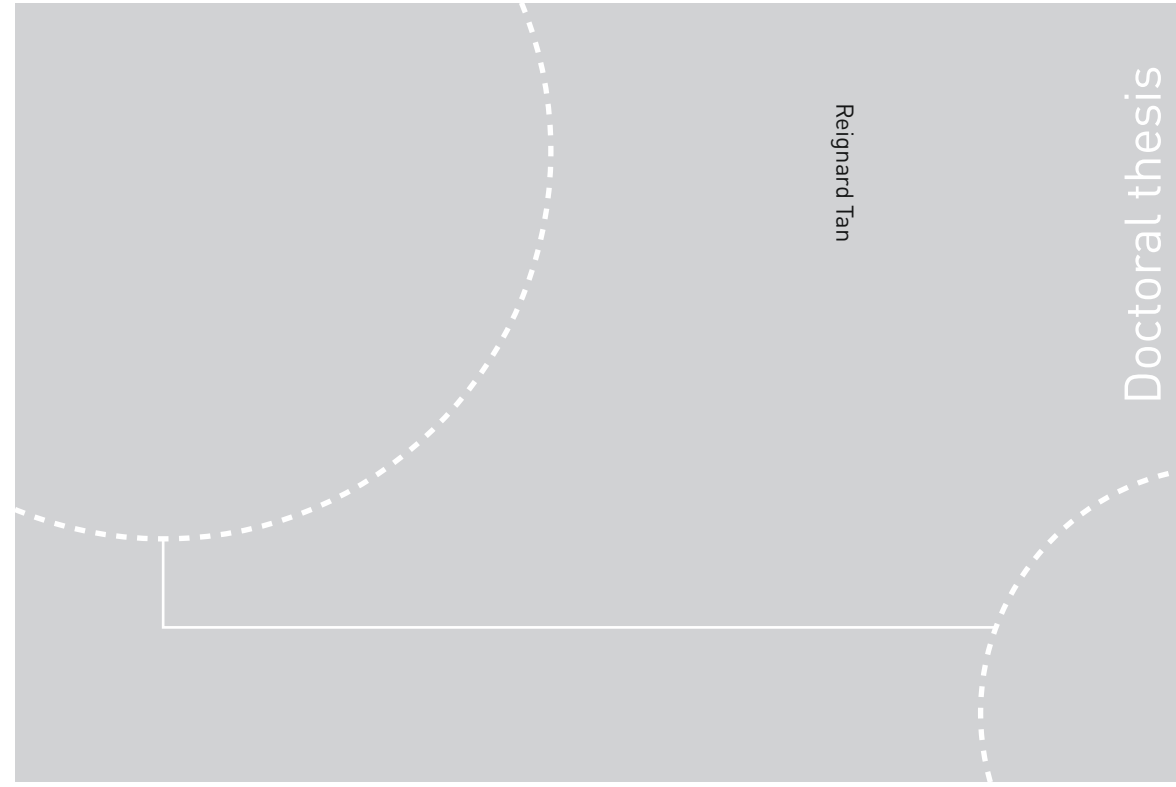


ISBN 978-82-326-3892-5 (printed ver.)
ISBN 978-82-326-3893-2 (electronic ver.)
ISSN 1503-8181



Doctoral theses at NTNU, 2019:147

Reignard Tan

Consistent crack width calculation methods for reinforced concrete elements subjected to 1D and 2D stress states

A mixed experimental, numerical and analytical approach

 **NTNU**
Norwegian University of
Science and Technology

Doctoral theses at NTNU, 2019: 147

NTNU
Norwegian University of Science and Technology
Thesis for the Degree of
Philosophiae Doctor
Faculty of Engineering
Department of Structural Engineering

 **NTNU**

 **NTNU**
Norwegian University of
Science and Technology

Reignard Tan

Consistent crack width calculation methods for reinforced concrete elements subjected to 1D and 2D stress states

A mixed experimental, numerical and analytical approach

Thesis for the Degree of Philosophiae Doctor

Trondheim, May 2019

Norwegian University of Science and Technology
Faculty of Engineering
Department of Structural Engineering

NTNU
Norwegian University of Science and Technology

Thesis for the Degree of Philosophiae Doctor

Faculty of Engineering
Department of Structural Engineering

© Reignard Tan

ISBN 978-82-326-3892-5 (printed ver.)
ISBN 978-82-326-3893-2 (electronic ver.)
ISSN 1503-8181

Doctoral theses at NTNU, 2019:147

Printed by NTNU Grafisk senter

Preface

This doctoral thesis is submitted in partial fulfilment of the requirements for the degree Philosophiae Doctor (PhD) at the Norwegian University of Science and Technology (NTNU). The research has been carried out at the Department of Structural Engineering at NTNU in Trondheim, Norway. The main supervisor has been Professor Terje Kanstad and the co-supervisors have been Professor Max Hendriks (NTNU and TU Delft), Professor Mette Geiker (NTNU) and MSc. Dan-Evert Brekke (Multiconsult).

The PhD project is a part of the ongoing research project Ferry-Free E39 carried out under the auspices of the Norwegian Public Roads Administration, work package 7.1.3: *Evaluation and improvement of crack width calculation methods for large-scale concrete structures*. NTNU and Ferry-Free E39 funded the PhD work. The research project Durable advanced Concrete Solutions (DaCS) financed by the Research Council of Norway (project no. 245645/O20) and several industrial partners contributed also with funding for the experimental work. The PhD project started in September 2015 and the thesis was submitted February 2019.

The thesis is written as a collection of papers and consists of two parts. The first part highlights the research significance, main objectives and limitations, and summarizes the appended papers and the main conclusions. The second part consists of five appended papers, of which two have been published, two are under review at international scientific peer-reviewed journals and one has been published in a conference proceedings.

The author, Reignard Tan, declares that this thesis with all its presented work is his own and contains no material that has previously been submitted for a degree at this university or any other institution.

Oslo/Trondheim, May, 2019.

Reignard Tan

Acknowledgements

Many have contributed and supported me in making this thesis possible. The past three and a half years have undoubtedly been the most exciting, amusing and challenging period in my life. I am forever grateful to have been given the privilege of doing a PhD.

First of all, I would like to thank my supervisors Professor Terje Kanstad, Professor Max Hendriks, Professor Mette Geiker and Dan-Evert Brekke for devoting your time and work to form a dreamteam to guide me through this journey. Terje, your composure, patience and never ending support have been indispensable to my motivation. Max, I strongly believe that I never would have fulfilled my goals and achievements in this PhD project without your supervision and level of scientific knowledge, as you are a true pleasure to work with. Mette, you simply raise the bar and I will be forever grateful for your great feedbacks to elevate the quality in my work. Dan-Evert, your experience, expertise and valuable input on this topic have indeed motivated me to pursue results that can be used for practical application and I thank you for always taking the time to have constructive discussions.

To my former leaders at Multiconsult, Per Horn, Christopher Løken and Egil Møen, who supported and encouraged me to grasp this opportunity. To my leaders now, Kjetil Slåttedalen and Andreas Andenæs, I truly appreciate your fight to carry on the backing from Multiconsult and I look forward to work for this great firm again. I would also like to express my gratitude to other colleagues at Multiconsult, in particular Magnus Møllegaard and my PhD-colleagues Morten Engen and Finn-Idar Grøtta Giske who I shared office with at Skøyen.

I would like to thank friends and colleagues at NTNU, for sharing research, experiences, achievements and even frustrations with you. Special thanks to Kristoffer Eileraas, Ola Opkvitne and Giedrius Žirgulis who helped me with the experimental work in the laboratory and for your contributions to my first journal paper. Thank you also to Simen Kvam for the great job you did on your master project, which I benefited a lot from in my work. I would also like to extend my gratitude to Professor Walter Kaufmann for having me as your guest at ETH Zürich and the opportunity of observing experiments on your ever so exciting and impressive laboratory.

To my mother, Leonora Tan, who has been the biggest inspiration in my life. I thank you for everything you have done for me and for laying the foundation to fulfil all my dreams in life. I appreciate also all the love and support from my family, in-laws and friends, especially my best friends Erik Espiritu, Imran Mir and Marvin Vergara who always have been there for me in both good and bad times.

And last but not the least, to my wife and the love of my life, Maria. Getting this degree would never have been possible without your everlasting grace, presence and support and I will always be forever grateful for that. Despite my many achievements during this PhD project and in life, nothing will ever measure up to getting married to you September 15th, 2018.

Abstract

Predicting crack widths in reinforced concrete (RC) structures is important for Serviceability Limit State (SLS) design. Crack widths exceeding the requirements can impair the functionality of a structure, limit its use and even reduce the service life. Calculation methods for predicting crack widths in one-way bearing structural elements have been developed for several decades and are relatively straightforward in use for design of conventional RC ties, beams and slabs. This is not the case for more complicated structural elements with large reinforcing bars (rebars) and covers, such as shear walls, two-way bearing slabs and shells typically occurring in *large-scale concrete structures*. Complete guidelines for predicting crack widths in such cases do not exist, and the influence of large rebars and covers on the cracking behaviour of RC structures is still not clear. Large-scale concrete structures are among others intended to be used for the planned coastal highway route “Ferry-free E39” in Norway.

The main objective in this thesis was formulated to facilitate a calculation model capable of predicting crack widths in large-scale concrete structures consistently. The study is subdivided into two parts as i) evaluation and ii) improvement of the current practice.

The evaluation reveals that the semi-empirical formulas recommended by Eurocode 2 (EC2) and *fib* Model Code 2010 (MC2010) yield inconsistent crack width predictions, particularly in cases of large rebars and covers. EC2 prove to yield overly conservative crack width predictions, in average predicting twice the size of maximum crack widths measured from an experimental study of RC ties. This could have severe economic consequences in a typical design situation.

An improved crack width calculation model was formulated by using the basic principles in solid mechanics, which lead to deriving and solving the second order differential equation for the slip using the bond-slip law recommended by MC2010, however, with adjusted parameters to account for the behaviour of RC ties. This resulted in the Modified Tension Chord Model (MTCM), essentially replacing the Tension Chord Model (TCM) in the Cracked Membrane Model (CMM), to formulate the Modified Cracked Membrane Model (MCMM) that is capable of predicting crack widths in large-scale concrete structures.

Comparison with crack widths measured from experiments reported in the literature showed that the MCMM predicted crack widths consistently and with a mean for the modelling uncertainty for crack width predictions being fairly close to one but still on the conservative side regardless of rebar and cover size. A simplified approach was formulated as an alternative method to the MCMM, in addition to a generalized expression for predicting tension stiffening normal to a crack, a feature currently missing in EC2 and MC2010. The simplified approach was consistent in its predictions but more conservative than the MCMM, as expected. The results in the thesis suggest that both the MCMM and the simplified approach show great potential for yielding consistent crack width predictions of large-scale concrete structures, and in general better predictions than offered by EC2 and MC2010 for

SLS design. Finally, the thesis offers complete guidelines for predicting crack widths in large-scale concrete structures subjected to in-plane loading.

Keywords: Crack widths, crack spacing, tension stiffening, calculations, large-scale concrete structures, membrane elements.

Table of contents

Part I – Extended summary

1	Introduction.....	1
1.1	Background and motivation.....	1
1.2	Objectives and limitations	2
1.3	Outline of the thesis.....	3
2	Cracking and tension stiffening	4
2.1	General.....	4
2.2	RC ties, beams and one-way bearing slabs.....	5
2.3	RC membranes and shells.....	6
3	Summary of papers	8
3.1	The work seen in context.....	8
3.2	Paper I.....	9
3.3	Paper IIa.....	9
3.4	Paper IIb	10
3.5	Paper III	10
3.6	Paper IV.....	10
4	Application to members subjected to bending.....	12
5	Comparison with EC2 and MC2010.....	13
6	Design case study.....	16
7	Conclusion	17
7.1	Concluding remarks.....	17
7.2	Recommendations for future research.....	18
8	List of notations	20
9	References.....	22

Part II – Appended papers

- Paper I *Experimental and theoretical investigation of crack width calculation methods for RC ties*
- Paper IIa *A numerical investigation of the cracking behaviour of reinforced concrete-tie elements*
- Paper IIb *An investigation of the strain profile over the cover in reinforced concrete elements subjected to tension*
- Paper III *Analytical calculation model for predicting the cracking behaviour of reinforced concrete ties*

Paper IV *Modified cracked membrane model for consistent crack width predictions of reinforced concrete structures subjected to in-plane loading*

Appendices

Appendix A *Solution procedure for the modified cracked membrane model*

Appendix B *MATLAB script for CHLM iteration procedure*

List of publications

Appended journal publications

Tan, R., Eileraas, K., Opkvitne, O., Žirgulis, G., Hendriks, M.A.N., Geiker, M., Brekke, D.E. & Kanstad, T. *Experimental and theoretical investigation of crack width calculation methods for RC ties*. Structural Concrete, 19(5), 1436-1447, 2018.

Tan, R., Hendriks, M.A.N., Geiker, M. & Kanstad, T. *A numerical investigation of the cracking behaviour of reinforced-concrete tie elements*. Magazine of Concrete Research, <https://doi.org/10.1680/jmacr.18.00156>, 1-13, 2018.

Tan, R., Hendriks, M.A.N., Geiker, M. & Kanstad, T. *Analytical calculation model for predicting the cracking behavior of reinforced concrete ties*. Under review, 2019.

Tan, R., Hendriks, M.A.N., Geiker, M. & Kanstad, T. *Modified cracked membrane model for consistent crack width predictions of reinforced concrete structures subjected to in-plane loading*. Under review, 2019.

Appended conference publication

Tan, R., Hendriks, M.A.N. & Kanstad, T. *An investigation of the strain profile over the cover in reinforced concrete elements subjected to tension*. Proceedings for 5th fib Congress, Melbourne, Australia, Oct. 7 to 11, 2018.

Conference publications

Tan, R., Hendriks, M.A.N., Geiker, M., Brekke, D.E. & Kanstad, T. *Evaluation and Improvement of Calculation Methods for Large-Scale Concrete Structures in Service Limit States*. Proceedings of the 11th fib International PhD Symposium in Civil Engineering, The University of Tokyo, Tokyo, Japan, Aug. 29 to 31, 2016.

Tan, R., Hendriks, M.A.N. & Kanstad, T. *Evaluation of Current Crack Width Calculation Methods According to Eurocode 2 and fib Model Code 2010*. High Tech Concrete: Where Technology and Engineering Meet. Proceedings of the 2017 fib Symposium, Maastricht, the Netherlands, June 12 to 14, 2017.

Tan, R., Hendriks, M.A.N., Geiker, M., Brekke, D.E. & Kanstad, T. *Evaluation and improvement of crack width calculation methods for large concrete structures*. Proceedings of the XXIII Nordic Concrete Research Symposium, Aalborg, Denmark, Aug. 21 to 23, 2017.

Tan, R., Hendriks, M.A.N., Geiker, M., Brekke, D.E. & Kanstad, T. *Evaluation of crack width calculation methods according to Eurocode 2 and fib Model Code 2010 and suggestions to improvements*. Workshop proceedings No. 12 from a Nordic mini-seminar on Crack Width Calculation Methods for Large Concrete Structures, Oslo, Norway. Aug. 29 to 30, 2017.

Tan, R., Hendriks, M.A.N., Geiker, M. & Kanstad, T. *Crack width calculation methods for large-scale concrete structures for the Ferry-Free E39*. Proceedings for the IABSE Conference Kuala Lumpur 2018, Kuala Lumpur, Malaysia, Apr. 25 to 27, 2018.

Other publications

Tan, R. & Engen, M. *Crack width calculation methods for large concrete structures*. Workshop proceedings No. 12 by the Nordic Concrete Federation, Norsk Betongforening, Oslo, Norway, 88 pp., 2017.

Technical presentations

Tan, R. *Diagonal Cracking and Excessive Deformations in Concrete Cantilever Bridges*. 2nd Nordic mini-seminar on residual service life & capacity of deteriorated concrete structures, Oslo, Norway, June 1 to 2, 2016.

Declaration of authorship

Reignard Tan has planned and conducted the work in the abovementioned publications, evaluated the results, written the papers and this thesis. Some of the co-authors in Paper I (Eileraas, K., Opkvitne, O. & Žirgulis, G.) contributed in the laboratory by preparing the specimens for testing, conducting the experiments and documenting the results. The co-authors also contributed with discussions of methods and results in addition to reviewing the manuscripts.

Part I – Extended summary

1 Introduction

1.1 Background and motivation

Limiting crack widths in reinforced concrete (RC) structures is an important design criterion for Serviceability Limit State (SLS). Serviceability design is in general important since the aim is to reflect the behaviour of a structure for its intended use (Balázs, et al., 2013). Cracking occurs whenever the tensile strength of concrete is reached and is often caused by volumetric changes in young hardening concrete, loads and imposed deformations (Leonhardt, 1988). The *fib* Model Code 2010 (MC2010) (fib, 2013) specifies appearance, tightness and durability as the main reasons for limiting the crack widths. Exceeding the limit state set by one of these during design does not necessarily mean that the structure should be rejected, but indicates a risk of reducing the functionality and/or the service life, and should be avoided (Basteskår, Engen, Kanstad, & Fosså, 2018). The appearance criteria is with regard to the aesthetics of a structure as well as to avoid concern by the casual observer (Haldane, 1976), while the tightness criteria is to prevent or limit leakage (Beeby, 1978). Cracking of the concrete cover can cause ingress of harmful substances that could lead to corrosion of steel reinforcement (Castel, 2000; Vidal, Castel, & François, 2004; Pease, 2011; Hornbostel & Geiker, 2017; Boschmann Käthler, Angst, Wagner, Larsen, & Elsener, 2017), which might pose a threat to the durability of a structure. A typical design criterion for SLS requires that the crack widths predicted by a chosen calculation method w_{cr} are less or equal to the limiting value w_{lim} , i.e. as

$$w_{cr} \leq w_{lim} \quad (1)$$

This thesis focuses on predicting crack widths in *large-scale concrete structures* subjected to in-plane loading. Large-scale concrete structures are in this thesis synonymous with RC structures having member dimensions that can be several meters in height, sections with large reinforcing bar (rebar) diameters and large covers, and members subjected to the eight force resultants typically occurring in shell structures as depicted in Figure 1(a). Such large-scale concrete structures are normally observed for dams, gravity based structures, bridges, silos, containers, etc., and are also intended to be used for the RC structures planned for the coastal highway route “Ferry-free E39” in Norway. The “Ferry-free E39” is a research project launched by the Norwegian Public Roads Administration (NPRA) with the aim of replacing eight ferry-crossings along the west coast of Norway with bridges and tunnels. Some of the crossings are up to 5 km long with fjord depths up to 1300 m. The NPRA recommends that the design methods should follow the guidelines provided in N400 (NPRA, 2015), which specifies covers being up to 130 mm in RC structures exposed to marine environment. Moreover, large rebars often in bundles and over several layers are typically used for large-scale concrete structures, as depicted in Figure 1(b). The N400 (NPRA, 2015) also recommends that the calculation method in Eurocode 2 (EC2) (CEN, 2004) is used for predicting crack widths. However, shortcomings can be mentioned.

- 1) neither EC2 nor MC2010 provide complete guidelines for predicting crack widths in RC structures subjected to in-plane shear and normal forces,
- 2) accounting for the effects of large rebars and covers are not clear when using EC2 and MC2010.

This suggests that the recommended practice is not fully capable of predicting crack widths in large-scale concrete structures. Furthermore, experience feedback indicate that EC2 tends to yield overly conservative and inconsistent crack width predictions for uniaxial stress states, particularly in cases of large rebars and covers.

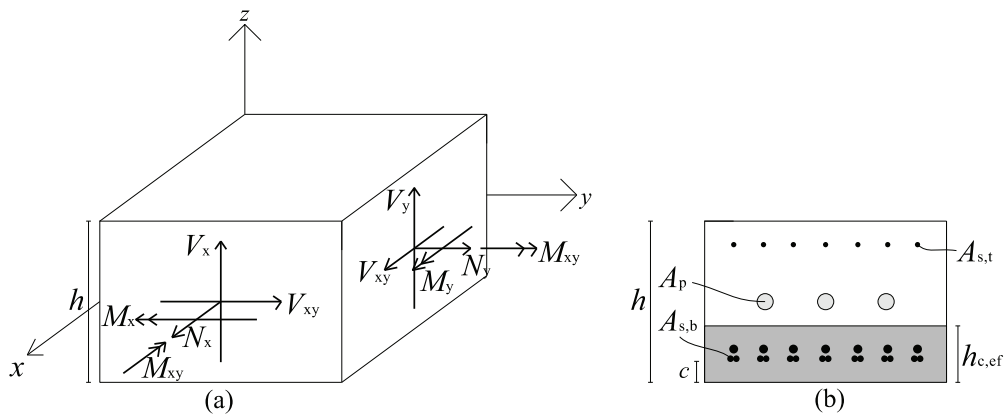


Figure 1: (a) Shell member subjected to the eight force resultants. (b) Typical section in large-scale concrete structures.

1.2 Objectives and limitations

The main objective of this PhD study is to provide a calculation method capable of predicting crack widths in large-scale concrete structures subjected to in-plane loading. This will be done by

- 1) evaluating the current practice experimentally and theoretically,
- 2) developing a tension stiffening model mechanically based on the physical behaviour of RC ties and that is capable of predicting crack widths consistently regardless of geometry, material and loading conditions,
- 3) formulating a calculation model that predicts crack widths in orthogonally RC structures subjected to in-plane loading.

The work in this PhD study is limited to predicting crack widths mainly caused by in-plane loading meaning that out-of-plane shear is neglected. Cracking caused by volumetric changes in young hardening concrete and hardened concrete such as plastic shrinkage, plastic settlement, heat of hydration, internal and external temperature differences within a member, and other imposed deformations in general will not be addressed in particular. The same

applies to consequences related to cracking, meaning that only the left hand side of the inequality in Eq. (1) will be addressed in this study. Moreover, undeformed rebars and load levels close to the ultimate load capacity will not be addressed in particular, i.e. for steel stresses after the onset of yielding.

1.3 Outline of the thesis

This thesis is written on the basis of five papers, of which four are either published or submitted for journal publication and one has been published in a conference proceedings. First, the basic concepts of cracking and tension stiffening, which formed the basis for all papers in this thesis, are discussed. Secondly, a summary of the main findings in the papers are given. Then, an application to members subjected to bending and comparison with EC2 and MC2010 are shown before a design case study follows. Finally, main conclusions from the PhD study are drawn before proposing further research.

2 Cracking and tension stiffening

2.1 General

The basic concepts of cracking and tension stiffening is discussed to better understand the essence of this thesis. Many approaches for predicting cracking of members subjected to uniaxial stress states such as RC ties, beams and one-way bearing slabs have been developed for several decades, where some use formulations based on empirical considerations (Kaar & Hognestad, 1965; Ferry-Borges, 1966; Base, Read, Beeby, & Taylor, 1966; Gergely & Lutz, 1968; Broms, 1968; Rizkalla & Hwang, 1984; Schiessl & Wölfel, 1986; Janovic & Kupfer, 1986), some use mechanical approaches (Saliger, 1936; Somayaji & Shah, 1981; Noakowski, 1985; Farra & Jaccoud, 1992; Russo & Romano, 1992; Balázs, 1993; Marti, Alvarez, Kaufmann, & Sigrist, 1998; Khalfallah, 2006; fib, 2010) while others use concepts of fracture mechanics (Bazant & Oh, 1983; Oh & Kang, 1987) as pointed out by Borosnyói & Balázs (2005). In contrast, few approaches have been proposed for members subjected to biaxial stress states such as RC membranes and shells (Cerioni, Michelini, & Bernardi, 2007; Giordano & Mancini, 2009; Barre, et al., 2016). The work in this thesis shows how the basic concepts of cracking and tension stiffening in RC ties can be extended to predict the cracking behaviour of members subjected to biaxial stress states, while also accounting for the effects of large rebars and covers.

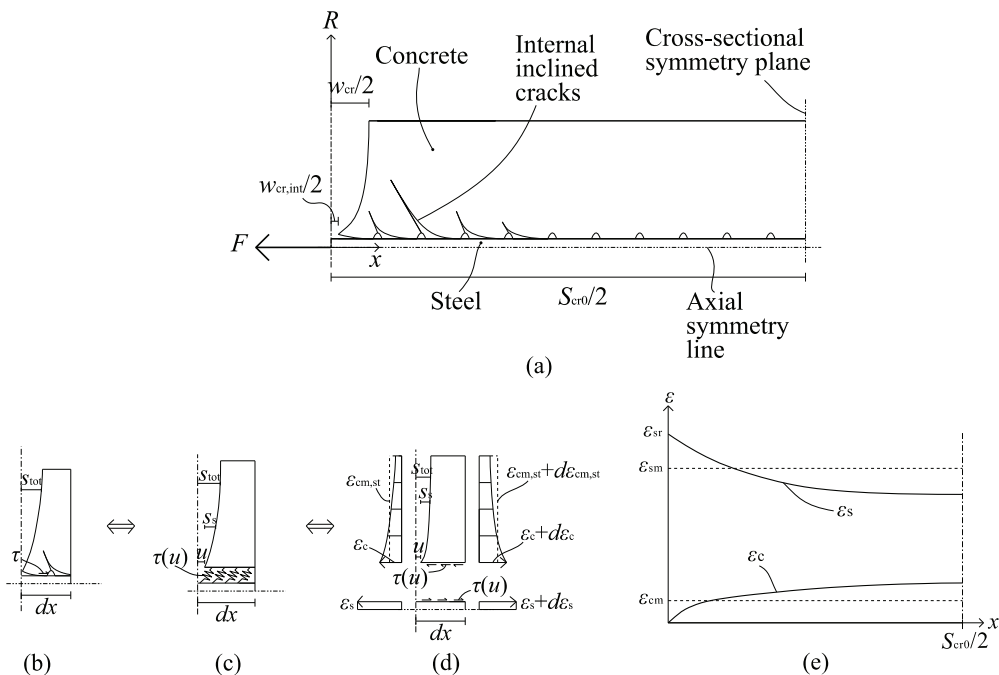


Figure 2: (a) Cracking of RC tie. (b) Arbitrary section in an RC tie. (c) The bond behaviour smeared to the interface between concrete and steel. (d) Strain profiles over the cover in an infinitesimal slice of the RC ties. (e) Strain profiles for the steel and concrete over the crack spacing.

2.2 RC ties, beams and one-way bearing slabs

The concept of cracking and tension stiffening is elucidated by discussing the physical behaviour of RC ties subjected to tensile forces. Figure 2(a) depicts a typical deformation configuration reported from several investigations in the literature (Watstein & Mathey, 1959; Broms, 1968; Husain & Ferguson, 1968; Yannopoulos, 1989; Beeby, 2004; Tammo, Lundgren, & Thelandersson, 2009; Borosnyói & Snóbli, 2010; Berrocal, Löfgren, Lundgren, Görander, & Halldén, 2016). It is observed that the internal inclined cracks cause the crack width at the interface $w_{cr,int}$ to be significantly smaller than that on the concrete surface w_{cr} . The research of Goto (1971) and Tammo and Thelandersson (2009) concludes that this is a consequence of the interlocking of the bar lugs and the confining concrete. A consideration of the arbitrary section depicted in Figure 2(b) suggests that the bond transfer is governed by the internal cracking behaviour of concrete. A simplification to describe this mechanical behaviour would be to assume steel and concrete as elastic materials and smear the nonlinearity related to the internal cracking behaviour to the interface (Saliger, 1936; Russo & Romano, 1992; Balázs, 1993; Khalfallah, 2006; fib, 2010; Debernardi & Taliano, 2016), e.g. as springs shown in Figure 2(c). The simplification implies that the deformation caused by internal inclined cracks is equivalent to slip occurring between steel and concrete at an arbitrary section. Furthermore, assuming that the spring behaviour is known from a bond-slip law yields a static equivalent section of an arbitrary section in an RC tie as depicted in Figure 2(d). The equilibrium for steel and concrete is obtained as

$$E_s A_s \frac{d\varepsilon_s}{dx} = -\tau(u) \sum \pi \phi_s \quad (2)$$

and

$$\psi E_c A_c \frac{d\varepsilon_c}{dx} = \tau(u) \sum \pi \phi_s \quad (3)$$

respectively. Here, u is the slip, τ is the bond stress, ϕ_s is the rebar diameter, ε_s and ε_c are steel and concrete strains respectively at the interface, E_s and E_c are Young's modulus for steel and concrete respectively and A_s and A_c are steel and concrete areas respectively. The strain variation parameter $\psi = \varepsilon_{cm,st}/\varepsilon_c \leq 1$ accounts for the presence of a nonlinear strain profile over the concrete cover and thus that plane sections do not remain plane in RC ties (Edwards & Picard, 1972), where $\varepsilon_{cm,st}$ are mean concrete strains over the cover.

Furthermore, the kinematic compatibility is obtained as

$$-u' = \varepsilon_s - \varepsilon_c \quad (4)$$

These three equations yield the second order differential equation (SODE) for the slip as

$$u'' - \chi \tau(u) = 0 \quad (5)$$

where $\chi = \zeta(\sum\pi\phi_s/E_sA_s)(1 + \xi)$, $\xi = \alpha_E\rho_s/\psi$, $\alpha_e = E_s/E_c$ and $\rho_s = A_s/A_c$ are constants. The term $\sum\pi\phi_s$ indicates the sum of perimeters of rebars contributing to bond in a section, while $\zeta \leq 1$ is factor accounting for the effect that rebar spacing has on the bond transfer. The solution to Eq. (5) provides a tension stiffening model that is dependent on the chosen bond-slip law $\tau(u)$ (Jiang, Shah, & Andonian, 1984; Russo & Romano, 1992; Balázs, 1993; Marti, Alvarez, Kaufmann, & Sigrist, 1998; Debernardi & Taliano, 2016). Proposals for bond-slip laws can be found in Rehm (1961), Nilson (1968), Martin (1973), Mirza and Houde (1979), Eligehausen et al. (1983), Pedziwiatr (2008), Muhamad et al. (2011) and Hong and Park (2012). Furthermore, steel and concrete strains are obtained by Eq. (2), (3) and (4) for a given load after having solved Eq. (5), see Figure 2(e). It is noticed that the steel strains reduce for increasing values of x up to the plane of symmetry $S_{cr0}/2$, which is caused by the bond transfer or, expressed more rigorously, the tension stiffening (Bresler & Bertero, 1968; Scott & Gill, 1987; Beeby & Scott, 2004; Beeby & Scott, 2005; Caldentey, Peiretti, Iribarren, & Soto, 2013). Finally, the crack width is obtained as the difference between the integrated steel and concrete strains over the crack spacing and can be expressed as

$$w_{cr} = S_{cr0}(\varepsilon_{sm} - \varepsilon_{cm}) \quad (6)$$

The concept can be extended to RC members subjected to bending by assuming that the effective concrete area surrounding the rebars is treated as an RC tie (CEB, 1985; Braam, 1990; Balázs, et al., 2013), see Figure 1(b). This is similar to the approach recommended by MC2010, implying that bending stresses can be accounted for by multiplying crack widths predicted with $(h - x_c)/(d - x_c)$ where x_c is the height of the compression zone. This would yield crack widths predicted that are comparable to crack widths measured at the “extreme tensile fibre” of the member.

2.3 RC membranes and shells

The concept of cracking and tension stiffening in RC ties can be applied to RC membranes as well. The main difference is that cracks in RC membranes do not form normal to the reinforcement directions as it does for RC ties, but rather in a skew angle due to the presence of shear stresses in addition to normal stresses as depicted in Figure 3(a). This implies that cracks tend to form normal to the direction of the *maximum principle strains* as observed in the experiments of (Vecchio & Collins, 1982; Marti & Meyboom, 1992; Khalifa, 1986; Kirschner & Collins, 1986; Laskar, Wang, Hsu, & Mo, 2007). Crack widths for RC membranes can thus be expressed as

$$w_{cr} = S_{cr}(\varepsilon_1 - \varepsilon_{c1}) \quad (7)$$

at which S_{cr} is the crack spacing and $(\varepsilon_1 - \varepsilon_{c1})$ represents the tension stiffening normal to the crack. Here, ε_1 are maximum principle strains for the RC membrane including the tension stiffening effect of the reinforcement and ε_{c1} are maximum principle strains for concrete. An expression to determine the tension stiffening normal to the crack in RC membranes is a feature currently missing in both EC2 and MC2010, and complete guidelines for predicting

crack widths in such conditions do not exist as highlighted previously. There are some methods capable of predicting crack widths in RC membranes in the literature, e.g. the Modified Compression Field Theory (MCFT) developed by Vecchio and Collins (1986), Collins and Mitchell (1997), Bentz (2000), and Bentz et al. (2006), the rotating angle softened-truss-model (RA-STM) developed by Hsu (1988), Pang and Hsu (1995), Hsu and Mo (2010), Bernardo et al. (2018), and the cracked membrane model (CMM) developed by Kaufmann (1998), Kaufmann and Marti (1998), Foster and Marti (2003), Dabbagh and Foster (2006) and Pimentel et al. (2010). However, these models were formulated with the primary objective of predicting the ultimate load capacity rather than the crack widths. This implied incorporating tension stiffening using simplified approaches, i.e. without having to solve the SODE for the slip in Eq. (5) explicitly for a chosen bond-slip law to obtain steel and concrete strains. Nevertheless, tension stiffening can be incorporated mechanically in RC membranes by combining it with the compression field approach (Kaufmann, 1998; Kaufmann & Marti, 1998). In shortness, this involves obtaining equilibrium of steel and concrete stresses at the crack in terms of the mean strains in the RC membrane.

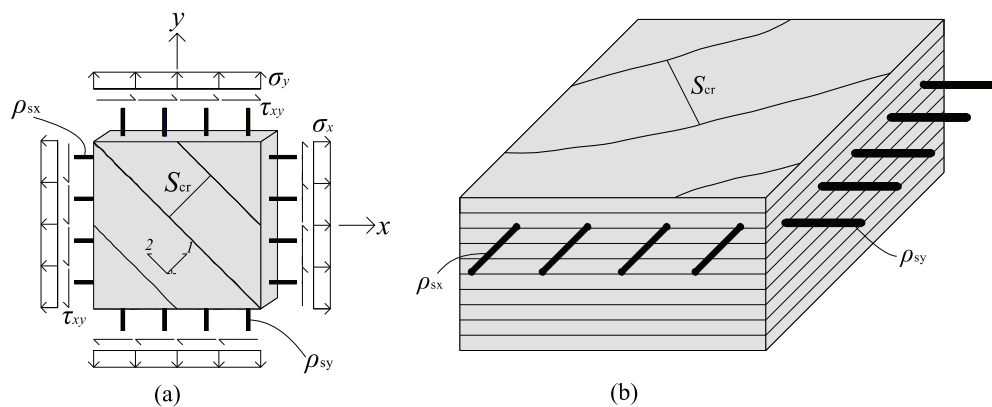


Figure 3: (a) RC membrane. (b) RC shell.

The concept of cracking and tension stiffening for RC membranes can further be extended to RC shells, e.g. by implementation to a layered approach (Seelhofer, 2009), see Figure 3(b). Each layer is thus treated as an RC membrane where the equilibrium of forces is formulated at a cracked section.

3 Summary of papers

3.1 The work seen in context

Figure 4 shows how the papers are interrelated to accommodate the main objectives in this thesis. The evaluation of the current practice in Paper I led to the conclusions that improvements of crack width calculation methods for large-scale concrete structures were needed. This mainly because EC2 and MC2010 do not account for the effects of large rebars and covers properly, and the fact that they do not provide complete guidelines for predicting crack widths in RC structures subjected to in-plane loading. To better understand the effects of rebar and cover, and in general the cracking behaviour of RC ties, virtual experiments using NLFEA were conducted in Papers IIa and IIb. These results formed the basis of the Modified Tension Chord Model (MTCM) formulated in Paper III, which later replaced the Tension Chord Model (TCM) in the Cracked Membrane Model (CMM) to formulate the Modified Cracked Membrane Model (MCMM) in Paper IV. It was seen that the MCMM was capable of predicting crack widths in RC members subjected to in-plane loading consistently and with a mean for the modelling uncertainty for crack width predictions being fairly close to one but still on the conservative side regardless of rebar and cover size, thus accommodating the objectives in this PhD study.

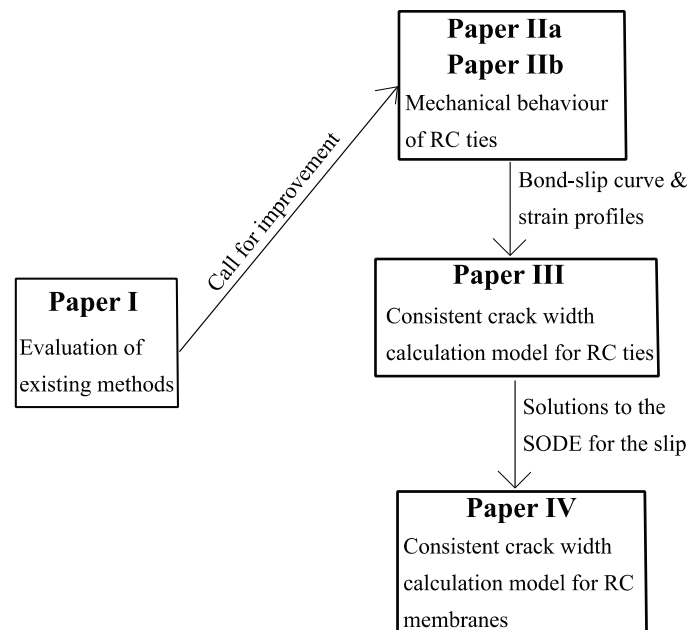


Figure 4: Interrelation of papers

3.2 Paper I

This paper investigates the semi-empirical formulas for predicting crack widths in RC ties recommended by EC2, MC2010 and EC2 with the German National Annex (DIN) (DIN, 2011) experimentally and theoretically. For this purpose, the concept of modelling uncertainty for crack width predictions was applied. The main objective was to investigate the application of the respective codes to sections having large rebars and covers. It was seen that the semi-empirical formulas were derived based on using the same mechanical concept that lead to the SODE for the slip in Eq. (5). However, instead of solving it explicitly, simplifications were made, resulting in a formulation that is in conflict with the basic principles of solid mechanics. This lead to, among others, the equilibrium being violated in the formula for calculating the maximum crack spacing in EC2 and MC2010 due to the inclusion of the cover term. DIN, however, has abandoned the cover term. Comparison with experiments on eight RC ties showed that the codes predicted the maximum crack widths measured inconsistently, particularly in cases of large rebars and covers. In fact, EC2 predicted crack widths that in average were twice the maximum crack widths measured in the experiments. MC2010 and DIN gave better predictions in terms of the mean, but with a relatively large number of predictions on the nonconservative side. No conclusions could be drawn on which of the codes were to be preferred other than that all three codes look to have a limited range of applicability. It was suggested that a more mechanical consistent crack width calculation model should be formulated to better account for the effects of large rebars and covers by (a) selecting a proper bond-slip law suited for the behaviour of RC ties, (b) accounting for the strain variation over the concrete cover and (c) solving the SODE for the slip explicitly.

3.3 Paper IIa

The main objectives in this paper were formulated to (i) better understand the cracking behaviour of RC ties as well as the influence of rebar and cover, and (ii) obtain a proper bond-slip law to be used in solving the SODE for the slip. For this purpose, virtual experiments using nonlinear finite element analysis (NLFEA) on cylindrical RC ties were conducted. The FE-model allowed for the formation of internal inclined and splitting cracks and was seen to conform to the experimental behaviour of RC ties reported in the literature. The important concepts of *comparatively lightly loaded members* (CLLM) and *comparatively heavily loaded members* (CHLM) introduced by Russo and Romano (1992), which forms the boundary conditions when solving the SODE for the slip, were investigated thoroughly and verified in this study. CLLM and CHLM are analogous to the concepts of *crack formation stage* and *stabilized cracking stage* respectively. Furthermore, it was found that the crack spacing was a geometry dependent parameter mechanically governed by the size of the cover and not the rebar. However, it was argued that this was not necessarily the case in real life structures as the scatter of the tensile strength influences the crack pattern thus causing an interaction of the rebar and cover to determine the finite crack spacing. Anyway, increasing the rebar size had a beneficial effect in reducing the steel strains and thus the crack width for a given load level. It was seen that a local bond-slip curve accounts for the effects that both internal inclined and splitting cracks have on reducing the bond transfer, and that using only one bond-slip curve is

sufficient to describe the average bond behaviour of an RC tie with arbitrary geometry. In fact, it was seen that the bond-slip law proposed by Eligehausen et al. (1983) and later adopted by MC2010 with adjusted parameters $\tau_1 = 5.0$ MPa, $s_1 = 0.1$ mm and $\alpha = 0.35$, tends to serve as a mean for all bond-slip curves obtained from the virtual experiments.

3.4 Paper IIb

This paper investigates strain profiles over the cover by conducting NLFEA of cylindrical RC ties. The main objective was to obtain a reasonable value for the strain variation parameter ψ defined in Eq. (3), which describes the relation between mean concrete strains and concrete strains at the interface. It was found that ψ more or less remained constant over the entire bar length except for a region close to the primary crack. Virtual experiments on six different RC ties revealed that a constant value of $\psi = 0.70$ was reasonable, irrespective of the location over the bar length, geometry and load level.

3.5 Paper III

This paper was motivated by the conclusions in Paper I suggesting that a mechanically consistent crack width calculation model capable of accounting for the effects of large rebars and covers should be formulated. This paper derived the SODE for the slip based on the mechanical behaviour of RC ties discussed in Paper IIa and IIb. It accounts for the effects of (i) internal cracking on the bond transfer using the proposed bond-slip law in Paper IIa, (ii) nonlinear strain profiles over the cover using the strain variation parameter proposed in Paper IIb and (iii) rebar spacing. The last effect is a feature currently lacking in the semi-empirical formulas recommended by EC2 and MC2010. The SODE for the slip was solved analytically yielding closed form solutions for CLLM and non-closed form solutions for CHLM. A solution strategy was provided that facilitates a practical application of the calculation model, which was the main drawback of using similar approaches previously. Comparison with RC ties experimentally and theoretically investigated in the literature showed that the calculation model could predict crack spacing and crack widths consistently, irrespective of the rebar and cover size.

3.6 Paper IV

This paper formulated the Modified Cracked Membrane Model (MCMM) capable of predicting crack widths in RC membranes subjected to in-plane loading. The paper was motivated by the main objective in this PhD study of facilitating a calculation model capable of predicting crack widths in large-scale concrete structures. The calculation model was derived using the basic concepts of the Cracked Membrane Model (CMM), essentially the main difference being a replacement of the Tension Chord Model (TCM) with the Modified Tension Chord Model (MTCM) to determine steel stresses at the crack in terms of the mean strains. The MTCM is a tension stiffening model based on using the solutions obtained for the SODE for the slip in Paper III. A simplified approach was also proposed as an alternative

method to the MCMM. Furthermore, a generalized expression for determining the tension stiffening normal to the crack was formulated, a paramount feature to predict crack widths in RC membranes currently missing in EC2 and MC2010. Comparison to a total of 101 maximum crack widths measured experimentally from 37 test specimen suggests that the MCMM shows greater potential for predicting crack widths than the CMM. This could be justified by a mean for the modelling uncertainty for crack width predictions being fairly close to one but still on the conservative side, as well as the better and more consistent crack width predictions of the MCMM particularly in cases of large rebars and covers. It was thus argued that the MCMM offers a wider range of applicability than the CMM mainly owing to the mechanical improvement of the MTCM to the TCM, at which all cracking stages are accounted for through the concepts of CLLM and CHLM. The simplified approach was also seen to yield consistent predictions but in average being more conservative than the MCMM and the CMM, as expected. Hence, the results suggest that the MCMM and the simplified approach show great potential for yielding consistent and reliable crack width predictions of large-scale concrete structures.

4 Application to members subjected to bending

Papers III and IV show that the MTCM and the MCMM can be applied to predict crack widths in RC elements subjected to uniform in-plane shear and normal loads. However, they can also be extended to predict the cracking behaviour of members subjected to bending as mentioned in section 2.2. The effect of cover is included by determining the effective height surrounding the rebars as

$$h_{c,ef} = \min \left[2.5 \left(c + \frac{\phi_s}{2} \right), \frac{h}{2} \right] \quad (8)$$

This means that the effect of cover increases the concrete area confining the rebars, which in turn increases the crack spacing in the MTCM and implicitly the crack widths as well. This is analogous to the discussions in Paper IIa and Paper III.

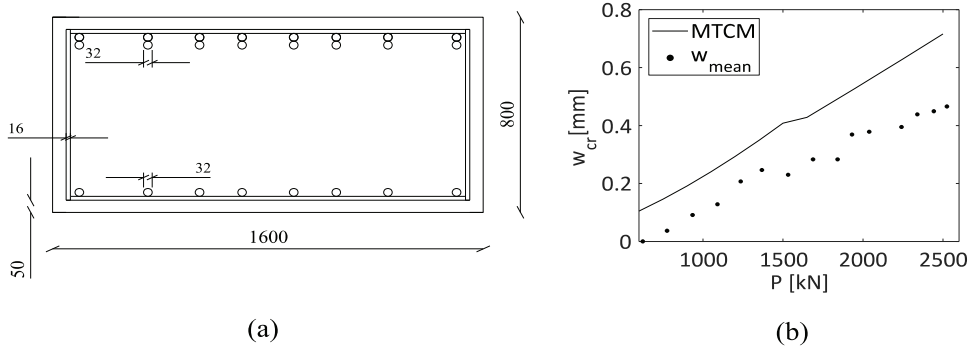


Figure 5: (a) RL6 section. (b) Comparison of mean crack widths measured for RL6 and crack widths predicted by the MTCM

The French research project CEOS.fr (Barre, et al., 2016) conducted a four point bending test on the beam designated as RL6 using a concrete class C50/60 and two bundled 32 mm rebars in the tensile zone, see Figure 5(a). The total length of the beam was 6 m of which 1.6 m were subjected to pure bending. Comparison of crack widths predicted by the MTCM and the mean of eight crack widths measured at the concrete surface in the pure bending zone is shown in Figure 5(b). The equilibrium was determined using the layered approach mentioned previously in section 2.3. It is observed that the crack widths predicted show a similar developing trend as the mean and are all on the conservative side. This shows that the application of the MTCM to members subjected to bending is reasonable.

5 Comparison with EC2 and MC2010

Table 1 shows a comparison of the crack spacing measured for the RC ties addressed in Paper I and II, and the corresponding maximum crack spacing predicted by MTCM, EC2 and MC2010. The crack spacing were predicted using the effective concrete area as highlighted in the previous chapter. The relationship between the maximum crack spacing predicted by the MTCM and the mean crack spacing measured, i.e. S_{cr0}/S_{crm0} , is in average 1.99 for the investigated RC ties under the assumption that the ratio is log-normally distributed. The average for EC2 and MC2010, on the other hand, is 3.16 and 2.22 respectively. The average for the MTCM is thus closest to the recommended value of 1.7 by CEB (1985) and Braam (1990), a factor that formed the basis for predicting the characteristic crack widths according to EC2 and MC2010. Furthermore, the standard deviation and coefficient of variation were 0.44 and 0.22 respectively for the MTCM, 0.83 and 0.26 respectively for EC2 and 0.58 and 0.26 respectively for MC2010. This suggests that the MTCM predicts the crack spacing more consistently than EC2 and MC2010 regardless of rebar and cover size, with all predictions being on the conservative side.

Table 1 – Crack spacing of investigated specimens

	Member	Measured [mm]		MTCM [mm]	EC2 [mm]			MC2010 [mm]		
		S_{crm0}	S_{cr0}	S_{cr0}	Cover	Bond	S_{cr0}	Cover	Bond	S_{cr0}
Paper I	S- ϕ 20-c40	163	250	390	136	372	508	80	304	384
	S- ϕ 32-c40	178	240	342	136	246	382	80	201	281
	S- ϕ 20-c90	217	290	422	306	433	739	180	354	534
	S- ϕ 32-c90	266	320	361	306	271	577	180	221	401
Paper II	Bresler and Bertero (1968)	203	-	301	210	325	535	124	265	389
	Yannopoulos (1989)	90	-	181	102	123	225	60	100	160
	ϕ 20c40	105	-	224	136	170	306	80	139	219
	ϕ 32c40	109	-	207	136	133	269	80	109	189
	ϕ 20c90	260	-	470	306	680	986	180	556	736
	ϕ 32c90	272	-	434	306	478	784	180	390	570

Table 1 shows the contribution of the cover and the bond term to the maximum crack spacing according to EC2 and MC2010. It is seen that they both predict the crack spacing overly conservative particularly in cases with large rebars and covers, e.g. for the specimens S- ϕ 20-c90, S- ϕ 32-c90, ϕ 20c90 and ϕ 32c90. This is primarily owing to the excessive contribution of the cover term, which in the predictions by EC2 already is observed to be larger than the maximum crack spacing measured for S- ϕ 20-c90 and only slightly smaller than the maximum crack spacing measured for S- ϕ 32-c90. MC2010 shows somehow better predictions in comparison, however, still yielding inconsistent predictions for specimens having different rebar dimensions but similar cover. EC2 and MC2010 assumes that the mean bond stress for the bond term is proportional to the tensile strength of concrete only, i.e. as

$\tau_{bm} = kf_{ctm}$ where k is constant. This is mechanical inconsistent with the findings in Paper IIa where it was found that the bond stress distribution and thus the mean bond stress is heavily dependent on the rebar, cover and the load level. These effects are accounted for in the MTCM through the chosen bond-slip law, which explains the more consistent and better crack spacing predictions.

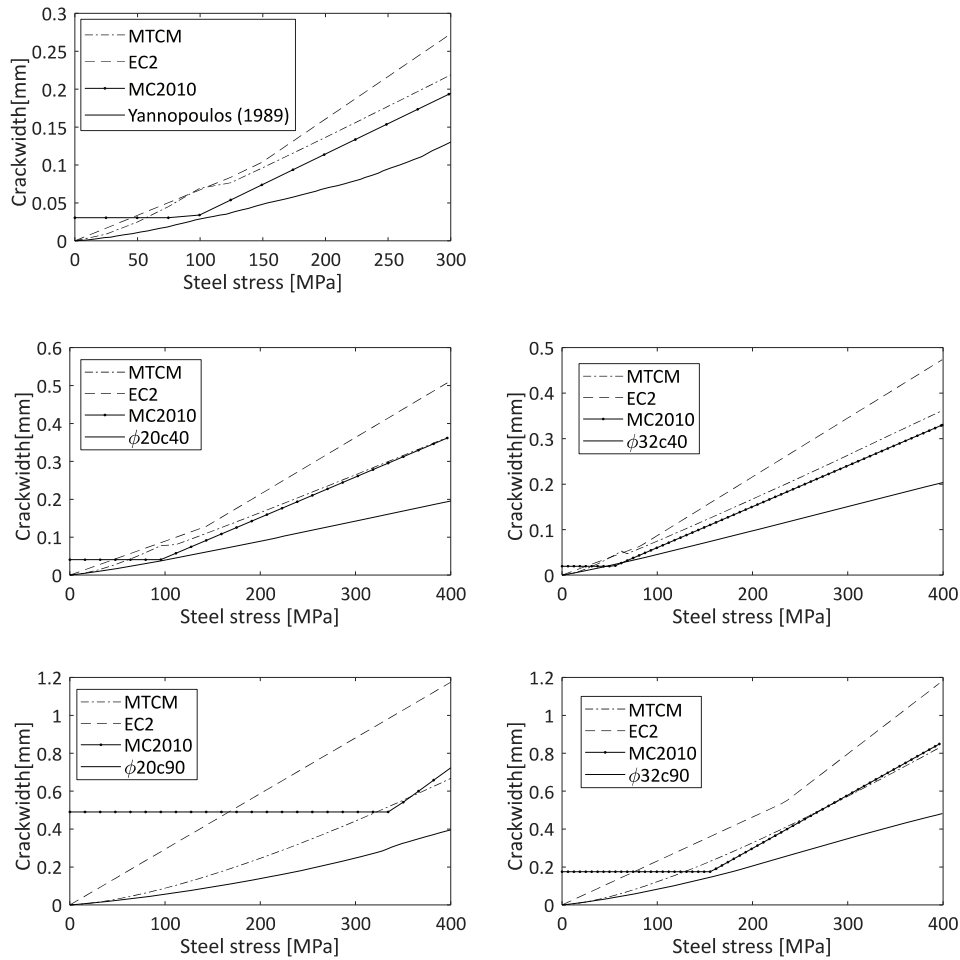


Figure 6 – Development of crack widths for some of the investigated specimens in Table 1.

Figure 6 shows comparison of the crack widths predicted and the mean crack widths measured for some of the investigated specimens in Table 2. It is seen that predictions by the MTCM in overall exhibit a developing trend quite similar to the mean crack widths measured, and conform as such better to the observed behaviour of the specimens than the predictions by EC2 and MC2010. This is particularly pronounced for specimen $\phi 20c90$, at which EC2 and MC2010 show peculiar predictions even for relatively large steel stresses (> 300 MPa). This is mainly caused by the fact that they do not account for the crack formation stage properly,

which for cases of large covers were observed to be governing even at large steel stresses in Paper IIa. Moreover, the derivation of the difference in steel and concrete strains, i.e. $(\epsilon_{sm} - \epsilon_{cm})$, according to EC2 and MC2010 in Paper I shows that they do not account for the member length in determining the tension stiffening. This is again mechanically inconsistent with the findings in Paper IIa as well as other investigations in the literature (Bresler & Bertero, 1968; Scott & Gill, 1987; Russo & Romano, 1992; fib, 2000) at which the member length indeed was found to be governing for the tension stiffening. These effects are accounted for in the MTCM through the concepts of CLLM and CHLM, which is a mechanical improvement to EC2 and MC2010. Comparison with the Yannopoulos (1989) specimen shows that the MTCM also can be applied for specimens having relatively small rebars and covers, which in this case were 16 mm and 30 mm respectively. This means that the MTCM is not restricted to predicting crack widths for cases with large rebars and covers only, thus suggesting that the MTCM offers a wider range of applicability than EC2 and MC2010.

6 Design case study

A simple case study of the test specimen S- ϕ 20-c90 from Paper I is now performed to elucidate the impact of using EC2, MC2010 and the MTCM to predict crack widths in a typical design situation. It is assumed a crack width requirement of $w_{lim} = 0.35$ mm and that the load of 736 kN given in Table 3 from Paper I governs. This would yield crack widths $w_{cr,EC2} = 0.65$ mm, $w_{cr,MC2010} = 0.33$ mm and $w_{cr,MTCM} = 0.43$ mm according to the predictions by EC2, MC2010 and MTCM respectively for the reinforcement configuration in S- ϕ 20-c90. Thus, only the crack width predicted by MC2010 satisfies the assumed requirement in this case. Typical measures for reducing the crack widths predicted in a design situation would be to 1) keep the reinforcement area constant by reducing the rebar diameter and increasing the number of rebars to reduce the crack spacing, or 2) increase the reinforcement area to reduce the steel strains as recommended in Paper II. Ideally, to be considered in the indicated order, from an economical point of view. However, it can be shown for option 1) that EC2 and the MTCM would require so many rebars that it in practice would be impossible to cast the RC tie, leaving option 2) as the only realistic action. Table 2 shows that for the investigated case an increase of 76% of the reinforcement area $A_{s,inc}$ is necessary when using EC2, while an increase of 25% is necessary when using the MTCM to satisfy the assumed crack width requirement. This simple case study shows that the dramatic increase in reinforcement area when using EC2 could have severe economic consequences for the design and might lead to rejecting the structure in other cases. Remarkably, the maximum crack width measured for S- ϕ 20-c90 at this load level, $w_{max} = 0.31$ mm, would already have satisfied the assumed crack width requirement $w_{lim} = 0.35$ mm.

Table 2 - Table showing crack widths predicted for test specimen S- ϕ 20-c90 from Paper I with varying reinforcement configurations

	n_{ϕ_s}	ϕ_s	A_s	$A_{s,inc}$	w_{cr}
EC2	9	25	4418	1.76	0.31
MC2010	8	20	2513	1.00	0.33
MTCM	10	20	3142	1.25	0.30

7 Conclusion

7.1 Concluding remarks

Evaluation of the semi-empirical formulas recommended by Eurocode 2 (EC2), *fib* Model Code 2010 (MC2010) and EC2 with German National Annex (DIN) showed that they predict crack widths inconsistently, particularly in cases of large rebars and covers. EC2 yields overly conservative crack width predictions, which can lead to severe economic consequences in design. MC2010 and DIN showed better crack width predictions in terms of the mean for the modelling uncertainty, however, with a relatively large number of predictions on the nonconservative side. The inconsistent predictions by the codes is a consequence of the mechanical formulation of the formulas being in conflict with the basic principles in solid mechanics, making them dependent on empirical adjustments. This suggests that EC2, MC2010 and DIN have a limited range of applicability. An improved crack width calculation method should be formulated, by (i) using a proper bond-slip law, (ii) accounting for nonlinear strains over the cover and (iii) solving the second order differential equation (SODE) for the slip explicitly.

The crack spacing was by virtual experiments found to be governed mechanically by the size of the cover and not the rebar. However, this is necessarily not the case in real life structures due to the influence of the scatter of concrete tensile strength on generating a random crack pattern, causing an interaction of the rebar and cover through the concepts of *Comparatively Lightly Loaded Members* (CLLM) and *Comparatively Heavily Loaded Members* (CHLM) to determine the finite crack spacing. Moreover, increasing the rebar size is the most effective way of reducing the steel strains and thus the crack widths for a given cover. The bond-slip curve of MC2010 with adjusted parameters can be used to describe the bond transfer of an arbitrary RC tie. Nonlinear strain profiles over the cover can also be accounted for by using a constant value for the strain variation parameter. This enables an analytical approach to solving the SODE for the slip explicitly to formulate the Modified Tension Chord Model (MTCM), which was derived using the basic principles in solid mechanics.

A replacement of the Tension Chord Model (TCM) with the MTCM in the Cracked Membrane Model (CMM) resulted in the Modified Cracked Membrane Model (MCMM). The MCMM predicts crack widths in RC members subjected to in-plane loading consistently and with a mean for the modelling uncertainty for crack width predictions being fairly close to one but still on the conservative side, regardless of rebar and cover size, member dimension, material parameters and loading condition. A simplified approach was also formulated as an alternative method to the MCMM, in addition to a generalized expression for predicting the tension stiffening normal to a crack to supplement its absence in EC2 and MC2010. The simplified approach was also consistent but more conservative than the MCMM, as expected. Hence, the results in this thesis suggest that both the MCMM and the simplified approach yield consistent and reliable crack width predictions. The thesis offers also complete guidelines for predicting crack widths in large-scale concrete structures subjected to in-plane loading, thus accommodating the main objectives formulated in this PhD study.

7.2 Recommendations for future research

The work in this thesis facilitated a calculation model capable of predicting crack widths in large-scale concrete structures subjected to in-plane loading for SLS design. However, there is still room for improvements and recommendations for future research to compliment the field of interest are

- To investigate the semi-empirical formulas for calculating crack widths recommended by EC2 and MC2010 further to discover their range of applicability. It would be relevant for design purposes to investigate at which rebar and cover dimensions the semi-empirical formulas yield acceptable crack width predictions. This can be done by applying the concept of modelling uncertainty for crack width predictions on more experimental and theoretical data, similar to the approach in Paper I, Empelmann et al. (2016) and Empelmann and Busse (2018). This applies also for the MCMM. Verification against crack patterns in real life structures is also recommended, as well as investigating the scale-effect on the cracking behaviour.
- To investigate the significance of including CLLM for design purposes. The semi-empirical formulas recommended by EC2 and MC2010 was formulated mainly to predict crack widths for the stabilized cracking stage only. However, it was seen in Paper IIa that the crack formation stage could be governing even at relatively large steel stresses in cases with large covers.
- To investigate the effect of rebar spacing experimentally and theoretically to discover a proper value for ζ that can be used in the MTCM, a parameter briefly discussed in Paper III. A proper value for ζ has the potential of further improving the consistency in the model. A theoretical approach could be to conduct nonlinear finite element analysis (NLFEA) using similar assumptions as in Paper IIa. Similar considerations are recommended for the effective concrete area surrounding the rebars in members subjected to bending.
- To investigate how the influence of tensile strength on generating a random crack pattern can be accounted for in the MTCM, as it has a large influence on the cracking behaviour in real life structures.
- To investigate how out-of-plane shear can be included in the MCMM to account for 3D stress states.
- To investigate the application of the MCMM for NLFEA of RC structures. This can be done by formulating a material model based on the framework presented in Paper IV.
- To investigate how the MTCM could be simplified to be used in code-type formulations as an alternative approach to EC2 and MC2010. This can be done by conducting parametric studies of the model. Statistical analysis could also be applied to further investigate how the calculation model itself affects the modelling uncertainty for crack width predictions similar to the approach by Markova and Sykora (2016) and Mlcoch et al. (2017).

- To investigate the application of the MCMM for predicting the cracking behaviour of RC structures subjected to the combination of loads and imposed deformations. This is particularly relevant for design of RC structures that are statically indeterminate.
- To investigate how the MCMM can be applied to predict crack widths in disturbed regions, e.g. in strut and tie approaches.

8 List of notations

A_c	Sectional area
A_p	Area of prestressing steel
$A_{s,b}$	Area of rebars at bottom of section
A_s	Area of rebars
$A_{s,t}$	Area of rebars at top of section
E_c	Young's modulus concrete
E_s	Young's modulus steel
f_{ctm}	Tensile strength of concrete
c	Concrete cover
F	Force in rebar at cracked section
h	Height of section
$h_{c,ef}$	Effective height surrounding rebars in tensile zone
M_x	Moment in x-direction
M_{xy}	Torsional moment
M_y	Moment in y-direction
N_x	Axial force in x-direction
N_y	Axial force in x-direction
$n\phi_s$	Number of rebars
R	Coordinates in radial direction
S_{cr}	Crack spacing for biaxial stress states
S_{cr0}	Maximum crack spacing for uniaxial stress states
S_{crm0}	Mean crack spacing for uniaxial stress states
S_s	Slip over section caused by elastic shear deformations of concrete
S_{tot}	Total slip over section
u	Slip at interface
V_x	Out-of-plane shear force in x-direction
V_{xy}	In-plane shear force
V_y	Out-of-plane shear force in y-direction
x	Coordinates in x-direction
x_c	Height of compressions zone in members subjected to bending

y	Coordinates in y-direction
z	Coordinates in y-direction
w_{cr}	Crack width predicted at the concrete surface
$w_{cr,int}$	Crack width at the inter
w_{lim}	Crack width requirement
w_{mean}	Mean of crack widths measured
ε_1	Maximum principle strains
ε_c	Concrete strains at interface
ε_{c1}	Maximum principle strains in concrete
ε_{cm}	Mean concrete strains at interface
$\varepsilon_{cm,st}$	Mean concrete strains over the section
ε_s	Steel strains at interface
ε_{sm}	Mean steel strains at interface
ϕ_s	Rebar diameter
ρ_{sx}	Reinforcement ratio in x-direction
ρ_{sy}	Reinforcement ratio in y-direction
σ_x	Normal stress in x-direction
σ_y	Normal stress in y-direction
τ	Bond stress at the interface
τ_{bm}	Mean bond stress at the interface
τ_{xy}	Shear stress

9 References

- Balázs, G. (1993). Cracking Analysis Based on Slip and Bond Stresses. *ACI Materials Journal*, 90(4), 340-348.
- Balázs, G., Bisch, P. B., Borosnyói, A., Burdet, O., Burns, C., Ceroni, F., . . . Vráblík, L. (2013). Design for SLS according to fib Model Code 2010. *Structural Concrete*, 14(2), 99-123.
- Barre, F., Bisch, P., Chauvel, D., Cortade, J., Coste, J. F., Dubois, J. P., . . . Toutlemonde, F. (2016). *Control of Cracking in Reinforced Concrete Structures: Research Project CEOS.fr (Civil Engineering and Geomechanics)*. London, UK: ISTE Ltd.
- Base, G. D., Read, J. B., Beeby, A. W., & Taylor, H. J. (1966). *An investigation of the crack control characteristics of various types of bar in reinforced concrete beams, Report 18, Part 1*. London: Cement and Concrete Association.
- Basteskár, M., Engen, M., Kanstad, T., & Fosså, K. (2018). A review of literature and code requirements for the crack width limitations for design of concrete structures in serviceability limit state. *Structural Concrete*, 1-11.
doi:<https://doi.org/10.1002/suco.201800183>
- Bazant, Z., & Oh, B. (1983). Spacing of Cracks in Reinforced Concrete. *Journal of Structural Engineering*, 109(9), 2066-2085.
- Beeby, A. (1978). Cracking: what are crack width limits for? *Concrete: the journal of the Concrete Society*, 31-33.
- Beeby, A. (2004). The influence of the parameter ϕ/ρ_{ef} on crack widths. *Structural Concrete*, 15(3), 317-330.
- Beeby, A., & Scott, R. (2004). Insights into the cracking and tension stiffening behaviour of reinforced concrete tension members revealed by computer modelling. *Magazine of Concrete Research*, 56(3), 179-190.
- Beeby, A., & Scott, R. (2005). Cracking and deformation of axially reinforced members subjected to pure tension. *Magazine of Concrete Research*, 57(10), 611-621.
- Bentz, E. (2000). *Sectional Analysis of Reinforced concrete Members*. Toronto, Canada: PhD-thesis, Department of Civil Engineering, University of Toronto.
- Bentz, E., Vecchio, F., & Collins, M. (2006). Simplified Modified Compression Field Theory for Calculating Shear Strength of Reinforced Concrete Elements. *ACI Structural Journal*, 103(4), 614-624.
- Bernardo, L., Lyrio, A., Silva, J., & Horowitz, B. (2018). Refined Softened Truss Model with Efficient Solution Procedure for Prestressed Concrete Membranes. *Journal of Structural Engineering*, 144(6), 04018045-1-12.
- Berrocal, C. G., Löfgren, I., Lundgren, K., Görander, N., & Halldén, C. (2016). Characterisation of bending cracks in R/FRC using image analysis. *Cement and Concrete Research*, 90, 104-116.
- Borosnyói, A., & Balász, G. (2005). Models for flexural cracking in concrete: the state of the art. *Structural Concrete*, 6(2), 53-62.
- Borosnyói, A., & Snóbli, I. (2010). Crack width variation within the concrete cover of reinforced concrete members. *Építőanyag - Journal of Silicate Based and Composite Materials*, 62(3), 70-74.

- Boschmann Käthler, A., Angst, U., Wagner, M., Larsen, C., & Elsener, B. (2017). *Effect of cracks on chlorideinduced corrosion of steel in concrete - a review*. Norwegian Public Roads Administration reports.
- Braam, C. (1990). *Control of crack width in deep reinforced concrete beams*. Delft, the Netherlands: PhD-thesis, TU Delft.
- Bresler, B., & Bertero, V. (1968). Behavior of Reinforced Concrete Under Repeated Load. *Journal of the Structural Division*, 94(6), 1567-1590.
- Broms, B. (1968). Theory of the calculation of crack width and crack spacing in reinforced concrete members. *Cement och Betong*, 1, 52-64.
- Caldentey, A., Peiretti, H., Iribarren, J., & Soto, A. (2013). Cracking of RC members revisited: influence of cover, ϕ/ρ_s , e_f and stirrup spacing – an experimental and theoretical study. *Structural Concrete*, 14(1), 69-78.
- Castel, A. (2000). *Coupled mechanical/corrosion problem in reinforced concrete members (Couplage mécanique et corrosion dans les éléments de béton armé)*, PhD thesis. Toulouse, France: Paul Sabatier University.
- CEB. (1985). *CEB Design Manual on Cracking and Deformations*. Lausanne, Switzerland: École Polytechnique Fédérale du Lausanne.
- CEN. (2004). *EN 1992-1-1 Eurocode 2: Design of concrete structures - Part 1-1: General rules and rules for buildings*. Brussels, Belgium: European Committee for Standardization.
- Cerioni, R., Michelini, I., & Bernardi, P. (2007). Multi-directional modeling of crack pattern in 2D R/C members. *Engineering Fracture Mechanics*, 75(3-4), 615-628.
- Collins, M., & Mitchell, D. (1997). *Prestressed concrete structures*. New Jersey, USA: Prentice Hall, Inc.
- Dabbagh, H., & Foster, S. (2006). A Smeared - Fixed Crack Model for FE Analysis of RC Membranes Incorporating Aggregate Interlock. *Advances in Structural Engineering*, 9(1), 91-101.
- Debernardi, P., & Taliano, M. (2016). An improvement to Eurocode 2 and fib Model Code 2010 methods for calculating crack width in RC structures. *Structural Concrete*, 17(3), 365-376.
- DIN. (2011). *EN-1992-1-1/NA. 2001-01, National Annex - Nationally determined parameters - Eurocode 2: Design of concrete structures - Part 1-1: General rules and rules for buildings*.
- Dörr, K. (1978). Bond-behaviour of ribbed reinforcement under transversal pressure. *Proceedings of IASS Symposium on Nonlinear Behaviour of Reinforced Concrete Spatial Structures, 1*, Edited by G. Mehlhorn, H. Rühle and W. Zerna. Düsseldorf, Germany: Werner-Verlag.
- Edwards, A., & Picard, A. (1972). Theory of Cracking in Concrete Members. *Proceedings of the ASCE – Journal of the Structural Division*, 98(12), 2687-2700.
- Eligehausen, R., Popov, E., & Bertero, V. (1983). *Local bond stress-slip relationships of deformed bars under generalized excitations*. Berkeley, USA: Report No. UCB/EERC 83-23, University of California.

- Empelmann, M., & Busse, D. (2018). Prediction Accuracy of Code Provisions for the Calculation of Crack Widths. *Proceedings for the 5th fib Congress*. Melbourne, Australia.
- Empelmann, M., Sawicki, P., & Busse, D. (2016). *Comparison of analysis concepts for crack width limitations in accordance with EN 1992-1-1, DIN EN 1992-1-1/NA as well as Model Code 2010. Report Nr. P02-19-1A*. Braunschweig, Germany: iBMB, TU Braunschweig.
- Farra, B., & Jaccoud, J. (1992). Bond behaviour, tension stiffening and crack prediction of high strength concrete. *Proceedings of International Symposium "Bond in Concrete"*. Riga.
- Ferry-Borges, J. (1966). Cracking and Deformability of Reinforced Concrete Beams. *IABSE Publication*, 26, 75-95.
- fib. (2000). *Bond of reinforcement in concrete*. Lausanne, Switzerland: Sprint-Druck Stuttgart.
- fib. (2010). *Structural Concrete - Textbook on behaviour, design and performance* (Second ed., Vol. 2). Lausanne, Switzerland: fib nulletin No. 52.
- fib. (2013). *fib Model code for concrete structures 2010*. Berlin: Ernst & Sohn.
- Foster, S., & Marti, P. (2003). Cracked Membrane Model: Finite Element Implementation. *Journal of Structural Engineering*, 129(9), 1155-1163.
- Gergely, P., & Lutz, L. A. (1968). Maximum crack width in reinforced flexural members. *ACI SP-20, Causes, Mechanism and Control of Cracking in Concrete*, 87-117.
- Giordano, L., & Mancini, G. (2009). Crack Width Evaluation of Reinforced Concrete Membrane Elements. *Structural Engineering International*, 19(3), 256-261.
- Goto, Y. (1971). Crack formed in concrete around deformed tension bars. *ACI Journal*, 68(4), 244-51.
- Haldane, D. (1976). The importance of crackings in reinforced concrete members. *Proceedings of International Conference on The Performance of Building Structures*. Glasgow University.
- Hong, S., & Park, S. (2012). Uniaxial Bond Stress-Slip Relationship of Reinforcing Bars in Concrete. *Advances in Materials Science and Engineering*, 12 pp.
- Hornbostel, K., & Geiker, M. (2017). Influence of cracking on reinforcement corrosion. *Nordic miniseminar on crack width calculation methods for large concrete structures*. Oslo, Norway: Workshop proceedings No. 12 by the Nordic Concrete Federation.
- Hsu, T. (1988). Softened Truss Model Theory for Shear and Torsion. *ACI Structural Journal*, 85(6), 624-635.
- Hsu, T., & Mo, Y. (2010). *Unified theory of concrete structures*. Chichester, UK: Wiley.
- Husain, S., & Ferguson, P. (1968). *Flexural Crack Width at the Bars in Reinforced Concrete Beams*. Austin, TX, USA: The University of Texas at Austin, Research Report Number 102-1F.
- Janovic, K., & Kupfer, H. (1986). Zur Rissbildung im Stahlbeton- und Spannbetonbau. *Betonwerk und Fertigteil-Technik*, 12, 161-169.
- Jiang, D., Shah, S., & Andonian, A. (1984). Study of the Transfer of Tensile Forces by Bond. *ACI Journal*, 81(3), 251-259.

- Kaar, P., & Hognestad, E. (1965, January). High strength bars as concrete reinforcement. *Journal of Portland Cement Association*, 42-53.
- Kaklauskas, G. (2017). Crack Model for RC Members Based on Compatibility of Stress-Transfer and Mean-Strain Approaches. *Journal of Structural Engineering*, 143(9), 04017105-1-12.
- Kaufmann, W. (1998). *Strength and Deformations of Structural Concrete Subjected to In-Plane Shear and Normal Forces*. Zürich, Switzerland: PhD-thesis, Institute of Structural Engineering, Swiss Federal Institute of Technology.
- Kaufmann, W., & Marti, P. (1998). Structural Concrete: Cracked Membrane Model. *Journal of Structural Engineering*, 124(12), 1467-1475.
- Khalfallah, S. (2006). Cracking analysis of reinforced concrete tensioned members. *Structural Concrete*, 7(3), 111-116.
- Khalifa, J. (1986). *Limit Analysis and Design of Reinforced Concrete Shell Elements*. Toronto, Canada: PhD-thesis, Department of Civil Engineering, University of Toronto.
- Kirschner, U., & Collins, M. (1986). *Investigating the Behaviour of Reinforced Concrete Shell Elements*. Toronto, Canada: University of Toronto, Department of Civil Engineering, Publication No. 86-09.
- Laskar, A., Wang, J., Hsu, T., & Mo, Y. (2007). *Rational Shear Provisions for AASHTO LRFD Specifications: Technical Report. Report No. FHWA/TX-07/0-4759-1*. Houston, Texas, USA: Department of Civil & Environmental Engineering, Cullen College of Engineering, University of Houston.
- Leonhardt, F. (1988, Jul-Aug). Cracks and Crack Control in Concrete Structures. *PCI Journal*, 124-145.
- Markova, J., & Sykora, M. (2016). Uncertainties in crack width verification of reinforced concrete structures. *Risk, Reliability and Safety: Innovating Theory and Practice*. doi:10.1201/9781315374987-368
- Marti, P., & Meyboom, J. (1992). Response of Prestressed Concrete Elements to In-Plane Shear Forces. *ACI Structural Journal*, 89(5), 503-514.
- Marti, P., Alvarez, M., Kaufmann, W., & Sigrist, V. (1998). Tension Chord Model for Structural Concrete. *Structural Engineering International*, 8(4), 287-298.
- Martin, H. (1973). On the interrelation among surface roughness, bond and bar stiffness in the reinforcement subject to short-term loading (in German). *Deutscher Ausschuss Stahlbeton*(228), 1-50.
- Mirza, S., & Houde, J. (1979). Study of bond stress-slip relationships in reinforced concrete. *ACI Journal*, 76(1), 19-46.
- Mlcoch, M., Markova, M., & Sykora, M. (2017). Uncertainty in crack width estimates according to fib Model Code 2010. *Civil Engineering Series*, 17(1), 155-158.
- Muhamad, R., Mohamed Ali, M., Oehlers, A., & Sheikh, H. (2011). Load-slip relationships of tension reinforcement in reinforced concrete members. *Engineering Structures*, 33(4), 1098-1106.
- Nilson, A. (1968). Nonlinear analysis of reinforced concrete by the finite element method. *ACI Journal*, 65(9), 757-766.

- Noakowski, P. (1985). Verbundorientierte, kontinuierliche Theorie zur Ermittlung der Rissbreite. *Beton- und Stahlbetonbau*, 7, 185–190.
- NPRA. (2015). *N400 Bruvrosjektering: Prosjektering av bruer, ferjekaier og andre bærende konstruksjoner*. Statens vegvesens håndbokserie: Vegdirektoratet.
- Oh, B., & Kang, Y. (1987). New Formulas for Maximum Crack Width and Crack Spacing in Reinforced Concrete Flexural Members. *ACI Structural Journal*, 85(2), 103-112.
- Pang, X., & Hsu, T. (1995). Behavior of reinforced concrete membrane elements in shear. *ACI Structural Journal*, 92(6), 665-679.
- Pease, B. (2011). *Influence of concrete cracking on ingress and reinforcement corrosion*. Lyngby, Denmark: PhD-thesis, Section for Construction Materials, Department of Civil Engineering, Technical University of Denmark.
- Pedziwiatr, J. (2008). Influence of internal cracks on bond in cracked concrete structures. *ARCHIVES OF CIVIL AND MECHANICAL ENGINEERING*, 8(3), 91-105.
- Pimentel, M., Brühwiler, E., & Figueiras, J. (2010). Extended cracked membrane model for the analysis of RC panels. *Engineering Structures*, 32(8), 1964-1975.
- Rehm, G. (1961). On the fundamentals of steel-concrete bond (in German). *Deutscher Ausschuss für Stahlbeton*(138), 59 pp.
- Rizkalla, S. H., & Hwang, L. S. (1984). Crack prediction for members in uniaxial tension. *ACI Journal*, 82(6), 572-579.
- Russo, G., & Romano, F. (1992). Cracking Response of RC Members Subjected to Uniaxial Tension. *Journal of Structural Engineering*, 118(5), 1172-1190.
- Saliger, R. (1936). High-grade steel in reinforced concrete. *Proceedings of the 2nd Congress of the International Association for Bridge and Structural Engineering, Berlin-Munich, Germany* (pp. 293-315). Switzerland: ETH Zürich.
- Schiessl, P., & Wölfel, E. (1986). Konstruktionsregeln zur Beschränkung der Rissbreite. *Beton- und Stahlbetonbau*, 8-15.
- Scott, R., & Gill, P. (1987). Short-term distributions of strain and bond stress along tension reinforcement. *The Structural Engineer*, 65B(2), 39-48.
- Seelhofer, H. (2009). *Ebener Spannungszustand im Betonbau Grundlagen und Anwendungen*. Zürich, Switzerland: PhD-thesis, Institute for Structural Engineering, Swiss Federal Institute of Technology.
- Somayaji, S., & Shah, S. P. (1981). Bond stress versus slip relationship and cracking response of tension members. *ACI Journal*, 78(3), 217–225.
- Tammo, K., & Thelandersson, S. (2009). Crack behavior near reinforcing bars in concrete structures. *ACI Structural Journal*, 106(3), 259-267.
- Tammo, K., Lundgren, K., & Thelandersson, S. (2009). Nonlinear analysis of crack widths in reinforced concrete. *Magazine of Concrete Research*, 61(1), 23-34.
- Vecchio, F., & Collins, M. (1982). *The response of reinforced concrete to in-plane shear and normal stresses*. Toronto, Canada: Department of Civil Engineering, University of Toronto.
- Vecchio, F., & Collins, M. (1986). The Modified Compression-Field Theory for Reinforced Concrete Elements Subjected to Shear. *ACI Structural Journal*, 83(2), 219-231.
- Vidal, T., Castel, A., & François, R. (2004). Analyzing crack width to predict corrosion in reinforced concrete. *Cement and Concrete Research*, 34(1), 165-174.

- Watstein, D., & Mathey, R. (1959). Width of cracks in concrete at the surface of reinforcing steel evaluated by means of tensile bond specimens. *ACI Journal*, 56(7), 47-56.
- Yannopoulos, P. (1989). Variation of concrete crack widths through the concrete cover to reinforcement. *Magazine of Concrete Research*, 41(147), 63-68.

Part II – Appended papers

Paper I

Experimental and theoretical investigation of crack width calculation
methods for RC ties

Tan, R., Eileraas, K., Opkvitne, O., Žirgulis, G., Hendriks, M.A.N., Geiker, M., Brekke, D.E.
& Kanstad, T.

Structural Concrete, 2018, 19(5), 1436-1447

TECHNICAL PAPER

Experimental and theoretical investigation of crack width calculation methods for RC ties

Reignard Tan¹  | Kristoffer Eileraas¹ | Ola Opkvitne¹ | Giedrius Žirgulis¹ | Max A. N. Hendriks^{1,2} | Mette Geiker¹ | Dan-Evert Brekke³ | Terje Kanstad¹

¹Department of Structural Engineering, NTNU, Norwegian University of Science and Technology, Trondheim, Norway

²Faculty of Civil Engineering and Geosciences, Delft University of Technology, Delft, The Netherlands

³Multiconsult ASA, Oslo, Norway

Correspondence

Reignard Tan, Multiconsult ASA, att. Reignard Tan, Postboks 265 Skøyen, 0213 Oslo, Norway.
Email: reignard.tan@multiconsult.no

This paper theoretically and experimentally investigates the semi-empirical formulas recommended by Eurocode 2 (EC2), *fib* Model Code 2010 (MC2010), and Eurocode 2 with the German National Annex (DIN) for calculating crack widths in reinforced concrete. It is shown that the formulas can be derived from the principles for the idealized behavior of RC ties. However, instead of explicitly solving the resulting differential equations, the use of simplifications leads to inconsistent formulas. An experimental study was carried out involving the testing of eight RC ties to discover the modeling uncertainty of the formulas. It was found that EC2 substantially overestimated the crack widths for the RC ties. MC2010 and DIN seemed to predict the crack widths better, but gave rather a large number of non-conservative crack width predictions. These experimental results, combined with the theoretical study, suggest that a more consistent calculation model should be formulated by explicitly solving the resulting differential equation.

KEYWORDS

calculation methods, cover, crack widths, experiments, large-scale concrete structures, modeling uncertainty, RC ties, semi-empirical formulas, tension stiffening

1 | INTRODUCTION

There are several methods for calculating crack widths, and a comprehensive summary of them is provided in Borosnyói and Balász.¹ This study focuses on the semi-empirical formulas for calculating crack widths in cases with relatively large bar diameters and covers, recommended by Eurocode 2 (EC2),² *fib* Model Code (MC2010),³ and Eurocode 2 with the German National Annex (DIN).⁴

This study is a part of an ongoing research project with the overall objective of improving crack width calculation methods for large-scale concrete structures, that is, for large cross sections and thick concrete members. New revisions of EC2 and MC2010 are also currently under way, and this study seeks to contribute by enhancing the crack width

calculation methods currently recommended by these codes. The main reason for including DIN in this study is that, unlike EC2 and MC2010, it excludes the cover term in calculating crack distance. The significance of the cover term has been the subject of major discussion in the development of the semi-empirical formulas. Some investigators argue that it should be abandoned,⁵ while others claim that it should be dominant.^{6–8}

The aim of this study is to investigate how well the formulas comply with the behavior of RC ties, from both a theoretical and an experimental point of view. First, the idealized behavior of RC ties is discussed, after which the background theory and the main assumptions used when deriving the semi-empirical formulas is revisited. Then, an experimental study of some relatively large RC ties is presented, which are assumed to be representative of the tensile zones of large cross sections exposed to bending. Finally,

Discussion on this paper must be submitted within two months of the print publication. The discussion will then be published in print, along with the authors' closure, if any, approximately nine months after the print publication.

the modeling uncertainty and the theoretical background of the semi-empirical formulas is assessed and investigated.

2 | THE THEORETICAL BACKGROUND FOR CRACK WIDTH CALCULATIONS OF RC TIES

2.1 | The idealized behavior of RC ties

For simplicity, the idealized behavior of RC ties is discussed in terms of axisymmetry and using the concept of *slip* as in *fib* bulletin No. 10.⁹

2.1.1 | General

Figure 1 depicts an axisymmetric plane in a RC tie exposed to a tensile force in the steel reinforcement bar ends. The steel bar is shown elongated more than the embedding concrete, and the relative displacement between the materials at an arbitrary section over the transfer length, L_t , is considered the slip. The slip consists of two contributions: the relative displacement at the interface between concrete and steel, s_i , and the elastic shear deformation in the concrete section, s_s (see Section 1 in Figure 1). The sum of the two contributions is the total slip, s_{tot} . The slip at the interface between concrete and steel is normally caused by the nonlinear behavior of the bond due to chemical adhesion and the formation of internal and splitting cracks.^{10–13} The slip caused by elastic shear deformation is a consequence of the force applied at the steel bar end being transmitted to the embedding concrete.^{14,15}

The slip can be conceptually visualized by considering the three different sections in Figure 1. Both contributions to the total slip are present at Section 1 ($s_{tot} = s_s + s_i$). At Section 2, however, the contribution to the total slip is solely due to the elastic shear deformation ($s_{tot} = s_s$). There is no slip at Section 3 implying that any deformation in the concrete and steel is fully compatible, that is, there is no relative displacement between the materials. This section also marks the end of the transfer length, L_t .

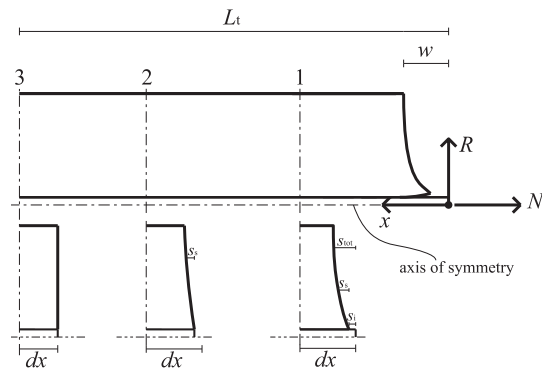


FIGURE 1 Idealized behavior of RC ties and the definition of slip

2.1.2 | Analytical static model

Treating every aspect of the nonlinear behaviour of bond can be rather complicated in an analytical static model, and simplifications are needed. One possible simplification is conceptually shown in Figure 2 by assuming that the sections are statically equivalent. Briefly summarized, the simplification involves treating concrete and steel as elastic materials and lumping all the nonlinearity to the interface between concrete and steel by applying a proper bond-slip law. Several authors in the literature^{5,16–18} have acknowledged this analytical static approach.

2.1.3 | Equilibrium and compatibility

The equilibrium and the compatibility of an arbitrary section over the transfer length can now be formulated in accordance with the static model in Figure 2c. This means that the equilibrium relationships for concrete and steel can respectively be obtained as:

$$\int_{A_c} d\sigma_c dA_c = \tau(s_i) \pi \phi dx, \quad (1)$$

and

$$d\sigma_s A_s = -\tau(s_i) \pi \phi dx. \quad (2)$$

Note that an integral is generally necessary in Equation (1) since a certain strain distribution in the concrete section is assumed to occur due to the presence of elastic shear deformation. The strain distribution in the steel section is assumed constant. Furthermore, the relative displacement at the interface between concrete and steel in Figure 2c leads to the following compatibility equation for the derivative of the slip:

$$s_i'(x) = \frac{ds_i}{dx} = \varepsilon_{si} - \varepsilon_{ci}. \quad (3)$$

2.1.4 | The slip

Using Equations (1), (2) and (3), and assuming that Hooke's law of elasticity applies for concrete and steel, that Poisson's

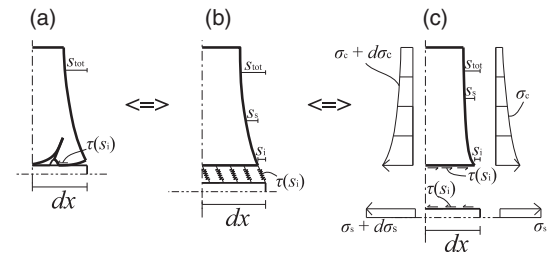


FIGURE 2 Statically equivalent sections: (a) "True" behavior of bond nonlinearity caused by loss of adhesion and formation of internal and splitting cracks; (b) Bond nonlinearity lumped as spring behavior to the interface between concrete and steel; (c) Simplified static model assuming that the bond nonlinearity in the spring can be modeled with a proper bond-slip law

ratio can be neglected, and that the strain distribution over the concrete section does not vary over the transfer length leads to the following second order ordinary differential equation for the slip:

$$\frac{d^2 s_i}{dx^2} - \chi \tau(s_i) = 0. \quad (4)$$

where χ is a constant governing the stiffness relationship between the concrete and steel. To solve Equation (4), the following boundary conditions can be applied in the *crack formation stage* and the *stabilized cracking stage* respectively:

$$s_i(L_t) = 0, \quad (5a)$$

$$s_i'(L_t) = 0, \quad (5b)$$

and

$$s_i(L_t) = 0, \quad (6a)$$

$$s_i'(L_t) > 0. \quad (6b)$$

The crack width, crack distance, longitudinal stress, and strain distribution for the materials can now be obtained by explicitly solving Equation (4), provided that a proper bond-slip law is applied and that a certain strain distribution over the concrete section is assumed beforehand.

2.2 | Semi-empirical formulation

The semi-empirical formulas recommended by EC2, MC2010, and DIN for calculating the crack width can be derived by using the same principles as in the idealized behavior of RC ties previously discussed. However, it will be shown that simplifications are used instead of explicitly solving Equation (4) to obtain expressions for the crack width, crack distance, longitudinal stress, and strain distribution of the concrete and steel.

2.2.1 | The characteristic crack width

By considering the cracked segment of a RC tie in the stabilized cracking stage (see Figure 3), the following compatibility equation can be easily derived:

$$w_k = S_{r,\max} (\epsilon_{sm} - \epsilon_{cm}) = 2L_{t,\max} (\epsilon_{sm} - \epsilon_{cm}), \quad (7)$$

where w_k is the characteristic crack width, and $(\epsilon_{sm} - \epsilon_{cm})$ is the difference in longitudinal steel and concrete mean strains over the maximum crack distance, $S_{r,\max}$, which is defined as twice the maximum transfer length, $L_{t,\max}$.

2.2.2 | Transfer length

The transfer length was originally formulated using the so-called *slip theory* and the *no-slip theory*.¹⁵ In the slip theory, a slip in the interface between concrete and steel is assumed to occur due to bond failure.¹⁹ This means solving Equation (1) under the assumption that the bond-slip function is constant (i.e., $\tau(s_i) = \tau_{bms}$), that plane sections remain plane, and that the concrete stresses at the end of the transfer length do not exceed the mean tensile strength of concrete f_{ctm} in the stabilized cracking stage, which leads to the following equation for the transfer length:

$$L_{tr} = \frac{1}{4} \frac{f_{ctm} \phi}{\tau_{bms} \rho_s}, \quad (8)$$

where $\rho_s = A_s/A_{c,ef}$ is the reinforcement ratio of the RC tie.

In contrast, the no-slip theory assumes that slip does not occur in the interface between the concrete and steel.²⁰ This means that any slip is solely due to the presence of elastic shear deformation in the concrete section, which reduces the concrete surface stresses and implies that plane sections do not remain plane as in Section 2 in Figure 1. However, no mathematical relationships can be derived and a “traditional engineering rule” is applied instead, with the claim that the transfer length is proportional to the size of the cover c as in:

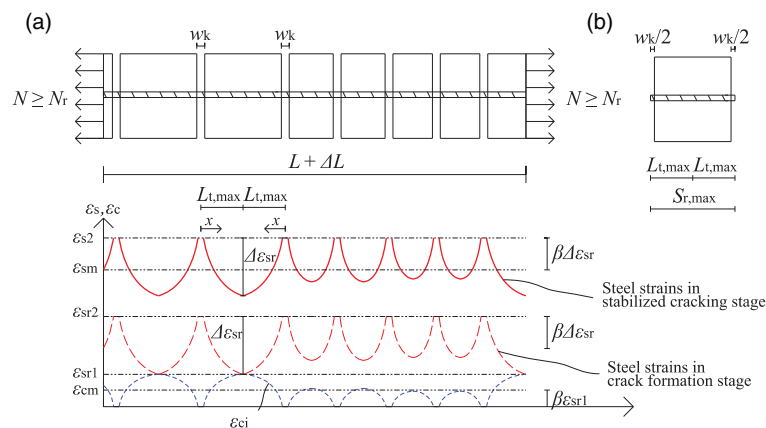


FIGURE 3 Cracked RC tie: (a) Strain distribution in a fully cracked RC Tie; (b) Cracked segment in an RC tie

$$L_{t\alpha} = k_{\alpha}c, \quad (9)$$

where the constant k_{α} is empirically determined.

In principle, either theory can be used to calculate the transfer length. However, both theories represent the reported behavior of RC ties in the literature only to a certain extent.^{21–26} This resulted in the pragmatic merger of the theories to form the following equation for the maximum transfer length at the time it was formulated¹⁴:

$$L_{t, \max} = L_{t\alpha} + L_{t\tau} = k_{\alpha}c + \frac{1}{4} \frac{f_{ctm} \phi}{\tau_{bms} \rho_s}. \quad (10)$$

It can be shown that EC2 and MC2010 have adopted this combined concept, however, altering the perception of the contribution related to the no-slip theory. This term seems rather related to the fact that the internal cracks become smaller and eventually close as the distance increases from the steel bar in cases of large covers instead of the elastic shear deformations, which normally are considered negligible.²⁷ DIN, however, has abandoned the cover term and calculates the maximum transfer length according to Equation (8), though not exceeding $L_{t\tau} = \frac{1}{41.8} \frac{\sigma_s \phi}{f_{ctm}}$, which accounts for the fact that the transfer length varies in the crack formation stage as stated by.^{5,17,18}

2.2.3 | Mean strains

The mean strains can be derived by assuming a certain longitudinal strain distribution for the concrete and steel in the RC tie in Figure 3a. Assuming that the mean strains for concrete and steel can be expressed by the same integration constant β yields the following mean strain expressions for steel and concrete respectively:

$$\varepsilon_{sm} = \varepsilon_{s2} - \beta \Delta \varepsilon_{sr}, \quad (11)$$

and

$$\varepsilon_{cm} = \beta \varepsilon_{sr1}. \quad (12)$$

Using that $\Delta \varepsilon_{sr} = \varepsilon_{sr2} - \varepsilon_{sr1}$ and subtracting (12) from (11) yields the following expression for the difference in mean strains:

$$\varepsilon_{sm} - \varepsilon_{cm} = \varepsilon_{s2} - \beta \varepsilon_{sr2}, \quad (13)$$

where $\varepsilon_{s2} = \sigma_s/E_s$ are the steel strains in a crack in the stabilized cracking stage, $\varepsilon_{sr2} = \sigma_{sr}/E_s$ are the steel strains right after a crack has formed in the crack formation stage, and $\varepsilon_{sr1} = f_{ctm}/E_c$ are the concrete strains across the section at cracking. The steel stresses right after a crack has formed can be expressed as $\sigma_{sr} = \frac{f_{ctm}}{\rho_s} (1 + \alpha_c \rho_s)$ when considering the behavior of a RC tie in the crack formation stage, where $\alpha_c = E_s/E_c$. Inserting these relationships in Equation (13) finally yields the expression for the difference in mean strains in the stabilized cracking stage as:

$$\varepsilon_{sm} - \varepsilon_{cm} = \frac{\sigma_s - \beta \frac{f_{ctm}}{\rho_s} (1 + \alpha_c \rho_s)}{E_s}. \quad (14)$$

A similar expression can be derived in the crack formation stage by considering the steel strain distribution for this cracking stage in Figure 3a. The mean steel strains can then be expressed as: $\varepsilon_{sm} = \varepsilon_{sr2} - \beta \Delta \varepsilon_{sr}$. Using the same procedure as above yields the following expression for the difference in mean strains in the crack formation stage:

$$\varepsilon_{sm} - \varepsilon_{cm} = \frac{\sigma_{sr}}{E_s} (1 - \beta). \quad (15)$$

EC2, MC2010 and DIN have all adopted Equation (14) for the stabilized cracking stage. In the crack formation stage, however, only MC2010 uses Equation (15), while EC2 and DIN use the following expression instead:

$$\varepsilon_{sm} - \varepsilon_{cm} = 0.6 \frac{\sigma_s}{E_s}. \quad (16)$$

Hence, Equations (15) and (16) yields the lower boundary for the difference in mean strains.

3 | EXPERIMENTAL STUDY

3.1 | Geometry, material properties, and test set-up

The behavior of four square cross sections (400 × 400 mm), reinforced with eight deformed steel bars, was experimentally investigated. The bar diameter was either 20 or 32 mm, while the cover was either 40 or 90 mm (see Figure 4). The RC ties were pulled in tension and had a total length of 3 m, of which 2 m were assumed to be representative for the crack pattern due to the anchorage zones at each end. See Figure 5 for the test set-up.

The concrete quality was B45 MF40, which is a Norwegian concrete typically used for bridges with a water-to-cement ratio of 0.4. The cement type was Norcem Standard FA Cement and conforms to the requirements of CEM II/B-M 42,5R according to NS-EN 197-1:2011.²⁸ The specimens were cured under wet conditions to avoid drying shrinkage. Table 1 shows the compressive strength, tensile strength, and Young's modulus after 28 days. The reinforcement quality was B500NC according to NS 3576²⁹ with a yield strength of 500 MPa and Young's modulus 200,000 MPa. The threaded rods used in the anchorage zone had a steel quality denoted as 8.8, that is, with a yield limit of 640 MPa and an ultimate strength of 800 MPa.

An additional set of four parallel RC ties were cast, giving a total of eight RC ties to be investigated in the experimental study. Two identical RC ties were loaded to different loading regimes corresponding to either the crack formation or the stabilized cracking stage. The objective was to study the internal crack pattern at the two load levels by injecting

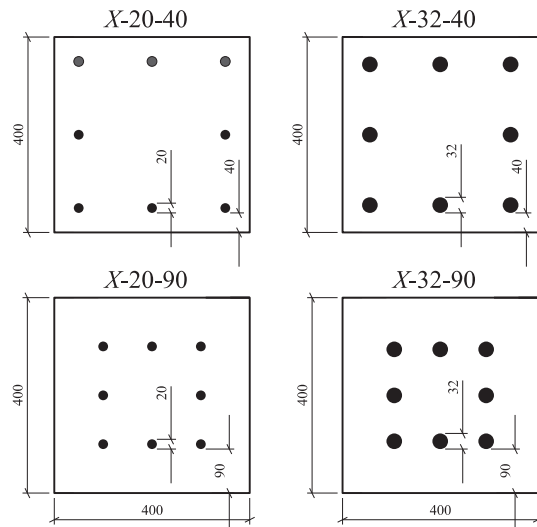


FIGURE 4 Cross sections of RC ties

epoxy resin in the cracks. These results will be documented in a subsequent paper, while this paper mainly focuses on the surface cracks. The RC ties were named $X-\phi-c$, where X represents the loading regime either as the crack formation

(F) or stabilized cracking stage (S), ϕ represents the steel bar diameter and c represents the cover (see Table 2 and Figure 4).

The tensile force from the loading rig was transferred to the RC tie by mounting a 30 mm thick steel plate with welded ribs onto four M36 rods that were embedded in the anchorage zone at each end (see Figure 5b). The anchorage of the steel rods inside the specimen was strengthened with steel nuts, while stirrups, additional longitudinal reinforcement, and externally prestressed steel frames were mounted to prevent anchorage failure. The load was applied in a deformation-controlled procedure with a velocity of 0.2–0.4 mm/min. Strain gauges were utilized to monitor eccentricities caused by the self-weight of the RC ties or geometric deviations before cracking. The strain measurements showed that these effects were small, which was confirmed by the fact that cracks were usually observed to form instantaneously through the whole section.

3.2 | Measuring technique using image analysis

The development of surface cracks was documented using a digital single-lens reflex (DSLR) camera with a 50 mm $f/2.5$ macro lens mounted to a tripod system (see Figure 6a,b). Each crack formed was measured section-wise over a length of

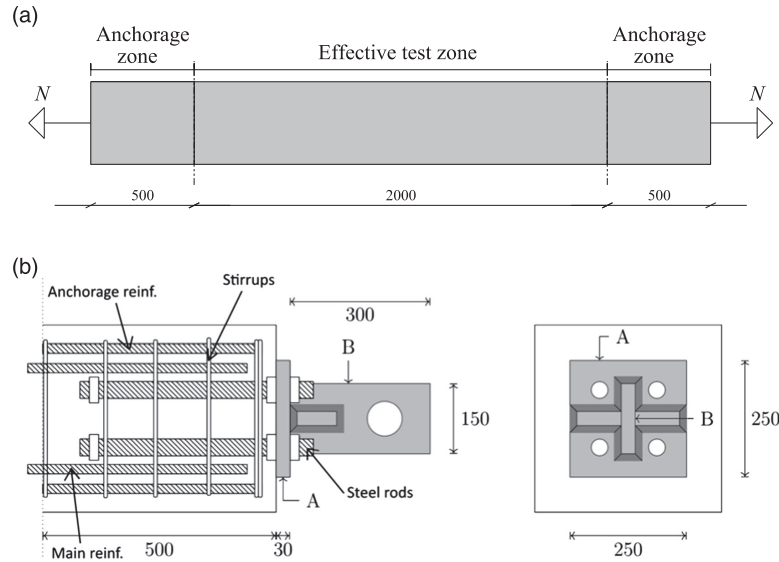


FIGURE 5 Test set-up: (a) Test set-up for RC ties; (b) Anchorage zone details

TABLE 1 Material properties of concrete at 28 days

Specimen	Date of test	Measured f_c [MPa]	Mean f_c [MPa]	Measured f_{ct} [MPa]	Mean f_{ct} [MPa]	Measured E_c [GPa]	Mean E_c [GPa]
1	March 03, 2017	74.1		3.98		27.3	
2	March 03, 2017	73.2	74.3	4.03	4.14	27.2	27.4
3	March 03, 2017	75.5		4.41		27.6	

TABLE 2 Statistical properties showing the number of total measured crack widths n_{tot} , the mean \bar{y}_{tot} and the variance s_{tot} in a member. $s_{tot,w}^2/s_{tot}^2$ indicates the contribution of the within-cracks variation to the total variance, while $w_{0.50}$ and $w_{0.95}$, respectively, shows the median and 95%-fractile. These values are obtained by assuming that the crack widths are log-normally distributed

Member	P [kN]	σ_s [MPa]	n_{tot}	\bar{y}_{tot}	s_{tot}	$s_{tot,w}^2/s_{tot}^2$	$w_{0.50}$ [mm]	$w_{0.95}$ [mm]
F-20-40	503	200	42	-2.53	0.31	0.77	0.08	0.13
S-20-40	520	207	6	-2.27	0.11	1.00	0.10	0.13
	667	265	6	-2.07	0.12	1.00	0.13	0.16
	808	321	68	-2.05	0.32	0.61	0.13	0.22
F-32-40	753	117	51	-2.90	0.22	0.71	0.06	0.08
S-32-40	743	115	30	-3.15	0.27	0.65	0.04	0.07
	1,012	157	50	-2.91	0.34	0.84	0.05	0.10
F-20-90	585	233	30	-1.93	0.21	0.74	0.15	0.21
S-20-90	574	228	42	-1.99	0.26	0.60	0.14	0.21
	736	293	42	-1.64	0.27	0.50	0.19	0.31
	1,003	399	54	-1.44	0.31	0.36	0.24	0.40
F-32-90	804	125	41	-2.47	0.37	0.68	0.08	0.16
S-32-90	805	125	36	-2.36	0.34	0.44	0.09	0.17
	1,004	156	47	-2.27	0.42	0.27	0.10	0.21
	1,201	187	47	-2.11	0.40	0.31	0.12	0.24
	1,363	212	45	-1.91	0.34	0.35	0.15	0.27

40 mm to the level of the reinforcement (see Figure 6c,d,e). This is in agreement with the recommendations in MC2010, that is, that the crack width measured at the elevation of the reinforcement is comparable to the characteristic crack width. Each section measured was afterwards processed and analyzed in the open source program Fiji (ImageJ) (2012).³⁰ The average crack width for each section measured was then obtained by applying a user-supplied subroutine to the program. Only the crack widths along the vertical faces were documented due to the time consuming measuring technique. This resulted in up to six section average crack width measurements for each crack formed (see Figure 6d).

One of the main advantages of using this imaging technique is that the inhomogeneous propagation of formed cracks could be properly accounted for, for example, cracks do not form in a straight line and crack widths vary over the concrete surface (see Figure 6e).

3.3 | Statistical analysis for determining crack widths and modeling uncertainty

The crack widths that are of primary interest from the experimental study and that are comparable to the characteristic crack width, w_k , are the 95%-fractile of the crack widths measured, $w_{0.95}$, for each RC tie. To obtain this value, the statistical method of Engen et al.³¹ was used to account for the uncertainty related to the limited number of section average crack width measurements for each formed crack. Generally, the mean and the variance of the crack width for a formed crack i with n_i section average crack width measurements can be estimated as:

$$\bar{y}_i = \frac{1}{n_i} \sum_{j=1}^{n_i} y_{i,j} \quad (17)$$

and

$$S_i^2 = \frac{1}{n_i - 1} \sum_{j=1}^{n_i} (y_{i,j} - \bar{y}_i)^2, \quad (18)$$

where $y_{i,j}$ is the j th section average crack width measurement of crack i . See Figure 6c,d for practical examples of the indexing. Furthermore, it can be shown that the mean and the variance of a group with m formed cracks in a RC tie can be respectively estimated as:

$$\bar{y}_{tot} = \frac{1}{n_{tot}} \sum_{i=1}^m n_i \bar{y}_i, \quad (19)$$

and

$$S_{tot}^2 = \frac{\sum_{i=1}^m ((n_i - 1) S_i^2)}{n_{tot} - 1} + \frac{\sum_{i=1}^m (n_i \bar{y}_i^2) - n_{tot} \bar{y}_{tot}^2}{n_{tot} - 1} = s_{tot,w}^2 + s_{tot,b}^2, \quad (20)$$

where $n_{tot} = \sum_{i=1}^m n_i$ is the total number of section average crack width measurements in a group with m formed cracks in a RC tie. It should be noted that S_{tot}^2 includes both the variation of the crack width within a formed crack, $s_{tot,w}^2$, and the variation in the crack width between cracks, $s_{tot,b}^2$, in a RC tie. The standard deviation (SD), S_{tot} , and the coefficient of variation, V_{tot} , for a group with m formed cracks can now be obtained based on the mean, \bar{y}_{tot} , and variance, S_{tot}^2 .

Assuming that the crack widths are normally distributed, a future prediction of the 95%-fractile of the crack width in a RC tie can be estimated as:

$$w_{0.95} = \bar{y}_{tot} - t_{\alpha=95\%,v} S_{tot} \sqrt{\frac{d+2}{d+1}}, \quad (21)$$

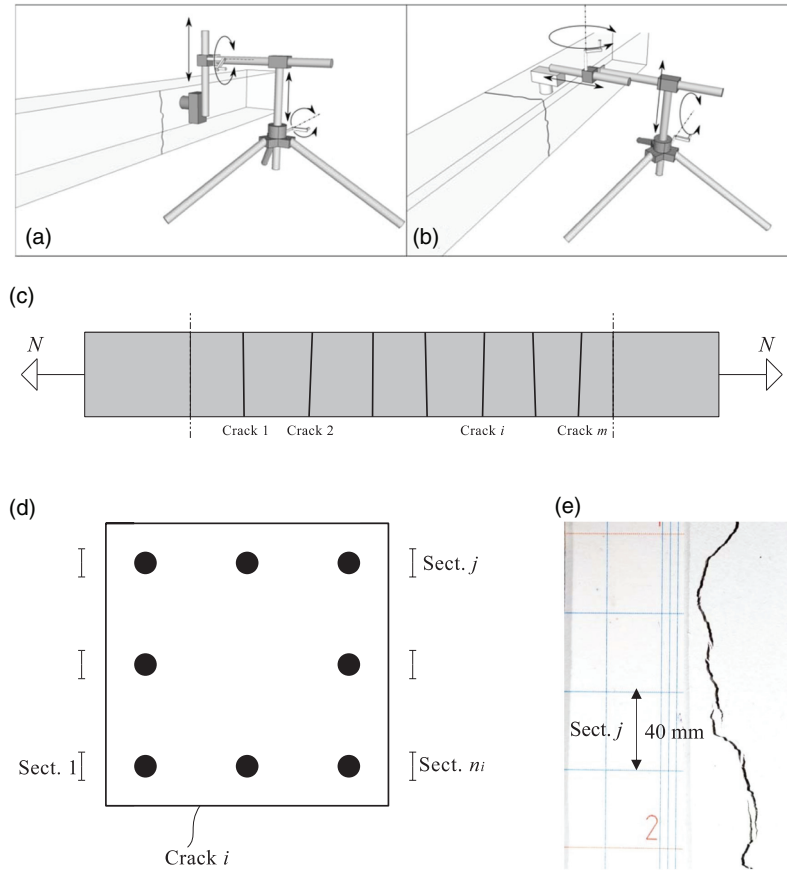


FIGURE 6 Measuring crack widths: (a) Set-up for measuring crack widths with DSLR camera section-wise at vertical faces; (b) Set-up for measuring crack widths with DSLR camera section-wise at top faces; (c) Numbering of the cracks formed; (d) n_j measured section crack widths at the level of the reinforcement for the formed crack i ; (e) Cracks were averaged over a length of 40 mm at section j due to the inhomogeneous propagation of cracks

where $t_{\alpha = 95\%, \nu}$ is the 95%-fractile of the t-distribution with $\nu = n_{tot} - 1$ degrees of freedom. Based on the estimated 95%-fractile of the crack width, $w_{0,95}$, the modeling uncertainty, θ , can now be calculated as:

$$\theta = \frac{w_{0,95}}{w_k} \quad (22)$$

where w_k is the characteristic crack width calculated using the semi-empirical formulas recommended in EC2, MC2010, or DIN. The crack width measured, $w_{0,95}$, can be obtained by assuming both a normal and log-normal distribution of the crack widths. The difference is small and, in the following, only the results assuming log-normally distributed crack widths are presented in accordance with CEB.³² This means that the natural logarithm of the section average crack width measurement is assumed normally distributed, thus replacing $y_{i,j}$ with $\ln y_{i,j}$ in Equations (17) and (18). The modeling uncertainty is assumed to be log-normally distributed in accordance with the suggestions in the JCSS Probabilistic Model Code.³³

4 | EXPERIMENTAL RESULTS

4.1 | The modeling uncertainty

The ratio, $s_{tot,w}^2/s_{tot}^2$, in Table 2 indicates that the contribution of the within-cracks variation to the total variance, S_{tot}^2 , is significant and justifies the use of Equations (17) to (21). The ratio of $s_{tot,w}^2/s_{tot}^2 = 1$ in the first two load steps for S-20-40 can be explained by the fact that only one crack was measured. Furthermore, the relatively low ratio, $s_{tot,w}^2/s_{tot}^2$, in the last load steps for S-20-90 and S-32-90 can be explained by the observed variation in crack distances for these members.

The characteristic and measured crack widths at the respective load steps for the RC ties are given in Table 3. The mean material properties in Table 1 were used in determining the characteristic crack widths. Furthermore, the characteristic crack widths determined in accordance with EC2 and MC2010 were based on using the integration constant $\beta = 0.6$ since the RC ties could be considered to be subject to short-term loading

TABLE 3 Load steps and the corresponding crack widths and cracking stages in each member

Member	Load		Crack width				Cracking stage			
	P [kN]	σ_s [MPa]	w_k , EC2	w_k , MC2010	w_k , DIN	$w_{0.95}$	EC2	MC2010	DIN	Observed
F- ϕ 20-c40	503	200	0.34	0.25	0.16	0.13	F	F	F	F
S- ϕ 20-c40	520	207	0.35	0.25	0.17	0.13	F	F	F	F
	667	265	0.45	0.25	0.28	0.16	F	F	F	S
	808	321	0.55	0.31	0.36	0.22	F	S	S	S
F- ϕ 32-c40	753	117	0.14	0.08	0.08	0.08	F	F	F	F
S- ϕ 32-c40	743	115	0.14	0.08	0.08	0.07	F	F	F	S
	1,012	157	0.19	0.12	0.11	0.10	F	S	S	S
F- ϕ 20-c90	585	233	0.52	0.31	0.22	0.21	F	F	F	F
S- ϕ 20-c90	574	228	0.51	0.31	0.21	0.21	F	F	F	F
	736	293	0.65	0.31	0.31	0.31	F	F	F	S
	1,003	399	0.88	0.59	0.50	0.40	F	S	S	S
F- ϕ 32-c90	804	125	0.22	0.11	0.08	0.16	F	F	F	F
S- ϕ 32-c90	805	125	0.22	0.11	0.08	0.17	F	F	F	F
	1,004	156	0.27	0.15	0.11	0.21	F	S	S	S
	1,201	187	0.32	0.21	0.15	0.24	F	S	S	S
	1,363	212	0.38	0.26	0.18	0.27	S	S	S	S

only, while a factor of $\beta = 0.4$ was used for DIN in accordance with the provisions in this Annex. It was assumed that the effective concrete area was equal to the cross-sectional area, that is, $A_{c, ef} = A_c$. This is reasonable since it was observed that the RC ties usually seemed to crack through the whole section. This assumption was tested by pouring water into the cracks in the top face and observing that it leaked through the whole of the bottom face for RC tie S-32-40, which had the smallest crack widths and a low cover.

The modeling uncertainty for the respective formulas is graphically plotted in Figure 7 and summarized in Table 4, which shows the mean μ_θ , the SD σ_θ , the coefficient of variation V_θ , and the minimum and maximum values for the modeling uncertainty. The number of observations in which the crack widths measured exceed the crack widths calculated is also shown, that is, $n(\theta_s > 1)$. In total, 16 values for the crack widths measured $w_{0.95}$ were obtained from the experiments (see Table 2), which gives 16 observations for the modeling uncertainty. The median $w_{0.5}$ is also given to elucidate the scatter of the measurements.

The results show that EC2 has the lowest SD and coefficient of variation, implying that the scatter of the modeling

uncertainty around the mean is lower than with MC2010 and DIN. However, EC2 consistently predicts crack widths substantially on the conservative side, which is shown by the low mean value and the relatively low maximum value for the modeling uncertainty. In practice, this implies that EC2 consistently predicts crack widths that are on average more than half the size of the largest crack widths measured (95%-fractile) in the RC ties. Nevertheless, all of the predicted crack widths according to EC2 are on the conservative side.

MC2010 and DIN seem to predict the crack widths better in terms of the mean for the modeling uncertainty. However, the relatively high SD and coefficient of variation for both codes yields a larger scatter around the mean than with EC2. This implies that MC2010 and DIN predict the crack widths more inconsistently than EC2 and do so occasionally on the nonconservative side. In fact, MC2010 predicts five and DIN predicts seven crack widths that are on the nonconservative side, which are relatively large numbers compared to the total observations for the modeling uncertainty. This is particularly pronounced for the RC ties with large bar diameters and covers (see Table 3). It should be mentioned though, that the reported modeling uncertainties are representative for this

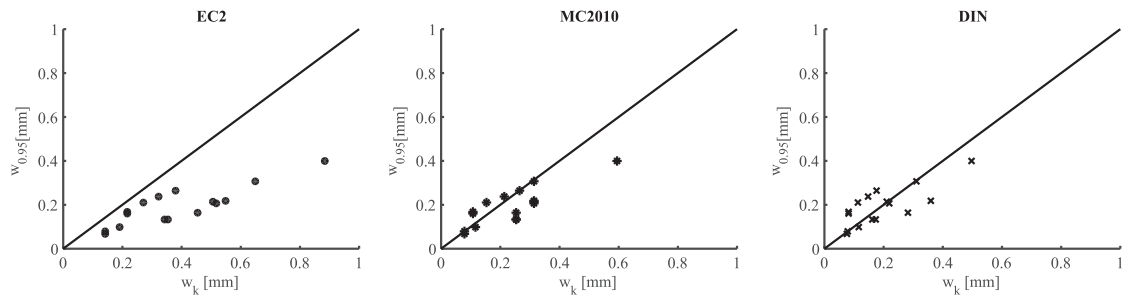


FIGURE 7 The modeling uncertainty for EC2, MC2010 and DIN

TABLE 4 Statistical properties for the modeling uncertainty showing mean μ_θ , SD σ_θ , coefficient of variation V_θ , minimum and maximum observed values and the number of observations where $\theta > 1$

	μ_θ	σ_θ	V_θ	Min	Max	$n(\theta > 1)$
EC2	0.54	0.17	0.32	0.36	0.78	0
MC2010	0.93	0.38	0.40	0.52	1.58	5
DIN	1.17	0.55	0.47	0.58	2.03	7

experimental series and are not intended to serve as a generalization for the performance of the formulas.

4.2 | Crack distances

Table 5 shows the maximum calculated crack distance and the maximum measured crack distances for the RC ties in the stabilized cracking stage, which should be comparable according to the discussions in Section 2.2.2 above. The mean values are also shown. The table shows that EC2 and MC2010 predict the maximum crack distances on the conservative side in all cases, while DIN underestimates the maximum measurements for S-32-40 and S-32-90. The table also elucidates that the maximum crack distances are more influenced by the cover than the bar diameter. The measured values show that the maximum crack distance increases with increasing cover for a constant reinforcement ratio. This seems to comply with the formulas recommended by EC2 and MC2010, which acknowledge the significance of the cover in calculating the maximum crack distance. However, the increase in the maximum crack distance due to the influence of the cover seems to be dramatically overestimated in EC2, which can be seen from the contribution of the no-slip term, $2L_{\alpha}$, to the maximum crack distance. MC2010 appears to predict the increase better. Nevertheless, DIN actually gives the best overall agreement with the measured maximum crack distances.

5 | DISCUSSION

5.1 | Semi-empirical formulas in theory

The composed transfer length in Equation (10) is conceptually visualized in Figure 8 in accordance to the origin of the formula, which shows that plane sections remain plane and that a slip in the interface between concrete and steel occurs at Section 1 as assumed in the slip theory. Compatibility in deformation is restored on the right-hand side of Section 2, which also marks the end of the transfer length according to

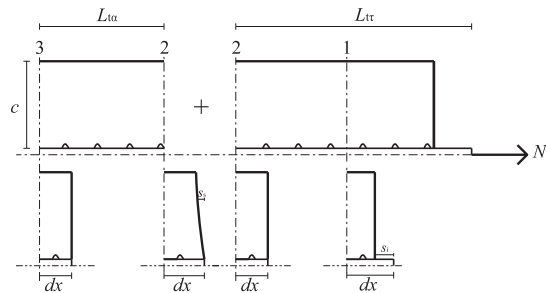


FIGURE 8 Composed transfer length formulas conceptually visualized

the slip theory. The addition of the transfer length according to the no-slip theory implies a sudden incompatibility in deformation on the left-hand side of Section 2, which means that plane sections no longer remain plane due to the presence of elastic shear deformation. Compatibility is restored at Section 3, which marks the end of the transfer length according to the no-slip theory as well as the end of the composed transfer length. In other words, the combined concept implies that compatibility and incompatibility in deformation both occur at the same time at Section 2, and that compatibility in deformation occurs twice within the same composed transfer length, at Sections 2 and 3. Although the cover term in the transfer length formula recommended by EC2 and MC2010 has a different physical meaning than originally formulated, does not change the fact that the current formulation is in conflict with the basic principles of solid mechanics and violates the equilibrium for the concrete section in Equation (1). Moreover, a merging of the slip and the no-slip theory, two theories based on exactly opposite assumptions, can be considered inconsistent, ambivalent and controversial from a statics point of view.

5.2 | Semi-empirical formulas in practice

An important physical factor is how well the semi-empirical formulas according to EC2, MC2010 and DIN capture the cracking behavior in the crack formation stage and the stabilized cracking stage. This can be monitored by using Equations (14), (15) and (16) to indicate the cracking state of the RC ties at the current load level and then comparing it to the observed experimental behavior (see Table 3). This shows that EC2 assumes that the RC ties are in the crack formation stage

TABLE 5 Crack distances. L_{α} and L_{τ} , respectively, indicates the contribution from the no-slip and the slip theory to the maximum transfer length $L_{t, \max}$, where the calculated maximum crack distance is given as $S_{r, \max} = 2L_{t, \max}$. The measured values from the experiments for the maximum crack distance and the mean crack distance $S_{r, m}$ are also shown

Member	Load		EC2 [mm]			MC2010 [mm]			DIN [mm]	Measured values [mm]	
	P [kN]	σ_s [MPa]	$2L_{\alpha}$	$2L_{\tau}$	$S_{r, \max}$	$2L_{\alpha}$	$2L_{\tau}$	$S_{r, \max}$	$S_{r, \max}$	$S_{r, \max}$	$S_{r, m}$
S-20-40	808	321	136	433	569	80	354	434	353	250	163
S-32-40	1,012	157	136	271	407	80	221	301	221	240	178
S-20-90	1,003	399	306	433	739	180	354	534	353	290	217
S-32-90	1,363	212	306	271	577	180	221	401	221	320	266

except for one load step. This applies even to relatively large steel stresses, such as 321 MPa for S-20-40 and 399 MPa for S-20-90 in the last load steps. MC2010 and DIN seem to capture this better than EC2. For MC2010, the better compliance between the predicted and observed behavior seems to be related to the fact that the difference in mean strains are explicitly derived based on the assumed behavior of the RC ties in the crack formation stage, as shown in Section 2.2.3. The better compliance for DIN seems to be related to the fact that the tension stiffening factor $\beta = 0.4$ seems to fit better than $\beta = 0.6$ in the stabilized cracking stage. Recent studies in the literature also support the idea of reducing the tension stiffening factor in the stabilized cracking stage.^{5,34}

The experimental study suggests that the maximum crack distance is significantly influenced by the cover, which is supported by another experimental study in the literature.³⁵ More remarkable is the limited influence of the bar diameter, which contradicts the beneficial effect of using large bar diameters in reducing the transfer length according to the slip term in Equation (10) and as observed in Table 5. Moreover, DIN does not acknowledge that the crack distance increases with increasing cover under the assumption that $A_{c,ef} = A_c$, which contradicts the observed behavior of the RC ties in this experimental study. An interesting point, however, is that DIN gives the best overall agreement with the maximum crack distances measured. These contradictory observations, combined with the theoretical study, suggest that the effect of cover and bar diameter should be implemented more consistently than is done in the current semi-empirical formulas.

5.3 | Suggestions for improvements

One suggestion for a more consistent calculation model is to solve Equation (4) explicitly, by applying a proper bond-slip law that takes into account the bond nonlinearity in RC ties and by assuming an appropriate strain distribution over the cover in Equation (1). In this way, the contribution to the total slip can be consistently accounted for at each section of the RC tie without violating the equilibrium, which is an effect the semi-empirical formulas are essentially attempting to model. Moreover, one of the main advantages of explicitly solving Equation (4) is that it is not necessary to assume a certain longitudinal strain distribution for concrete and steel to obtain the crack widths. Instead, the chosen bond-slip law and the contribution of the embedding concrete will explicitly account for the tension stiffening. The challenge is then limited to determining the bond-slip law properties and the strain distribution in the concrete, for instance, by conducting physical and numerical studies. Some of the authors in this paper are currently working on such improvements.

It should be mentioned though, that these suggestions lead to more complex crack width calculations that primarily are intended for large-scale concrete structures, that is, where the use of large covers and bar diameters is typical. The

simplifications in the semi-empirical formulas, however, seem adequate in conventional cases.

6 | CONCLUSION

The behavior of RC ties has been investigated from both an experimental and a theoretical point of view. The aim was to study the applicability of the semi-empirical formulas recommended by EC2, MC2010 and DIN in predicting crack widths for large-scale concrete structures, where large bar diameters and covers typically are used. The theoretical study showed that the semi-empirical formulas could be derived by using the principles of the idealized behavior of RC ties. However, instead of solving the resulting differential equation explicitly, simplifications are made, resulting in semi-empirical formulas that account for the physical behavior of RC ties in a rather inconsistent manner that is also in conflict with the basic principles of solid mechanics.

The conducted experimental study showed that EC2 consistently predicted crack widths that were substantially on the conservative side. MC2010 and DIN seemed to predict the crack widths better, but the relatively large standard deviation and coefficient of variation for the modeling uncertainty resulted in a large number of predicted crack widths on the nonconservative side. This was particularly pronounced for large bar diameters and covers. The experimental study also showed that the cover governs the crack distance and thus the crack widths, which is acknowledged by the semi-empirical formulas in EC2 and MC2010, yet DIN actually gave the best agreement with the crack distances measured even though the cover term is abandoned in this code. The reported modeling uncertainties are representative for this experimental series and are not intended to serve as a generalization for the performance of the formulas.

These contradictory observations, combined with the theoretical study, suggest that a more consistent calculation model should be formulated for large-scale concrete structures. It is proposed that the influence of cover and tension stiffening can be addressed more consistently by (a) selecting a proper bond-slip law, (b) assuming an appropriate strain distribution over the concrete cover, and (c) explicitly solving the differential equations for the slip.

ACKNOWLEDGMENTS

The work presented in this paper is a part of an ongoing PhD-study funded by the research projects Ferry-free E39 and Durable Advanced Concrete Structures (DaCS).

NOTATIONS

A_c	concrete area
$A_{c,ef}$	effective concrete area
A_s	steel area

c	cover	μ_θ	mean value for the modeling uncertainty
d_x	infinitesimal increase x-coordinate	σ_c	concrete stress
E_c	concrete Young's modulus	σ_s	steel stress
E_s	steel Young's modulus	σ_{sr}	steel stress at a crack in crack formation stage
f_{ctm}	mean tensile strength for concrete	σ_θ	SD for the modeling uncertainty
j	section in a crack	ρ_s	reinforcement ratio
k_α	empirical constant in the no-slip theory	τ	bond stress
L_τ	transfer length	τ_{bms}	mean bond stress
$L_{\tau, \max}$	maximum transfer length	φ	steel bar diameter
$L_{t\alpha}$	transfer length according to no-slip theory	χ	stiffness relationship between concrete and steel
$L_{t\tau}$	transfer length according to slip theory		
n_i	number of section average crack width measurements for a crack in a RC tie		
n_{tot}	total number of section average crack width measurements for a group of cracks in a RC tie		
m	total number of cracks in a RC tie		
P	applied force in the RC ties		
s_i	slip at interface between concrete and steel		
s_s	slip caused by shear deformations in the concrete section		
s_{tot}	total slip in a section over the transfer length		
S_i^2	variance of section average crack width measurements for a crack		
S_{tot}^2	variance of total section average crack width measurements for a group of cracks in a RC tie		
$S_{r, \max}$	maximum crack distance		
V_θ	coefficient of variation for the modeling uncertainty		
$w_{0, 95}$	95%-fractile of the measured crack widths		
w_k	characteristic crack width		
$w_{k, DIN}$	characteristic crack width recommended by DIN		
$w_{k, EC2}$	characteristic crack width recommended by EC2		
w_k	characteristic crack width recommended by MC2010		
MC2010			
X	loading regime for RC ties in either crack formation stage or stabilized cracking stage		
$y_{i, j}$	average crack width measurement for the j th section in a crack		
\bar{y}_i	mean of section average crack width measurements for a crack		
\bar{y}_{tot}	mean of total section average crack width measurements for a group of cracks in a RC tie		
α_e	modular ratio		
β	tension stiffening factor		
$\Delta \epsilon_{sr}$	difference in steel strains at a crack and at the end of transfer length in crack formation stage		
ϵ_{ci}	longitudinal concrete strains at interface		
ϵ_{cm}	longitudinal mean concrete strains		
ϵ_{s2}	steel strains at a crack in stabilized cracking stage		
ϵ_{sr1}	steel strains at the end of the transfer length in crack formation stage		
ϵ_{sr2}	steel strains in crack in crack formation stage		
ϵ_{sm}	longitudinal mean steel strains		
ϵ_{si}	longitudinal steel strains at interface		

ORCID

Reignard Tan  <http://orcid.org/0000-0001-8190-6215>

REFERENCES

- Borosnyói A, Balász GL. Models for flexural cracking in concrete: The state of the art. *J Struct Concr*. 2005;6(2):53–62.
- CEN. EN 1992-1-1, Eurocode 2: Design of Concrete Structures—Part 1-1: General Rules and Rules for buildings. Brussels: European Committee for Standardization; 2004.
- fib. *fib Model code for concrete structures 2010*. International Federation for Structural Concrete. Berlin: Ernst & Sohn, 2013.
- DIN: EN-1992-1-1/NA. 2011-01, National Annex – Nationally determined parameters – Eurocode 2: Design of concrete structures – Part 1-1: General rules and rules for buildings; 2011.
- Debernardi PG, Taliano M. An improvement to Eurocode 2 and *fib* model code 2010 methods for calculating crack width in RC structures. *J Struct Concr*. 2016;17(3):365–376.
- Broms B. Theory of the calculation of crack width and crack spacing in reinforced concrete members. *Cement och Betong*. 1968;1:52–64. [In Swedish].
- Gergely P, Lutz LA. Maximum crack width in reinforced concrete flexural members. Causes, Mechanisms and Control of Cracking in Concrete, SP-20. Farmington Hills, MI: American Concrete Institute, 1968; p. 87–117.
- Beeby A. The influence of the parameter ϕ/ρ_{eff} on crack widths. *J Struct Concr*. 2004;5(2):71–83.
- fib. Bond of reinforcement in concrete – State-of-art report. *fib bulletin No. 10*. Lausanne, Switzerland; 2000.
- Goto Y. Cracks formed in concrete around deformed tension bars. *ACI J*. 1971;68(4):244–251.
- Dörr, K. Bond-behaviour of ribbed reinforcement under transversal pressure, Proceedings of IASS Symposium on Nonlinear Behaviour of Reinforced Concrete Spatial Structures, Darmstadt, 1, Edited by G. Mehlhorn, H. Rühle and W. Zerna, Werner-Verlag, Düsseldorf, Germany, 1978.
- Jiang DH, Shah SP, Andonian AT. Study of the transfer of tensile forces by bond. *ACI J*. 1984;81(3):251–259.
- Tammo K, Lundgren K, Thelandersson S. Nonlinear analysis of crack widths in reinforced concrete. *Mag Concr Res*. 2009;61(1):23–34.
- Ferry-Borges J. Cracking and deformability of reinforced concrete beams. Vol 26. IABSE Publications, Zürich, Switzerland, 1966;p. 75–95.
- Beeby AW. The prediction of crack widths in hardened concrete. *Struct Eng*. 1979;57A(1):9–17.
- fib. *Structural Concrete – Textbook on behaviour, design and performance*, Second edition, Volume 2. *fib bulletin No. 52*. Lausanne, Switzerland; 2010.
- Russo G, Romano F. Cracking response of RC members subjected to uniaxial tension. *J Struct Eng*. 1992;118(5):1172–1190.
- Balász GL. Cracking analysis based on slip and bond stresses. *ACI Mater J*. 1993;90(4):340–348.
- Saliger R. High-grade steel in reinforced concrete. Proceedings Second Congress of the International Association for Bridge and Structural Engineering. Berlin-Munich, 1936 (cited according to Ref. [15]).
- Base GD, Read JB, Beeby AW, Taylor HPJ. An investigation of the crack control characteristics of various types of bar in reinforced concrete beams. Research Report 18, Part 1. London, UK: Cement and Concrete Association, 1966.
- Scott RH, Gill PAT. Short-term distributions of strain and bond stress along tension reinforcement. *Struct Eng*. 1987;65B(2):39–48.

22. Yannopoulos PJ. Variation of concrete crack widths through the concrete cover to reinforcement. *Mag Concr Res.* 1989;41(147):63–68.
23. Fantilli AP, Mihashi H, Vallini P. Crack profile in RC, R/FRC and R/HFRC members in tension. *Mater Struct.* 2007;40:1099–1114.
24. Tammo K, Thelandersson S. Crack behavior near reinforcing bars in concrete structures. *ACI Struct J.* 2009;106(3):259–267.
25. Borosnyói A, Snóbli I. Crack width variation within the concrete cover of reinforced concrete members. *Építőanyag—J Silicate Based Compos Mater.* 2010;62(3):70–74.
26. Berrocal C, Löfgren I, Lundgren K, Görander N, Halldén C. Characterisation of bending cracks in R/FRC using image analysis. *Cem Concr Res.* 2016;90:104–116.
27. Braam, CR. Control of crack width in deep reinforced concrete beams [PhD thesis]. TU Delft, Delft, the Netherlands; 1990.
28. NS: EN-197-1: 2011. Cement – Part 1: Composition, specifications and conformity criteria for common cements. SN/K 007; 2011.
29. NS: 3576-1: 2005. Steel for the reinforcement of concrete – Dimensions and properties – Part 1: Ribbed bars B500NA. SN/K 089; 2005 [In Norwegian].
30. Schneider CA, Rasband WS, Eliceiri KW. NIH image to ImageJ: 25 years of image analysis. *Nat Methods.* 2012;9(7):671–675.
31. Engen M, Hendriks MAN, Köhler J, et al. Predictive strength of ready-mixed concrete: Exemplified using data from the Norwegian market. *Structural Concrete.* 2017;1–14.
32. CEB. CEB design manual on cracking and deformations. Lausanne, Switzerland: École Polytechnique Fédérale du Lausanne, 1985.
33. JCSS. Probabilistic Model Code, 12th draft. Joint Committee on Structural Safety; 2001.
34. CEOS.fr. Control of cracking in reinforced concrete structures. London and Hoboken: ISTE Ltd and John Wiley & Sons, Inc, 2016.
35. Caldentey AP, Peiretti HC, Iribarren JP, Soto AG. Cracking of RC members revisited: Influence of cover, ϕ/ρ_s , e_f and stirrup spacing – An experimental and theoretical study. *J Struct Concr.* 2013;14(1):69–78.

AUTHOR'S BIOGRAPHIES



Reignard Tan, PhD-candidate
Department of Structural Engineering
NTNU, Norwegian University of Science and Technology Rich.
Birkelandsvei 1A 7491 Trondheim, Norway
reignard.tan@multiconsult.no



Kristoffer Eileraas, M.Sc
Department of Structural Engineering
NTNU, Norwegian University of Science and Technology Rich.
Birkelandsvei 1A 7491 Trondheim, Norway
kristoffer.eileraas@afconsult.com



Ola Opkvitne, M.Sc
Department of Structural Engineering
NTNU, Norwegian University of Science and Technology Rich.
Birkelandsvei 1A 7491 Trondheim, Norway
ola.opkvitne@ramboll.no



Giedrius Žirgulis, PhD
Department of Structural Engineering
NTNU, Norwegian University of Science and Technology Rich.
Birkelandsvei 1A 7491
Trondheim, Norway
giedrius.zirgulis@gmail.com



Max A. N. Hendriks, PhD, Professor
Department of Structural Engineering
NTNU, Norwegian University of Science and Technology Rich.
Birkelandsvei 1A 7491 Trondheim, Norway
Faculty of Civil Engineering and Geosciences Delft University of Technology
Stevinweg 1, 2628CN Delft, The Netherlands
max.hendriks@ntnu.no



Mette Geiker, PhD, Professor
Department of Structural Engineering
NTNU, Norwegian University of Science and Technology Rich. Birkelandsvei 1A 7491 Trondheim, Norway
mette.geiker@ntnu.no



Dan-Evert Brekke, M.Sc
Multiconsult ASA
Postboks 265 Skøyen
0213 Oslo, Norway
dan.evert.brekke@multiconsult.no



Terje Kanstad, PhD, Professor
Department of Structural Engineering
NTNU, Norwegian University of Science and Technology Rich.
Birkelandsvei 1A 7491 Trondheim, Norway
terje.kanstad@ntnu.no

How to cite this article: Tan R, Eileraas K, Opkvitne O, et al. Experimental and theoretical investigation of crack width calculation methods for RC ties. *Structural Concrete.* 2018;19:1436–1447. <https://doi.org/10.1002/suco.201700237>

Paper IIa

A numerical investigation of the cracking behaviour of reinforced
concrete-tie elements

Tan, R., Hendriks, M.A.N., Geiker, M. & Kanstad, T.

Magazine of concrete research, 2018, 1-13, <https://doi.org/10.1680/jmacr.18.00156>

Cite this article

Tan R, Hendriks MAN, Geiker M and Kanstad T
 A numerical investigation of the cracking behaviour of reinforced-concrete tie elements.
Magazine of Concrete Research,
<https://doi.org/10.1680/jmacr.18.00156>

Research Article

Paper 1800156
 Received 26/03/2018; Revised 25/07/2018;
 Accepted 28/08/2018

Keywords: bond/cracks & cracking/
 finite element methods

ICE Publishing: All rights reserved

A numerical investigation of the cracking behaviour of reinforced-concrete tie elements

Reignard Tan

PhD candidate, Department of Structural Engineering, Norwegian University of Science and Technology, Trondheim, Norway (corresponding author: reignard.tan@multiconsult.no) (Orcid:0000-0001-8190-6215)

Max A. N. Hendriks

Professor, Department of Structural Engineering, Norwegian University of Science and Technology, Trondheim, Norway; Faculty of Civil Engineering and Geosciences, Delft University of Technology, Delft, the Netherlands (Orcid:0000-0001-9507-3736)

Mette Geiker

Professor, Department of Structural Engineering, Norwegian University of Science and Technology, Trondheim, Norway (Orcid:0000-0003-4952-8394)

Terje Kanstad

Professor, Department of Structural Engineering, Norwegian University of Science and Technology, Trondheim, Norway (Orcid:0000-0003-0760-2322)

The cracking behaviours of reinforced-concrete (RC) ties are investigated by conducting virtual experiments using non-linear finite-element analysis. The assumptions in the model are verified by benchmarking the classical experiments of B. Bresler and V. V. Bertero as conducted in 1968 and P. J. Yannopoulos, conducted in 1989, which shows good agreement in the comparison of steel strains, development of crack widths and crack spacing. Furthermore, virtual experiments on four different RC ties show that the size of the cover and not the bar diameter governs the crack spacing and thus implicitly the crack width. An increase of the bar diameter has a beneficial effect in reducing the steel stress and the associated steel strains, which in turn reduces the crack width. Finally, a single bond-slip curve is sufficient in describing the average bond transfer of an arbitrary RC tie.

Notation

A_c	area of concrete
A_s	area of steel
c	cover
E_c	modulus of elasticity of concrete
E_s	modulus of elasticity of steel
F_c	force resultant of concrete
F_{cr}	cracking force of concrete
f_c	compressive strength of concrete
f_{ct}	tensile strength of concrete
f_y	yield strength of steel
G_f	tensile fracture energy of concrete
G_{fc}	compressive fracture energy of concrete
L	bar length
N	applied force at steel bar ends
R	radial axis
s	slip
s_1	slip parameter in bond-slip curve according to <i>fib</i> Model Code 2010
s_f	specific distance from the loaded end
t_i	thickness of interface layer between concrete and steel
w_i	crack width at the steel bar surface
w_o	crack width at the specimen surface
x	position over the bar length
x_{cr}	crack spacing
x_i	x -coordinate of integration points adjacent to the steel and outer concrete surface
x_r	transfer length
α	curve parameter in bond-slip curve according to <i>fib</i> Model Code 2010
Δx	half finite-element length
ε_c	strains at outer concrete surface

ε_{ci}	concrete strains at integration points
ε_{ct}	cracking strain concrete
ε_s	strains at steel surface
ε_{si}	steel strains at integration points
ν_c	Poisson ratio of concrete
ν_s	Poisson ratio of steel
ρ_{eff}	reinforcement ratio
σ_s	steel stress
τ_1	bond stress parameter in bond-slip curve according to <i>fib</i> Model Code 2010
$\tau_{bm,x_{cr}}$	mean bond stress over the crack distance
ϕ	bar diameter

Introduction

In deriving an analytical crack width calculation model for reinforced-concrete (RC) elements, the roles of (a) bond at the steel-concrete interface and (b) cover become two key parameters (Balázs *et al.*, 2013; CEB, 1985). This paper investigates these two parameters using non-linear finite-element (FE) analyses (NLFEA), which were validated against classical experiments. The tensile strength of concrete is a third key parameter. This parameter has been investigated thoroughly in the research project of CEOS.fr (Barre *et al.*, 2016), in which the scale effect is accounted for in determining the concrete tensile strength, and will not be addressed in detail here.

The roles of bond and cover are implemented in the empirical formulation recommended by the American Concrete Institute (ACI, 2001) and in the semi-empirical formulation recommended by Eurocode 2 (CEN, 2004) and *fib* Model Code 2010 (MC2010) (*fib*, 2013) in a relatively simplified manner. The bond and cover terms in the crack spacing formula of

Axisymmetric model

The NLFEA were carried out using quadratic, axisymmetric, quadrilateral elements in the FE program 'Diana' (Diana FEA BV, 2016). A linear elastic material model was used for steel, while a non-linear fracture mechanics material model with rotating cracks based on a total strains formulation was used for concrete. The parabolic curve according to Feenstra (1993) was used for the compressive behaviour, whereas the softening curve according to Hordijk (1991) was used for the tensile behaviour. The Poisson effect was gradually reduced in accordance with the total strains formulation as the cracking damage progressed, while lateral influences on the compressive behaviour were neglected. Geometry, interface layer, loading and boundary conditions for the FE model are as shown in Figure 1(b). Symmetry allowed for modelling half of the length only.

Loads were monotonically increased in a displacement-controlled manner using regular Newton–Raphson iterations. The convergence criteria were force and energy based with the tolerance value of 0.01 and 0.001, respectively, in accordance with the Dutch guidelines for NLFEA of concrete structures (Belletti *et al.*, 2014; Hendriks *et al.*, 2017). The element size was adjusted to obtain approximately six to ten elements over the cover and one to three elements over the steel bar radius.

Interface elements between concrete and steel were chosen to have a thickness of $t_i = 0.1$ mm. A non-linear elasticity model with non-linear properties in the radial direction and a constant stiffness in the shear direction were chosen to allow for radial separation only in accordance with the assumptions discussed in the previous section. The elastic radial and shear moduli for the interface elements were derived from the modulus of elasticity for concrete, E_c – that is, respectively, as E_c/t_i and $E_c/[2(1+\nu_c)t_i]$. The elastic radial modulus was reduced with a factor of 10^{-05} when a tensile strain of $0.8f_{ct}/E_c$ at the interface was reached, in order to simulate the radial separation in a stable manner.

Validation of FE model

Test set-up

The classical experiments of Bresler and Bertero (1968) and Yannopoulos (1989) were benchmarked to investigate the validity of the assumptions in the FE model. The investigated RC tie named specimen H by Bresler and Bertero (1968) was 152 mm (6 in) in diameter, had a length of 406 mm (16 in) and was embedded with a deformed steel bar with dia. 28.7 mm (1.13 in) in the centre of the cross-section. The length of the specimen was chosen as twice the mean crack spacing obtained from the pilot studies of 1829 mm (72 in) long RC ties with similar sectional properties. The specimen was axially cyclic loaded in the steel bar ends in the experiments, and a notch was cut at the mid-length to induce a primary crack at this section. Strain gauges were mounted in a sawed-out canal in the centre of the steel bar to measure the steel strains over

the length. The reduction of the steel bar area due to the sawed-out canal was accounted for by subtracting an inner radius of 5.6 mm from the outer radius of the steel bar in the FE model. This corresponded to the given nominal area of 548 mm^2 (0.85 in^2) for the steel bar in the experiments.

The six RC ties investigated by Yannopoulos (1989) were 76 mm in diameter, had a length of 100 mm and were embedded with a deformed steel bar of dia. 16 mm in the centre of the cross-sections. The length of the specimens was limited to avoid formation of a new primary crack and was based on the mean crack spacing obtained from pilot studies carried out on 800 mm long RC ties with similar sectional properties. The RC ties were axially and monotonically loaded at the steel bar ends while measuring the development of the crack width.

The material parameters given in the experiments are summarised in Table 1 and were used in validating the FE model. Material parameters such as the Poisson ratio and the fracture energy were not given in the experiments and were derived in accordance with the recommendations in the Dutch guidelines for NLFEA of concrete structures (Hendriks *et al.*, 2017).

Comparison of steel strains, crack widths and crack spacing

The comparison of the steel strains obtained from the NLFEA and the experimental steel strains of Bresler and Bertero (1968) at four different load levels is shown in Figure 2(a). The two lowest load levels corresponding to steel stresses of 33 MPa and 65 MPa give good comparisons of the steel strains, as expected, since the experimental strains at these load levels are obtained from the first monotonic load cycle. The experimental strains at the two higher load levels corresponding to steel stresses of 195 MPa and 242 MPa, however, are obtained from the second load cycle. Cyclic loading is known to have a significant effect on the deterioration of bond even for the first repeated loads (Dörr, 1978; *fib*, 2000), which could explain the less stiff response of the experimental steel strains in the second load cycle compared to that obtained from the monotonic loading in the NLFEA. Nevertheless, the comparison of the steel strains obtained from the NLFEA and the experiments shows in general a good agreement.

A comparison of the development of the crack width with increasing steel stresses obtained in the experiments of Yannopoulos (1989) and in the NLFEA is shown in Figure 2(b). The comparison of the developed crack width also shows good agreement; however, it is observed that the NLFEA slightly overestimates the crack width for a given steel stress.

Separate NLFEA were conducted to investigate whether the FE model also could predict crack spacing similar to that

Table 1. Material parameters of the RC ties investigated in the experiments of Bresler and Bertero (1968) and Yannopoulos (1989)

Material parameters	Bresler and Bertero (1968)		Yannopoulos (1989)	
	Concrete	Steel	Concrete	Steel
Compressive strength, f_c : MPa	40.8	—	43.4	—
Tensile strength, f_{ct} : MPa	4.48	—	3.30	—
Yield strength, f_y : MPa	—	413	—	424
Modulus of elasticity, E_c and E_s : MPa	33 165	205 464	32 000	200 000
Poisson ratio, ν_c and ν_s	0.15	0.30	0.15	0.30
Tensile fracture energy, $G_f = \frac{73f_c^{0.18}}{1000}$: N/mm	0.142	—	0.144	—
Compressive fracture energy, $G_c = 250G_f$: N/mm	35.6	—	36.0	—

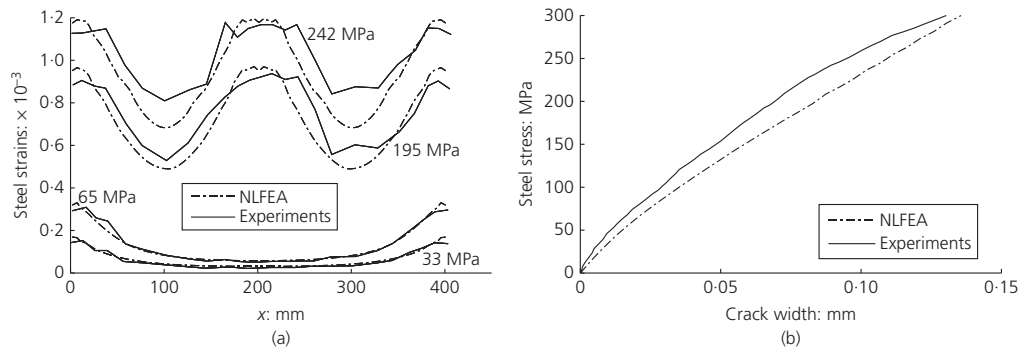


Figure 2. (a) Comparison of steel strains in the experiments of Bresler and Bertero (1968) with steel strains obtained in the NLFEA. (b) Comparison of crack widths in the experiments of Yannopoulos (1989) with crack widths obtained in the NLFEA

obtained in the pilot studies of Bresler and Bertero (1968) and Yannopoulos (1989) on longer specimens. The RC tie lengths were thus increased in the FE model to investigate this. The strain distribution in Figures 3(a) and 3(b), respectively, shows that a new crack formed in the NLFEA at a distance of approximately 200 mm from the loaded end for the long 'Bresler and Bertero' specimen and at approximately 80 mm for the long 'Yannopoulos' specimen. This corresponds well to the mean crack spacing of 203 mm and 90 mm, respectively, obtained in the experiments of Bresler and Bertero (1968) and Yannopoulos (1989) on longer specimens.

The good agreement in the comparison of steel strains, crack widths and crack spacing confirms the validity of the discussed assumptions, and further shows the ability of the FE model to simulate the physical behaviour of RC ties realistically.

The physical behaviour of RC ties

General

The physical behaviour of RC ties is now discussed and elucidated using the results from the NLFEA conducted on the 'Bresler and Bertero' specimen. Details for the test set-up were

presented in the section entitled 'Test set-up'. A contour plot of exaggerated radial displacements at a steel stress, $\sigma_s \approx 180$ MPa, which is just before a primary crack forms at the symmetry section, is shown in Figure 4(a). It is noticed that the concrete is separated radially from the steel bar close to the loaded end due to the inflicted shear stress at the concrete inner surface. The radial displacements are counteracted by the stiffness of the concrete in the hoop direction, causing a confining pressure to the steel bar. Splitting cracks arise if the hoop stresses exceed the tensile strength of concrete, as can be observed in Figure 4(b). Actually, the splitting cracks cause a build-up of radial and shear stresses close to the loaded end, before reaching the peaks at approximately the same location over the bar length, as can be observed in Figure 4(c). Further propagation of internal splitting cracks as the load increases causes additional movement of the stress peaks towards the symmetry section.

It should be mentioned that the maximum radial displacements in the analyses are of the magnitude of 10^{-2} mm, which is still small compared to typical rib dimensions. This justifies the assumption of claiming that the mechanical bond is maintained although the concrete is separated radially from

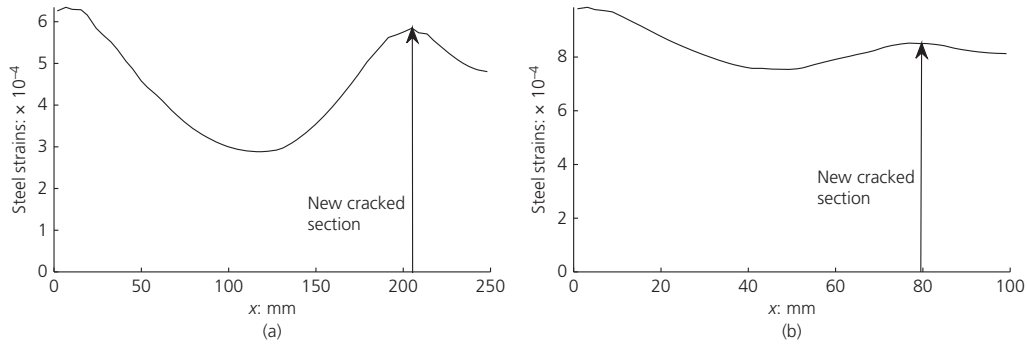


Figure 3. Steel strain distributions obtained from the NLFEA immediately after the formation of a new primary crack for (a) the long 'Bresler and Bertero' specimen ($L = 500$ mm) and (b) the long 'Yannopoulos' specimen ($L = 200$ mm)

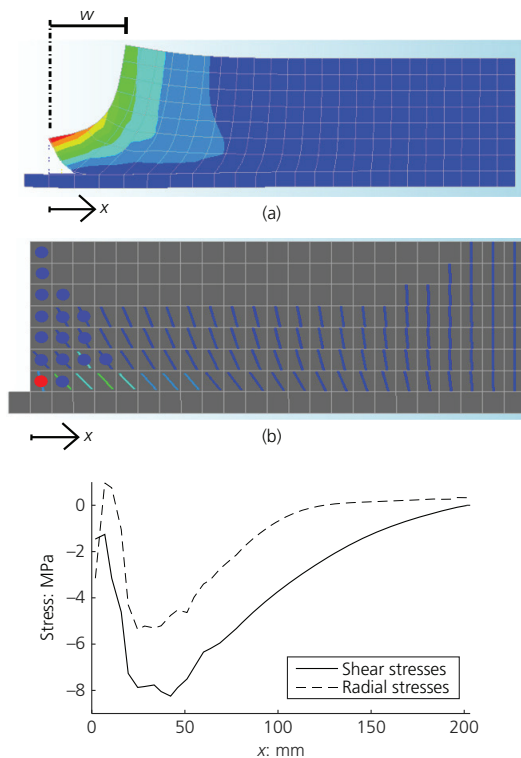


Figure 4. (a) Contour plot of radial displacements and the deformation configuration at $\sigma_s = 180$ MPa. (b) Corresponding plot of internally inclined cracks (straight lines) and splitting cracks (circles). (c) Corresponding shear and radial stresses. A full-colour version of this figure can be found on the ICE Virtual Library (www.icevirtuallibrary.com)

the steel bar. Finally, these observations suggest that the shear transfer is dependent on the stiffness of the confining concrete.

Lightly as opposed to heavily loaded members

The interaction of the load level and the specimen length is significant for the cracking behaviour of RC ties. Russo and Romano (1992) were the first to introduce the principles of the comparatively lightly loaded member (CLLM) behaviour and the comparatively heavily loaded member (CHLM) behaviour, which are conceptually visualised in Figures 5(a) and 5(b), respectively. The figures depict the steel and the corresponding concrete strain distribution of a long specimen with length $L = 500$ mm and a short specimen with length $L = 200$ mm, exposed to the same loading. To clarify, the arrows in Figure 5(b) indicate the corresponding concrete surface strains to the steel strains for the short specimen. The main difference is that the strains become compatible ($\epsilon_s = \epsilon_c$) at a certain distance x_r from the loaded end and remain constant along the remaining length in the case of CLLM, whereas in the case of CHLM the strains remain incompatible ($\epsilon_s > \epsilon_c$) over the entire specimen length. The point of compatibility x_r moves towards the symmetry section upon increasing the load, and will have moved completely to the symmetry section ($x_r = L/2$) for a sufficiently large load in the case of CLLM. Upon even further loading, strains become incompatible at the symmetry section and a primary crack will only have the possibility to form here if the concrete strains exceed the cracking strain. The specimen can then be said to have undergone a smooth transition from the CLLM behaviour to the CHLM behaviour. If the concrete strains exceed the cracking strain at any location prior to the symmetry section – that is, $\epsilon_c(x_r) \geq \epsilon_{ct}$, a new primary crack will instead form here, thus generating a new member length $L = x_r = x_{cr}$. The new member will then exhibit either a CLLM behaviour or a CHLM behaviour depending on the load level and the member length.

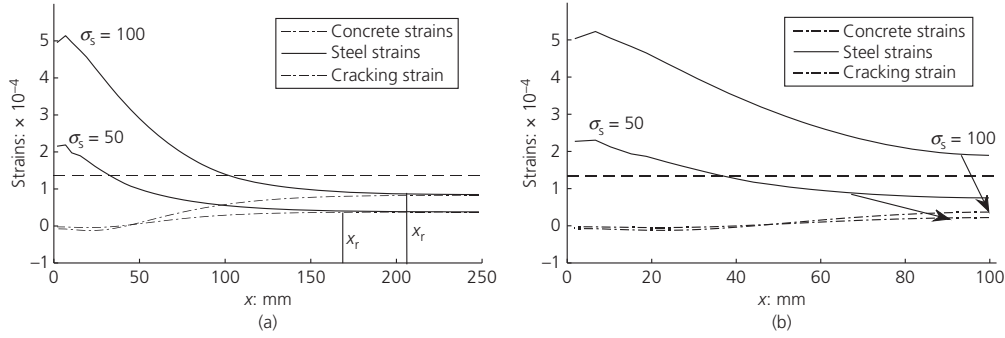


Figure 5. Strain distribution for the 'Bresler and Bertero' specimen at two similar load levels: (a) CLLM behaviour of a long specimen $L = 500$ mm; (b) CHLM behaviour of a short specimen $L = 200$ mm

An analogy of the CLLM and CHLM behaviour can be drawn to the so-called crack formation stage and stabilised cracking stage, respectively. However, they are not the same. This can be explained by the fact that a smooth transition between the CLLM and the CHLM behaviour is possible, which is not the case in the concept of the crack formation stage and stabilised cracking stage.

The influence of bar diameter and cover on the cracking behaviour of RC ties

Virtual experiments

The bar diameter and cover are essential parameters in calculating the crack spacing and the crack width in the semi-empirical formulas recommended by Eurocode 2 (CEN, 2004) and MC2010 (fib, 2013). Both parameters have been the subject of major discussions for several decades in developing the semi-empirical formulas (Base *et al.*, 1966; Beeby, 1979, 2004; Broms, 1968; Caldentey *et al.*, 2013; Ferry-Borges, 1966; Gergely and Lutz, 1968; Saliger, 1936; Tan *et al.*, 2018). For this purpose, the FE model established and verified in this study has been used to conduct virtual experiments on RC ties to better understand the influence of bar diameter and cover.

The behaviours of four circular specimens, reinforced with one concentric deformed steel bar, were investigated. The specimens were named $\phi 20c40$, $\phi 20c90$, $\phi 32c40$ and $\phi 32c90$, indicating that the bar diameter ϕ was either 20 or 32 mm and that the cover c was either 40 mm or 90 mm. A concrete grade C35 according to MC2010 (fib, 2013) was chosen for the concrete, while a Young's modulus of $E_s = 200\,000$ MPa and a yield strength of $f_y = 500$ MPa was chosen for the steel. The Poisson ratio and the fracture energy were derived in accordance with the recommendations in the Dutch guidelines for NLFEA of concrete structures (Hendriks *et al.*, 2017). The analysis procedure was to first conduct CLLM studies on longer specimens ($L = 700$ mm) to obtain a typical crack

spacing x_{cr} , after which a separate analysis on the cracked specimen was conducted to include the CHLM behaviour.

The influence of bar diameter

CLLM behaviour

The bond stress distributions for the CLLM behaviour of $\phi 20c40$ against $\phi 32c40$ and $\phi 20c90$ against $\phi 32c90$ are compared at the load levels just before a primary crack forms in Figures 6(a) and 6(b), respectively, with Table 2 showing the corresponding condition in the specimens. The comparison shows that the bond stress distributions are influenced greatly by the bar diameter and differ in general from one another. It is noticed, however, that the bond stress distributions align and become negligibly small ($\tau < 1$ MPa) at approximately the same location over the bar length, indicating the end of the transfer length and that a primary crack is about to form in the vicinity. The concrete force resultant at a distance x_r from the loaded end is obtained by integrating the bond stress distribution $\tau(x)$ as

$$1. \quad F_c(x_{cr}) = \int_0^{x_r=x_{cr}} \tau(x) \pi \phi dx = \tau_{bm,x_{cr}} \pi \phi x_{cr}$$

which is limited by the cracking force as

$$2. \quad F_{cr} = f_{ct} A_c$$

Although the bar diameter influences the bond stress distribution and thus the concrete force resultant in Equation 1, it does not significantly affect the limit value in Equation 2, nor does it influence the transfer length as pointed out for Figures 6(a) and 6(b). This means that a primary crack forms at approximately the same location over the bar length for

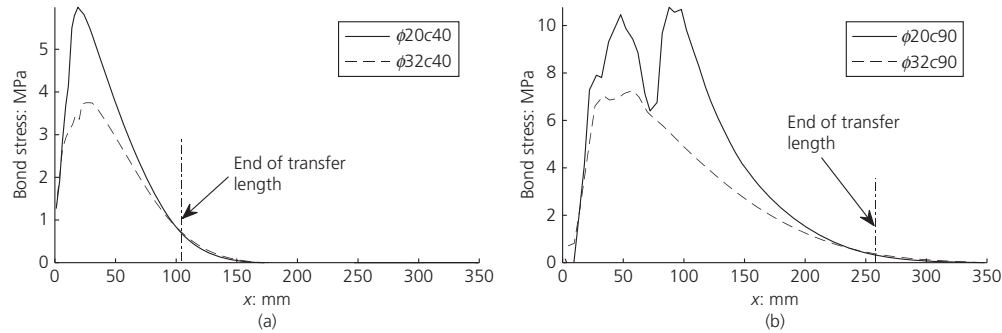


Figure 6. (a) Bond stress distribution for the CLLM behaviour of $\phi 20c40$ against $\phi 32c40$ at primary cracking in accordance with the load levels in Table 2. (b) Bond stress distribution for the CLLM behaviour of $\phi 20c90$ against $\phi 32c90$ at primary cracking in accordance with the load levels in Table 2

Table 2. CLLM behaviour of $\phi 20c40$ against $\phi 32c40$ and $\phi 20c90$ against $\phi 32c90$ showing the steel stress σ_s and the corresponding load level F just before a primary crack forms at a distance s_r from the loaded end, mean bond stress $\tau_{bm,x_{cr}}$ of the bond stress distribution over the crack distance x_{cr} , concrete force resultant at the section where a primary crack forms, $F_c(x_{cr}) = \tau_{bm,x_{cr}} \pi \phi x_{cr}$, and the cracking force, $F_{cr} = f_{ct} A_c$

RC tie	σ_s : MPa	F : kN	x_{cr} : mm	$\tau_{bm,x_{cr}}$: MPa	$F_c(x_{cr})$: kN	F_{cr} : kN
$\phi 20c40$	100.3	31.5	105	3.76	24.8	24.2
$\phi 32c40$	58.1	46.7	109	2.74	30.0	29.0
$\phi 20c90$	341.1	107.1	260	6.23	101.8	99.8
$\phi 32c90$	160.6	129.1	272	4.21	115.1	110.7

specimens having similar cover, irrespective of the bar diameter size, as also can be observed in Table 2.

CHLM behaviour

The strain distribution for the CHLM behaviour of $\phi 20c40$ against $\phi 32c40$ and $\phi 20c90$ against $\phi 32c90$ with specimen lengths similar to the crack spacing in Table 2 is shown in Figures 7(a) and 7(b), respectively, at two steel stress levels, while the development of the crack width with steel stresses is shown in Figures 7(c) and 7(d). It is observed that the bar diameter influences the strain distribution over the bar length for a given steel stress. The 20 mm specimens experience more variation in steel strains than the 32 mm specimens. This can be explained by the fact that the 32 mm specimens are exposed to a substantially higher load level than the 20 mm specimens for a given steel stress. This implies that the confining concrete for the 32 mm specimens is exposed to more internal cracking than the 20 mm specimens, which has a significant limiting effect on the tension stiffening. Less tension stiffening results in a larger crack width for a given steel stress, as can be observed in Figures 7(c) and 7(d), which can be explained by the following. The crack width is obtained by integrating the

difference in steel strains and concrete strains at the specimen surface over the bar length as

$$3. \quad w = \int_0^{x_{cr}} (\epsilon_s - \epsilon_c) dx$$

Acknowledging from Figures 7(a) and 7(b) that the concrete strains are negligible in the case of CHLM behaviour suggests that the major contribution to the crack width must be the steel strains. Hence, a larger reduction in steel strains over the specimen length results in smaller crack width. It should be mentioned, however, that large bar diameters have a beneficial effect in reducing the steel stress and the associated steel strains for a given load level, which in turn reduces the crack width.

The influence of cover

CLLM behaviour

The bond stress distributions for the CLLM behaviour of $\phi 20c40$ against $\phi 20c90$ and $\phi 32c40$ against $\phi 32c90$ are compared in Figures 8(a) and 8(b), respectively, at two different conditions, one at a similar load level ($\sigma_s \approx 50$ MPa and $\sigma_s \approx 35$ MPa) and the other corresponding to the load levels in Table 2, which is just before a primary crack forms. The comparison of the bond stress distributions at the similar load level shows that they are quite similar, implying that the cover size does not affect the bond transfer significantly for a given load level and bar diameter in the case of CLLM behaviour. However, comparing the bond stress distributions at the load levels just before a primary crack forms shows that both bond stresses and transfer lengths increase with increasing load level and cover, which can be explained mechanically by the following. A larger cover increases the cracking force in accordance

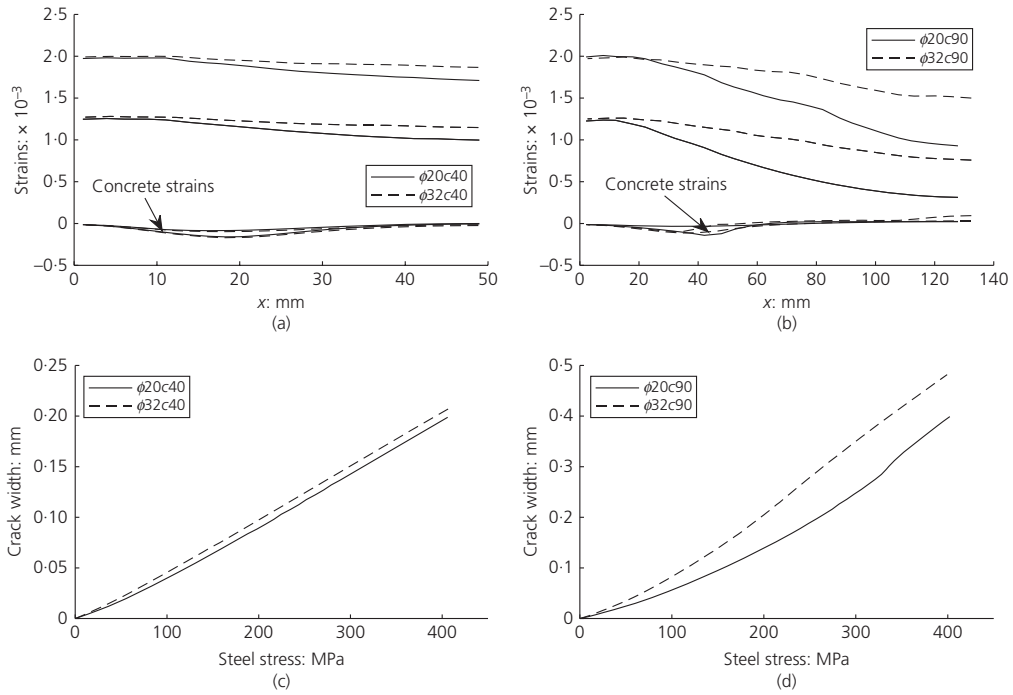


Figure 7. Strain distributions for (a) $\phi 20c40$ against $\phi 32c40$ and (b) $\phi 20c90$ against $\phi 32c90$ at steel stresses $\sigma_s = 250$ MPa and $\sigma_s = 400$ MPa. Development of crack widths with steel stresses for (c) $\phi 20c40$ against $\phi 32c40$ and (d) $\phi 20c90$ against $\phi 32c90$

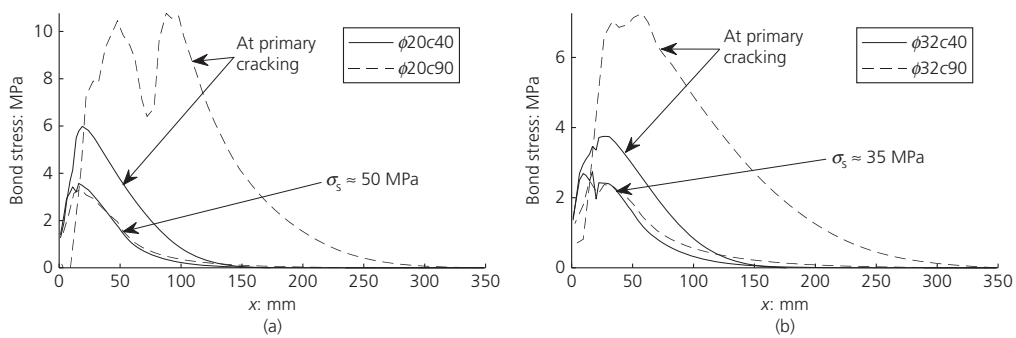


Figure 8. (a) Bond stress distribution for the CLLM behaviour of $\phi 20c40$ against $\phi 20c90$ at $\sigma_s \approx 50$ MPa and at primary cracking in accordance with the load levels in Table 2. (b) Bond stress distribution for the CLLM behaviour of $\phi 32c40$ against $\phi 32c90$ at $\sigma_s \approx 35$ MPa and at primary cracking in accordance with the load levels in Table 2

with Equation 2. The concrete force resultants, in accordance with Equation 1, however, remain approximately the same at the load level just before a primary crack forms in the specimen having a smaller cover, as the bond stress distributions

should be quite similar for a given load level. This means that the concrete force resultant for the specimen having a larger cover can only increase and approach its cracking force by increasing the load level. This in turn results in a larger bond

stress distribution and transfer length, which can also be observed in Table 2 by comparing mean bond stresses and crack spacing for specimens having similar bar diameter but different covers.

CHLM behaviour

The strain distribution for the CHLM behaviour of $\phi 20c40$ against $\phi 20c90$ and $\phi 32c40$ against $\phi 32c90$ with specimen lengths similar to the crack spacing in Table 2 is shown in Figures 9(a) and 9(b), while the development of the crack width with steel stresses is shown in Figures 9(c) and 9(d). The specimens $\phi 20c90'$ and $\phi 32c90'$ are included to represent the hypothetical case in which $\phi 20c90$ and $\phi 32c90$, respectively, were supposed to have the same specimen lengths as $\phi 20c40$ and $\phi 32c40$. It is noticed that the variation in steel strains and the development of crack width nearly remains the same for specimens having similar lengths and bar diameters but different covers. This means that it is the specimen length over which the steel strains are integrated that governs the crack width and not necessarily the cover itself. Hence, the cover does not explicitly influence the crack width per se, but contributes implicitly by increasing the crack spacing. Larger crack spacing simply results in larger crack width, as indicated in Figures 9(c) and 9(d).

The influence of bar diameter and cover on the crack spacing

The discussions regarding Figures 6(a) and 6(b) and Figures 8(a) and 8(b) suggest that the crack spacing is a geometrically dependent parameter, which is mainly governed by the size of the cover but not the bar diameter. A comparable conclusion was drawn by Broms (1968), Gergely and Lutz (1968), Beeby (2004) and Tan *et al.* (2018), primarily by discussing the limited influence of ϕ/ρ_{eff} on the development of crack widths observed in several published experiments. A mechanical explanation of this finding is that the concentrated forces inflicted at the steel bar ends at the moment of cracking, $F = \epsilon_{\text{ct}}(E_s A_s + E_c A_c) \approx f_{\text{ct}} A_c$, should be close for two specimens having similar cover but different bar diameters since the concrete area A_c remains almost the same as discussed earlier, see Table 2. This means that the concentrated forces inflicted at the steel bar ends should disperse in a similar fashion over the cover to obtain an even distribution of the stresses over the cross-section, further implying that the transfer lengths should also be close. Figure 10(a), which shows how the concrete force resultants gradually increase from the loaded end at the load levels corresponding to Table 2, supports this postulation. Further supporting evidence can be observed in Figure 10(b), which shows the development

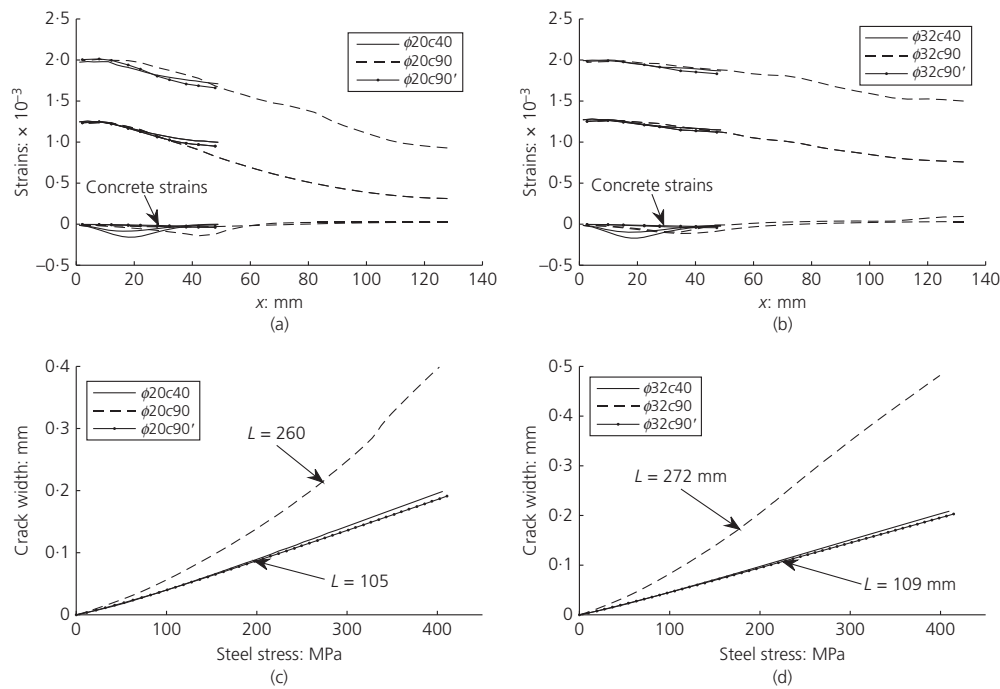


Figure 9. Strain distributions for (a) $\phi 20c40$ against $\phi 20c90$ and (b) $\phi 32c40$ against $\phi 32c90$. Development of crack widths with steel stresses for (c) $\phi 20c40$ against $\phi 20c90$ and (d) $\phi 32c40$ against $\phi 32c90$.

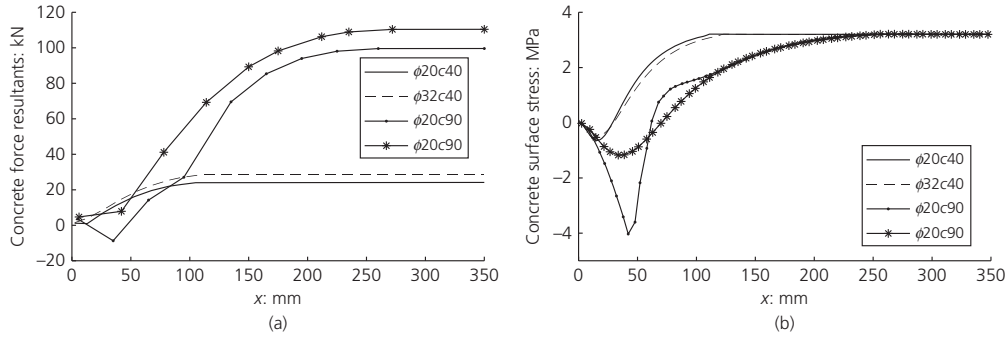


Figure 10. (a) Development of concrete force resultants over the bar length at cracking. (b) Development of concrete surface stresses over the bar length at cracking

of the corresponding concrete surface stresses over the respective transfer lengths.

Although the cover appears to be governing for the crack spacing in virtual experiments, in physical experiments the bar diameter could still have a substantial influence. This can mainly be attributed to the large scatter of the tensile strength of concrete in real-life structures (Barre *et al.*, 2016). The influence of the tensile strength will cause a structure to crack more randomly and not necessarily at the end of the transfer length during the crack formation. The division of the member length due to the random cracking will cause an interaction of the CLLM and CHLM behaviour at which both the cover and the bar diameter together play significant roles for the further development of the crack pattern.

Local bond-slip curve

Determining the local bond-slip curves

The slip distributions for the analysed specimens are approximated by numerically integrating the difference in steel and concrete strains over the bar lengths using the method of Riemann sum as

$$4. \quad s(x) = \int_x^{L/2} (\varepsilon_s - \varepsilon_c) dx \approx \sum_{i | x \leq x_i \leq (L/2)} (\varepsilon_{si} - \varepsilon_{ci}) \Delta x$$

where $s(x)$ is the slip at an arbitrary section x ; ε_s is strain at the steel surface; ε_c is strain at the outer concrete surface; x_i is the x -coordinate of integration points adjacent to the steel and outer concrete surface; ε_{si} and ε_{ci} are, respectively, the steel and concrete strains at these integrations points; and Δx is half the FE length.

A 2×2 integration scheme was applied for the FE. Furthermore, using the strains adjacent to the outer concrete surface implies that the slip is composed of two parts: the

relative displacement occurring at the interface between concrete and steel due to formation of internally inclined cracks and shear deformations occurring over the cover. This conforms to the definition of slip in accordance with *fib* bulletin number 10 (*fib*, 2000) and Tan *et al.* (2018). Local bond-slip curves are finally obtained by extracting the shear stresses in steel integration points adjacent to the steel bar surface at the location of the evaluated slip.

The local bond-slip curves

Local bond-slip curves at coordinates $x \approx 0$, $x = L/8$, $x = L/4$, $x = 3L/8$ and $x = L/2$ for steel stresses up to 400 MPa have been extracted from all of the analysed specimens in this study and plotted in Figure 11. Both CLLM and CHLM behaviour with specimen lengths corresponding to Figures 6–9 have been included in the plots. Figure 11 shows that the local bond-slip curves in general vary with the geometry of the RC tie. However, there are some significant resemblances. Except for the post-peak region, which occurs at relatively large steel stresses, the local bond-slip curves are seen to exhibit quite similar behaviour independent of the location over the bar length for a given geometry. The exceptions are the local bond-slip curves located in the vicinity of the primary crack ($x \approx 0$) owing to the combined formation of inclined and splitting cracks taking place here, as could be observed in Figure 4(b). This suggests that one local bond-slip curve is sufficient in describing the mean bond transfer for a certain RC tie. Moreover, the bond-slip curve includes the effect that the stiffness reduction of the confining concrete has on reducing the bond transfer due to internal cracking.

The local bond-slip curve proposed by Eligehausen *et al.* (1983) and later adopted by MC2010 (*fib*, 2013)

$$5. \quad \tau = \tau_1 \left(\frac{s}{s_1} \right)^\alpha$$

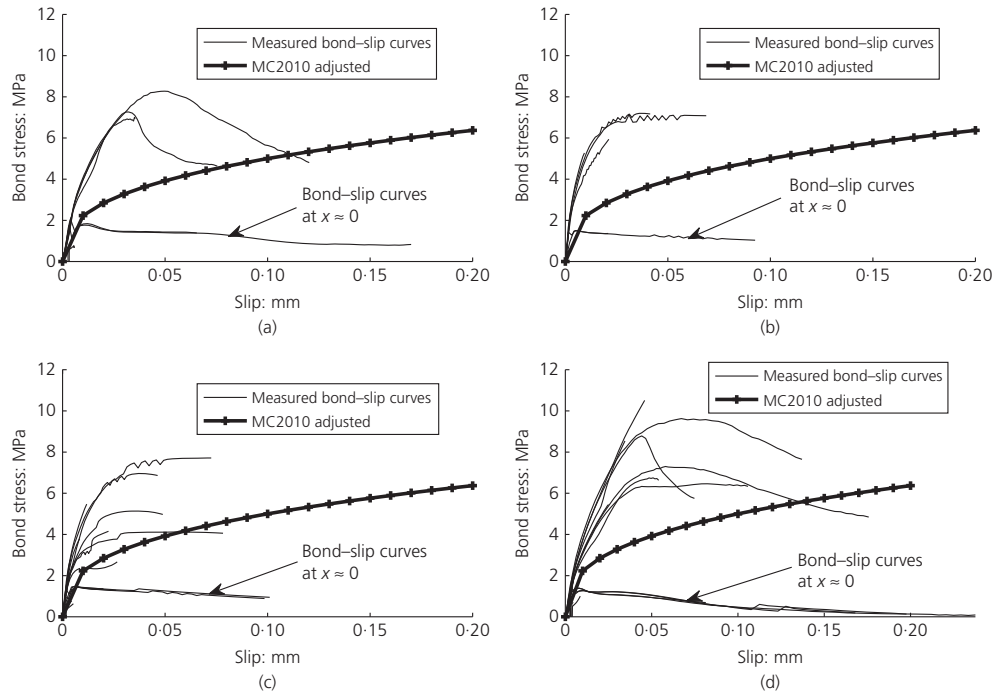


Figure 11. Local bond-slip curves for: (a) the ‘Bresler and Bertero’ specimens; (b) the ‘Yannopoulos’ specimens; (c) $\phi 20c40$ and $\phi 32c40$; (d) $\phi 20c90$ and $\phi 32c90$

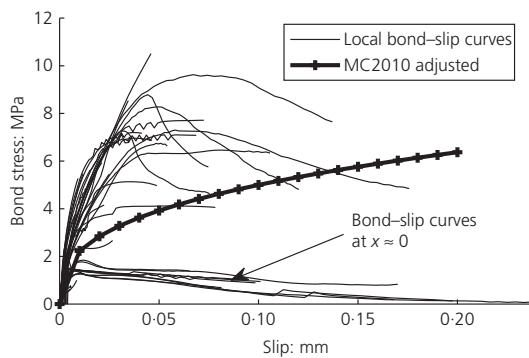


Figure 12. (a) Local bond-slip curves for all of the analysed specimens

is plotted with the parameters $\tau_1 = 5.0$ MPa, $s_1 = 0.1$ mm and $\alpha = 0.35$ in Figure 11, while Figure 12 shows all of the bond-slip curves obtained, plotted together with Equation 5. It is seen that the chosen parameters for Equation 5 tend to serve as a mean for all of the bond-slip curves obtained, irrespective

of geometry and location over the bar length. This has an important practical significance in the sense that only one bond-slip curve seems to be necessary in describing the average behaviour of an arbitrary RC tie. Moreover, solving the second order differential equation for the slip using the bond-slip curve in Equation 5 yields an analytical model that is capable of (i) replicating the NLFEA conducted in this paper and (ii) predicting consistent and conservative crack spacing and crack width. The latter is an approach the authors in this paper currently are developing.

Conclusions

Based on the findings in this study, the following conclusions can be drawn.

- The FE model used to conduct virtual experiments is based on the assumption that the concrete follows the longitudinal displacement field of steel at the interface, which has proven to predict the cracking behaviour of cylindrical RC ties quite accurately.
- Virtual experiments on four different RC ties show that the crack spacing can be proven mechanically to be a geometrically dependent parameter governed by the size

of the cover, and not the bar diameter. In physical experiments, however, the bar diameter could still have a substantial influence. This is due to the large scatter of the tensile strength, which will greatly influence the crack spacing and thus the interaction of the CLLM and CHLM behaviour.

- The cover size does not explicitly increase the crack width by itself, but contributes implicitly by increasing the crack spacing that the steel strains are integrated over. Larger crack spacing simply results in larger crack widths.
- Large bar diameters have a beneficial effect in reducing the steel stresses and the appurtenant steel strains, which in turn reduce the crack widths.
- A local bond–slip curve accounts for the effect that the stiffness reduction of the confining concrete has on the bond transfer due to internal cracking. Moreover, one bond–slip curve is sufficient to describe the average bond behaviour of an RC tie with arbitrary geometry. This has a practical significance that enables an analytical model capable of replicating the NLFEA results.

Acknowledgement

The work presented in this paper is part of an ongoing PhD study funded by the Norwegian Public Roads Administration as a part of the Coastal Highway Route E39 project.

REFERENCES

- ACI (American Concrete Institute) Committee (2001) *Control of Cracking in Concrete Structures (ACI 224R-01)*. ACI, Farmington Hills, MI, USA.
- Balázs GL (1993) Cracking analysis based on slip and bond stresses. *ACI Materials Journal* **90**(4): 340–348.
- Balázs GL, Bisch P, Borosnyói A et al. (2013) Design for SLS according to fib Model Code 2010. *Structural Concrete* **14**(2): 99–123.
- Barre F, Bisch P, Chauvel D et al. (2016) *Control of Cracking in Reinforced Concrete Structures: Research Project CEOS.fr (Civil Engineering and Geomechanics)*. ISTE Ltd, London, UK.
- Base GD, Read JB, Beeby AW and Taylor HPJ (1966) *An Investigation of the Crack Control Characteristics of Various Types of Bar in Reinforced Concrete Beams*. Cement and Concrete Association, London, UK, Research Report 18, Part 1.
- Beeby AW (1979) The prediction of crack widths in hardened concrete. *The Structural Engineer* **57A**(1): 9–17.
- Beeby AW (2004) The influence of the parameter ϕ/p_{eff} on crack widths. *Structural Concrete* **5**(2): 71–83.
- Belletti B, Damoni C, Hendriks MAN and de Boer A (2014) Analytical and numerical evaluation of the design resistance of reinforced concrete slabs. *Structural Concrete* **15**(3): 317–330.
- Borosnyói A and Snóbli I (2010) Crack width variation within the concrete cover of reinforced concrete members. *Építőanyag – Journal of Silicate Based and Composite Materials* **62**(3): 70–74.
- Bresler B and Bertero VV (1968) Behavior of reinforced concrete under repeated load. *Proceedings of the ASCE – Journal of the Structural Division* **94**(6): 1567–1590.
- Broms BB (1968) Theory of the calculation of crack width and crack spacing in reinforced concrete members. *Cement Och Betong* **1**: 52–64.
- Caldentey AP, Peiretti HC, Iribarren JP and Soto AG (2013) Cracking of RC members revisited: influence of cover, ϕ/p_{sef} and stirrup spacing – an experimental and theoretical study. *Structural Concrete* **14**(1): 69–78.
- CEB (Comité Euro-International du Béton) (1985) *CEB Design Manual on Cracking and Deformations*. École Polytechnique Fédérale du Lausanne, Lausanne, Switzerland.
- CEN (European Committee for Standardization) (2004) EN 1992-1-1 Eurocode 2: Design of concrete structures – Part 1-1: General rules and rules for buildings. European Committee for Standardization, Brussels, Belgium.
- Debernardi PG and Taliano M (2013) Effect of secondary cracks for cracking analysis of reinforced concrete tie. *ACI Materials Journal* **110**(2): 209–216.
- Debernardi PG and Taliano M (2016) An improvement to Eurocode 2 and fib Model Code 2010 methods for calculating crack width in RC structures. *Structural Concrete* **17**(3): 365–376.
- Diana FEA BV (2016) *DIANA Finite Element Analysis User's Manual Release 10.1*. Diana FEA BV, Delft, the Netherlands.
- Dörr K (1978) Bond-behaviour of ribbed reinforcement under transversal pressure. *Proceedings of IASS Symposium on Nonlinear Behaviour of Reinforced Concrete Spatial Structures*. Werner Verlag, Düsseldorf, Germany, vol. 1, pp. 13–24.
- Eligehausen R, Popov EP and Bertero VV (1983) *Local Bond Stress–Slip Relationships of Deformed Bars under Generalized Excitations*. University of California, Berkeley, CA, USA, Report No. UCB/EERC 83-23.
- Feenstra PH (1993) *Computational Aspects of Biaxial Stress in Plain and Reinforced Concrete*. PhD thesis, Delft University of Technology, Delft, the Netherlands.
- Ferry-Borges J (1966) *Cracking and Deformability of Reinforced Concrete Beams*. IABSE Publications, Zurich, Switzerland.
- fib (International Federation for Structural Concrete) (2000) *Bond of Reinforcement in Concrete – State-of-Art Report*. fib, Lausanne, Switzerland, fib bulletin no. 10.
- fib (2013) *fib Model Code for Concrete Structures 2010*. Wiley, Hoboken, NJ, USA.
- Gergely P and Lutz LA (1968) Maximum crack width in reinforced concrete flexural members. In *Causes, Mechanisms and Control of Cracking in Concrete* (Philleo RE (ed.)). American Concrete Institute, Farmington Hills, MI, USA, SP-20, pp. 87–117.
- Goto Y (1971) Crack formed in concrete around deformed tension bars. *ACI Journal* **68**(4): 244–251.
- Hendriks MAN, de Boer A and Belletti B (2017) *Guidelines for Nonlinear Finite Element Analysis of Concrete Structures (RTD:1016-1:2017)*. Rijkswaterstaat Centre for Infrastructure, Utrecht, the Netherlands.
- Hordijk DA (1991) *Local Approach to Fatigue of Concrete*. PhD thesis, Delft University of Technology, Delft, the Netherlands.
- Husain SI and Ferguson PM (1968) *Flexural Crack Width at the Bars in Reinforced Concrete Beams*. Center for Highway Research, The University of Texas at Austin, Austin, TX, USA, Research Report Number 102-1F.
- Jiang DH, Shah SP and Andonian AT (1984) Study of the transfer of tensile forces by bond. *ACI Journal* **81**(4): 251–259.
- Lutz LA (1970) Analysis of stresses in concrete near a reinforcing bar due to bond and transverse cracking. *ACI Journal* **67**(10): 778–787.
- Mirza SM and Houde J (1979) Study of bond stress–slip relationships in reinforced concrete. *ACI Journal* **76**(1): 19–46.
- Nilson AH (1972) Internal measurement of bond slip. *ACI Journal* **69**(7): 439–441.
- Russo G and Romano F (1992) Cracking response of RC members subjected to uniaxial tension. *Journal of Structural Engineering* **118**(5): 1172–1190.
- Saliger R (1936) High-grade steel in reinforced concrete. *Proceedings of the 2nd Congress of the International Association for Bridge and*

- Structural Engineering, Berlin-Munich, Germany*. ETH, Zürich, Switzerland, pp. 293–315.
- Somayaji S and Shah SP (1981) Bond stress versus slip relationship and cracking response of tension members. *ACI Journal* **78**(3): 217–225.
- Tammo K and Thelandersson S (2009) Crack behavior near reinforcing bars in concrete structures. *ACI Structural Journal* **106**(3): 259–267.
- Tammo K, Lundgren K and Thelandersson S (2009) Nonlinear analysis of crack widths in reinforced concrete. *Magazine of Concrete Research* **61**(1): 23–34, <https://doi.org/10.1680/mac.2009.61.1.23>.
- Tan R, Eileraas K, Opkvitne O *et al.* (2018) Experimental and theoretical investigation of crack width calculation methods for RC ties. *Structural Concrete*, <https://doi.org/10.1002/suco.201700237>.
- Watstein D and Mathey RG (1959) Width of cracks in concrete at the surface of reinforcing steel evaluated by means of tensile bond specimens. *ACI Journal* **56**(7): 47–56.
- Yannopoulos PJ (1989) Variation of concrete crack widths through the concrete cover to reinforcement. *Magazine of Concrete Research* **41**(147): 63–68, <https://doi.org/10.1680/mac.1989.41.147.63>.

How can you contribute?

To discuss this paper, please submit up to 500 words to the editor at journals@ice.org.uk. Your contribution will be forwarded to the author(s) for a reply and, if considered appropriate by the editorial board, it will be published as a discussion in a future issue of the journal.

Paper IIb

An investigation of the strain profile over the cover in reinforced
concrete elements subjected to tension

Tan, R., Hendriks, M.A.N. & Kanstad, T.

Proceedings for the 5th *fib* Congress, 7-11. Oct. 2018, Melbourne, Australia, ISBN 978-1-877040-14-6.

An investigation of the strain profile over the cover in reinforced concrete elements subjected to tension

Reignard Tan¹, Max A.N. Hendriks^{1,2} and Terje Kanstad¹

¹Norwegian University of Science and Technology, Department of Structural Engineering, Rich. Birkelandsvei 1A, 7491 Trondheim, Norway.

²Delft University of Technology, Faculty of Civil Engineering & Geosciences, Stevinweg 1, 2628CN Delft, the Netherlands.

Abstract:

The strain profile over the cover in reinforced concrete ties subjected to tension is investigated in this paper. This is normally neglected in the crack width calculation methods recommended by Eurocode 2 and *fib* Model Code 2010, meaning that it is assumed uniformly distributed over the cover. However, this assumption is questionable in the case of large covers. A pragmatic approach of accounting for the non-uniform strain profile over the cover in an analytical crack width calculation model can be by using the concept of the strain variation parameter ψ , which relates mean concrete strains over the cover to concrete strains at the steel bar surface at an arbitrary section over the bar length, x . Virtual experiments on six cylindrical concentrically reinforced concrete specimens were thus conducted by using nonlinear finite element analysis to establish a better understanding of the strain profile over the cover and, if possible, to obtain a proper value for $\psi(x)$. The results show that ψ more or less remains constant over the bar length, except for the region close to the loaded end. This means that assuming a constant value for ψ seems reasonable. The practical significance of this finding is that the non-uniform strain profile over the cover can be properly accounted for in deriving and solving the second order differential equation for the slip between concrete and steel. This would ultimately yield an analytical crack width calculation model that predicts crack widths consistently, also in cases for large covers and bar diameters.

Keywords: Crack width, FE-modelling, analytical calculations, strain profile, cover, large-scale concrete structures.

1 Introduction

The semi-empirical formulas for calculating crack widths recommended by Eurocode 2 (EC2) (CEN 2004) and *fib* Model Code 2010 (MC2010) (*fib* 2013) assumes a constant strain profile over the cover (CEB 1985). This implies that plane sections remain plane and that shear deformations over the cover are neglected, which contradicts the findings in *fib* bulletin 10 (2000) and Fantilli et al. (2007). Furthermore, the strain profile affects the equilibrium in determining the crack distance (CEOS.fr 2016, Tan & al. 2018). How it should be properly accounted for in an analytical crack width calculation model, however, is still not clear. The strain profiles over the cover are thus investigated in this paper by conducting virtual experiments on circular reinforced concrete (RC) ties concentrically reinforced with a steel bar using nonlinear finite element analysis (NLFEA).

This study is part of a research project that has an overall objective of improving crack width calculations specifically for large-scale concrete structures. Such structures are intended to be used at the “Ferry-free E39”, which is a coastal highway route along the West coast of Norway that involves several fjord crossings being up to several km long. The Norwegian Public Roads Administration guidelines

N400 (NPRA 2015) for design of bridge structures requires covers up to 120 mm in concrete structures exposed to marine environment. The semi-empirical formulas recommended by EC2 and MC2010, however, have a limited range of applicability and care should be taken when using these in predicting crack widths for large-scale concrete structures having large bar diameters and covers (Tan & al. 2018).

2 Strain distribution over the cover

The strain profile over the cover affects the equilibrium equations for the concrete in an RC tie (*fib* 2000) and becomes important in deriving and solving the second order differential equation for the slip. In such analytical crack width calculation model, elastic material laws are assumed for both concrete and steel, while a non-linear bond-slip law normally is used to account for the bond transfer between the materials (Balász 1993, Debernardi & Taliano 2016). A typical elastic concrete strain profile at an arbitrary section over the RC tie length in Fig. 1(a) is shown in Fig. 1(b). The concrete force resultant at an arbitrary section is thus expressed as

$$F_c(x) = \int_{A_c} \varepsilon_c E_c dA_c \quad (1)$$

where ε_c are concrete strains over the concrete area A_c and E_c is the Young's modulus. Note that an integral in Eq. (1) is necessary since the concrete strains typically are not uniformly distributed over the cover as depicted in Fig. 1(b). The integral in Eq. (1) can be conveniently solved in the ideal case of axisymmetry and if the concrete strain distribution over the concrete area is known. In most practical situations, however, this is not the case. A pragmatic approach can instead be formulated by assuming a relation between the strains at the interface between concrete and steel ε_{ci} , and the mean strains ε_{cm} over the concrete area A_c as

$$\psi(x) = \frac{\varepsilon_{cm}}{\varepsilon_{ci}} \quad (2)$$

This simplifies the integral in Eq. (1) to

$$F_c(x) = \varepsilon_{cm} E_c A_c = \psi(x) \varepsilon_{ci} E_c A_c \quad (3)$$

Edwards and Picard (1972) were the first to introduce the concept. They claimed that ψ remained constant over the entire RC length, which later became a paramount assumption that made it possible for Russo and Romano (1992) to solve the second order differential equation for the slip analytically when using a bond-slip law proposed by Eligehausen et al. (1983) and later adopted by MC2010. However, this assumption still needs more investigation. Not to mention, what a proper constant value for ψ would be since it seems reasonable that it varies with respect to the geometry of the RC tie.

3 Finite element model

NLFEA were carried out in the finite element (FE) program DIANA (DIANA FEA BV, 2016) using quadratic, axisymmetric, quadrilateral elements to account for the 3D behaviour of cylindrical RC ties. Geometry, boundary conditions and loading for the FE model were as shown in Fig. 1(a), while elastic material laws were assumed for both concrete and steel. The Poisson's ratio was neglected for concrete

($\nu_c = 0$), while a bond-slip power law proposed by Noakowski (1978) was used for the interface elements between concrete and steel to account for the non-linear bond transfer between the materials. This would yield an FE-model that is *partially* equivalent to the analytical crack width calculation model mentioned previously. Partially only, since the FE-model is a full 3D-model, while the analytical model can be considered a 1D-model that takes into account the 3D-effects by using a bond-slip model. The strain distribution over the cover in the two models though, should be equivalent.

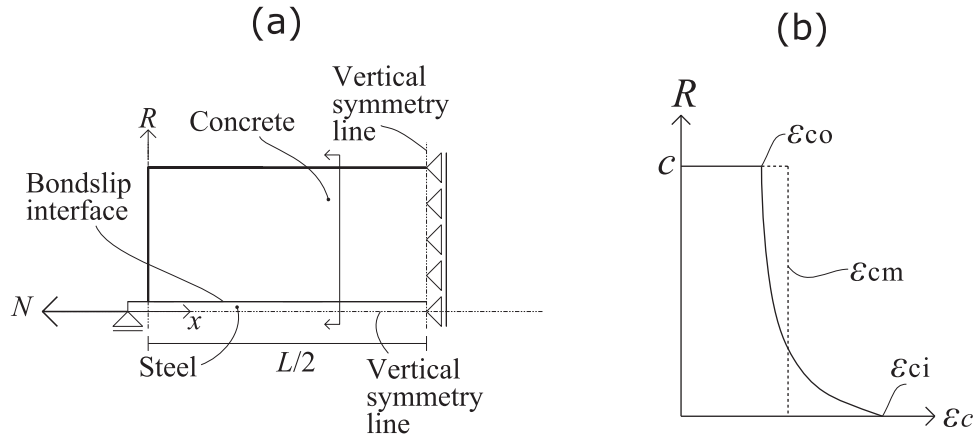


Fig. 1. (a) Geometry, boundary conditions and loading in the axisymmetric FE-model. (b) Typical strain distribution over the cover at an arbitrary section over the RC tie length.

The parameters in the bond-slip power law were adapted to fit the bond-slip law recommended by MC2010, but with adjusted parameters as $\tau_{bmax} = 6.0$ MPa, $s_1 = 0.1$ mm and $\alpha = 0.15$ to account for the tension behaviour of RC ties. The interface elements were chosen to have thickness $t_i = 0.1$ mm, with elastic radial and shear stiffness modulus derived from the modulus of elasticity for concrete E_c , i.e. respectively as E_c/t_i and $E_c/[2(1 + \nu_c)t_i]$. The element size was chosen so that 6-10 elements over the concrete cover and 1-3 elements over the steel bar radius were obtained. Loads in the steel bar ends were inflicted monotonically in a displacement controlled manner using regular Newton-Raphson iterations. The convergence criteria was force and energy based with tolerance values respectively as 0.01 and 0.001 in accordance to the Dutch Guidelines for NLFEA of Concrete Structures (Belletti & al. 2014, Hendriks & al. 2017).

4 Comparison with experiments

4.1 Test set-up

The classical experiments of Bresler and Bertero (1968) and Yannopoulos (1989) were benchmarked to investigate the credibility of the NLFEA. The cylindrical RC tie investigated by Bresler and Bertero (1968) was 152.4 mm in diameter, was concentrically reinforced with a 28.7 mm deformed steel bar, had a length of 406.4 mm and was cyclic loaded in the steel bar ends. A circumferential notch was cut at the mid-length of the specimen to induce cracking. Furthermore, steel strains along the bar length were measured by mounting strain gauges in a sawed-out canal at the centre of the embedded steel bar. The compressive strength, tensile strength and modulus of elasticity for concrete were respectively reported

as 40.8 MPa, 4.48 MPa and 33165 MPa, while the yield strength and modulus of elasticity for steel respectively were reported as 413 MPa and 205464 MPa.

The six cylindrical RC ties investigated by Yannopoulos (1989) were 76 mm in diameter, was concentrically reinforced with a 16 mm deformed steel bar and had a length of 90 mm. Loads were inflicted monotonically at the steel bar ends while measuring the development of the crack widths. The length of the specimen was chosen to avoid the formation of a new crack. The compressive strength, tensile strength and modulus of elasticity for concrete were respectively reported as 43.4 MPa, 3.30 MPa and 32000 MPa, while the yield strength and modulus of elasticity for steel were respectively reported as 424 MPa and 200000 MPa.

Only the modulus of elasticity and Poisson's ratio were used in the NLFEA since elasticity was assumed for both concrete and steel. The Poisson's ratio for steel was not reported in neither experiments, but was chosen as 0.30 in both benchmark analyses in accordance with the Dutch Guidelines for NLFEA of Concrete structures (Hendriks & al. 2017). The Poisson's for concrete was neglected as explained earlier.

4.2 Comparison of steel strains and crack widths

Steel strains obtained along the steel bar length in the experiments of Bresler and Bertero (1968) and the NLFEA are compared at four different load levels in Fig. 2(a). The steel strains corresponding to 33 MPa and 65 MPa are obtained from the first monotonic load cycle in the experiments, while the steel strains corresponding to 195 MPa and 242 MPa are obtained from the second load cycle in which a primary crack has formed at the mid-length. The steel strains in the NLFEA at the two highest load levels are thus obtained by modelling half the specimen length only, since a crack cannot form in the FE-model due to the assumption of elastic concrete. Nevertheless, the comparison of steel strains show in general good agreement.

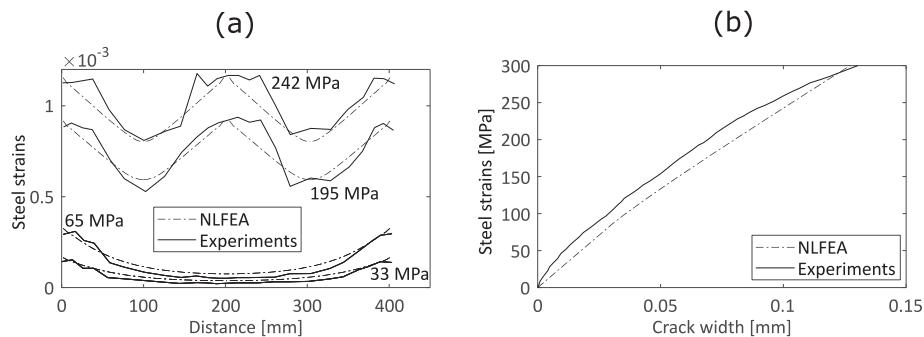


Figure 2. (a) Comparison of steel strains from the experiments of Bresler and Bertero (1968) and the NLFEA. (b) Comparison of the development of crack widths with increasing steel stresses from the experiments of Yannopoulos (1989) and the NLFEA.

The development of the crack widths with increasing steel stresses in the experiments of Yannopoulos (1989) and in the NLFEA are compared in Fig. 2(b). The resulting crack widths are obtained by subtracting the deformation at the outer concrete surface from the deformation at the steel bar surface at the specimen ends for a given steel stress. The comparison of the development of crack widths with steel stresses also shows good agreement.

The comparison of the experimental and NLFEA results shows that the FE-model is capable of simulating the behaviour of RC ties realistically, and this in a relatively simplified manner by using

elastic material laws and a local bond-slip curve proposed by Tan et. al (2018). This means that a study of the strain profile over the cover is reasonable by using the same FE-model.

4.3 Strain profile over the cover

The strain profile over the cover is now studied by using the results from the NLFEA of the Bresler and Bertero (1968) specimen. Figure 3(a) shows the strain profile over the cover at different locations over the bar length at the load level just before a crack forms at mid-length. A crack is assumed to form when the concrete force resultant becomes

$$F_c(s_r) = \int_{s_r} \tau(x) \pi \phi dx = f_{ctm} A_c \quad (4)$$

where s_r is the distance from the loaded end at which a crack forms, $\tau(x)$ is the bond stress distribution at a given load level obtained from the NLFEA, ϕ is the bar diameter size and f_{ctm} is the mean tensile strength of concrete. The dashed lines in Figure 3(a) indicate the corresponding mean strains in which the respective strain profiles have been averaged over the concrete area. It is observed that the strain profiles in general vary at different locations over the bar length.

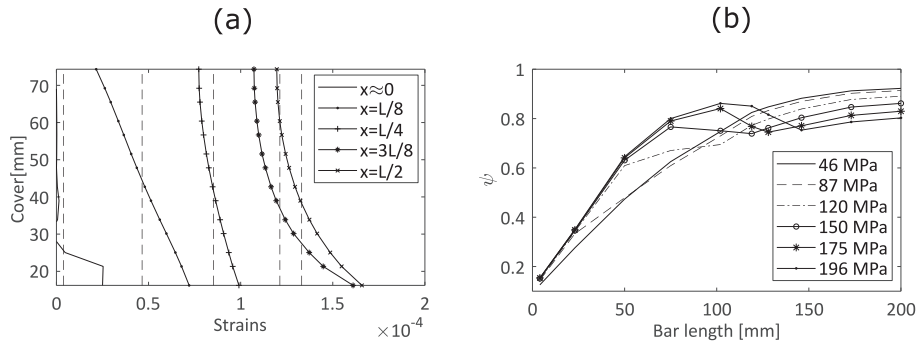


Fig. 3. (a) Strain distribution over the cover at different locations over the bar length at the load level just before a crack forms. (b) Comparison of ψ along the bar length at different load levels.

Figure 3(b) shows how ψ in general varies over the bar length at different load levels. It is immediately noticed though, that the load level does not influence ψ significantly. Furthermore, it is observed that ψ approaches a value of around 0.8 relatively close to the loaded end, especially for the load levels close to the load level at which a primary crack forms that in this case is at a steel stress of 196 MPa. This implies that ψ more or less remains constant over the bar length except for the region close to the loaded end.

4.4 Virtual studies of the strain profile over the cover

The validated FE-model is now used to conduct virtual studies on the strain profile over the cover with the purpose of determining a proper value for ψ . Four new specimens named $\phi 20c40$, $\phi 20c90$, $\phi 32c40$ and $\phi 32c90$ were investigated in addition to the specimens of Bresler and Bertero (1968) and Yannopoulos (1989). ϕ indicates that the bar diameter either is 20 mm or 32 mm, while c indicates that the cover either is 40 mm or 90 mm. A modulus of elasticity corresponding to a concrete grade of C35 according to MC2010 was used for the concrete, while the modulus of elasticity and the Poisson's ratio

respectively for steel were chosen as 200000 MPa and 0.30. The bond-slip curve for the interface elements was chosen similar to the previous.

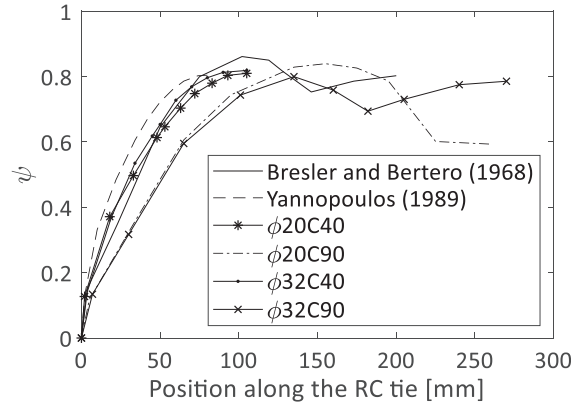


Fig. 4. ψ for all of the investigated specimens.

Fig. (4) shows ψ for the different specimens at the load level just before a crack forms in accordance to Eq. (4). It is noticed that ψ does not really exhibit a unique behaviour depending on the geometry of the specimen. In contrary, ψ appears to approach a similar value relatively close to the region at the loaded end. These observations justifies the important finding in Edwards and Picard (1972) of claiming that ψ remains constant along the bar length, irrespective of the geometry of the specimen and the load level. Finally, neglecting that the values goes towards zero at the loaded end yields that a constant value of $\psi = 0.70$ seems reasonable.

5 Discussions

Assuming a constant value for ψ has a practical significance in the sense that a non-uniform strain profile can be accounted for without explicitly assuming a certain distribution over the cover (*fib* 2000), which in Fig. 3(a) was observed to vary over the bar length. This is in particular practical for cross sections having the combination of large covers and large bar diameters that even may be in several layers or bundles, which is quite conventional in large-scale concrete structures. Assuming a strain distribution in such cases is certainly not straightforward and becomes impractical. Finally, a constant value for ψ provides that the second order differential equation for the slip can be solved analytically when using the bond-slip law according to MC2010. This would ultimately yield an analytical crack width calculation model that accounts for the effect of large covers and bar diameters more consistently compared to the formulation in EC2 and MC2010. The authors in this paper are currently working on such formulation.

6 Conclusions

The strain profile over the cover has been investigated in this paper by conducting virtual experiments on RC ties using NLFEA. The main purpose was to establish a better understanding and obtain a reasonable value for ψ , which describes the relation between mean concrete strains and concrete strains at the steel bar surface at an arbitrary section over the bar length. It was observed that ψ more or less

remained constant over the bar length except for a region close to the loaded end, irrespective of the geometry and the load level. Furthermore, virtual experiments on six different specimens showed that a constant value of ψ is reasonable. The practical significance of this finding is that the non-uniform strain distribution over the cover can be properly accounted for when deriving and solving the second order differential equation for the slip. This would ultimately yield an analytical crack width calculation model that predicts crack widths more consistently, also in cases of large covers and bar diameters.

Acknowledgement

The work presented in this paper is part of an ongoing PhD study funded by the Norwegian Public Roads Administration as a part of the Coastal Highway Route E39 project.

References

- Balász, G. L. (1993). "Cracking Analysis Based on Slip and Bond Stresses", *ACI Materials Journal*, 90(4), 340-348.
- Belletti, B., Damoni, C., Hendriks, M.A.N. et al. (2014). "Analytical and numerical evaluation of the design resistance of reinforced concrete slabs" *fib Journal Structural concrete*, 15(3), 317-330.
- Bresler, B. and Bertero, V.V. (1968). "Behavior of reinforced concrete under repeated load" *Proceedings of the ASCE – Journal of the Structural Division*, 94(6), 1567-1590.
- CEB Manual. (1985). "Cracking and Deformations", *École polytechnique fédérale de Lausanne*, Lausanne, Switzerland.
- CEN. (2004) EN-1992-1-1, "Eurocode 2, Design of concrete structures – Part 1-1: General rules and rules for buildings", Brussels, Belgium: CEN European Committee for Standardization.
- CEOS.fr. (2016) "Control of Cracking in Reinforced Concrete Structures", ISTE Ltd and John Wiley & Sons, Inc, London and Hoboken, UK and USA.
- Debernardi, P. G. and Taliano, M. (2016). "An Improvement of the Eurocode 2 and fib Model Code 2010 Methods for the Calculation of Crack Width in R.C Structures", *Structural Concrete Journal*, 17(3), 365-376.
- DIANA FEA BV. (2016). "DIANA Finite Element Analysis User's Manual Release 10.1", Delft, The Netherlands.
- Edwards, A.D., and Picard, A. (1972). "Theory of Cracking in Concrete Members", *Proceedings of the ASCE – Journal of the Structural Division*, 98(12), 2687-2700.
- Eligehausen, R., Popov, E.P. and Bertero V.V. (1983). "Local bond stress-slip relationships of deformed bars under generalized excitations", Report No. UCB/EERC 83-23, University of California, Berkeley, USA.
- Fantilli, A.P., Mihashi, H. and Vallini P. (2007). "Crack profile in RC, R/FRCC and R/HPFRCC members in tension", *Materials and Structures*, 40, 1099-1114.
- fib. (2000). "Bond of reinforcement in concrete – State-of-art report", *fib bulletin no. 10*, Lausanne, Switzerland.
- fib. (2013). "fib Model Code for concrete Structures 2010", Ernst & Sohn, Berlin.
- NPRA. (2015). "N400 Bruprosjektering: Prosjektering av bruer, ferjekaier og andre bærende konstruksjoner", N400 i Statens vegvesens håndbokserie, ISBN: 978-82-7207-680-0.
- Hendriks, M.A.N., de boer, A. and Belletti, B. (2017). "Guidelines for Nonlinear Finite Element Analysis of Concrete Structures", Rijkswaterstaat Centre for Infrastructure, Report RTD:1016-1:2017.
- Noakowski, P. (1978). "Die Bewehrung von Stahlbetonscheiben bei Zwangsbeanspruchung infolge Temperatur", *Deutscher Ausschluß für stahlbeton* 296.

- Russo, G., and Romano, F. (1992). "Cracking Response of RC Members Subjected to Uniaxial Tension", *Journal of Structural Engineering*, 118(5), 1172-1190.
- Tan, R., Eileraas, K., Opkvitne, O., et al. (2018). "Experimental and theoretical investigation of crack width calculation methods for RC ties", under review.
- Yannopoulos, P . J. (1989). *Variation of concrete crack widths through the concrete cover to reinforcement*. *Magazine of Concrete Research*, 41(147), 63-68, 1989.

Paper III

Analytical calculation model for predicting the cracking behavior of
reinforced concrete ties

Tan, R., Hendriks, M.A.N., Geiker, M. & Kanstad, T.

Accepted for publication at Journal of Structural Engineering, 2019

Analytical calculation model for predicting the cracking behavior of reinforced concrete ties

Reignard Tan¹, Max A.N. Hendriks^{1,2}, Mette Geiker¹, Terje Kanstad¹

¹NTNU, Norwegian University of Science and Technology, Department of Structural Engineering, Trondheim, Norway

²Delft University of Technology, Delft, the Netherlands

Abstract

This paper formulates an analytical calculation model for predicting the cracking behavior of reinforced concrete ties to provide more consistent crack width calculation methods for large-scale concrete structures in which large bar diameters and covers are used. The calculation model was derived based on the physical behavior of reinforced concrete ties reported from experiments and finite element analyses in the literature. The derivations led to a second order differential equation for the slip that accounts for the 3D effects of internal cracking by using a proper bond-slip law. The second order differential equation for the slip was solved completely analytically, resulting in a closed-form solution in the case of lightly loaded members and in a non-closed-form solution in the case of heavily loaded members. Finally, the paper provides a solution strategy to facilitate a practical and applicable method for predicting the complete cracking response. Comparison with experimental and finite element results in the literature demonstrated the ability of the calculation model to predict crack widths and crack spacing consistently and on the conservative side regardless of the bar diameter and cover.

Keywords

Crack widths, crack distances, analytical calculation model, bond-slip, RC ties, large-scale concrete structures.

1 Introduction

Predicting the cracking behavior of reinforced concrete (RC) structures consistently and accurately is not straightforward. This is reflected in the many approaches proposed in the literature (Borosnyói and Balázs 2005). Formulas based on empirical, semi-empirical, elastic analysis, and even fracture mechanics have all been proposed. Mechanical calculation models based on the internal cracking behavior of RC ties have also recently been proposed (Fantilli et al. 2007, Debernardi and Taliano 2016, Kaklauskas 2017).

The study presented in this paper is part of an ongoing research project with the overall objective of improving crack width calculation methods for the large-scale concrete structures planned for the coastal highway route “Ferry-free E39” in Norway. The Norwegian Public Roads Administration (NPRA) recommends that the design of such structures should follow

the guidelines provided in N400 (NPRA 2015), which state that the crack width calculation methods should be in accordance with the provisions in Eurocode 2 (EC2) (CEN 2004). However, Tan et al. (2018a) showed that the crack width formulas recommended by EC2 and the *fib* Model Code 2010 (MC2010) (*fib* 2013) predict the cracking behavior of structural elements inconsistently, particularly in cases of large covers and bar diameters. The analytical calculation model presented in this paper was based on solving the second order differential equation (SODE) for the slip when applying a bond-slip law first proposed by Eligehausen et al. (1983) and later adopted by MC2010. Other authors in the literature have used a similar approach (e.g. Russo and Romano 1992, Balász 1993, Debernardi and Taliano 2016), an approach which has recently been acknowledged in the state-of-the-art French research project CEOS.fr (2016) as an alternative way of calculating crack widths for large RC members. The main drawback in using this approach until now was the analytically complex solution of the SODE for the slip, thus resorting to numerical solution techniques instead and by that reducing the practical applicability of the approach. Moreover, the background of the SODE for the slip was never properly elaborated.

he aim of this research was to provide more realistic and consistent surface crack width calculation methods for large-scale concrete structures, where large covers in combination with large bar diameters in several layers and bundles are typically used, by deriving and solving the SODE for the slip completely analytically. First, the SODE for the slip was derived. Then, the SODE for the slip was solved analytically, after which a solution strategy for determining the complete cracking response was developed for the purposes of practical application. Finally, the application was demonstrated by comparing analytical predictions with experimental and finite element (FE) results reported in the literature.

The analytical model was derived using the concept of axisymmetry and applies first and foremost to such conditions. However, it will be shown that the model also has the ability to predict the cracking behavior of RC ties that deviate from such conditions by transforming an arbitrary cross section into an equivalent axisymmetric cross section. Moreover, predicting realistic and consistent surface crack widths is an important part of the structural design, and it might also be relevant for the aesthetics of a structure (Leonhardt 1988). On the other hand it is often argued that the crack width at the reinforcement appears more relevant in terms of durability. Predicting the latter, though, becomes rather complicated and was not addressed in this study.

2 The physical behavior of RC ties

A typical deformation configuration of RC ties according to several experimental studies reported in the literature (Watstein and Mathey 1959, Broms 1968, Husain and Ferguson 1968, Yannopoulos 1989, Beeby 2004 and Borosnyói and Snóbli 2010) is depicted in Fig. 1(a). Note that the crack width at the interface between concrete and steel $w_{cr,int}$ is considerably smaller than that on the concrete surface w_{cr} , which according to Goto (1972)

and Tammo and Thelanderrson (2009) is due to the rib interaction between concrete and steel. This causes the concrete to crack internally, which allows it to follow the displacement field of steel at the interface almost completely. This reported physical behavior formed the basis for ignoring the crack width at the interface in the FE model of Tan et al. (2018c). This imposed equal longitudinal displacements for concrete and steel at the interface as shown in Fig. 1(b), in which it should be noted that the crack width w_{cr} applies to the concrete surface only. The FE model was validated against the classical experiments of Bresler and Bertero (1968) and Yannopoulos (1989), where comparison of steel strains, the development of crack widths and the mean crack spacing showed good agreement. Furthermore, the FE model was also used to analyze cylindrical RC ties to better understand the cracking behavior. It was observed that the bond transfer at the interface caused radial displacements of the concrete, which in turn increased hoop stresses and strains. This resulted in internal splitting cracks and inclined cracks, depicted respectively as circles and straight lines in Fig. 1(b), when the principal stresses exceeded the tensile strength of the concrete. Moreover, deriving local bond-slip curves at different positions over the bar length showed that such curves include the effect that internal splitting and inclined cracks had on reducing the bond transfer. In other words, the local bond-slip curve describes how the 3D behavior of an RC tie affects the bond transfer. This shows that a single local bond-slip curve is sufficient to describe the mean bond transfer at the interface between concrete and steel for an arbitrary RC tie.

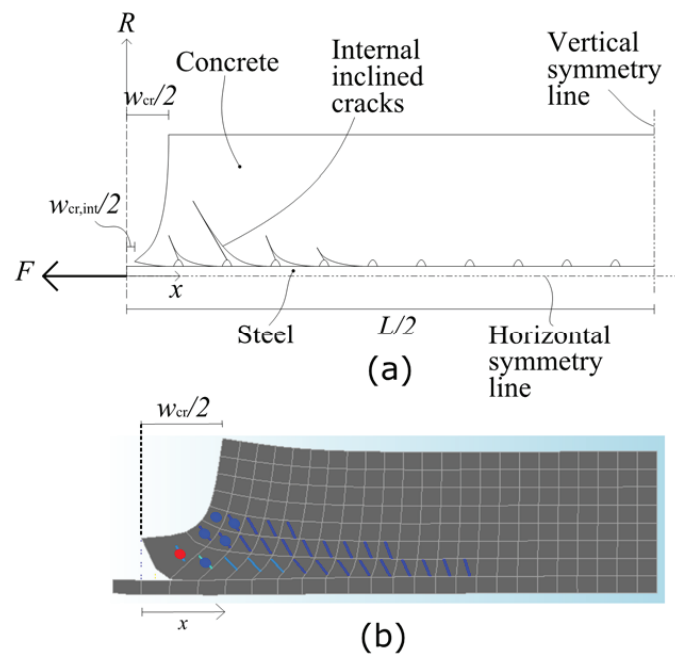


Fig. 1(a) Typical deformation configuration of RC ties with deformed steel bars observed in experiments. (b) FE model with assumptions in accordance with Tan et al. (2018c) showing a typical deformation configuration and crack plot, where straight lines indicate inclined internal cracks and circles indicate internal splitting cracks.

3 The mechanical crack width calculation model

3.1 Main assumptions

The analytical calculation model was derived based on the physical behavior of RC ties discussed in the previous section. However, some simplifications were made, and at first the concept of axisymmetry was also used for simplicity. Firstly, concrete and steel were both treated as elastic materials. Secondly, the nonlinearity of the internal cracking of the confining concrete was accounted for by lumping this behavior to the interface between the materials using a bond-slip law, i.e. claiming that the three sections in Fig. 2(a), (b) and (c) are statically equivalent. Note that a physical slip u occurs at the interface in Fig. 2(b) and (c) as a result of treating concrete and steel as elastic materials. This means that the total slip s_{tot} in the statically equivalent section in Fig. 2(c) is composed of two parts: the slip at the interface u caused by the formation of internal inclined cracks and the elastic deformations of the concrete caused by axial and shear deformations in the cover s_s . This also conforms to the definition of slip in *fib* bulletin 10 (2000). Assuming that the slip at the interface is equivalent to the deformation caused by internal inclined cracks implies in reality that the crack width at the interface can be ignored in the calculation model, so that the resulting crack width applies to the concrete surface. Furthermore, the Poisson's ratio for concrete can be ignored ($\nu_c = 0$) because the concrete is assumed to be exposed to heavy internal cracking as described in the previous section. Finally, the displacement field depicted in Fig. 3, which shows the deformed configuration of an arbitrary section in an RC tie subjected to loading at the rebar ends, can be assumed to apply for an arbitrary statically equivalent section.

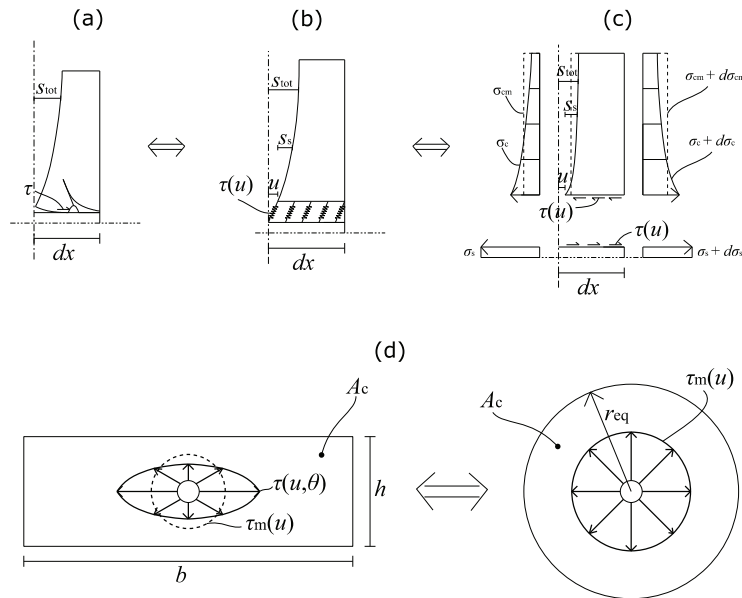


Figure 2(a) Internally cracked section typically observed in physical experiments. (b) The internal cracking behavior lumped as springs to the interface between concrete and steel. (c) Statically

equivalent section using a bond-slip law for the springs. (d) Equivalent cross sections when using the second order differential equation for the slip.

The continuum concept (Irgens 2008) is hereafter used to formulate the compatibility, material laws and equilibrium for concrete and steel.

3.2 Equations for concrete

3.2.1 General equations

The SODE for the concrete displacements was derived by using the cylindrical coordinates and the displacement field depicted in Fig. 3. Concrete strains at the interface ε_{ci} and the specimen surface ε_{co} were assumed to be related as

$$\psi(x) = \frac{\varepsilon_{co}}{\varepsilon_{ci}} \leq 1 \quad (1)$$

in which

$$\varepsilon_{ci} = \frac{dw_{ci}(x)}{dx} \quad (2)$$

and

$$\varepsilon_{co} = \frac{dw_{co}(x)}{dx} \quad (3)$$

where dw_{ci} and dw_{co} are differential displacements at the interface and at the specimen surface respectively. Note that the inequality in Eq. (1) is because the concrete strains at the specimen surface cannot exceed the concrete strains at the interface as a consequence of force being applied at the steel bar ends. The maximum longitudinal displacement of the concrete cover relative to the concrete interface is

$$-\Delta w_{cmax}(x) = w_{ci}(x) - w_{co}(x) \quad (4)$$

Moreover, longitudinal concrete displacements can be formulated as

$$w_c(R, x) = w_{ci}(x) + \Delta w_{cmax}(x) \bar{\psi}(R, x) \quad (5)$$

in which $\bar{\psi}$ is a shape function describing the variation in longitudinal displacements over the section and over the bar length. It was chosen to satisfy the following boundary conditions:

$$\begin{aligned} w_c(R_1, x) &= w_{ci}(x) \\ w_c(R_2, x) &= w_{co}(x) \end{aligned} \quad (6)$$

where R_1 and R_2 are the radial coordinates of respectively the interface and the specimen surface. It should be noted that Fig. 3 omits radial displacements for the concrete, while in the case of axisymmetry displacements in the hoop direction are non-existent. Omitting radial displacements contradicts the physical behavior of RC ties discussed previously, but using a bond-slip law $\tau(u)$, with τ denoting the bond stress, will take into account the 3D-effects that are excluded when radial displacements for the concrete are omitted. This means that Eq. (5) suffices in describing the displacement field for concrete. Now, using Green strains for small displacements yield the following non-zero components in the strain tensor for concrete:

$$\varepsilon_c = \frac{\partial w_c(R, x)}{\partial x} = \frac{dw_{ci}(x)}{dx} + \frac{\partial}{\partial x} [\Delta w_{cmax}(x) \bar{\psi}(R, x)] \quad (7)$$

$$\gamma_{cRx} = \gamma_{cR} = \frac{\partial w_c(R, x)}{\partial R} = \Delta w_{cmax}(x) \frac{d\bar{\psi}(R, x)}{dR} \quad (8)$$

where ε_c and $\gamma_{cRx} = \gamma_{cR}$ are longitudinal strains and engineering shear strains respectively. Consequently, Eq. (7) and (8), and ignoring the Poisson's ratio for concrete, yield the following non-zero components for the stress tensor:

$$\sigma_c = E_c \varepsilon_c \quad (9)$$

$$\tau_{cRx} = \tau_{cR} = \frac{1}{2} E_c \gamma_{cRx} \quad (10)$$

where σ_c and $\tau_{cRx} = \tau_{cR}$ are respectively the normal and the shear stresses, while E_c is the Young's modulus for concrete. Considering equilibrium for the concrete in Fig. 2(c) yields

$$\frac{dF_c(x)}{dx} = \tau(u) \sum \pi \phi_s \quad (11)$$

where τ is the bond stress dependent on the slip at the interface u , and $\sum \pi \phi_s$ is the total perimeter surrounding the steel bars in a cross section. The concrete force resultant can be formulated as

$$\psi(x) = \psi = \frac{\varepsilon_{cm}}{\varepsilon_{ci}} \leq 1 \quad (14)$$

in which

$$\varepsilon_{cm} = \frac{dw_{cm}(x)}{dx} = \psi \varepsilon_{ci} \quad (15)$$

are mean concrete strains and w_{cm} are mean displacements over the section, see Fig. 3, which in this particular case simplifies the shape function to

$$\bar{\psi} = 1 \quad (16)$$

Note that ψ in Eq. (14) is now assumed constant. Edwards and Picard (1972) were the first to introduce the concept of Eq. (14). This was later investigated more thoroughly by conducting nonlinear finite element analysis (NLFEA) on cylindrical RC ties in Tan et al. (2018b). It was concluded that although the shape function $\bar{\psi}$, first defined in Eq. (5) varied with respect to both R and x -coordinates over the bar length, the ratio in Eq. (14) remained more or less constant over the bar length except for a small region close to the loaded end. Actually, it was observed that a constant value of $\psi = 0.70$ over the entire bar length seemed reasonable independent of geometry and load level. The physical interpretation of Eq. (15) is that *plane sections that do not remain plane* are implicitly accounted for in determining the equilibrium. Now, replacing w_{co} with w_{cm} in Eq. (13) and inserting Eq. (14) and (16) simplifies the SODE for the longitudinal concrete displacements at the interface to

$$\psi A_c E_c \frac{d^2 w_{ci}(x)}{dx^2} = \tau(u) \Sigma \pi \phi_s \quad (17)$$

3.3 Equations for steel

Longitudinal displacements for steel were assumed uniform over its radius. And since the Poisson's ratio for concrete was ignored and axisymmetry applied for circular steel rebars means that Eq. (18)

$$w_s(R, x) = w_s(x) \quad (18)$$

suffices in describing the displacement field for steel. The following normal strain was thus the only non-zero component in the strain tensor when Green strains for small deformations were applied:

$$\varepsilon_s = \frac{dw_s(x)}{dx} \quad (19)$$

Moreover, the Poisson's ratio for steel was ignored ($\nu_s = 0$) as the lateral effects it had on bond were assumed to be included in the bond-slip curve. This led to the following normal stress being the only non-zero component in the stress tensor:

$$\sigma_s = E_s \varepsilon_s \quad (20)$$

where E_s is the Young's modulus for steel. The equilibrium of steel in Fig. 2(c) yields

$$\frac{dF_s(x)}{dx} = -\tau(u)\Sigma\pi\phi_s \quad (21)$$

Furthermore, the steel force resultant was obtained as

$$F_s(x) = \int_{A_s} \sigma_s dA_s = A_s E_s \frac{dw_s(x)}{dx} \quad (22)$$

when inserting Eq. (20) and (19) successively. Finally, inserting Eq. (22) in (21) yields

$$A_s E_s \frac{d^2 w_s(x)}{dx^2} = -\tau(u)\Sigma\pi\phi_s \quad (23)$$

which is the SODE for the steel displacements.

3.4 Compatibility

The slip was defined in terms of the displacement field depicted in Fig. 3 as

$$-u(x) = w_s(x) - w_{ci}(x) \quad (24)$$

Differentiating Eq. (24) once and inserting Eq. (2) and (19) provides the first derivative of the slip as

$$-u'(x) = \frac{dw_s(x)}{dx} - \frac{dw_{ci}(x)}{dx} = \varepsilon_s - \varepsilon_{ci} \quad (25)$$

3.5 The second order differential equation for the slip

Inserting Eq. (23) in (17) provides

$$\frac{d}{dx} \left[\frac{dw_{ci}(x)}{dx} + \xi \frac{dw_s(x)}{dx} \right] = 0 \quad (26)$$

where

$$\xi = \frac{\alpha_e \rho_s}{\psi} \quad (27)$$

$$\alpha_e = \frac{E_s}{E_c} \quad (28)$$

and

$$\rho_s = \frac{A_s}{A_c} \quad (29)$$

Inserting Eq. (25) and (23) successively in Eq. (26) yields the SODE for the slip as

$$\frac{d^2u(x)}{dx^2} - \chi\tau(u) = 0 \quad (30)$$

where

$$\chi = \frac{\sum \pi \phi_s}{A_s E_s} (1 + \xi) \quad (31)$$

By introducing

$$\zeta = \frac{\tau_m(u)}{\tau(u, \theta)} \leq 1 \quad (32)$$

where τ_m and $\tau(u, \theta)$ is respectively the mean and the maximum bond stress around the circumference of a steel bar in an arbitrary cross section, and further multiplying χ in Eq. (30) by ζ from Eq. (32) takes into account the bond stress τ not being constant around the circumference of the steel bar in non-axisymmetric cases, e.g. when the cover to the steel surface varies in a cross section as depicted in Fig. 2(d). In practice, this implies taking the distance between rebars into account, a parameter acknowledged by the research of Gergely and Lutz (1968) to be significant for the crack width. This means that the solution of Eq. (30) with χ multiplied by ζ from Eq. (32) involves transforming a cross section with an arbitrary geometry into a circular cross section with a radius r_{eq} such that the area A_c remains the same.

The analytical solution of Eq. (30) depends on the choice of the bond-slip law and a variety of choices can be found in the literature (Rehm 1961, Nilson 1972, Martin 1973, Dörr 1978, Mirza and Houde 1979, Hong and Park 2012). In this study, the local bond-slip law recommended by MC2010 was used:

$$\tau(u) = \tau_{\max} \left(\frac{u}{u_1} \right)^\alpha \quad (33)$$

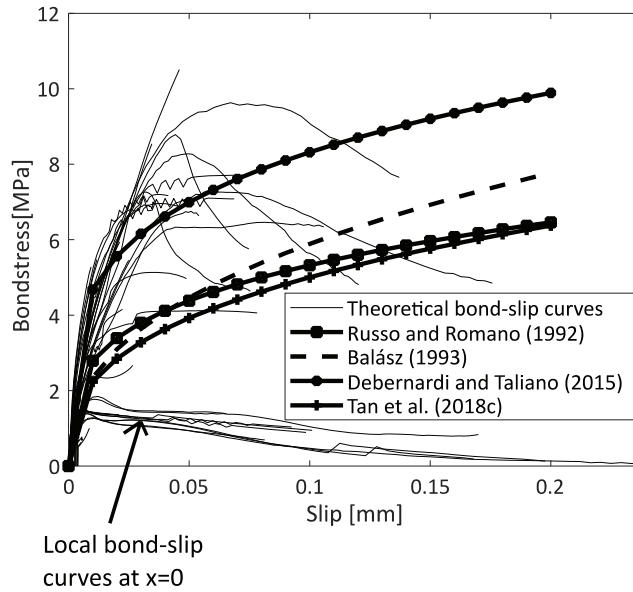


Figure 4. Local bond-slip curves according to Eq. (33) with adjusted parameters proposed by Russo and Romano (1992), Balász (1993), Debernardi and Taliano (2015) and Tan et al. (2018c) compared with theoretical local bond-slip curves obtained in the FE analysis of several RC ties at different positions over the bar length in Tan et al. (2018c).

Eq. (33) and its parameters were originally derived on the basis of pull-out tests of relatively short specimens, in which the concrete was in compression, thus differing considerably from the stress conditions in RC ties where the concrete is in tension (Pedziwiatr 2008). However, the investigation by Tan et al. (2018c) showed that Eq. (33) could be applied to represent the mean bond transfer over the specimen length by using the predefined parameters $\tau_{\max} = 5.0$ MPa, $u_1 = 0.1$ and $\alpha = 0.35$ when comparing it to the local bond-slip curves obtained from the FE analysis of several RC ties, see Fig. 4. Bond-slip curves proposed by other authors are also shown in the same figure. This means that inserting Eq. (33) in Eq. (30) finally yields the SODE

$$\frac{d^2u}{dx^2} - \chi \frac{\tau_{\max}}{u_1^\alpha} u^\alpha = 0 \quad (34)$$

Note that Eq. (34) has been derived and will be solved using the simplified equations for concrete.

4 The analytical crack width calculation model

4.1 General solutions

4.1.1 The slip

Eq. (34) is a non-linear homogenous SODE and can be solved analytically, by successively defining the second term as a function of the slip $f(u)$, moving it to the other side of the equal sign, multiplying both sides with the first derivative of the slip u' , applying the chain rule on the left-hand side of the equal sign and the substitution rule on the right-hand side, and subsequently integrating once, the first derivative of the slip is provided as

$$u' = \frac{du}{dx} = -\sqrt{2(\gamma u^\beta + C)} \quad (35)$$

where C is an integration constant and

$$\beta = 1 + \alpha \quad (36)$$

and

$$\gamma = \chi \frac{\tau_{\max}}{\beta u_1^\alpha} \quad (37)$$

Only the negative sign is included in Eq. (35) for compatibility with Eq. (25). Splitting the variables in Eq. (35) and integrating on both sides yields

$$x = B - \frac{1}{\sqrt{2}} \int (\gamma u^\beta + C)^{-\frac{1}{2}} du \quad (38)$$

where B is an integration constant. The integral can now be solved using the method proposed by Russo et al. (1990) and Russo and Romano (1992), where the binomial in Eq. (38) is developed as an infinite series of functions in accordance with Newton's binomial theorem, and then integrating each term. This results in two different general solutions that converge at distinct intervals

$$x = B_1 - \frac{1}{\sqrt{2}} \sum_{k=0}^{\infty} \binom{-\frac{1}{2}}{k} \gamma^k \left(\frac{1}{C}\right)^{\left(\frac{1}{2}+k\right)} \frac{u^{1+k\beta}}{1+k\beta} \text{ for } 0 < u < u_d \quad (39)$$

and

$$x = B_2 - \frac{1}{\sqrt{2}\gamma} \sum_{k=0}^{\infty} \binom{-\frac{1}{2}}{k} \left(\frac{C}{\gamma}\right)^k \frac{u^{\delta-k\beta}}{\delta-k\beta} \text{ for } u > u_d \quad (40)$$

where B_1 and B_2 are integration constants, and

$$\delta = \frac{1-\alpha}{2} \quad (41)$$

while

$$u_d = \left| \frac{C}{\gamma} \right|^{\frac{1}{\beta}} \quad (42)$$

is the value discerning Eq. (39) from (40). Note that the general solutions in Eq. (39) and (40) imply that the longitudinal coordinate x is a function of the slip value u as a consequence of splitting the variables in Eq. (35).

4.1.2 Strains

Successively inserting Eq. (2) and (19) in Eq. (26), integrating once, and applying $\varepsilon_{ci} = 0$ and $\varepsilon_s = F/E_s A_s = \varepsilon_{s0}$ at the loaded end, i.e. at $x = 0$, yields

$$\varepsilon_{ci} = \xi(\varepsilon_{s0} - \varepsilon_s) \quad (43)$$

Inserting Eq. (35) and (43) in Eq. (25) yields the steel strains

$$\varepsilon_s = \frac{\xi \varepsilon_{s0} + \sqrt{2(\gamma u^\beta + C)}}{1 + \xi} \quad (44)$$

while, inserting Eq. (44) in (43) provides the concrete strains

$$\varepsilon_{ci} = \xi \frac{\varepsilon_{s0} - \sqrt{2(\gamma u^\beta + C)}}{1 + \xi} \quad (45)$$

4.2 Boundary conditions

Boundary conditions must be established before calculating particular solutions. These are established by considering the concepts of *comparatively lightly loaded members* (CLLM) and *comparatively heavily loaded members* (CHLM) depicted in Fig. 5. Russo and Romano (1992) were the first to introduce these concepts, which were later acknowledged by *fib* bulletin 10 (2000). Briefly summarized, the main difference is that steel and concrete strains become compatible, $\varepsilon_s = \varepsilon_{ci}$, at a certain distance x_r from the loaded end in the case of CLLM, while the strains remain incompatible, $\varepsilon_s \neq \varepsilon_{ci}$, over the entire bar length in the case of CHLM. This further implies, in accordance with Eq. (24), that the slip becomes zero at distance x_r from the loaded end in the case of CLLM and at the symmetry section x_s in the case of CHLM. This yields the following boundary conditions in the case of CLLM behavior:

$$-u_r = 0 \quad (46)$$

$$-u'_r = \varepsilon_s - \varepsilon_{ci} = 0$$

at $x = x_r$, and in the case of CHLM behavior:

$$-u_s = 0 \quad (47)$$

$$-u'_s = \varepsilon_s - \varepsilon_{ci} > 0$$

at $x = x_s = \frac{L}{2}$.

4.3 Comparatively lightly loaded members (CLLM)

Applying the boundary conditions in Eq. (46) for Eq. (35) yields

$$C = 0 \quad (48)$$

Inserting Eq. (48) in (38), integrating once and applying the boundary conditions in Eq. (46) again yields the expression for the slip in the case of CLLM behavior

$$u = [\delta\sqrt{2\gamma}(x_r - x)]^{\frac{1}{\beta}} \quad (49)$$

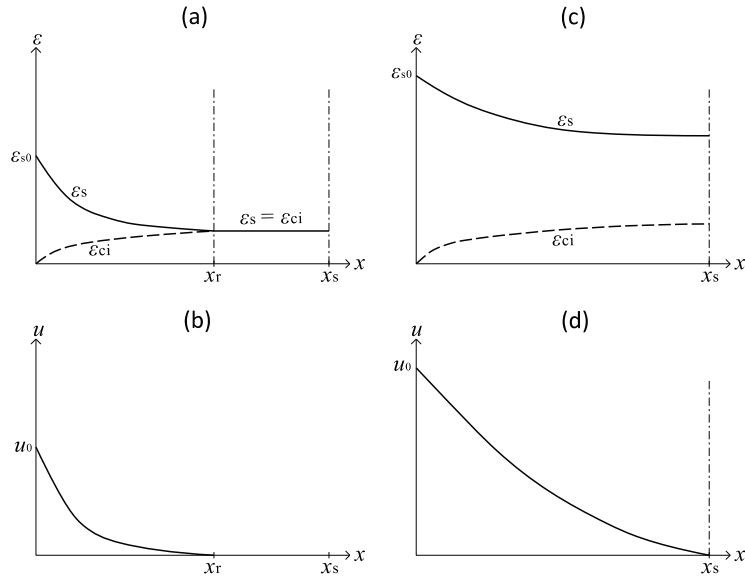


Figure 5(a) and (b) Strain and slip distribution in CLLM. (c) and (d) Strain and slip distribution in CHLM.

Inserting Eq. (48) in (44) and acknowledging that $\epsilon_s = \epsilon_{s0}$ at $x = 0$, provides the maximum slip at the loaded end as

$$u_0 = \left(\frac{\epsilon_{s0}^2}{2\gamma} \right)^{\frac{1}{\beta}} \quad (50)$$

Furthermore, inserting Eq. (50) in (49) for $x = 0$ yields the transfer length as

$$x_r = \frac{1}{\delta} \left[\varepsilon_{s0} \left(\frac{1}{2\gamma} \right)^{\frac{1}{2\delta}} \right]^{\frac{2\delta}{\beta}} \quad (51)$$

Note that the transfer length increases with increasing steel strains $\varepsilon_{s0} = F/E_s A_s$ at the loaded end. Expressions for the steel and concrete strains can be finally obtained by inserting Eq. (49) in respectively Eq. (44) and (45)

$$\varepsilon_s = \frac{\xi \varepsilon_{s0} + (2\gamma)^{\frac{1}{2\delta}} [\delta(x_r - x)]^{\frac{\beta}{2\delta}}}{1 + \xi} \quad (52)$$

$$\varepsilon_{ci} = \xi \frac{\varepsilon_{s0} - (2\gamma)^{\frac{1}{2\delta}} [\delta(x_r - x)]^{\frac{\beta}{2\delta}}}{1 + \xi} \quad (53)$$

One application of the particular solutions obtained could be in the case of two consecutive cracks formed with a considerable distance between them. This means that a certain region, $2(x_s - x_r)$, remains undisturbed as depicted in Fig. 5(a) and (b). This situation occurs typically in the so-called *crack formation stage*, in which the applied member load is relatively low and the distance between two consecutive cracks formed is relatively large.

4.4 Comparatively heavily loaded members (CHLM)

4.4.1 Particular solutions

Applying the boundary conditions in Eq. (47) in (35) yields

$$u'_s = -\sqrt{2C} \quad (54)$$

Acknowledging from Eq. (35) and Fig. 5 that u' is a real function yields

$$C > 0 \quad (55)$$

This means that the general solutions of Eq. (39) and (40) apply in the case of CHLM because $C \neq 0$. Now, inserting Eq. (35) in (25) and applying $\varepsilon_{ci} = 0$ and $\varepsilon_s = F/E_s A_s = \varepsilon_{s0}$ at the loaded end, i.e. at $x = 0$, yields

$$C = \frac{\varepsilon_{s0}^2}{2} - \gamma u_0^\beta \quad (56)$$

Furthermore, Eq. (55) and (56) imply that the maximum slip at the loaded end must satisfy

$$u_{0,\max} = \left(\frac{\varepsilon_{s0}^2}{2\gamma} \right)^{\frac{1}{\beta}} \quad (57)$$

Inserting Eq. (56) in (42) and acknowledging that Eq. (37) is a positive value provides

$$u_d = \left(\frac{\varepsilon_{s0}^2}{2\gamma} - u_0^\beta \right)^{\frac{1}{\beta}} \quad (58)$$

Now, applying the first condition in Eq. (47) to (39) yields

$$B_1 = \frac{L}{2} \quad (59)$$

Moreover, applying $u = u_0$ at $x = 0$ for Eq. (40) yields that B_2 can be expressed with binomial coefficients as

$$B_2 = \frac{1}{\sqrt{2\gamma}} \sum_{k=0}^{\infty} \binom{-\frac{1}{2}}{k} \left(\frac{C}{\gamma} \right)^k \frac{u_0^{\delta-k\beta}}{\delta - k\beta} \quad (60)$$

The particular solutions of Eq. (39) and (40) are now obtained using the integration constants in Eq. (56), (59) and (60). It should be noted, however, that the integration constants in Eq. (56) and (60) depend on the slip at the loaded end u_0 , so they must be obtained iteratively. This can be done conveniently by considering the two cases shown in Fig. 6.

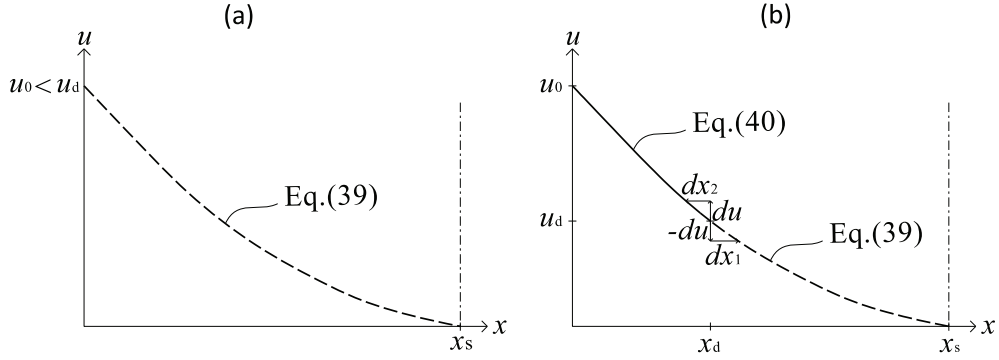


Figure 6(a) Case 1: solution for the slip using Eq. (39), i.e. $u_0 < u_d$. (b) Case 2: solution for the slip using Eq. (39) for $0 < u < u_d$ and Eq. (40) for $u_d < u < u_0$.

4.4.2 Case 1

The first case involves solving Eq. (39) with respect to the slip at the loaded end in its interval when $u_0 < u_d$ in accordance with Fig. 6(a). Inserting Eq. (59) in (39) and applying $u = u_0$ at $x = 0$ provides the function

$$f_1(u_0) = \frac{L}{2} - \frac{1}{\sqrt{2}} \sum_{k=0}^{\infty} \binom{-\frac{1}{2}}{k} \gamma^k \left(\frac{1}{C}\right)^{\left(\frac{1}{2}+k\right)} \frac{u_0^{1+\beta k}}{1+\beta k} = 0 \quad (61)$$

which is valid for the interval

$$0 \leq u_0 < \left(\frac{\varepsilon_{s0}^2}{4\gamma}\right)^{\frac{1}{\beta}} \quad (62)$$

when acknowledging that u_d in Eq. (39) is given by Eq. (58).

4.4.3 Case 2

Case 2 is where $u_0 > u_d$, which means that the solution for the slip u depends on both Eq. (39) and (40) due to the validity of the equations at its respective intervals, see Fig. 6(b). In other words, Eq. (39) is valid for slip values below u_d while Eq. (40) is valid for slip values above u_d . Now, accepting that Eq. (39) is valid for the slip value $u = u_d - du$ at the location $x_d + dx_1$ provides

$$x_d + dx_1 = \frac{L}{2} - \frac{1}{\sqrt{2}} \sum_{k=0}^{\infty} \binom{-\frac{1}{2}}{k} \gamma^k \left(\frac{1}{C}\right)^{\left(\frac{1}{2}+k\right)} \frac{(u_d - du)^{1+\beta k}}{1 + \beta k} \quad (63)$$

Similarly, accepting that Eq. (40) is valid for the slip value $u = u_d + du$ at the location $x_d - dx_2$ and inserting Eq. (60) provides

$$x_d - dx_2 = \frac{1}{\sqrt{2}\gamma} \sum_{k=0}^{\infty} \binom{-\frac{1}{2}}{k} \left(\frac{C}{\gamma}\right)^k \frac{u_0^{\delta-k\beta}}{\delta - k\beta} - \frac{1}{\sqrt{2}\gamma} \sum_{k=0}^{\infty} \binom{-\frac{1}{2}}{k} \left(\frac{C}{\gamma}\right)^k \frac{(u_d + du)^{\delta-k\beta}}{\delta - k\beta} \quad (64)$$

Note that du is an infinitesimal value for the slip, while dx_1 and dx_2 are infinitesimal values along the bar length in accordance with Fig. 6(b). Subtracting Eq. (64) from (63) provides the function

$$f_2(u_0) = \frac{L}{2} - \frac{1}{\sqrt{2}\gamma} \{f_{21}(u_0) - f_{22}(u_0)\} - \frac{1}{\sqrt{2}} f_{23}(u_0) - \Delta x = 0 \quad (65)$$

where

$$f_{21}(u_0) = \sum_{k=0}^{\infty} \binom{-\frac{1}{2}}{k} \left(\frac{C}{\gamma}\right)^k \frac{u_0^{\delta-k\beta}}{\delta - k\beta} \quad (66)$$

$$f_{22}(u_0) = \sum_{k=0}^{\infty} \binom{-\frac{1}{2}}{k} \frac{\left[\left(\frac{C}{\gamma}\right)^{\frac{k}{\delta-k\beta} + \frac{1}{\beta}} + du \left(\frac{C}{\gamma}\right)^{\frac{k}{\delta-k\beta}} \right]^{\delta-k\beta}}{\delta - k\beta} \quad (67)$$

$$f_{23}(u_0) = \sum_{k=0}^{\infty} \left(\frac{-\frac{1}{2}}{k} \right) \frac{\gamma^k \left[C^{\frac{2-\beta}{2\beta(1+k\beta)}} \left(\frac{1}{\gamma} \right)^{\frac{1}{\beta}} - du C^{-\frac{\frac{1}{2}+k}{1+k\beta}} \right]^{1+k\beta}}{1+k\beta} \quad (68)$$

and $\Delta x = dx_1 + dx_2$. Eq. (65) is valid for

$$u_0 > \left(\frac{\varepsilon_{s0}^2}{4\gamma} \right)^{\frac{1}{\beta}} \quad (69)$$

when acknowledging that u_d in Eq. (40) is given by Eq. (58).

4.4.4 Solution strategy

Russo and Romano (1992) give a convenient way of determining whether Case 1 or Case 2 governs by calculating Eq. (61) for a value of u_0 close to the upper limit value in Eq. (62),

e.g. as $u_{0\text{check}} = \left(\frac{\varepsilon_{s0}^2}{4\gamma} - du \right)^{\frac{1}{\beta}}$. Case 1 governs if the value calculated is negative. Case 2 governs if the value calculated is positive since the nature of Eq. (61) invokes that u_0 must increase to satisfy Eq. (61), which implies that Eq. (69) governs.

Newton-Raphson iterations are used to calculate the value of u_0 effectively after determining whether Case 1 or 2 governs

$$u_{0,i+1} = u_{0,i} - \frac{f_j(u_{0,i})}{f_j'(u_{0,i})} \quad (70)$$

where index i represents the number of iterations and index j represents the function in Eq. (61) for Case 1 or Eq. (65) for Case 2. Furthermore, it is suggested that an initial value of $u_{0,\text{init}} = \left(\frac{\varepsilon_{s0}^2}{4\gamma} \right)^{\frac{1}{\beta}} - du$ is used for Case 1 or $u_{0,\text{init}} = \left(\frac{\varepsilon_{s0}^2}{4\gamma} \right)^{\frac{1}{\beta}} + du$ is used for Case 2 to start the iterations in Eq. (70). The iterated value $u_{0,i+1}$, however, should never exceed Eq. (57) due to the requirement of Eq. (55). Convergence is achieved when $|u_{0,i+1} - u_{0,i}| < Tol$, at which Tol is a chosen tolerance value. Note that the derivatives of the functions in Eq. (61) and (65) are needed to solve Eq. (70) and are provided in Appendix A. Once the value of u_0 is obtained, the particular solutions of Eq. (39) and (40) are used to obtain the corresponding x values for the slip u along the bar length. In summary, CHLM involves determining whether Case 1 or 2 governs using Eq. (61) before the slip at the loaded end u_0 is calculated using Eq. (70).

4.4.5 Strains

The strain distributions for steel and concrete were obtained by using Eq. (44) and (45) respectively. Moreover, inserting Eq. (45) in (15), and acknowledging that the maximum concrete strains will occur at the symmetry section, i.e. where the slip $u = 0$, provides the maximum mean concrete strains as

$$\varepsilon_{cm,max} = \psi \xi \frac{\varepsilon_{s0} - \sqrt{2C}}{1 + \xi} < \varepsilon_{ct} \quad (71)$$

The violation of Eq. (71) implies that a crack has formed at the symmetry section, meaning a new member with length $L/2$ exists and that the CHLM response should be determined for the newly formed member.

4.5 Conditions at crack formation

The conditions at crack formation are shown in Fig. 7, where the transfer length increases with increasing load as highlighted for Eq. (51). The steel strain at the loaded end needed to extend the transfer length to the symmetry section is obtained by inserting $x_r = L/2$ in Eq. (51) so that

$$\varepsilon_{s0,S} = (2\gamma)^{\frac{1}{2\delta}} \left(\frac{L}{2} \delta \right)^{\frac{\beta}{2\delta}} \quad (72)$$

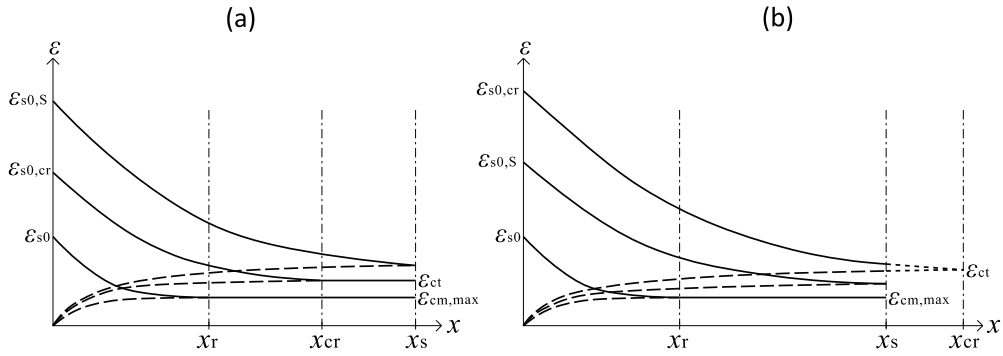


Figure 7(a) Condition 1. (b) Condition 2.

Furthermore, the maximum mean concrete strain at the end of the transfer length x_r is obtained by inserting Eq. (53) in (15) at $x = x_r$ so that

$$\varepsilon_{\text{cm,max}} = \frac{\psi\xi}{1+\xi} \varepsilon_{s0} \quad (73)$$

It is assumed that a crack forms when $\varepsilon_{\text{cm,max}} = \varepsilon_{\text{ct}}$, which means that the corresponding steel strain at the loaded end is

$$\varepsilon_{s0,\text{cr}} = \varepsilon_{\text{ct}} \frac{1+\xi}{\psi\xi} \quad (74)$$

So inserting Eq. (74) in (51) yields the distance from the loaded end at which a new crack can form or, expressed more rigorously, the *crack spacing*

$$x_{\text{cr}} = \frac{1}{\delta} \left[\varepsilon_{\text{ct}} \frac{1+\xi}{\psi\xi} \left(\frac{1}{2\gamma} \right)^{\frac{1}{2\delta}} \right]^{\frac{2\delta}{\beta}} \quad (75)$$

Eq. (72) to (75) are conceptually visualized in Fig. 7, providing two different conditions for the cracking response of a member. The continuous lines represent the steel strains, while the dashed lines represent the corresponding concrete strains. Note that the concrete strain for $\varepsilon_{s0,S}$ in Fig. 7(a) is unrealistic since the concrete tensile strength is exceeded. It is only included to elucidate the physical concept of Eq. (72). Condition 1 implies that a crack forms at a distance from the loaded end shorter than half the member length, i.e. $x_{\text{cr}} < x_S$, meaning that $\varepsilon_{s0,\text{cr}} < \varepsilon_{s0,S}$. This further implies that the cracking response of the member is governed by CLLM behavior as long $\varepsilon_{s0} < \varepsilon_{s0,\text{cr}}$, while CHLM behavior governs the cracking response as soon as $\varepsilon_{s0} > \varepsilon_{s0,\text{cr}}$. Condition 2 implies that a crack can form only at the symmetry section, $x_{\text{cr}} = x_S$, because $\varepsilon_{s0,\text{cr}} > \varepsilon_{s0,S}$. This means that a CLLM behavior governs the cracking response of the member as long $\varepsilon_{s0} < \varepsilon_{s0,S}$, while CHLM behaviour governs the cracking response as soon $\varepsilon_{s0} > \varepsilon_{s0,S}$. The physical interpretation of Condition 1 is that cracking can form at any location beyond x_r due to the unrestricted length of the member, while Condition 2 means that cracking can form only at the symmetry section due to the limited length of the member. Appendix B provides guidelines for determining which condition applies and whether CLLM or CHLM behavior governs the cracking response based on the a priori loading and the mechanical properties of the RC tie. For design purposes, however, only Condition 1 is relevant for determining the cracking response.

4.6 The crack width

Finally, the crack width is obtained as

$$w_{\text{cr}} = 2 \int_{x_r} (\varepsilon_s - \varepsilon_{\text{cm}}) dx \quad (76)$$

Inserting Eq. (15), (44) and (45) in Eq. (76) yields

$$w_{\text{cr}} = 2 \left(\frac{1}{1 + \xi} \right) [\xi \varepsilon_{s0} x_r (1 - \psi) + u_0 (1 + \psi \xi)] \quad (77)$$

In summary, the crack width is a function of the applied load $\varepsilon_{s0} = F/A_s E_s$, the transfer length x_r , and the slip at the loaded end u_0 . For design purposes, i.e. Condition 1, the crack width is determined by calculating u_0 and x_r , which in the case of CLLM behavior is obtained by the closed-form solutions in Eq. (50) and (51). A solution strategy is provided in subsection 4.4.4 to calculate u_0 efficiently in the case of CHLM behavior, but here x_r is replaced with $\frac{x_{\text{cr}}}{2}$, where x_{cr} is the crack spacing obtained using the closed-form solution in Eq. (75). Note that the crack width obtained w_{cr} applies to the face at the loaded rebar end, i.e. as depicted in Fig. 1. This means that the calculation model conservatively assumes that a crack has been formed before loading, which allows for predicting crack widths regardless of the load level.

4.7 Comparison with equivalent calculation models

The calculation model described was evaluated against the equivalent models proposed by Russo and Romano (1992), Balász (1993) and Debernardi and Taliano (2016). The models are equivalent in the sense that the SODE for the slip, i.e. Eq. (34), is solved. However, some significant differences should be highlighted. The models of Balász (1993) and Debernardi and Taliano (2016) neglect the elastic shear deformation over the cover, i.e. they assume $\psi = 1$ in Eq. (14). Another significant difference in Debernardi and Taliano (2016) is that the bond stress distribution over the bar length is altered locally by using a linear descending branch close to the primary crack, which complicates the solution of Eq. (34). These authors assume that internal inclined cracks form in this region and continue to form towards the symmetry section as the load increases. The FE analysis by Lutz (1970) and by Tan et al. (2018c) on RC ties show that a build-up of bond stresses occurs close to a primary crack and that the peak of the bond stress distribution tends to move towards the symmetry section as the load increases, as assumed by Debernardi and Taliano (2016). However, this physical phenomenon is a consequence not of internal inclined cracks, but of internal splitting cracks forming close to the primary crack, which is reflected by the characteristic bond-slip curves at $x \approx 0$ in Fig. 4. In fact, the FE analysis showed that internal inclined cracks also formed beyond the bond stress distribution peak, which means they cannot occur in direct conjunction with the descending branch alone. This also means that a single bond-slip curve should suffice to represent the mean local bond-slip behavior over the bar length, as shown in Fig. 4 and

discussed in Section 2, and should already include the total effect of both internal splitting and internal inclined cracks have on reducing the bond transfer.

The calculation model presented in this paper was particularly inspired by the work of Russo and Romano (1992). However, there are some significant differences: (i) a primary crack is assumed to form when, $\varepsilon_{cm} = \varepsilon_{ct}$, implying that concrete stresses are unevenly distributed even at the zero-slip section in accordance with the observations in Fantilli et al. (2008) and Tan et al. (2018b); (ii) the influence of the distance between steel bars can be accounted for by Eq. (32); and (iii) a completely analytical solution strategy is provided to solve Eq. (34) for practical applications. In addition, the derivations using continuum mechanics formulation yield a mechanically sound model that describes how the 3D behavior of RC ties can be simplified into a 1D model when using a proper bond-slip law. However, the main advantage of the model presented in this paper, and that of Russo and Romano (1992), is that Eq. (34) is solved completely analytically, in contrast to Balász (1993) and Debernardi and Taliano (2016), who only provide analytical solutions in the case of CLLM behavior.

Using the bond-slip curve recommended by Tan et al. (2018c) implies that the bond stresses should be related to the deformations in the outer surface of the concrete rather than at the steel-concrete interface, which contradicts the compatibility in Eq. (24). However, the elastic shear deformation over the cover is normally considered to be negligible, although it does seem to affect the elastic stress and strain distribution (Braam 1990, Tan et al. 2018b). This justifies the combined use of the chosen bond-slip curve, the compatibility in Eq. (24), and the concept of ψ in Eq. (14).

5 Application

5.1 Comparison with axisymmetric RC ties

5.1.1 General

This section compares strains and crack widths obtained analytically with the classical experiments of Bresler and Bertero (1968) and Yannopoulos (1989), and the FE analysis of Tan et al. (2018c) on cylindrical RC ties concentrically reinforced with a steel bar loaded at the steel bar ends. The bond-slip parameters, $\tau_{max} = 5.0$ MPa, $u_1 = 0.1$ mm and $\alpha = 0.35$ were chosen, while $\psi = 0.70$ was adopted in accordance with Tan et al. (2018b). The factor $\zeta = 1$ was chosen due to axisymmetry. The infinite series used for calculating the response in the case of CHLM behavior was truncated after 10 terms, while the parameters $\Delta x = 0.1$ and $du = 5.8 \cdot 10^{-5}$ were chosen in accordance with Russo and Romano (1992).

5.1.2 Comparison with experimental data

Bresler and Bertero (1968) measured the strain distribution over the bar length by mounting several strain gauges in a groove cut along the center of several reinforcing steel bars. The reinforcing steel bars were first cut longitudinally into two halves, after which the groove was

milled along the center of the two parts. After mounting the strain gauges in this groove, the two halves were tack-welded together to minimize the impact on the exterior of the reinforcing bars. The specimen investigated, denoted “Specimen H”, was 406.4 mm (16 in) long and 152.4 mm (6 in) in diameter concentrically reinforced with a 28.7 mm (1.13 in) deformed steel bar. The length of the specimen was chosen as twice the mean crack spacing of 203.2 mm (8 in) obtained from pilot studies conducted on 1829 mm (72 in) long RC ties with similar sectional properties. A notch was cut around the circumference at mid-length to induce cracking here. The compressive strength, tensile strength, and Young’s modulus for the concrete were reported as respectively 40.8 MPa (5.92 ksi), 4.48 MPa (0.65 ksi), and 33165 MPa (4810 ksi), while the yield strength and Young’s modulus for the steel were reported as 413 MPa (60 ksi) and 205464 MPa (29800 ksi) respectively. The reduction of the steel area due to the groove was taken into account in the analytical calculations by using the reported steel area $A_s = 548 \text{ mm}^2$ (0.85 in²), while the notch was taken into account by reducing the reported tensile strength by a factor of 0.7. This led to cracking at mid-length in the analytical calculations for higher load levels as shown in Fig. 8(a). It should be noted that the analytical steel strains represent the mean of the experimental steel strains.

The six specimens investigated by Yannopoulos (1989) were 76 mm in diameter concentrically reinforced with a 16 mm deformed steel bar and were 100 mm long. The length of the specimens was based on the mean crack spacing of 90 mm obtained from pilot studies conducted on 800 mm long RC ties with similar sectional properties and was chosen to prevent new cracks from forming between the loaded ends. The compressive strength, tensile strength, and Young’s modulus for concrete were reported respectively as 43.4 MPa, 3.30 MPa and 32000 MPa, while the yield strength and Young’s modulus for steel were reported as 424 MPa and 200000 MPa respectively. The specimen length in the analytical calculations was chosen to be similar to that in the experiments. Fig. 8(b) shows the average crack width development at the loaded ends reported for the six specimens investigated. The analytical calculations predicted slightly larger crack widths. Nevertheless, the comparison shows good agreement.

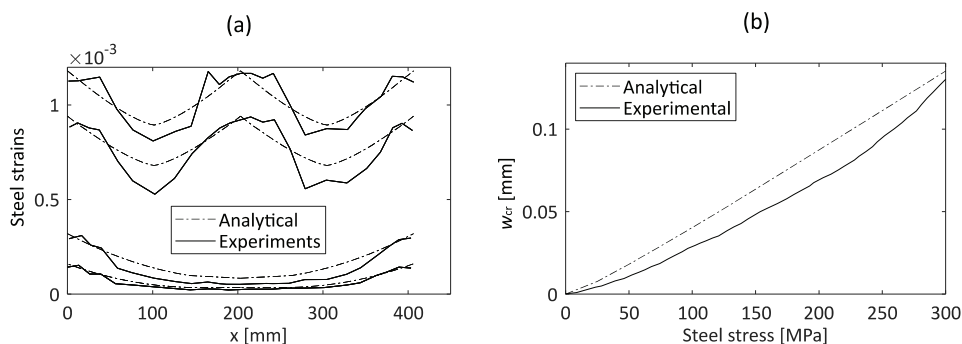


Figure 8(a) Comparison of steel strains predicted with steel strains reported in the experiments of Bresler and Bertero (1968) over the bar length. (b) Comparison of crack widths predicted with crack

widths reported in the experiments of Yannopoulos (1989) using similar specimen length $L = 100 \text{ mm}$ similar to that in the experiments.

5.1.3 Comparison with FE analysis

Tan et al. (2018c) conducted NLFEA on four cylindrical RC ties denoted $\phi 20c40$, $\phi 32c40$, $\phi 20c90$, and $\phi 32c90$ using axisymmetric elements, with ϕ and c respectively indicating steel bar diameter and cover. The concrete was given material properties corresponding to a concrete grade C35 in accordance with MC2010 and a non-linear fracture mechanics material model based on total strain formulation with rotating cracks. The crack bandwidth was chosen to be dependent on the total area of the finite elements in line with the smeared crack approach. The steel was chosen to have linear elastic material properties with a Young's modulus of 200000 MPa and a Poisson's ratio of 0.3. Furthermore, interface elements were used to allow for radial separation but no physical slip, as depicted in Fig. 1(b). In summary, the approach implied smearing out internal inclined and splitting cracks that would have localized at the tip of each bar rib if they were modelled discretely. This was found to give good agreement in comparison with the steel strains, development of crack widths, and mean crack spacing observed in the experiments.

Table 1. Comparison of crack spacing predicted with mean crack spacing reported in the experiments of Bresler and Bertero (1968) and Yannopoulos (1989), and the FE analysis of Tan et al. (2018c).

	Experimental and FE analysis	Predicted
RC tie	Mean [mm]	Analytical [mm]
Bresler and Bertero (1968)	203	301
Yannopoulos (1989)	90	181
$\phi 20c40$	105	224
$\phi 32c40$	109	207
$\phi 20c90$	260	470
$\phi 32c90$	272	434

Fig. 9 shows the comparison of steel strain distributions over the bar lengths at three different stress levels for the specimens, again noting that the analytical model predicts the mean of the experimental steel strains. The first stress level shows the CLLM behavior just before a crack forms at a certain distance from the loaded end, while the two higher stress levels show the

CHLM behavior for specimen lengths similar to the crack spacing obtained in the FE analysis, see Table 1. Note that the strain distribution is shown for only half the specimen length due to symmetry. In general, the analytical calculations make conservative predictions of the CLLM behavior, which also is reflected in the comparison of the predicted crack spacing in Table 1. The table also shows that the analytical model predicts crack spacing consistently and on the conservative side regardless of the bar diameter and cover size. The conservative prediction of the crack spacing can be attributed to the bond-slip parameters chosen. Fig. 10 shows the development of crack widths in specimens with lengths similar to the FE analysis crack spacing in Table 1 and indicates that the analytical model makes quite accurate predictions of crack widths for a given specimen length.

Fig. 11 shows comparisons of the development of crack widths based on specimen lengths similar to the crack spacing predicted by the analytical model in Table 1. The analytical model yields Condition 2 and CHLM behavior in general, which allows for cracking at mid-length at higher load levels and occurs for all of the specimens except $\phi 20c90$. The graphs also show that the analytical model predicts crack widths on the conservative side in general.

5.2 Comparison with non-axisymmetric RC ties

The French research project CEOS.fr (2016) conducted experiments on two identical quadratic RC ties identified as Ties 4 and 5 which were pulled in tension. The ties were 355 mm in width and height, had a length of 3200 mm, and were reinforced with eight 16 mm rebars. A concrete grade C40/50 was used, while the yield strength and Young's modulus of steel were reported as 529 MPa and 200000 MPa respectively. The cover to the rebars was 45 mm. Fig. 12(a) shows a comparison of the development of predicted crack widths with the maximum crack widths measured. The analytical calculations were based on using specimen lengths similar to the crack spacing predicted analytically in Table 2. The factor $\zeta = 1$ was chosen for simplicity. The deviation between Tie 4 and Tie 5 in the maximum crack widths measured seems to be due to the difference in maximum crack spacing reported in Table 2. Nevertheless, the maximum crack spacing predictions were conservative, and the crack widths predicted show relatively good agreement with the maximum crack widths measured.

Tan et al. (2018a) conducted experiments on eight quadratic RC ties identified as $X-\phi-c$, where X represents the loading regime the RC tie was exposed to, either at the crack formation stage (F) or the stabilized cracking stage (S), while ϕ and c represent the rebar diameter and cover respectively. The rebar diameter was either 20 mm or 32 mm, while the cover was either 40 mm or 90 mm. The ties were 400 mm in width and height, had a length of 3000 mm, and were reinforced with eight rebars. The concrete compressive and tensile strength were reported as 74.3 MPa and 4.14 MPa respectively, while the Young's modulus was reported as 27.4 GPa. The yield strength and Young's modulus of the steel were reported as 500 MPa and 200000 MPa respectively. Fig. 12(b) shows the comparison of maximum crack widths measured $w_{0.95}$ and crack widths predicted w_{cr} using the concept of modelling uncertainty, i.e. as $\theta = w_{0.95}/w_{cr}$.

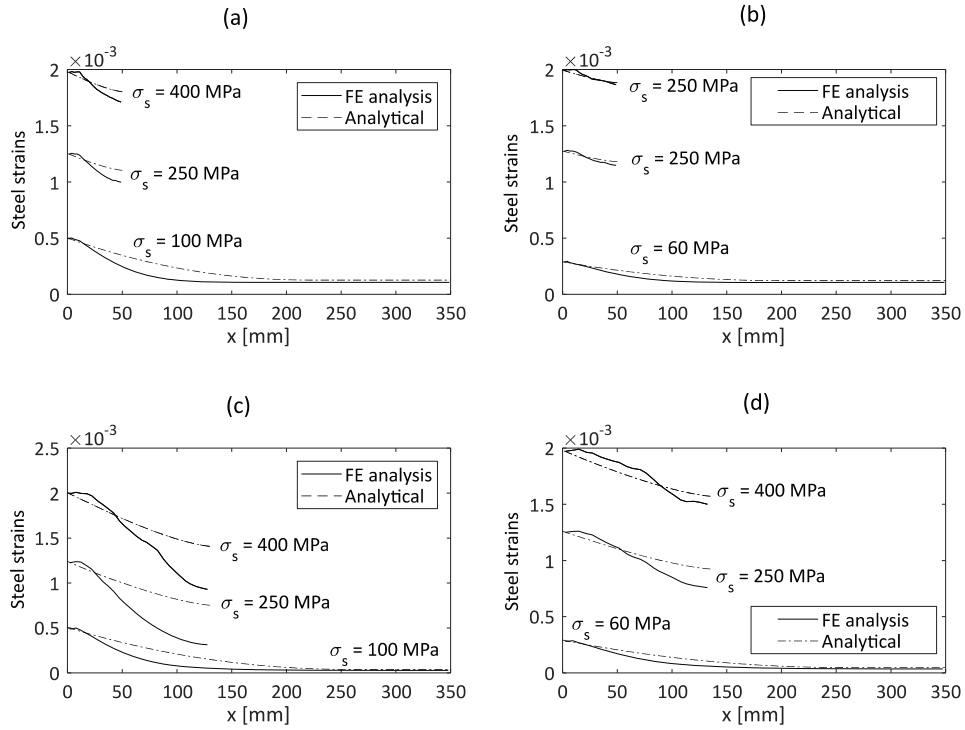


Figure 9. Comparison of steel strains predicted with steel strains reported over the bar length in the FE analysis of Tan et al. (2018c). (a) Specimen $\phi 20c40$. (b) Specimen $\phi 32c40$. (c) Specimen $\phi 20c90$. (d) Specimen $\phi 32c90$.

Table 2. Comparison of crack spacing predicted with crack spacing reported in the experiments of CEOS.fr (2016) and Tan et al. (2018a).

RC tie	Experimental		Predicted
	Mean [mm]	Maximum [mm]	Analytical [mm]
Tie 4	160	257	370
Tie 5			
S-20-40	163	250	422
S-32-40	178	240	361
S-20-90			
S-32-90			

6 Discussion

The conservative predictions of the crack widths in Fig. 11 are due to the nature of Eq. (75), which, together with the predefined bond-slip parameters, provides an upper limit for the crack spacing or, expressed more rigorously, for the maximum crack spacing. This is equivalent to the concept of calculating the maximum crack widths according to the semi-empirical formulas in EC2 and MC2010. However, unlike EC2 and MC2010, Eq. (75) is not assumed to vary from once to twice this value. Furthermore, Figs. 8b) and 10 show the ability of the model to predict accurate crack widths given a specimen length. The observations in Figs. 8a) and 9 suggest that the analytical model can predict the mean behavior of experimental steel strains, which is a direct result of using just one local bond-slip curve to represent the bond transfer over the specimen length. This means that the effect internal inclined and splitting cracks has on reducing the bond transfer locally is smeared over the specimen length in the analytical model. The consequence of using only one local bond-slip curve is that the bond stresses reach their maximum at the cracked section ($x = 0$), which contradicts the physical behavior of RC ties discussed previously. This is due to the fact that the selected bond-slip curve causes bond stresses to increase with increasing slip as can be observed in Fig. 4. This is elucidated in Fig. 13, which shows the corresponding bond stresses to the steel strains predicted in Fig. 9. One solution to this problem would be to use different bond-slip curves depending on the location over the specimen length, but this would substantially complicate the solutions to the analytical model. So, the use of just one local bond-slip curve provides a practical yet mechanically sound calculation model that has proven capable of predicting the development of crack widths and crack spacing consistently and on the conservative side, regardless of the mechanical properties and loading of the RC ties. Another advantage of using a bond-slip curve, as opposed to assuming a constant bond stress distribution e.g. in EC2 and MC2010, is that the mean bond stresses become dependent on the load level and the geometry of RC tie, thus conforming to the theoretical observations made by Tan et al. (2018c). This should provide more realistic predictions of the crack spacing.

Fig. 14 shows the corresponding concrete strains at the interface, ε_{ci} , to the steel strains predicted in Fig. 9 at load levels 250 MPa and 400 MPa, whereas the dashed lines represent the resultant of concrete strains in a section according to Eq. (15), i.e. as $\varepsilon_{cm} = \psi\varepsilon_{ci}$. It is observed that both the concrete stresses at the interface and the resultants of concrete stresses increase with increasing load level. This is due to the increase of the bond transfer between the load levels of 250 MPa and 400 MPa as represented by the increase of the areas under the curves shown in Fig. 13. Furthermore, this would cause a crack to form at the zero-slip section even in the case of CHLM behavior if the mean concrete strains exceed the tensile strength of concrete, as shown in Fig. 11. This conforms to the discussions of transient cracking of RC ties addressed in *fib* bulletin No. 10 (*fib* 2000). This feature though, can easily be neglected in the calculation model for design situations as a conservative approach. The main reason for including ψ in Eq. (14) was to account for the fact that nonlinear strain profiles occur over the concrete cover (Tan 2018b), which is a mechanical improvement to the assumption of claiming that plane sections remain plane in RC ties as per (Saliger 1936,

Balász 1993, CEN 2004, *fib* 2013 and Debernadi and Taliano 2016). It can be shown though, that different values of ψ in general have limited effect on the crack width predictions.

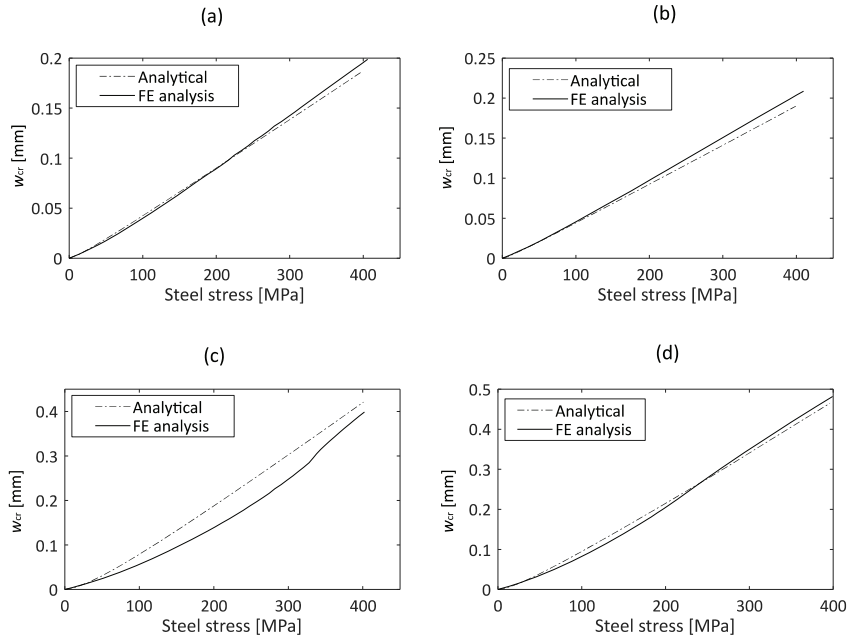


Fig. 10. Comparison of crack widths predicted (in specimens with lengths similar to FE analysis mean crack spacing reported in Table 1) with crack widths reported in the FE analysis of Tan et al. (2018c). (a) Specimen $\phi 20c40$, $L = 105$ mm. (b) Specimen $\phi 32c40$, $L = 109$ mm. (c) Specimen $\phi 20c90$, $L = 260$ mm. (d) Specimen $\phi 32c90$, $L = 272$ mm.

Fig. 12 shows that the analytical model presented can be applied to predict crack widths in non-axisymmetric RC ties as well. In these calculations, simple assumptions were made such as that the whole concrete area contributed in tension $A_{c,ef} = A_c$ and choosing $\zeta = 1$. This led to similar crack spacing predictions for RC ties with similar reinforcement ratios but different covers, which contradicts the experimental data in Table 2. It is well-known that the cover has a significant influence on crack spacing, and therefore crack widths, as reported by Broms (1968), Gergely and Lutz (1968), Caldentey et al. (2013) and Tan et al. (2018a). One approach to taking the cover into account could be to use the provisions in EC2 and MC2010 for calculating an effective reinforcement ratio, $\rho_{s,ef} = A_s/A_{c,ef}$, to predict the cracking behavior. This is exemplified in Table 3, which shows the crack spacing predictions when the effective height surrounding the rebars, i.e. $h_{c,ef} = \min[2.5(c + \phi/2), h/2]$, is used to determine the effective reinforcement ratios. Comparison of specimens having similar geometrical reinforcement ratios, e.g. S-20-40 against S-20-90 and S-32-40 against S-32-90, shows that the crack spacing predictions increase for specimens having larger covers owing to the difference in effective reinforcement ratios. However, the increase in crack spacing predictions for specimens with larger covers is seen to be underestimated compared to the

experimental evidence. This could also be related to assuming $\zeta = 1$, which is questionable particularly for RC ties with 90 mm cover because the bond stress distribution surrounding the perimeter of the rebars is probably not uniform, as elucidated in Fig. 2(d). However, determining a proper value for ζ is not straightforward and requires further study, e.g. by conducting FE analysis of non-axisymmetric RC ties. Nevertheless, the model with the introduction of the factor ζ and an effective reinforcement ratio based on the cover size shows great potential in predicting the cracking behavior of non-axisymmetric RC ties as well.

Table 3. Comparison of crack spacing reported in the experiments of Tan et al. (2018a) and crack spacing predicted using effective reinforcement ratios.

RC tie	Experimental		Predicted
	Mean [mm]	Maximum [mm]	Analytical [mm]
S-20-40	163	250	390
S-32-40	178	240	342
S-20-90	217	290	422
S-32-90	266	320	361

The calculation model using the simplified equations for concrete can predict crack widths both in the *crack formation stage* and the *stabilized cracking stage* through the concepts of CLLM and CHLM, and is as such different from the calculation methods recommended by EC2 and MC2010 which apply to the stabilized cracking stage only. Furthermore, assuming ψ not equal to one implies that the mean concrete strains over the section in general is different from the concrete strains at the interface further implying that the concrete stresses in each section are assumed unevenly distributed, even at the zero-slip section, a concept first introduced by Edwards and Picard (1972). This means that a crack forms when the resultant of concrete stresses at the zero-slip section is equal to the mean value of the tensile strength as pointed out for Eq. (74). Finally, using only one bond-slip curve means that bond stresses are different from null at the cracked section. These assumptions enabled a practical approach to solve the SODE for the slip.

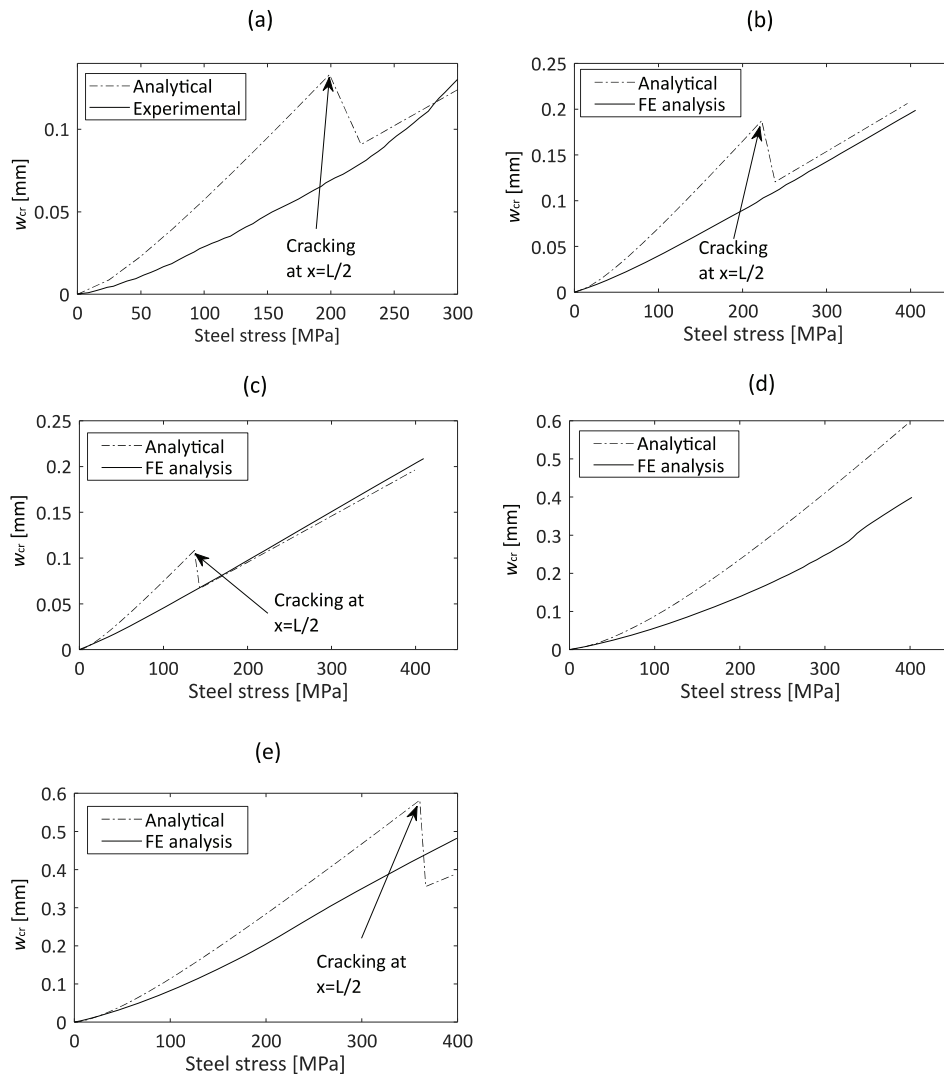


Fig. 11. Comparison of crack widths predicted (in specimens with lengths similar to crack spacing predicted in Table 1) with crack widths reported in the experiments of Yannopoulos (1989) and the FE analysis of Tan et al. (2018c). (a) Yannopoulos (1989) specimen, $L = 181$ mm. (b) Specimen $\phi 20c40$, $L = 224$ mm. (c) Specimen $\phi 32c40$, $L = 207$ mm. (d) Specimen $\phi 20c90$, $L = 470$ mm. (e) Specimen $\phi 32c90$, $L = 434$ mm.

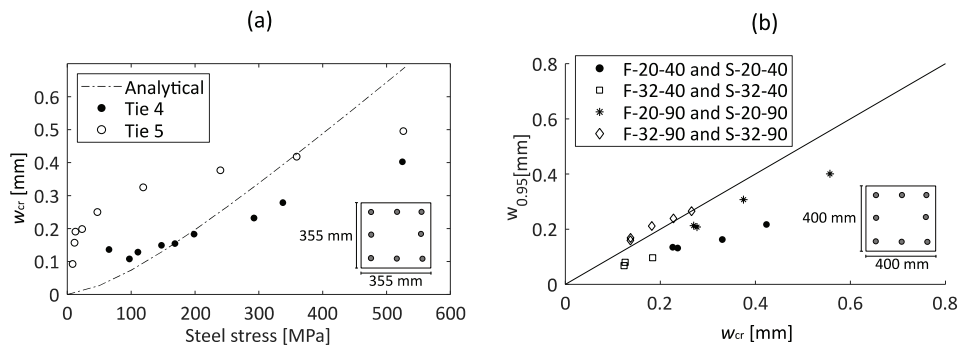


Fig. 12. Comparison of crack widths predicted (in specimens with lengths similar to crack spacing predicted in Table 2) with crack widths reported in experiments. (a) CEOS.fr (2016). (b) Tan et al. (2018a).

The model allows for treating problems such as *imposed deformations*, where the mechanical loading becomes directly dependent on the crack pattern or, expressed more rigorously, the stiffness of the member. Moreover, the authors of this paper are also currently working on the application of the analytical model to more general cases, such as non-cylindrical RC ties, tensile zones in structural elements exposed to bending, and RC membrane elements exposed to biaxial stress states at which cracks form at a skew angle to an orthogonal reinforcement grid.

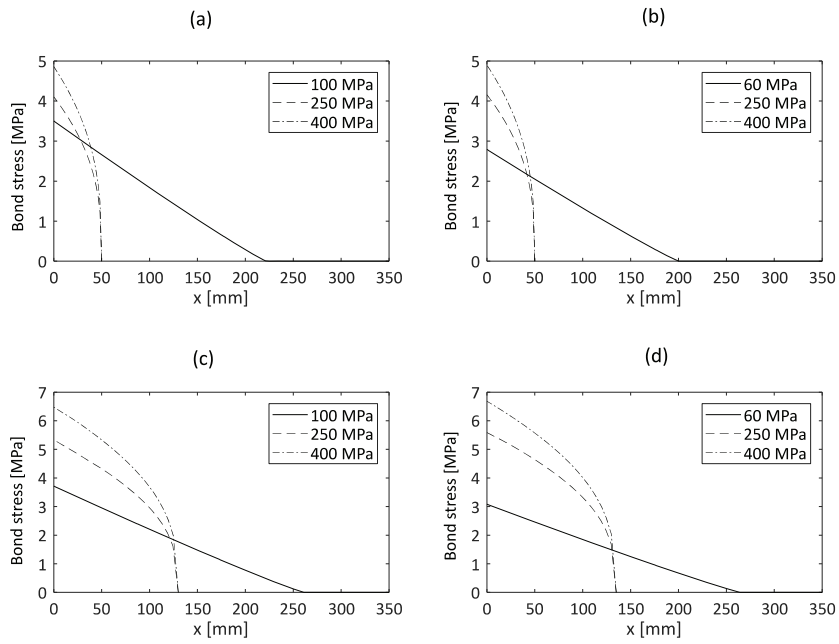


Fig. 13. Bond stresses corresponding to the steel strains predicted in Fig. 9. (a) Specimen $\phi 20c40$. (b) Specimen $\phi 32c40$. (c) Specimen $\phi 20c90$. (d) Specimen $\phi 32c90$.

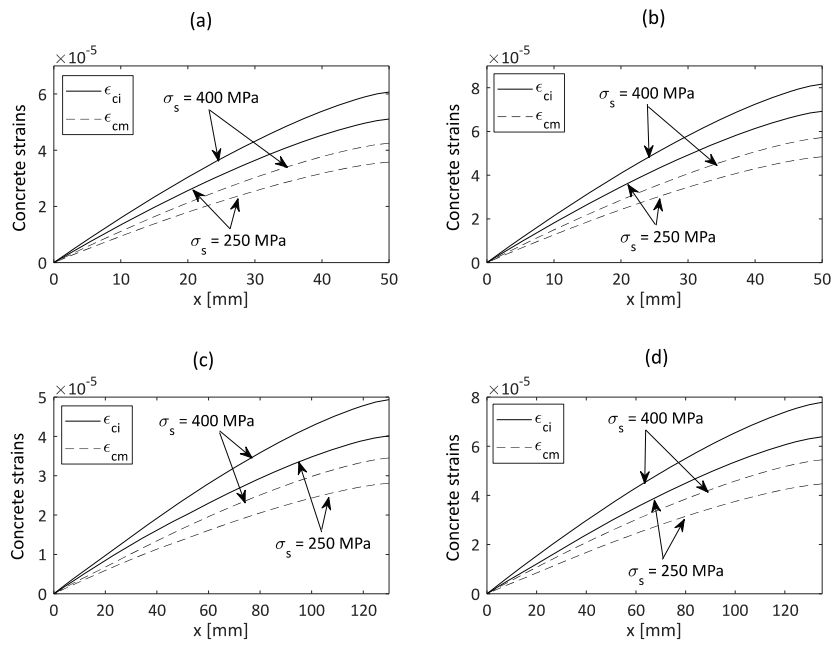


Fig. 14. Concrete strains corresponding to the steel strains predicted in Fig. 9. (a) Specimen $\phi 20c40$. (b) Specimen $\phi 32c40$. (c) Specimen $\phi 20c90$. (d) Specimen $\phi 32c90$.

7 Conclusions

A new analytical crack width calculation model has been formulated to provide more consistent crack width calculations for large-scale concrete structures, where large covers and bar diameters are typically used. The calculation model was derived based on the uniaxial behavior of axisymmetric RC ties. Furthermore, the model includes the effect of internal cracking on the bond transfer, a non-uniform strain distribution over the concrete area and a non-uniform bond stress distribution surrounding the perimeter of the steel bar in non-axisymmetric cases. The latter accounts for the effect of steel bar spacing in practice.

The SODE for the slip has been solved completely analytically, yielding closed-form solutions in the case of comparatively lightly loaded member (CLLM) behavior and non-closed-form solutions in the case of comparatively heavily loaded member (CHLM) behavior. One solution strategy and method for determining the complete cracking response has been provided for the purposes of facilitating a practical applicable calculation model, the lack of which has been the major drawback in using previous equivalent models. The comparison with experimental and finite element results in the literature shows that the calculation model predicts an average strain distribution based on using a single local bond-slip curve to represent the bond transfer. The comparisons demonstrate the ability of the calculation model to predict crack widths accurately given a member length. Finally, the model has proven capable of predicting crack spacing and crack widths consistently and in general on the conservative side regardless of the bar diameter and cover, even for non-axisymmetric RC ties.

Acknowledgement

The work presented in this paper is part of an ongoing PhD study funded by the Norwegian Public Roads Administration as a part of the Coastal Highway Route E39 project.

Appendix A

Function derivatives in the case of CHLM behavior for Case 1.

$$f_1'(u_0) = -\frac{1}{\sqrt{2}} \sum_{k=0}^{\infty} \binom{-\frac{1}{2}}{k} \gamma^k \left[\gamma \beta u_0^{\beta-1} \left(\frac{1}{2} + k \right) C^{-\frac{3}{2}-k} \frac{u_0^{1+k\beta}}{1+k\beta} + C^{-\left(\frac{1}{2}+k\right)} u_0^{k\beta} \right] \quad (78)$$

Function derivatives in the case of CHLM behavior for Case 2.

$$f_2'(u_0) = -\frac{1}{\sqrt{2}\gamma} [f_{21}'(u_0) - f_{22}'(u_0)] - \frac{1}{\sqrt{2}} f_{23}'(u_0) \quad (79)$$

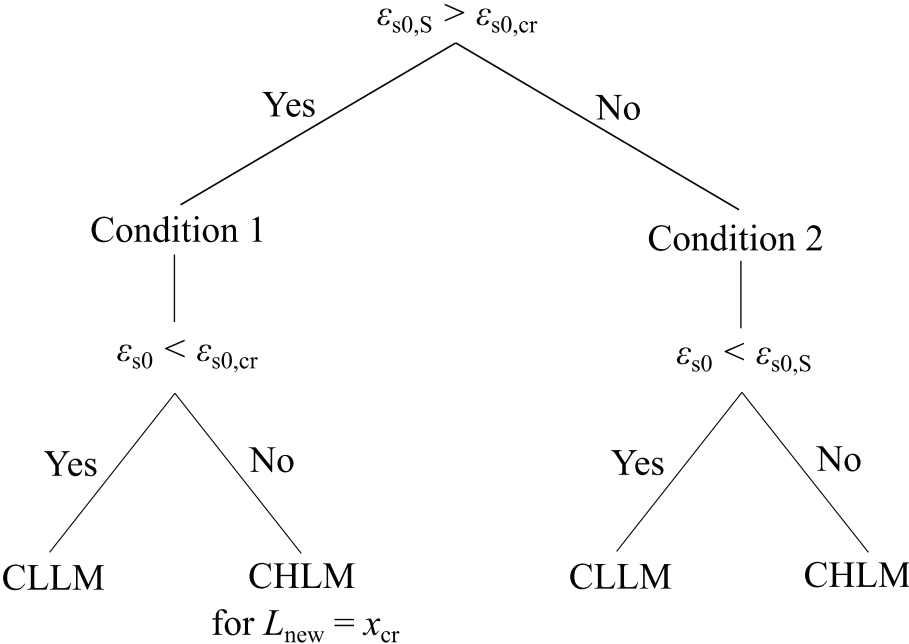
$$f_{21}'(u_0) = \sum_{k=0}^{\infty} \binom{-\frac{1}{2}}{k} \left(\frac{1}{\gamma} \right)^k \left[C^k u_0^{\delta-k\beta-1} - \frac{\gamma \beta k C^{k-1}}{\delta - k\beta} u_0^{\beta(1-k)+\delta-1} \right] \quad (80)$$

$$f_{22}'(u_0) = \sum_{k=0}^{\infty} \binom{-\frac{1}{2}}{k} \left[\left(\frac{C}{\gamma} \right)^{\frac{k}{\delta-k\beta} + \frac{1}{\beta}} + du \left(\frac{C}{\gamma} \right)^{\frac{k}{\delta-k\beta}} \right]^{\delta-k\beta-1} \cdot \left(-\gamma \beta u_0^{\beta-1} \right) \cdot \left[\left(\frac{1}{\gamma} \right)^{\frac{k}{\delta-k\beta} + \frac{1}{\beta}} \left(\frac{k}{\delta - k\beta} + \frac{1}{\beta} \right) C^{\frac{k}{\delta-k\beta} + \frac{1}{\beta} - 1} + du \left(\frac{1}{\gamma} \right)^{\frac{k}{\delta-k\beta}} \left(\frac{k}{\delta - k\beta} \right) C^{\frac{k}{\delta-k\beta} - 1} \right] \quad (81)$$

$$\begin{aligned}
f_{23}'(u_0) &= \sum_{k=0}^{\infty} \binom{-\frac{1}{2}}{k} \gamma^k \left[\left(\frac{1}{\gamma}\right)^{\frac{1}{\beta}} C^{\frac{2-\beta}{2\beta(1+k\beta)}} - du C^{-\frac{\frac{1}{2}+k}{1+k\beta}} \right]^{k\beta} \\
&\quad \cdot (-\gamma \beta u_0^{\beta-1}) \\
&\quad \cdot \left\{ \left(\frac{1}{\gamma}\right)^{\frac{1}{\beta}} \left[\frac{2-\beta}{2\beta(1+k\beta)} \right] C^{\left[\frac{2-\beta}{2\beta(1+k\beta)} - 1 \right]} \right. \\
&\quad \left. + du \left[\frac{\frac{1}{2}+k}{1+k\beta} \right] C^{-\left[\frac{\frac{1}{2}+k}{1+k\beta} + 1 \right]} \right\}
\end{aligned} \tag{82}$$

Appendix B

A method for determining the complete cracking response, in which $\epsilon_{s0,s}$, $\epsilon_{s0,cr}$ and x_{cr} are determined by Eq. (72), (74) and (75) respectively, while ϵ_{s0} is the steel strain at the loaded end. CLLM and CHLM are abbreviations for *Comparatively Lightly Loaded Members* and *Comparatively Heavily Loaded Members* respectively.



References

- Balázs, G.L. (1993). "Cracking Analysis Based on Slip and Bond Stresses." *ACI Materials Journal*, 90(4), 340-348.
- Barre, F., Bisch, P., Chauvel, D., et al. (2016). "Control of Cracking in Reinforced Concrete Structures." ISTE Ltd and John Wiley & Sons, Inc, London and Hoboken, UK and USA.
- Beeby, A.W. (2004). "The influence of the parameter ϕ/ρ_{eff} on crack widths." *fib Journal Structural Concrete*, 5(2), 71-83.
- Borosnyói, B., and Balázs, G.L. (2005). "Models for flexural cracking in concrete: the state of the art" *fib Journal Structural Concrete*, 6(2), 53-62.
- Borosnyói, A., and Snóbli, I. (2010). "Crack width variation within the concrete cover of reinforced concrete members." *Építőanyag – Journal of Silicate Based and Composite Materials*, 62(3), 70-74.
- Bresler, B. and Bertero, V.V. (1968). "Behavior of reinforced concrete under repeated load." *Proceedings of the ASCE – Journal of the Structural Division*, 94(6), 1567-1590.
- Braam, C.R. (1990). "Control of crack width in deep reinforced concrete beams [PhD thesis]." TU Delft, Delft, the Netherlands.
- Broms, B. (1968). "Theory of the calculation of crack width and crack spacing in reinforced concrete members." *Cement och Betong*, No. 1, 52-64.
- Caldentey, A.P., Peiretti, H.C., Iribarren, J.P., and Soto, A.G. (2013). "Cracking of RC members revisited: influence of cover, $\phi/\rho_{s,ef}$ and stirrup spacing – an experimental and theoretical study." *fib Journal Structural Concrete*, 14(1), 69-78.
- CEN. (2004). "EN 1992-1-1 Eurocode 2: Design of concrete structures – Part 1-1: General rules and rules for buildings." European Committee for Standardization, Brussels, Belgium.
- Debernardi, P.G., and Taliano, M. (2016). "An improvement to Eurocode 2 and *fib* Model Code 2010 methods for calculating crack width in RC structures." *fib Journal Structural Concrete*, 17(3), 365-376.
- Dörr, K. (1978). "Bond-Behaviour of Ribbed Reinforcement under Transversal Pressure. IASS Symposium on Nonlinear Behaviour of Reinforced Concrete Spatial Structures." *Werner Verlag*, Düsseldorf, Germany, Vol. 1, pp. 13-24.
- Edwards, A.D., and Picard, A. (1972). "Theory of Cracking in Concrete Members." *Proceedings of the ASCE – Journal of the Structural Division*, 98(12), 2687-2700.
- Eligehausen, R., Popov, E.P., and Bertero, V.V. (1983). "Local bond stress-slip relationships of deformed bars under generalized excitations: experimental results and analytical model." Report No. UCB/EERC 83/23, University of California, Berkeley, USA.
- Fantilli, A.P., Mihashi, H., and Vallini, P. (2007). "Crack profile in RC, R/FRCC and R/HPFRCC members in tension." *Materials and Structures*, 40, 1099-1114.
- fib*. (2000). "Bond of reinforcement in concrete – State-of-the-art report." *fib bulletin No. 10*, Lausanne, Switzerland.
- fib*. (2013). "*fib* Model Code for Concrete Structures 2010. International Federation for Structural Concrete." Ernst & Sohn, Berlin.
- Gergely, P., and Lutz, L.A. (1968). Maximum Crack Width in Reinforced Concrete Flexural

- Members. Causes, Mechanisms and Control of Cracking in Concrete, SP-20, American Concrete Institute, Farmington Hills, MI, USA, pp. 87-117.
- Goto, Y. (1971) "Crack formed in concrete around deformed tension bars." *ACI Journal*, 68(4), 244-251.
- Hong, S., and Park, S.K. (2012). "Uniaxial Bond Stress-Slip Relationship of Reinforcing Bars in Concrete." *Advances in Materials Science and Engineering*. 2012 (2012), Article ID 328570.
- Husain, S.I., and Ferguson, P.M. (1968). "Flexural crack width at the bars in reinforced concrete beams. Research Report Number 102-1F." Center for Highway Research, The University of Texas at Austin, USA.
- Irgens, F. (2008). *Continuum Mechanics*, Springer, Bergen, Norway.
- Kaklauskas, G. (2017). "Crack Model for RC Members Based on Compatibility of Stress-Transfer and Mean-Strain Approaches." *J. Struct. Eng.*, 143(9). 10.1061/(ASCE)ST.1943-541X.0001842.
- Leonhardt, F. (1988). "Cracks and Crack Control in Concrete Structures." *PCI Journal*, Jul-Aug, pp. 124-145.
- Lutz, L.A. (1970) "Analysis of Stresses in Concrete Near a Reinforcing Bar Due to Bond and Transverse Cracking." *ACI Journal*, 67(10): 778-787.
- Martin, H. (1973). "On the interrelation among surface roughness, bond and bar stiffness in the reinforcement subject to short-term loading (in German)." *Deutscher Ausschuss Stahlbeton*, (228), 1-50.
- Mirza, S.M., and Houde, J. (1979). "Study of Bond Stress-Slip Relationships in Reinforced Concrete." *ACI Journal*, 76(1): 19-46.
- Nilson, A.H. (1972). "Internal Measurement of Bond Slip." *ACI Journal*, 69(7), 439-441.
- NPRA. (2015). "N400 Bruprosjektering: Prosjektering av bruer, ferjekaier og andre bærende konstruksjoner." *N400 in Statens vegvesens håndbokserie*, ISBN: 978-82-7207-680-0.
- Pedziwiatr, J. (2008). "Influence of internal cracks on bond in cracked concrete structures." *Archives of Civil and Mechanical Engineering*, 8(3), 91-105.
- Rehm, G. (1961). "On the fundamentals of the steel-concrete bond (in German)." *Deutscher Ausschuss für Stahlbeton*, (138), 1-59.
- Russo, G., Zingone, G., and Romano, F. (1990). "Analytical Solution for Bond-Slip of Reinforcing Bars in R.C. Joints." *J. Struct. Eng.*, [10.1061/\(ASCE\)0733-9445\(1990\)116:2\(336\)](https://doi.org/10.1061/(ASCE)0733-9445(1990)116:2(336)).
- Russo, G., and Romano, F. (1992). "Cracking Response of RC Members Subjected to Uniaxial Tension." *J. Struct. Eng.*, [10.1061/\(ASCE\)0733-9445\(1992\)118:5\(1172\)](https://doi.org/10.1061/(ASCE)0733-9445(1992)118:5(1172)).
- Tan, R., Eileraas K., Opkvitne, O., et al. (2018a). "Experimental and theoretical investigation of crack width calculation methods for RC ties." *fib Journal Structural Concrete*, 1-12. <https://doi.org/10.1002/suco.201700237>.
- Tan, R., Hendriks, M.A.N., and Kanstad, T. (2018b). "An investigation of the strain profile over the cover in reinforced concrete elements subjected to tension." Proceedings of the 5th *fib Congress*, October 2018, Melbourne, Australia.
- Tan, R., Hendriks, M.A.N., Geiker, M., and Kanstad, T. (2018c). "A numerical investigation

of the cracking behaviour of reinforced concrete tie elements.” Accepted for publication in the *Magazine of Concrete Research*.

<https://doi.org/10.1680/jmacr.18.00156>.

Tammo, K., and Thelandersson, S. (2009). “Crack behavior near reinforcing bars in concrete structures.” *ACI Structural Journal*, 106(3), 259-267.

Watstein, D., and Mathey, R.G. (1959). “Width of Cracks in Concrete at the Surface of Reinforcing Steel Evaluated by Means of Tensile Bond Specimens.” *ACI Journal*, 56(7), 47-56.

Yannopoulos, P.J. (1989). “Variation of concrete crack widths through the concrete cover to reinforcement.” *Magazine of Concrete Research*, 41(147), 63-68.

Paper IV

Modified cracked membrane model for consistent crack width
predictions of reinforced concrete structures subjected to in-plane
loading

Tan, R., Hendriks, M.A.N., Geiker, M. & Kanstad, T.

Under review, 2019

Modified cracked membrane model for consistent crack width predictions of reinforced concrete structures subjected to in-plane loading

Reignard Tan¹, Max A.N. Hendriks^{1,2}, Mette Geiker¹, Terje Kanstad¹

¹NTNU, Norwegian University of Science and Technology, Department of Structural Engineering, Trondheim, Norway

²Delft University of Technology, Delft, the Netherlands

Abstract

The modified cracked membrane model (MCMM) presented in this paper was formulated to facilitate a mechanical calculation model that predicts crack widths in reinforced concrete (RC) structures subjected to in-plane loading for all cracking stages. It was formulated using the basic concepts of the existing cracked membrane model (CMM). Furthermore, a generalized approach for predicting the tension stiffening normal to a crack was formulated, an approach currently lacking in Eurocode 2 and *fib* Model Code 2010. A simplified approach for predicting the cracking behaviour of RC membranes was also proposed. Comparison with a total of 101 maximum crack widths measured experimentally on 37 test specimen from the literature showed that the MCMM provided good and consistent crack width predictions even for the cases of large rebars and covers, at which the CMM was seen to struggle. The results in this paper suggests that both the MCMM and the simplified approach show great potential for yielding reliable crack width predictions in RC membranes.

Keywords

Crack widths, crack spacing, calculation model, RC membranes, in-plane loading, tension stiffening, modelling uncertainty.

1 Introduction

There are many approaches for predicting crack widths in reinforced concrete (RC) structures exposed to uniaxial stress conditions and a comprehensive summary of them is provided in Borosnyói and Balász (2005). These calculation methods can be used to predict the cracking behaviour of one-way bearing structural elements such as RC ties, beams and slabs. However, they become inadequate for more complicated structural elements such as orthogonally RC membranes, two-way bearing slabs and shells. Such structural elements can in most practical cases be treated as components subjected to in-plane loading thus necessitating more comprehensive calculation methods, e.g. the modified compression field theory (MCFT) developed by Vecchio and Collins (1986), Collins and Mitchell (1997), Bentz (2000) and Bentz et al. (2006), the rotating angle softened-truss-model (RA-STM) developed by Hsu (1988), Pang and Hsu (1995), Hsu and Mo (2010) and Bernardo et al. (2018) and the cracked membrane model (CMM) developed by Kaufmann (1998), Kaufmann and Marti (1998),

Foster and Marti (2003), Dabbagh and Foster (2005) and Pimentel et al. (2010). The three models have all proven to predict deformations and ultimate load capacity of structural elements subjected to in-plane loading, such as orthogonally RC membranes quite convincingly. Common for the models is that equilibrium of stresses is obtained iteratively in terms of the mean strains. The main differences between the models are that i) equilibrium was formulated in terms of average stresses and average strains between cracks for the MCFT and the RA-STM, while equilibrium of stresses was formulated at the cracks for the CMM and ii) tension stiffening was incorporated using empirical constitutive laws for the MCFT and the RA-STM, while tension stiffening was incorporated using the fully mechanical based tension chord model (TCM) developed by Marti et al. (1998) for the CMM. Nonetheless, all three models could potentially predict crack widths under the presumption of assuming that a finite crack pattern had formed. In other words, the models can in principle predict crack widths in RC membranes for the *stabilized cracking stage* only.

The semi-empirical calculation methods for predicting crack widths recommended by Eurocode 2 (EC2) (CEN 2004) and *fib* Model Code 2010 (MC2010) (*fib* 2013) were partially based on the same mechanical concept as the TCM (Tan et al. 2018a). However, EC2 and MC2010 do not provide complete guidelines for predicting cracking widths in RC membranes, i.e. they only offer a way of predicting the crack spacing but not the tension stiffening normal to the crack. There have been some proposals for this in the literature, though without avoiding incorporating tension stiffening in an empirical manner (Cerioni et al. 2007, Giordano and Mancini 2009). Using empirical constitutive laws for the tension stiffening can limit the models' range of applicability as it in general depends on the bond behaviour between concrete and steel, and is further governed mechanically by the cover, diameter of the reinforcing steel bars (rebars), rebar spacing and load level (Lutz 1970, Goto 1971, Nilson 1972, Dörr 1978, Mirza and Houde 1979, Somayaji and Shah 1981, Jiang et al. 1984, Tammo et al. 2009, Tan et al. 2018b). Further comparing the comprehensive calculation methods shows that the CMM offers the possibility of altering the basic components that govern its mechanical behaviour quite conveniently. It can thus be argued that the CMM offers greater potential in predicting the cracking behaviour of RC membranes subjected to in-plane loading than the MCFT and RA-STM. A statement also acknowledged by the state-of-the-art French research project CEOS.fr (Barre et al. 2016).

This study is part of an ongoing research project with the overall objective of improving crack width calculation methods for large-scale concrete structures planned for the coastal high-way route "Ferry-free E39" in Norway. Use of large covers being up to 130 mm is specified by the Norwegian Public Roads Administration (NPRA) guidelines N400 (NPRA 2015) for marine structures. In addition, large rebar diameters, often in bundles and over several layers, are typically used for the cross-sections of such large-scale concrete structures. It was shown by Tan et al. (2018a) that Eurocode 2 with German National Annex (DIN 2011), which essentially is similar to the TCM, predicted maximum crack widths inconsistently and in average on the nonconservative side particularly for the combination of large rebars and covers. This led to formulating the *modified tension chord model* (MTCM), which has proven to predict the cracking behaviour of RC ties more consistently and on the conservative side

regardless of cover and rebar size (Tan et al. 2019). In this paper, the CMM is used to formulate a new calculation model for predicting the response of orthogonally RC membranes, later referred to as the *modified cracked membrane model* (MCMM). In shortness, the MCMM incorporates tension stiffening using the MTCM instead of the TCM to account for the cracking behaviour in the *crack formation stage* and the stabilized cracking stage, as well as after yielding of reinforcement. Tan et al. (2018b) showed that the crack formation stage could be governing even at relatively large steel stresses in cases with large covers.

First, the basic principles in the CMM are discussed after which the MTCM is derived and incorporated in the MCMM together with a set of chosen constitutive models for concrete, reinforcing steel and prestressing steel. Based on the MCMM, a simplified approach for predicting crack widths in RC membranes is proposed. Then, crack widths predicted by the MCMM, CMM and the simplified approach are compared to a total of 101 maximum crack widths measured from experiments on 37 test specimen reported in the literature. Finally, the modelling uncertainty for the three models is discussed.

2 Cracked membrane model

2.1 The basic principles

The equilibrium equations of stresses at cracks can be obtained by e.g. orienting the unit vectors \mathbf{n} and \mathbf{e} in the direction of the inflicted stresses σ_x , σ_y and τ_{xy} (Irgens 2008) as shown in Fig. 1

$$\begin{aligned} \sigma_x = & \sigma_{c1} \cos^2 \theta_{cr} + \sigma_{c2} \sin^2 \theta_{cr} \\ & - 2\tau_{c12} \sin \theta_{cr} \cos \theta_{cr} + \rho_{sx}\sigma_{srx} + \rho_{px}\sigma_{prx} \end{aligned} \quad (1)$$

$$\begin{aligned} \sigma_y = & \sigma_{c1} \sin^2 \theta_{cr} + \sigma_{c2} \cos^2 \theta_{cr} \\ & + 2\tau_{c12} \sin \theta_{cr} \cos \theta_{cr} + \rho_{sy}\sigma_{sry} + \rho_{py}\sigma_{pry} \end{aligned} \quad (2)$$

$$\tau_{xy} = (\sigma_{c1} - \sigma_{c2}) \sin \theta_{cr} \cos \theta_{cr} + \tau_{c12}(\cos^2 \theta_{cr} - \sin^2 \theta_{cr}) \quad (3)$$

where σ_{c1} are concrete stresses normal to the crack, σ_{c2} are concrete stresses parallel to the crack, τ_{c12} are shear stresses at the crack, σ_{srx} and σ_{sry} are rebar stresses at the crack in x and y-direction respectively, ρ_{sx} and ρ_{sy} are steel reinforcement ratios in x and y-direction respectively, σ_{prx} and σ_{pry} are prestressing steel stresses at the crack in x and y-direction respectively, ρ_{px} and ρ_{py} are prestressing steel ratios in x and y-direction respectively and θ_{cr}

is the angle between a unit vector normal to the crack and the global x -direction. The cracks are assumed free to rotate implying null shear stresses at cracks, i.e. $\tau_{c12} = 0$, and that the cracked plane is coincident with the plane of principal strains. Using the concept of rotating cracks can in terms of serviceability be justified since the angle rotations in most cases are negligibly small prior to yielding of rebars. It also simplifies the calculations considerably. Internal stresses in Eq. (1) to (3) are finally obtained through a set of chosen constitutive models for concrete, steel and tension stiffening in terms of the global mean strains ϵ_x , ϵ_y and γ_{xy} .

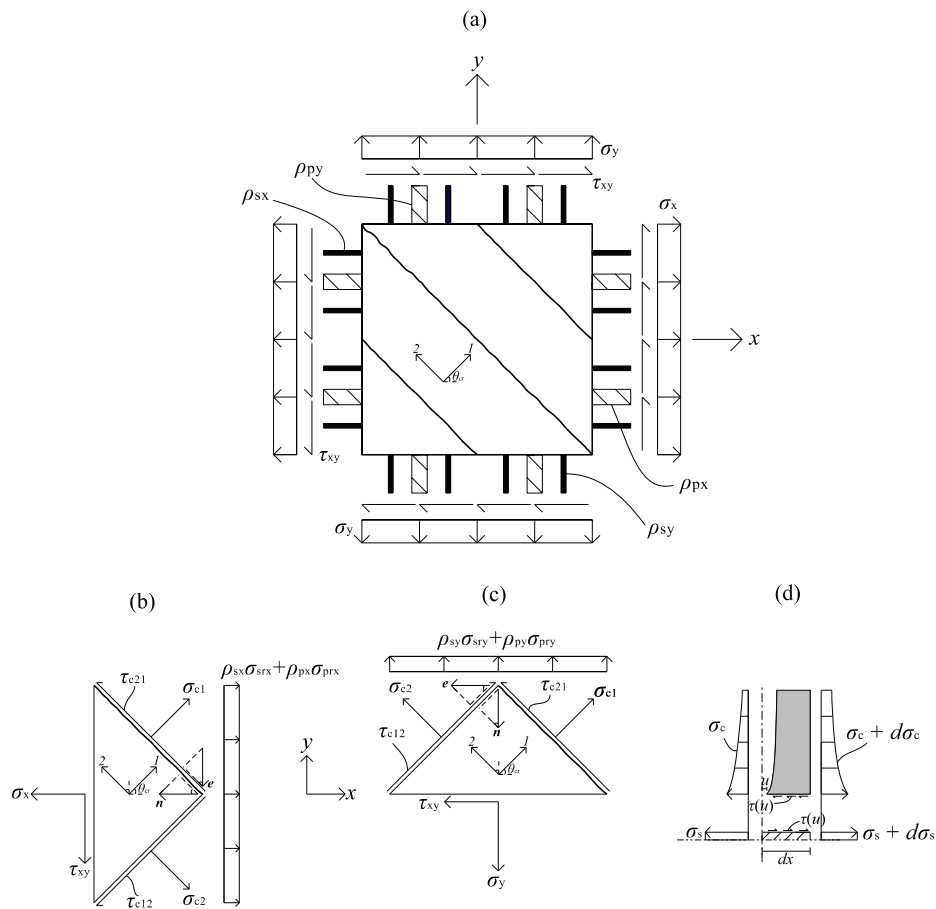


Figure 1(a) Cracked RC membrane. (b) and (c) Equilibrium of stresses at the crack in x - and y -direction. (d) Stresses, deformations and slip for a differential element in an RC tie.

2.2 Tension chord model

The second order differential equation (SODE) for the slip u was derived by considering equilibrium, compatibility and linear elastic material laws for steel and concrete for a differential element in an RC tie, see Fig. 1(d), or e.g. as discussed by Saliger (1936), Russo and Romano (1992), Balász (1993), Khalfallah (2006), *fib* bulletin No. 52 (2010) and Debernardi and Taliano (2016)

$$\frac{d^2u}{dx^2} - \chi\tau(u) = 0 \quad (4)$$

where σ_{c1} are concrete stresses normal to the crack, σ_{c2} are concrete stresses parallel to the crack, τ_{c12} are shear stresses at the crack, σ_{srx} and σ_{sry} are rebar stresses at the crack in x and y-direction respectively, ρ_{sx} and ρ_{sy} are steel reinforcement ratios in x and y-direction respectively, σ_{prx} and σ_{pry} are prestressing steel stresses at the crack in x and y-direction respectively, ρ_{px} and ρ_{py} are prestressing steel ratios in x and y-direction respectively and θ_{cr} is the angle between a unit vector normal to the crack and the global x-direction. The cracks are assumed free to rotate implying null shear stresses at cracks, i.e. $\tau_{c12} = 0$, and that the cracked plane is coincident with the plane of principal strains. Internal stresses in Eq. (1) to (3) are finally obtained through a set of chosen constitutive models for concrete, steel and tension stiffening in terms of the global mean strains ε_x , ε_y and γ_{xy} .

3 Modified cracked membrane model

3.1 Modified tension chord model

3.1.1 General

The modified tension chord model (MTCM) is a tension stiffening model based on solving the SODE for the slip in Eq. (4) completely analytically using the bond-slip law of Eligehausen et al. (1983) and later adopted by MC2010

$$\tau(u) = \tau_{\max} \left(\frac{u}{u_1} \right)^\alpha \quad (5)$$

Here, $u_1 = 0.1$ mm, $\tau_{\max} = 5.0$ MPa and $\alpha = 0.35$ being the chosen bond-slip parameters to account for the behaviour of RC ties according to the recommendations in Tan et al. (2018b). The conceptual difference between the TCM and MTCM is visualized in Fig. 2(a) for steel stresses prior to yielding, in which the continuous and dashed lines represent steel strains ε_s and the corresponding concrete strains ε_c respectively. The linear curves show that the strains vary over the bar length with a constant slope of $4\tau_{b0}/\phi_s$ for the TCM, while nonlinear strains in general are observed for the MTCM. Furthermore, the tension stiffening can be

subdivided into three regimes depending on if the steel stresses over the bar length are; 1) below yielding, 2) partially below and above yielding or 3) above yielding as pointed out by Kaufmann (1998) and Kaufmann and Marti (1998), see Fig. 2(b). An output from the MTCM is usually the mean steel strains ε_{sm} as a function of the steel stresses σ_{sr} at the crack similar to the concept of any other tension stiffening model, e.g. EC2, MC2010 or the TCM. The challenge, however, is to “go the other way around” and determine the steel stresses at the crack σ_{sr} as a function of mean strains ε_{sm} instead. For solving this inverse problem for Regime 1, the analytical solutions to the SODE for the slip fully provided in Russo and Romano (1992) and Tan et al. (2019) are used. For Regime 2 and 3, the closed form solutions provided by Kaufmann (1998) and Kaufmann and Marti (1998) are used, however, with modifications for the stepped, rigid-perfectly plastic bond-slip law to avoid abrupt change in stiffness between Regime 1 and 2. Moreover, the factor $\psi = 0.70$ was for the MTCM adopted according to the recommendations in Tan et al. (2018c), which was seen to remain constant and equal to this value except for a region close to the loaded end, regardless of the cover size, rebar diameter, load level and even material properties in the case of axisymmetry.

3.1.2 Regime 1

The response in Regime 1 is grouped into two concepts as *comparatively lightly loaded members* (CLLM) and *comparatively heavily loaded members* (CHLM), which in principle are analogous to the crack formation stage and the stabilized cracking stage respectively. The concept of CLLM is depicted in Fig. 3(a) and (b) in which the transfer length S_{r0} denotes the abscissa where steel and concrete strains become compatible and the slip becomes zero. It moves towards the symmetry section $L/2$ upon increasing the load and a new crack is formed at the location where the concrete strains exceed the tensile strength of concrete, i.e. $S_{r0} = S_{cr0}$ if $\varepsilon_c(S_{r0}) = \varepsilon_{c,max} \geq \varepsilon_{ct}$. Here, $\varepsilon_{ct} = f_{ct}/E_c$, f_{ct} being the tensile strength of concrete, while S_{cr0} is the crack spacing. The concept of CHLM governs thereafter the response for the newly cracked member in which it is observed that steel and concrete strains remain incompatible over the entire crack spacing although the slip is zero at the symmetry section as depicted in Fig. 3(c) and (d). In summary, the main difference between the two concepts is that strains become compatible at a certain location over the bar length for CLLM, while strains remain incompatible over the entire bar length for CHLM. This provided two sets of boundary conditions yielding closed form solutions for CLLM and non-closed form solutions for CHLM. General expressions for the steel strains and concrete strains independent of the concept were obtained as

$$\varepsilon_s = \frac{\xi \varepsilon_{sr} - u'}{1 + \xi} \quad (6)$$

$$\varepsilon_c = \psi \xi \frac{\varepsilon_{sr} + u'}{1 + \xi} \quad (7)$$

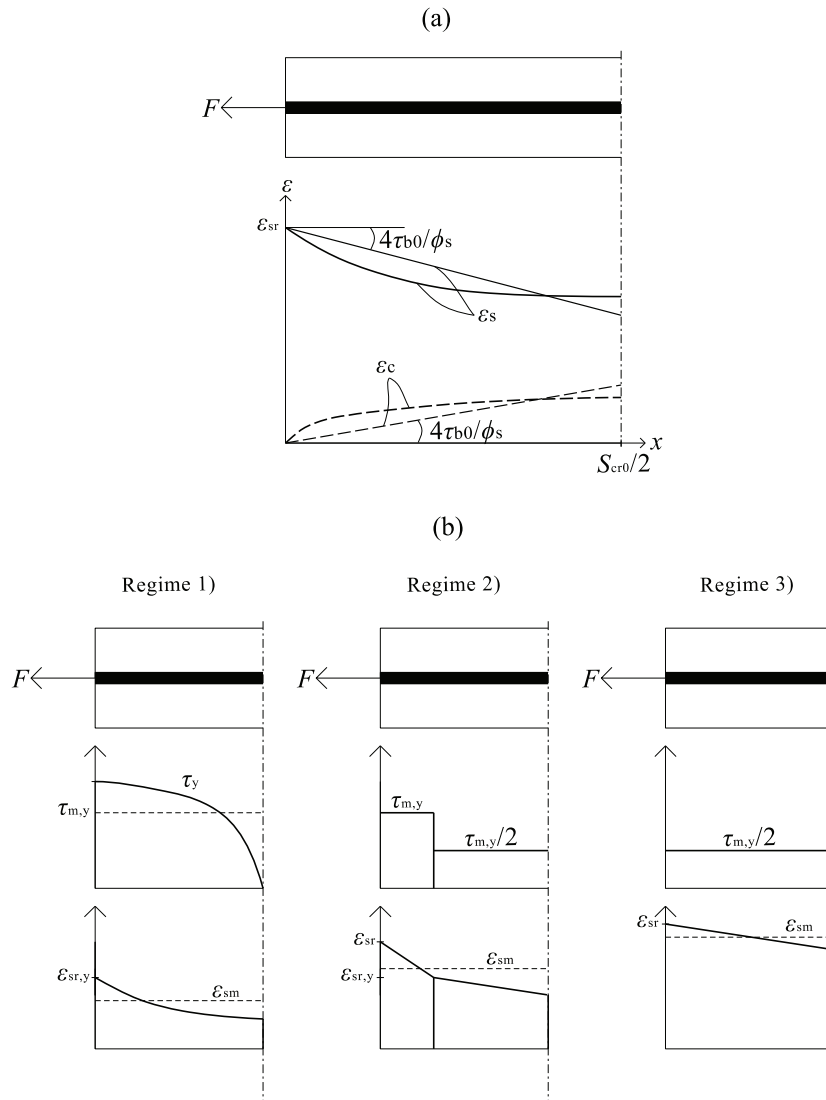


Figure 2(a) Steel and concrete strains distribution over the bar length. Linear strains represent the concept of TCM, while nonlinear strains represent the concept of MTCM. (b) Regime 1 represents steel stresses over the bar length prior to yielding. Regime 2 represents steel stresses over the bar length that partially are below and above yielding. Regime 3 represents steel stresses over the entire bar length that are above yielding.

in which $-u' = \epsilon_s - \epsilon_c$ was the derivative of the slip and $\epsilon_{sr} = \sigma_{sr}/E_s$ was the steel strain at the crack. The expressions for mean steel strains and mean concrete strains are for CLLM obtained by integrating Eq. (6) and (7) respectively over the transfer length S_{r0}

$$\varepsilon_{sm} = \frac{1}{S_{r0}} \frac{\xi \varepsilon_{sr} S_{r0} + u_{r,CLLM}}{1 + \xi} \quad (8)$$

$$\varepsilon_{cm} = \frac{\psi \xi \varepsilon_{sr} S_{r0} - u_{r,CLLM}}{S_{r0} (1 + \xi)} \quad (9)$$

in which the transfer length was defined as

$$S_{r0} = \frac{1}{\delta} \left[\varepsilon_{sr} \left(\frac{1}{2\gamma} \right)^{\frac{1}{2\delta}} \right]^{\frac{2\delta}{\beta}} \quad (10)$$

while the slip at the crack was obtained as, see Fig. 3(b)

$$u_{r,CLLM} = \left(\frac{1}{2\gamma} \right)^{\frac{1}{\beta}} \varepsilon_{sr}^{\frac{2}{\beta}} \quad (11)$$

with the constants $\gamma = \chi \tau_{\max} / (\beta u_1^\alpha)$, $\beta = 1 + \alpha$ and $\delta = (1 - \alpha) / 2$. Inserting Eq. (10) and (11) in (8), substituting ε_{sm} with a known value for the mean strains ε_m and multiplying with the Young's modulus for steel yields an expression for the steel stresses at the crack as

$$\sigma_{sr} = \frac{1 + \xi}{\delta + \xi} \varepsilon_m E_s \quad (12)$$

An expression for the steel stresses at the crack as a function of the mean strains is derived conveniently due to the closed form solution of the slip at the crack provided for CLLM. This is not the case for CHLM since the slip at the crack $u_{r,CHLM}$ only could be obtained iteratively as a function of ε_{sr} . Thus, a solution to obtain ε_{sr} for CHLM for a known value of the mean strain ε_m is by assuming

$$\varepsilon_{sr} = \frac{\varepsilon_m}{\beta_s} \quad (13)$$

where $\beta_s = 1$ is chosen initially. The expressions for mean steel strains and mean concrete strains are obtained in a similar fashion as for CLLM, however, this time around by integrating Eq. (6) and (7) over half the crack spacing $S_{cr0}/2$ according to Fig. 3(c)

$$\varepsilon_{sm} = \frac{1}{\frac{S_{cr0}}{2}} \frac{\xi \varepsilon_{sr} \frac{S_{cr0}}{2} + u_{r,CHLM}}{1 + \xi} \quad (14)$$

$$\varepsilon_{cm} = \frac{\psi \xi}{\frac{S_{cr0}}{2}} \frac{\varepsilon_{sr} \frac{S_{cr0}}{2} - u_{r,CHLM}}{1 + \xi} \quad (15)$$

in which the theoretical maximum crack spacing was defined as

$$S_{cr0} = \frac{1}{\delta} \left[\varepsilon_{ct} \frac{1 + \xi}{\psi \xi} \left(\frac{1}{2\gamma} \right)^{\frac{1}{2\delta}} \right]^{\frac{2\delta}{\beta}} \quad (16)$$

The maximum slip $u_{r,CHLM}$ is determined iteratively as a function of ε_{sr} using the solution strategy provided in (Tan et al., 2019). If $\varepsilon_{sm} \neq \varepsilon_m$, new values of $\beta_s = \varepsilon_{sm}/\varepsilon_{sr} \leq 1$, ε_{sr} using Eq. (13) and ε_{sm} using Eq. (14) are calculated. Finally, steel stresses at the crack are obtained by multiplication of Eq. (13) with the Young's modulus for steel

$$\sigma_{sr} = \frac{\varepsilon_m}{\beta_s} E_s \quad (17)$$

3.1.3 Regime 2 and 3

Regime 2 and 3, which represent steel stresses over the crack spacing after the onset of yielding, is in general not relevant in terms of serviceability but are needed to properly account for cases where the reinforcement ratio in one direction differs greatly from the other direction. This could cause yielding for the reinforcement with lowest reinforcement ratio while the other remains elastic. The expressions for the steel stresses provided in the TCM (Kaufmann, 1998; Kaufmann and Marti, 1998) are used as a simplification. However, one important modification in relation to the stepped, rigid-perfectly plastic bond-slip law is applied. Instead of directly relating the mean bond stresses to the tensile strength of concrete as $\tau(u) = \tau_{b0} = 2f_{ct}$ and $\tau(u) = \tau_{b1} = f_{ct}$, they are rather taken as the mean bond stress $\tau_{m,y}$ of the bond stress distribution τ_y at the onset of yielding of the rebar at the crack, i.e. when $\varepsilon_{sr} = \varepsilon_{sr,y} = f_{sy}/E_s$ where f_{sy} is the yield stress. This means that $\tau(u) = \tau_{m,y}$ for steel

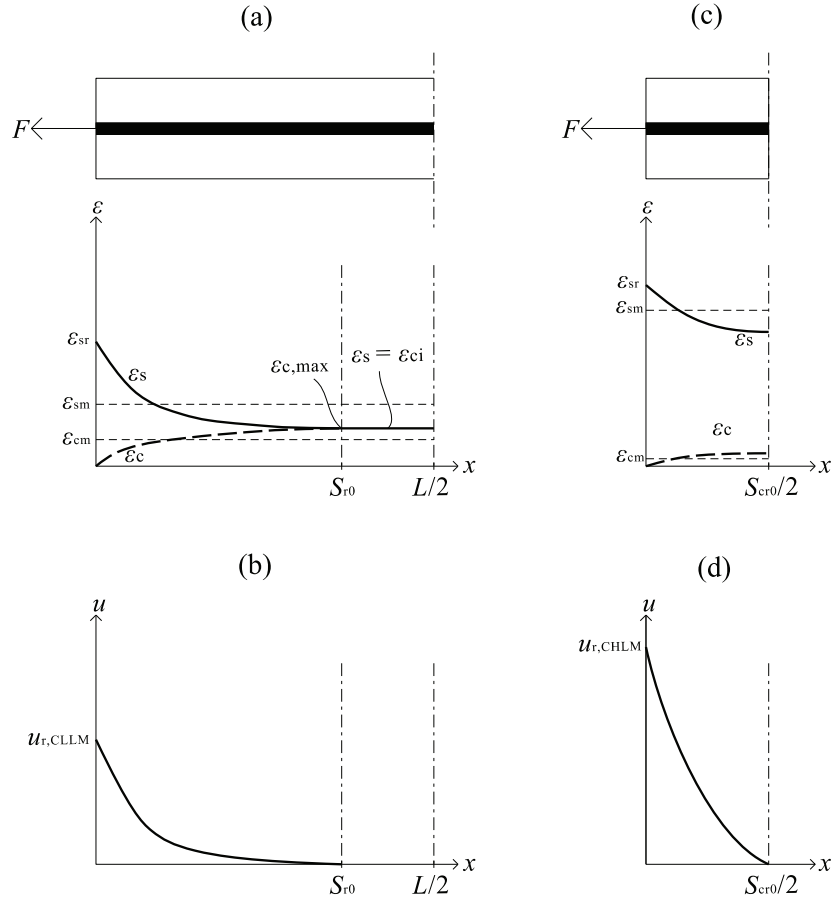


Figure 3(a) Steel and concrete strains distribution over the bar length for the concept of CLLM. (b) Slip over the bar length for the concept of CLLM. (c) Steel and concrete strains distribution over the bar length for the concept of CHLM. (d) Slip over the bar length for the concept of CHLM.

stresses prior to yielding and $\tau(u) = \tau_{m,y}/2$ for steel stresses after the onset of yielding, see Fig. 2(b). This is mainly to avoid abrupt change in stiffness in the transition between Regime 1 and 2. The expression for Regime 2 becomes

$$\sigma_{sr} = f_{sy} + 2 \frac{\frac{\tau_{m,y} S_{cr0}}{\phi_s} - \sqrt{(f_{sy} - E_s \epsilon_m) \frac{\tau_{m,y} S_{cr0}}{2 \phi_s} \left(2 - \frac{E_s}{E_{sh}}\right) + \frac{E_s}{E_{sh}} \frac{\tau_{m,y}^2 S_{cr0}^2}{2 \phi_s^2}}}{2 - \frac{E_s}{E_{sh}}} \quad (18)$$

or $\frac{f_{sy}}{E_s} - \frac{\tau_{m,y}S_{cr0}}{\phi_s E_s} < \epsilon_m \leq \frac{f_{sy}}{E_s} + \frac{\tau_{m,y}S_{cr0}}{2\phi_s E_{sh}}$, while the expression for Regime 3 becomes

$$\sigma_{sr} = f_{sy} + \left(\epsilon_m - \frac{f_{sy}}{E_s} \right) E_{sh} + \frac{\tau_{m,y}S_{cr0}}{2\phi_s} \quad (19)$$

for $\epsilon_m > \frac{f_{sy}}{E_s} + \frac{\tau_{m,y}S_{cr0}}{2\phi_s E_{sh}}$.

3.1.4 Constitutive model

The stress-strain curves for the constitutive models of MTCM, TCM and naked steel are plotted in Fig. 4 with two different reinforcement configurations. Fig. 4(a) applied to an RC tie with $\rho_s = 2.93\%$, $\phi_s = 19.5$ mm, $f_{sy} = 492$ MPa and $\tau_{m,y} = 4.196$ MPa, while Fig. 4(b) applied to an RC tie with $\rho_s = 0.97\%$, $\phi_s = 11.3$ mm, $f_{sy} = 479$ MPa and $\tau_{m,y} = 4.673$ MPa. The Young's modulus for steel was set to $E_s = 200000$ MPa, while the cylinder strength, tensile strength and the Young's modulus for concrete was set to $f_c = 42.5$ MPa, $f_{ct} = 3.17$ MPa and $E_c = 34000$ MPa respectively in both cases. The bar length was set equal to the crack spacing determined by the MTCM and TCM as 265 mm and 161 mm respectively in Fig. 4(a) and as 286 mm and 311 mm respectively in Fig. 4(b). It is observed that the TCM is slightly stiffer in its response than the MTCM. Furthermore, it is noticed a drop of steel stresses for the MTCM at $\epsilon_m \approx 1 \cdot 10^{-3}$ in Fig. 4(a), which can be explained by the fact that the CHLM behaviour allows for a crack to form at the centre of the crack spacing if the concrete strains at this location exceed the tensile strength of concrete, i.e. when $\epsilon_c(S_{cr0}/2) \geq \epsilon_{ct}$, as recommended by Russo and Romano (1992) and Tan et al. (2019).

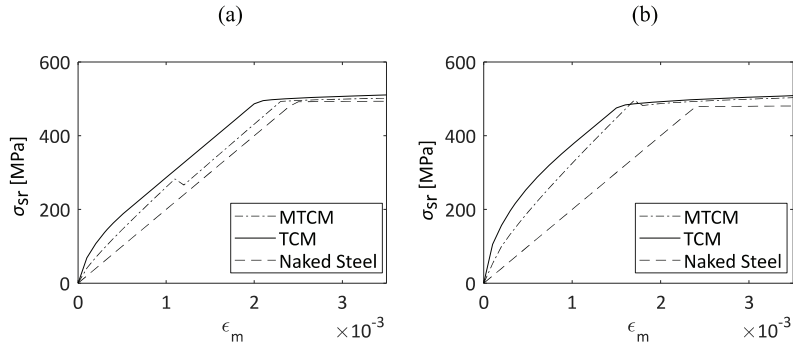


Figure 4(a) Stress strain curve for an RC tie with $\rho_s = 2.93\%$, $\phi_s = 19.5$ mm, $f_{sy} = 492$ MPa and $\tau_{m,y} = 4.196$ MPa. Bar lengths are set to 265 mm and 161 mm for the MTCM and the TCM respectively. (b) Stress strain curve for an RC tie with $\rho_s = 0.97\%$, $\phi_s = 11.3$ mm, $f_{sy} = 479$ MPa and $\tau_{m,y} = 4.673$ MPa. Bar lengths are set to 286 mm and 311 mm for the MTCM and TCM.

3.2 Modified tension chord model at biaxial stress conditions

3.2.1 General

The MTCM at biaxial stress conditions caused by in-plane loading is discussed by considering the development of maximum principle stresses of concrete between cracks. The consideration of Mohr's circle of concrete stresses at cracks and between cracks depicted in Fig. 5 yields an expression for the development of maximum principle stresses in the concrete as

$$\sigma_{c1b} = \frac{f_{ct}}{2}(\lambda_x + \lambda_y) - \frac{\tau_{xy}}{2}(\tan \theta_{cr} + \cot \theta_{cr}) \quad (20)$$

$$+ \sqrt{\left[\frac{\tau_{xy}}{2}(\cot \theta_{cr} - \tan \theta_{cr})\right]^2 - \frac{f_{ct}}{2}(\lambda_x - \lambda_y) + \tau_{xy}^2} \leq f_{ct}$$

under the assumption that θ_{cr} and τ_{xy} remain the same, where $\lambda_x = \varepsilon_{cx,max}/\varepsilon_{ct}$ and $\lambda_y = \varepsilon_{cy,max}/\varepsilon_{ct}$. In general,

$$\lambda = \frac{\varepsilon_{c,max}}{\varepsilon_{ct}} \leq 1 \quad (21)$$

where $\varepsilon_{c,max}$ are maximum concrete strains at the end of the transfer length S_{r0} , see Fig. 3(a), in which the expression according to Russo and Romano (1992) and Tan et al. (2019) is adopted

$$\varepsilon_{c,max} = \frac{\psi \xi}{1 + \xi} \varepsilon_{sr} \quad (22)$$

Here, ε_{sr} is determined from Eq. (12) implying that λ becomes a value dependent on the steel stresses at the crack. The limiting value in Eq. (21) is chosen such that the transfer length S_{r0} never is larger than the crack spacing S_{cr0} in the uniaxial direction. Furthermore, it can be proven that the limit state in Eq. (20), i.e. when $\sigma_{c1b} = f_{ct}$, only is attained for $\lambda_x = \lambda_y = 1$. This also means that the cracking response in biaxial stress conditions is determined either by the concept of CLLM or CHLM similar to uniaxial stress conditions as depicted in Fig. 6.

3.2.2 CLLM

The concept of CLLM at biaxial stress conditions implies that $\lambda_x < 1$, $\lambda_y < 1$ and $\sigma_{c1b} < f_{ctm}$, meaning only a distinct region $S_r/2$ to each side of the crack experiences

incompatibility in strains, see Fig. 6(a). By geometry, two conditions for the transfer length apply

$$S_r = \begin{cases} 2S_{rx0} \cos|\theta_{cr}| & \text{if } S_{rx0} \cos|\theta_{cr}| \geq S_{ry0} \sin|\theta_{cr}| \\ 2S_{ry0} \sin|\theta_{cr}| & \text{if } S_{rx0} \cos|\theta_{cr}| < S_{ry0} \sin|\theta_{cr}| \end{cases} \quad (23)$$

in which S_{rx0} and S_{ry0} are determined from Eq.(10), while steel stresses at the crack are determined using Eq. (12).

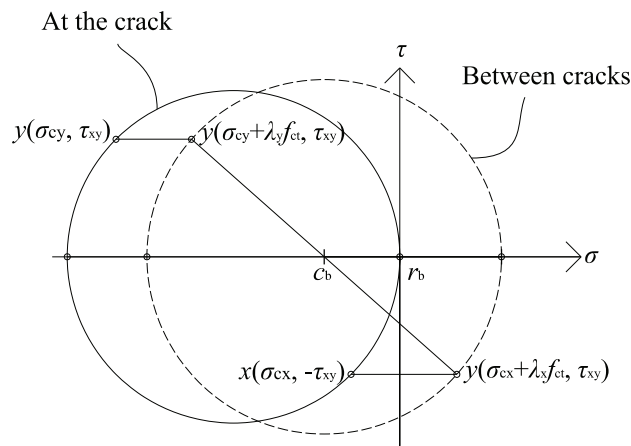


Figure 5 Figure of Mohr's circle of stresses for the concrete at cracks and between cracks inspired by Kaufmann and Marti (1998).

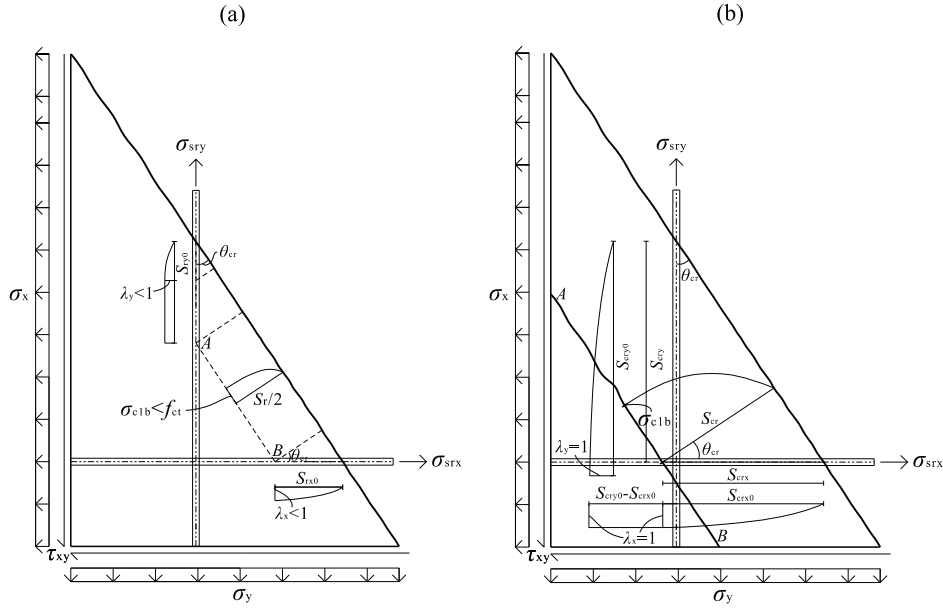


Figure 6(a) CLLM at biaxial stress conditions. (b) The limit state and CHLM at biaxial stress conditions.

3.2.3 CHLM

It is assumed that the concept of CHLM governs as long as either $\lambda_x = 1$, $\lambda_y = 1$ or $\sigma_{c1b} = f_{ct}$ occur. The choice means that the reinforcement in one direction can be governed by CLLM behaviour ($\lambda < 1$), while the other can be governed by CHLM behaviour ($\lambda = 1$), which typically occur in cases with orthotropic reinforcement configurations and for load situations with low shear stresses compared to the normal stresses. This means that CHLM governs as long as one of the reinforcement directions is governed by CHLM behaviour. Fig. 6(b) shows the case when $\lambda_x = 1$, $\lambda_y = 1$ and $\sigma_{c1b} = f_{ct}$ occur simultaneously. By geometry and the fact that the limit state, i.e. $\sigma_{c1b} = f_{ctm}$, only is attained for $\lambda_x = 1$ and $\lambda_y = 1$ yields two conditions for the crack spacing that is chosen to apply

$$\left. \begin{aligned} S_{crx} &= S_{crx0} \\ S_{cr} &= S_{crx} \cos|\theta_{cr}| \\ S_{cry} &= \frac{S_{cr}}{\sin|\theta_{cr}|} \end{aligned} \right\} \text{if } S_{crx0} \cos|\theta_{cr}| \geq S_{cry0} \sin|\theta_{cr}| \quad (24)$$

or as

$$\left. \begin{array}{l} S_{\text{cry}} = S_{\text{cry}0} \\ S_{\text{cr}} = S_{\text{cry}} \sin|\theta_{\text{cr}}| \\ S_{\text{crx}} = \frac{S_{\text{cr}}}{\cos|\theta_{\text{cr}}|} \end{array} \right\} \text{if } S_{\text{crx}0} \cos|\theta_{\text{cr}}| < S_{\text{cry}0} \sin|\theta_{\text{cr}}| \quad (25)$$

meaning that the skew crack spacing simply is governed by the angle θ_{cr} and the theoretical maximum crack spacing in uniaxial directions determined from Eq. (16). Fig. 6 shows the case where $S_{\text{rx}0} \cos|\theta| > S_{\text{ry}0} \sin|\theta|$ and $S_{\text{crx}0} \cos|\theta| > S_{\text{cry}0} \sin|\theta|$, in which it is noticed that line AB in Fig. 6(a) later forms to a crack in Fig. 6(b). Steel stresses at the crack are determined in a similar fashion as discussed for Eq. (17), however, by substituting the crack spacing $S_{\text{cr}0}$ in Eq. (14) with S_{crx} and S_{cry} . Similar substitution applies for Eq. (18) and (19) in Regime 2 and 3.

3.2.4 Crack width

The crack width is for the concept of CLLM determined as

$$w_{\text{cr}} = S_{\text{r}}(\varepsilon_1 - \varepsilon_{\text{c}1}) \quad (26)$$

and for the concept of CHLM as

$$w_{\text{cr}} = S_{\text{cr}}(\varepsilon_1 - \varepsilon_{\text{c}1}) \quad (27)$$

where ε_1 and $\varepsilon_{\text{c}1}$ are mean maximum principle strains for the RC membrane and the concrete respectively determined as

$$\varepsilon_1 = \frac{\varepsilon_{\text{smx}} + \varepsilon_{\text{smy}}}{2} + \sqrt{\left(\frac{\varepsilon_{\text{smx}} - \varepsilon_{\text{smy}}}{2}\right)^2 + \left(\frac{\gamma_{\text{xy}}}{2}\right)^2} \quad (28)$$

$$\varepsilon_{\text{c}1} = \frac{\varepsilon_{\text{cmx}} + \varepsilon_{\text{cmy}}}{2} + \sqrt{\left(\frac{\varepsilon_{\text{cmx}} - \varepsilon_{\text{cmy}}}{2}\right)^2 + \left(\frac{\gamma_{\text{cxy}}}{2}\right)^2} \quad (29)$$

Conservatively neglecting the concrete shear strains γ_{cxy} and subtracting Eq. (29) from (28) yields

$$\varepsilon_1 - \varepsilon_{c1} = \frac{(\varepsilon_{smx} - \varepsilon_{cmx}) + (\varepsilon_{smy} - \varepsilon_{cmy})}{2} \quad (30)$$

$$+ \sqrt{\left(\frac{\varepsilon_{smx} - \varepsilon_{smy}}{2}\right)^2 + \left(\frac{\gamma_{xy}}{2}\right)^2 - \left|\frac{\varepsilon_{cmx} - \varepsilon_{cmy}}{2}\right|}$$

which is approximately the same as

$$\varepsilon_1 - \varepsilon_{c1} \approx \frac{(\varepsilon_{smx} - \varepsilon_{cmx}) + (\varepsilon_{smy} - \varepsilon_{cmy})}{2} \quad (31)$$

$$+ \sqrt{\left[\frac{(\varepsilon_{smx} - \varepsilon_{cmx}) - (\varepsilon_{smy} - \varepsilon_{cmy})}{2}\right]^2 + \left(\frac{\gamma_{xy}}{2}\right)^2}$$

The expression in Eq. (31) was formulated with the purpose of serving as a generalized approach for predicting tension stiffening in skew cracks, an expression currently lacking in EC2 and MC2010. The expression is thus dependent on i) the difference between the mean strains, $\varepsilon_{sm} - \varepsilon_{cm}$, making it compatible with any other tension stiffening model for uniaxial stress conditions and ii) the shear strains γ_{xy} known from equilibrium.

3.3 Steel

Bilinear material behaviour is assumed for both reinforcing steel and prestressing steel as shown in Fig. 7.

3.4 Concrete

The constitutive model elaborated in Foster and Marti (2003) is here adopted for the compressive behaviour of concrete, see Fig. 8(a). Briefly summarized, the compressive curve by Thorenfeldt et al. (1987) was adopted using the calibrated decay factor proposed by Collins and Porasz (1989) for the post peak behaviour of conventional and high strength concrete. Furthermore, the stress and strain peak was adjusted by the factor k_c , which was obtained using the model of Vecchio and Collins (1986) to account for weakening of concrete when subjected to biaxial tension compression, i.e. $k_c \leq 1$. The effect of confinement, i.e. when $k_c > 1$, is by the authors of this paper conservatively neglected.

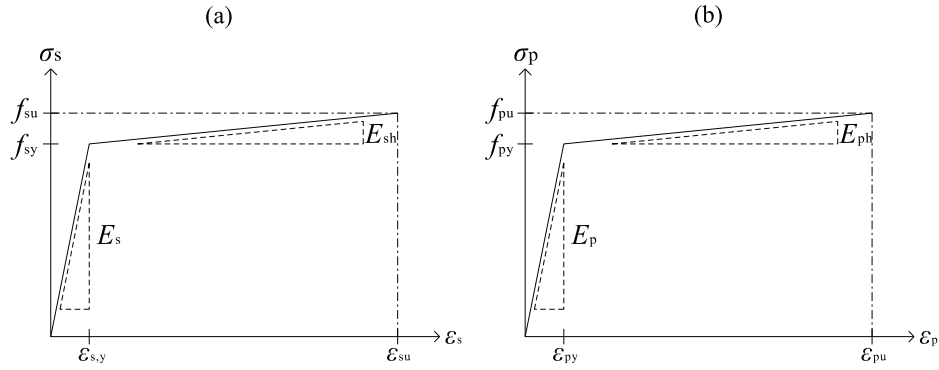


Figure 7(a) Bilinear behaviour of reinforcing steel bars. (b) Bilinear behaviour of prestressing steel.

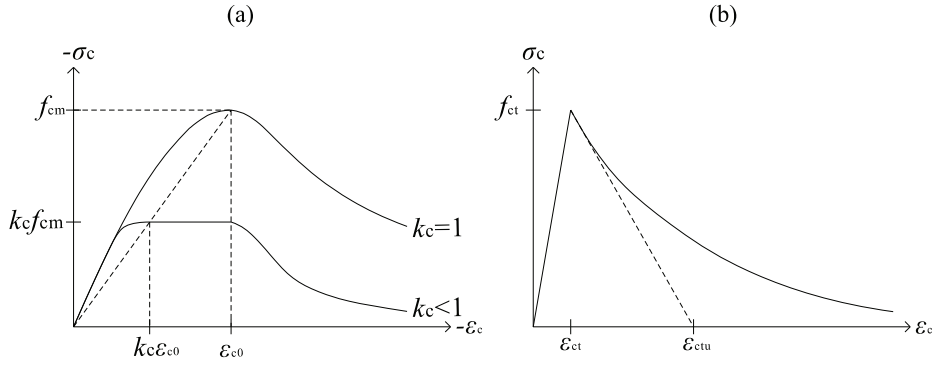


Figure 8(a) Compressive behaviour of concrete using the constitutive model of Foster and Marti (2003). (b) Tensile behaviour of concrete using the exponential curve recommended by the Dutch guidelines for NLFEA (Hendriks et al., 2017).

Tension softening is in general neglected, except for the condition when both principle strains are positive, i.e. $\epsilon_1 \geq \epsilon_2 > 0$. This can occur in load situations with low shear stresses compared to the normal stresses and is recommended to be included only to ensure numerical stability since combining tension softening with tension stiffening can appear inconsistent. The exponential curve recommended by the Dutch guidelines for nonlinear finite element analyses (NLFEA) of concrete structures (Belletti et al., 2014, Hendriks et al., 2017) is chosen for the tension softening of concrete, see Fig. 8(b). Here, $\epsilon_{ctu} = G_f / [\max(S_{crx0}, S_{cry0}) f_{ct}]$ where it is for simplicity assumed that the fracture energy is smeared over the maximum crack spacing in either x or y direction.

3.5 Constitutive relationships

The equilibrium in Eq. (1) to (3) can be written as

$$\boldsymbol{\sigma}_{xy} = \mathbf{D}_{xy} \boldsymbol{\varepsilon}_{xy} \quad (32)$$

in which the equilibrium in Eq. (32) is determined iteratively by updating the material elasticity tensor $\mathbf{D}_{xy} = \mathbf{D}_{cxy} + \mathbf{D}_{sxy} + \mathbf{D}_{pxy}$ using the secant stiffness. Here,

$$\mathbf{D}_{cxy} = \mathbf{T}' \mathbf{D}_{c12} \mathbf{T} \quad (33)$$

where \mathbf{T} is the strain transformation tensor to the principal plane and

$$\mathbf{D}_{c12} = \frac{1}{1 - \nu_{c12}\nu_{c21}} \begin{bmatrix} E_{c1} & \nu_{c12}E_{c1} & 0 \\ \nu_{c21}E_{c2} & E_{c2} & 0 \\ 0 & 0 & (1 - \nu_{c12}\nu_{c21})G_{c12} \end{bmatrix} \quad (34)$$

is the concrete elasticity tensor adopted from (Darwin and Pecknold, 1977; Foster and Marti, 2003). Here, ν_{c12} and ν_{c21} were the Poisson's ratio's taken as zero after cracking, and $(1 - \nu_{c12}\nu_{c21})G_{c12} = 1/4[E_{c1}(1 - \nu_{c12}) + E_{c2}(1 - \nu_{c21})]$. The secant modules are determined from the chosen constitutive laws for concrete as $E_{c1} = \sigma_{c1}/\varepsilon_1$ and $E_{c2} = \sigma_{c2}/\varepsilon_2$. The elasticity tensors for reinforcing and prestressing steel are

$$\mathbf{D}_{sxy} + \mathbf{D}_{pxy} = \begin{bmatrix} \rho_{sx}E_{sx} & 0 & 0 \\ 0 & \rho_{sy}E_{sy} & 0 \\ 0 & 0 & 0 \end{bmatrix} + \begin{bmatrix} \rho_{px}E_{px} & 0 & 0 \\ 0 & \rho_{py}E_{py} & 0 \\ 0 & 0 & 0 \end{bmatrix} \quad (35)$$

in which the secant modules are determined as $E_{sx} = \sigma_{srx}/\varepsilon_x$, $E_{sy} = \sigma_{sry}/\varepsilon_y$, $E_{px} = \sigma_{prx}/\varepsilon_x$ and $E_{py} = \sigma_{pry}/\varepsilon_y$. Tension stiffening is neglected for the prestressing steel.

4 Simplified approach to calculate crack widths for RC membranes

The MCMM should provide more realistic estimates of the crack widths and deformations at a given load level. However, this would require some local iterations within the equilibrium iterations in the case of CHLM as discussed for Eq. (17), which *might* increase the calculation time. If the crack widths are of primary interest, a simplification to eliminate the local iterations would be to treat rebars as *unbonded*, i.e. using the constitutive law for naked reinforcing steel in Fig. 7a) instead of the MTCM to determine the equilibrium in Eq. (32). The tension stiffening is a posteriori accounted for by assuming that steel strains at the crack are $\varepsilon_{srx} = \varepsilon_x$ and $\varepsilon_{sry} = \varepsilon_y$ in determining λ_x and λ_y from Eq. (21) and (22), after which the mean strains ε_{smx} and ε_{smy} are determined from the concept of either CLLM or CHLM to predict the crack width. This approach is analogous to predicting crack widths using the steel

stresses at a cracked section, similar to as one would have done in a practical design situation for uniaxial stress conditions. The approach is conservative compared to using the MCMM.

5 Comparison with experimental results

5.1 General

Experimental results and predictions by the MCMM, the CMM using the TCM of Seelhofer (2009) and the simplified approach are compared in the following. A similar comparison was conducted by Kaufmann and Mata-Falc3n 2017. The framework presented in section 3 was used for the MCMM predictions, meaning that tension stiffening using the MTCM was accounted for in obtaining the equilibrium in Eq. (32) and thus the load-deformation response. Tension softening was excluded in the predictions of the MCMM, CMM and the simplified approach.

5.2 Predicted response of shear panels

The response predicted by the MCMM is now compared to a selection of experimental results of orthogonally RC panels available in the literature (Vecchio and Collins 1982, Khalifa 1986, Marti and Meyboom 1992, Zhang and Hsu 1998, Laskar et al. 2007), see Table 1 for a summary of the material parameters. In summary, the selection consisted of panels with isotropic and anisotropic rebar layout, high strength concrete, prestressing and even unique loading conditions. The panels were loaded in pure shear except for PV25, which additionally was loaded in axial compression proportional to the shear stress level as $\sigma_x = \sigma_y = -0.69\tau_{xy}$, and PV28, which additionally was loaded in axial tension proportional to the shear stress level as $\sigma_x = \sigma_y = 0.32\tau_{xy}$. Furthermore, PP2 was prestressed in x-direction with prestressing steel ratio $\rho_{px} = 0.29\%$, yield stress $f_{pyx} = 910$ MPa, Young's modulus $E_{px} = 200$ GPa and an applied initial strain of $\varepsilon_{p0x} = 3.53\%$, while panel TA2 was prestressed in x-direction with prestressing steel ratio $\rho_{px} = 0.84\%$, yield stress $f_{pyx} = 1303$ MPa, Young's modulus $E_{px} = 200$ GPa and an applied initial strain of $\varepsilon_{p0x} = 4.93\%$. Note that TA2 was not reinforced with rebars in x-direction. The variety of panels selected for comparison was chosen mainly to investigate the ability of the MCMM to predict consistent load-deformation responses.

Table 1. Material parameters for selected RC panels.

Panel	Ref.	f_{cm} [MPa]	ε_{c0} [‰]	ϕ_{sx} [mm]	ρ_{sx} [%]	f_{syx} [MPa]	E_{sx} [MPa]	ϕ_{sy} [MPa]	ρ_{sy} [%]	f_{syy} [MPa]	E_{sy} [MPa]
PV25	Vecchio and	19.3	1.8	6.35	1.78	466	200	6.35	1.78	466	200
PV28	Collins (1982)	19	1.85	6.35	1.78	483	200	6.35	1.78	483	200
SE6	Khalifa (1986)	40	2.5	19.5	2.93	492	200	11.3	0.32	479	200
PP2	Marti and Meyboom (1992)	28.1	2.38	16	1.29	486	200	11.3	0.64	480	200
VA3	Zhang and Hsu (1998)	94.6	2.45	19.5	3.41	455	200	19.5	3.41	455	200
TA2	Laskar et al. (2007)	41.3	1.9	-	-	-	-	12.8	0.77	415	192

Comparison of experimental results and model predictions are shown in Fig. 9. As mentioned previously, the simplified approach does not include for tension stiffening in determining the equilibrium and yields thus larger deformations compared to the MCMM and CMM. It is also observed that there in general are small discrepancies between the MCMM and CMM, although the response after yielding of rebars looks to be slightly improved for the MCMM. Nevertheless, consistent and good predictions of the deformations and the ultimate load capacity are in general observed for both MCMM and CMM.

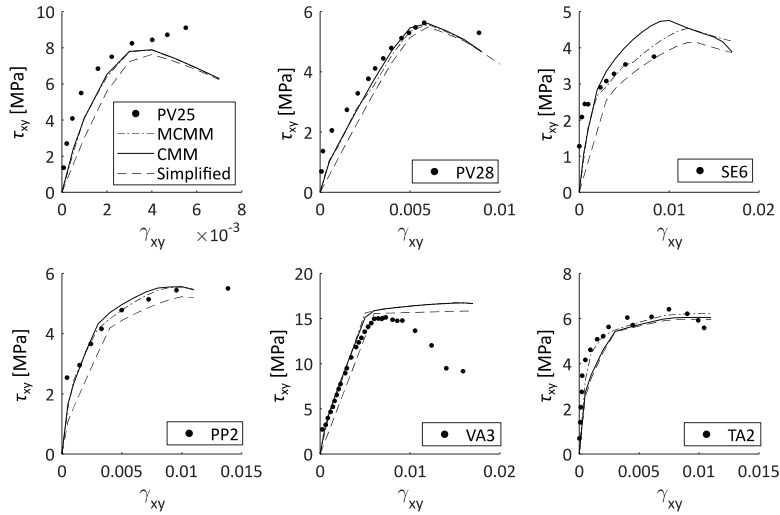


Figure 9 Comparison between responses predicted by the MCMM, CMM and the simplified approach with experimental results.

5.3 Crack widths

Comparison of crack widths predicted by the models are now compared to a selection of experimental results available in the literature at which the maximum crack widths measured were documented properly. The selection consisted of the test series by Tan et al. (2018a) on the RC ties X-20-40, X-32-40, X-20-90 and X-32-90, S and CS test series by Dyngeland (1989), panel PP1 by Marti and Meyboom (1992), A and B test series by Pang (1991) and KS test series by Proestos (2014). A summary including loading, reinforcement layout, maximum crack widths measured experimentally w_{\max} and crack widths predicted w_{cr} is given in Table 2. Further details regarding material properties, mechanical properties and test setup were else fully provided in the respective references. The axially loaded RC ties were included mainly to investigate how well the MCMM and the CMM captures the effects of large rebars and covers. Moreover, it is noticed that the S and CS panels were axially loaded only, however, with varying inclination for the orthogonal rebar grid in which α_s denotes the angle counter clockwise between the longitudinal reinforcement and the global x-direction. This was conveniently accounted for in the calculations by obtaining steel stresses at the crack in terms of the mean strains in the α_s -direction for the tension stiffening of the longitudinal reinforcement and the mean strains normal to the α_s -direction for the tension stiffening of the transversal reinforcement.

Fig. 10(a) shows comparison of mean and maximum crack widths measured experimentally and crack widths predicted by the models for six of the panels in Table 2. Corresponding load deformations responses are also included in Fig. 10(b). It is in general observed good agreement between maximum crack widths measured and crack widths predicted as well as between load deformation responses. The exception is CS2, at which the models yield quite conservative predictions. This can be explained by the fact that transversal pressure was applied normal to the loading direction, which would have beneficial effect on the tension stiffening as discussed by Dyngeland (1989). Similar was observed in the experiments by Dörr (1978) at which it was seen that the tension stiffening enhanced with increasing confining pressure for uniaxially loaded specimens. This beneficial effect is not captured by the MCMM nor the CMM since the bond-slip curves adopted were based on the behaviour of uniaxial loaded RC ties in tension. Similar trend was observed for PV25. Furthermore, the discontinuity observed for the MCMM and the simplified approach is caused by the transition between the CLLM and CHLM.

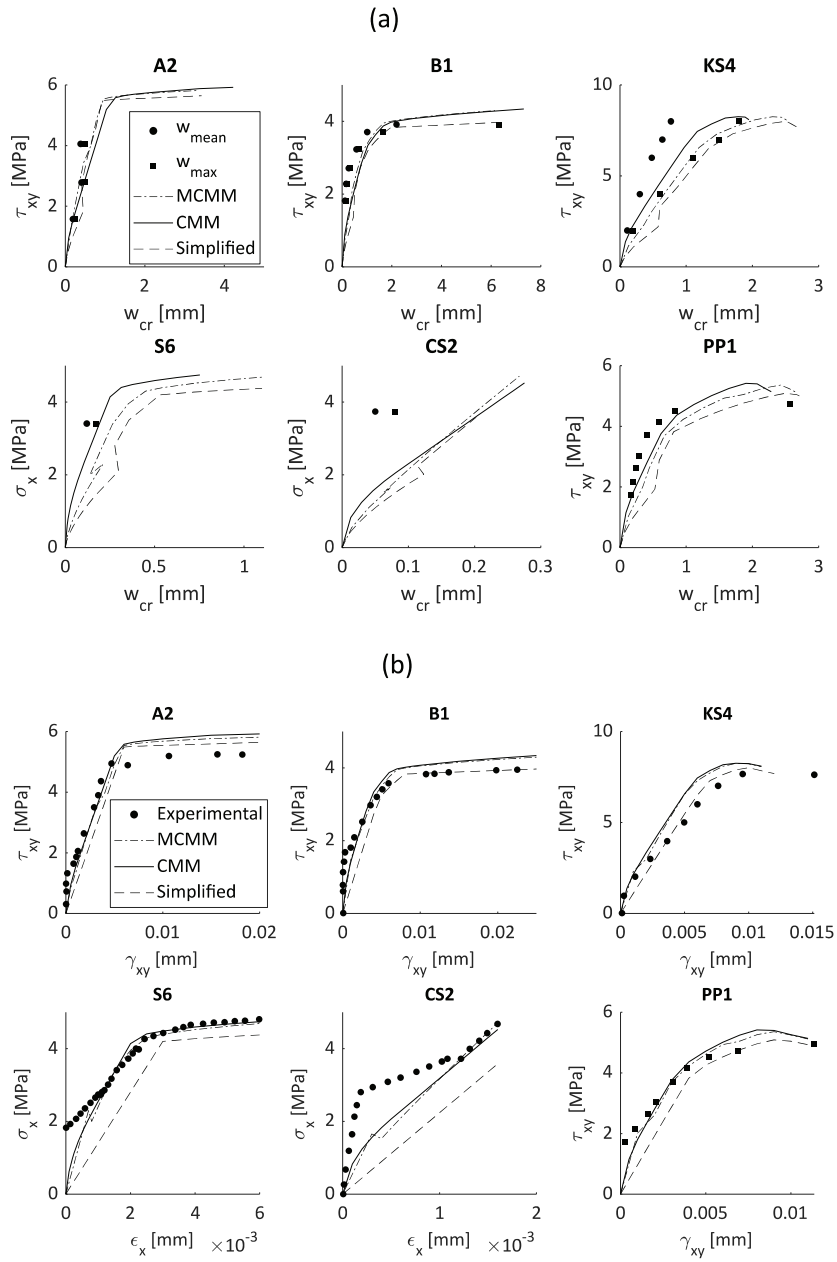


Figure 10(a) Comparison between mean and maximum crack widths measured experimentally and crack widths predicted by the MCMM, CMM and the simplified approach. (b) Comparison between corresponding load deformation responses predicted by the MCMM, CMM and the simplified approach with experimental results.

Table 2. Crack widths for investigated specimen.

Dimension [mm]	Panel	τ_{xy}	σ_x	σ_y	α_s [deg]	Cover [mm]	ϕ_{sx}	ϕ_{sy}	ρ_{sx}	ρ_{sy}	W_{max}	$W_{cr,MCM}$	$W_{cr,CMM}$	$W_{cr,simp}$	θ_{MCM}	θ_{CMM}	θ_{simp}
3000x400x400	X-20-40	-	3,14	-	0	40	20,00	-	1,57	-	0,13	0,24	0,11	0,24	0,55	1,25	0,55
		-	3,25	-							0,13	0,26	0,12	0,26	0,52	1,14	0,52
		-	4,17	-							0,16	0,37	0,19	0,37	0,44	0,85	0,44
			-	5,05	-						0,22	0,42	0,28	0,42	0,51	0,78	0,51
	X-32-40	-	4,71	-	0	40	32,00	-	4,02	-	0,08	0,15	0,05	0,15	0,55	1,58	0,55
		-	4,64	-							0,07	0,14	0,05	0,14	0,47	1,38	0,47
		-	6,33	-							0,10	0,18	0,09	0,18	0,53	1,09	0,53
	X-20-90	-	3,66	-	0	90	20,00	-	1,57	-	0,21	0,30	0,15	0,30	0,68	1,42	0,68
		-	3,59	-							0,21	0,30	0,14	0,30	0,72	1,51	0,72
		-	4,60	-							0,31	0,43	0,23	0,43	0,72	1,33	0,72
			-	6,27	-						0,40	0,56	0,40	0,56	0,72	1,01	0,72
	X-32-90	-	5,03	-	0	90	32,00	-	4,02	-	0,16	0,16	0,06	0,16	0,99	2,76	0,99
-		5,03	-							0,17	0,16	0,06	0,16	1,04	2,91	1,04	
-		6,28	-							0,21	0,18	0,09	0,18	1,16	2,42	1,16	
		-	7,51	-						0,24	0,23	0,12	0,23	1,05	2,05	1,05	
		-	8,52	-						0,27	0,27	0,14	0,27	1,00	1,89	1,00	
630x630x100	S1	-	3,76	-	0	10	8,00	8,00	1,12	-	0,15	0,21	0,18	0,21	0,72	0,84	0,72
	S2	-	3,56	-	0				1,12	-	0,14	0,19	0,16	0,19	0,72	0,86	0,72
	S3	-	3,80	-	45,00				1,12	1,12	0,29	0,33	0,40	0,40	0,87	0,72	0,72
	S4	-	3,49	-	45,00				1,12	1,12	0,30	0,30	0,35	0,37	1,00	0,85	0,82
	S5	-	2,67	-	45,00				0,56	1,12	0,41	0,83	0,45	1,74	0,49	0,90	0,23
	S6	-	3,41	-	18,40				1,12	1,12	0,17	0,27	0,19	0,35	0,64	0,90	0,49
	S7	-	3,45	-	18,40				1,12	0,37	0,32	0,81	0,49	1,04	0,40	0,65	0,31
	S8	-	3,41	-	18,40				1,12	1,12	0,16	0,27	0,19	0,35	0,60	0,84	0,46
	CS1	-	3,74	-4,67	0				1,12	-	0,08	0,20	0,21	0,20	0,40	0,38	0,40
	CS2	-	3,74	-9,34	0				1,12	-	0,08	0,20	0,21	0,20	0,40	0,38	0,40

KS7	7	-2,8	-2,8						0,75	0,77	0,54	0,90	0,98	1,38	0,84	
	9	-3,6	-3,6						1,30	1,04	0,78	1,19	1,25	1,66	1,09	
	2	-	-	0	54	16	12,8	2,09	1,35	0,20	0,18	0,08	0,29	1,12	2,54	0,69
KS8	5	-	-						0,65	0,52	0,35	0,60	1,24	1,85	1,08	
	7	-	-						0,80	0,78	0,55	0,87	1,03	1,46	0,92	
	9	-	-						1,20	1,14	0,75	1,20	1,05	1,59	1,00	
KS9	2	0,8	0,8	0	54	16	12,8	2,09	1,35	0,10	0,28	0,13	0,47	0,36	0,75	0,22
	3	1,2	1,2						0,50	0,38	0,26	0,47	1,33	1,90	1,07	
	5	2	2						0,90	0,75	0,53	0,85	1,20	1,70	1,06	
KS10	2	-	-	0	54	16	16	1,57	1,04	0,15	0,29	0,11	0,49	0,52	1,31	0,30
	4	-	-						0,60	0,63	0,39	1,38	0,95	1,55	0,43	
	6	-	-						1,10	1,19	0,74	1,40	0,93	1,49	0,78	
KS10	2	-0,6	-0,6	0	54	16	16	1,57	1,04	0,40	0,18	0,07	0,30	2,23	5,75	1,35
	5	-1,5	-1,5						0,60	0,55	0,32	1,16	1,09	1,88	0,52	
	8	-2,4	-2,4						1,00	1,13	0,70	1,33	0,88	1,44	0,75	
	9	-2,7	-2,7						1,50	1,30	0,83	1,51	1,15	1,82	0,99	

6 The modelling uncertainty for crack width predictions

The modelling uncertainty for crack widths predictions, i.e.

$$\theta = \frac{w_{\max}}{w_{\text{cr}}} \quad (36)$$

was investigated for the MCMM, CMM and the simplified approach. The statistical properties of θ were obtained using the method of Engen et al. (2017) and Tan et al. (2018a), which implied assuming log-normal distribution for the modelling uncertainty in accordance with the recommendations in JCSS Probabilistic Model Code (2001). This means that the natural logarithm of θ is assumed normal distributed. Values for θ are shown in Table 2, presented graphically in Fig. 11 and summarized in Table 3 showing the statistical properties for the modelling uncertainty such as mean, variance, standard deviation *SD*, coefficient of variation *COV*, minimum and maximum values for θ and the number of observations $n(\theta > 1)$ at which the crack widths measured exceed the crack widths predicted. A total of 101 observations for θ were obtained from Table 2. The summary suggests that the MCMM and the simplified approach show greater potential for predicting crack widths than the CMM.

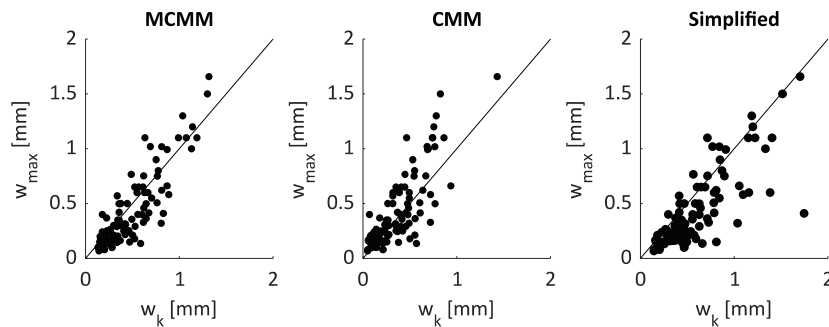


Figure 11 Maximum crack widths measured experimentally versus crack widths predicted by the MCMM, CMM and the simplified approach for the 101 observations for the modelling uncertainty.

Table 3. Modelling uncertainty for crack width predictions.

Model	Mean	Variance	<i>SD</i>	<i>COV</i>	Min	Max	$n(\theta > 1)$
MCMM	0,88	0,19	0,40	0,45	0,23	2,23	36
CMM	1,28	0,27	0,72	0,56	0,24	5,75	61
Simplified	0,73	0,21	0,35	0,48	0,19	1,54	19

7 Discussion

The results show that the simplified approach provided most conservative predictions, as expected. This can be explained by the fact that the simplified approach predicts crack widths using shear strains γ_{xy} when tension stiffening is neglected. Furthermore, it is observed that the CMM yielded a mean value for the modelling uncertainty on the nonconservative side while being more inconsistent in its predictions than the MCMM and the simplified approach which is reflected by the observations that it has the largest SD and COV. Table 2 shows that the CMM in particular underestimated the crack widths considerably for RC ties with the combination of large rebar and cover, e.g. X-32-90. The MCMM, on the other hand, provided a mean closest to one on the conservative side and yielded more consistent predictions in comparison which can be observed by the fact that it exhibits the lowest COV. This statement can also be backed up from a mechanical point of view since the MCMM accounts for all cracking stages through the concepts of CLLM and CHLM behaviour, whereas the CMM in principle applies to the stabilized cracking stage only. Also, solving the SODE for the slip using the MC2010 bond-slip law in the MTCM is a mechanical improvement to the TCM, and should better account for the effects of large rebars and covers as well as rebar spacing, thus offering wider range of applicability as discussed by Tan et al. (2019).

It is noticed from Table 3 that the *COV* is relatively large in comparison with the *COV* for the modelling uncertainty of the ultimate load capacity reported in e.g. Bentz et al. (2006) and Pimentel et al. (2010). Relatively large *COV* for the modelling uncertainty of crack widths predicted have also been reported in recent studies (Empelmann et al. 2016, Tan et al. 2018a, Empelmann and Busse 2018). This is first and foremost owing to the large scatter in tensile strength of concrete and its influence on generating a random crack pattern as discussed by Barre et al. (2016) and Tan et al. (2018b). Secondly, the modelling uncertainty for predicting the maximum crack widths becomes sensitive to the many physical uncertainties related to the chosen measuring technique. Most simply measure the maximum crack widths by the eye, others use more refined measuring techniques such as image analysis or digital image correlation while some use statistics to determine the 95%-quantile of the maximum crack widths measured. Another important physical aspect is related to where the maximum crack widths measured apply at the specimen surface, since they in general vary significantly depending on if they are measured over the rebar or between two adjacent rebars as discussed by Dawood and Marzouk (2011), not to mention the uncertainties related to the calculation model itself (Markova and Sykora 2016, Mlcoch et al. 2017).

All three models can be extended to predict the cracking behaviour of RC shell sections, e.g. by implementation to a layered approach. The authors of this paper are currently working on such an approach. It is also recommended to conduct further probabilistic analysis on the modelling uncertainty for crack width predictions to better understand the main parameters influencing the cracking behaviour. Such studies can be important in developing crack width calculation models in general.

8 Conclusions

The modified cracked membrane model (MCMM) presented in this paper was formulated to facilitate a mechanical calculation model that is able to predict crack widths in orthogonally reinforced concrete (RC) membranes subjected to in-plane loading. It was formulated using the basic concepts of the cracked membrane model (CMM), the essential difference being a replacement of the tension chord model (TCM) with the modified tension chord model (MTCM). A generalized expression to determine the tension stiffening normal to the crack in RC membranes was formulated, a feature currently missing in Eurocode 2 and *fib* Model Code 2010. Also, a simplified approach for predicting crack widths in RC membranes was proposed. The crack widths predicted by the MCMM, the cracked membrane model (CMM) and the simplified approach were compared to a total of 101 maximum crack widths measured experimentally on 37 test specimens to discover the modelling uncertainty. The CMM showed a mean value for the modelling uncertainty on the nonconservative side and yielded more inconsistent crack width predictions in particular for the combination of large rebars and covers. The MCMM, on the other hand, provided a mean closest to one on the conservative side and was observed to be more consistent in terms of having the lowest coefficient of variation in comparison with the CMM, which could be attributed to its mechanical improvement, hence, offering a wider range of applicability. The simplified approach yielded in average most conservative predictions as expected. Finally, the results in this paper suggests that both the MCMM and the simplified approach show great potential for yielding reliable crack width predictions in RC membranes, whereas the MCMM showed good predictions of deformations and ultimate capacity as well.

Acknowledgement

The work presented in this paper is part of an ongoing PhD study funded by the Norwegian Public Roads Administration as a part of the Coastal Highway Route E39 project.

Notations

A_c	Sectional area
A_s	Area rebar
c_b	Center of Mohr's circle of concrete stresses between cracks
dx	Differential element in an RC tie
E_c	Young's modulus concrete
E_p	Young's modulus prestressing steel
E_{ph}	Young's modulus prestressing steel after yielding
E_s	Young's modulus rebar
E_{sh}	Young's modulus rebar after yielding
f_{cm}	Compressive strength concrete
f_{ct}	Tensile strength concrete
f_{pu}	Ultimate strength prestressing steel
f_{py}	Yield strength prestressing steel
f_{su}	Ultimate strength rebar
f_{sy}	Yield strength rebar
G_f	Tensile fracture energy concrete
k_c	Reduction factor for compressive strength of concrete due to tensile strains
L	Bar length
r_b	Radius of Mohr's circle of concrete stresses between cracks
S_{cr}	Crack spacing at biaxial stress conditions
S_{crx}	Crack spacing in x-direction at biaxial stress conditions
S_{cry}	Crack spacing in y-direction at biaxial stress conditions
S_{crx0}	Maximum crack spacing in x-direction
S_{cry0}	Maximum crack spacing in y-direction
S_{cr0}	Crack spacing at uniaxial stress conditions
S_r	Transfer length at biaxial stress conditions
S_{r0}	Transfer length at uniaxial stress conditions
S_{rx0}	Transfer length in x-direction
S_{ry0}	Transfer length in y-direction
u	Slip
$u_{r,CHLM}$	Slip at the crack for CHLM
$u_{r,CLLM}$	Slip at the crack for CLLM
u'	Derivative of slip
w_{cr}	Crack width predicted
$w_{cr,CMM}$	Crack widths predicted by the cracked membrane model
$w_{cr,MCMM}$	Crack widths predicted by the modified cracked membrane model
$w_{cr,simp}$	Crack widths predicted by the simplified approach
w_{max}	Crack width measured experimentally
x	Coordinates in x-direction
y	Coordinates in y-direction

ε_1	Mean maximum principle strains
ε_c	Concrete strains
ε_{c0}	Concrete strains corresponding to the compressive strength of concrete
ε_{c1}	Mean maximum principle strains in concrete
ε_{ct}	Concrete strains corresponding to tensile strength of concrete
ε_{cx}	Concrete strains in x-direction
ε_{cy}	Concrete strains in y-direction
$\varepsilon_{c,max}$	Maximum concrete strains
ε_{cm}	Mean concrete strains
ε_{cmx}	Mean concrete strains in x-direction
ε_{cmy}	Mean concrete strains in y-direction
ε_m	Mean strains
ε_p	Prestressing steel strains
ε_{py}	Prestressing steel strains at yielding
ε_{pu}	Prestressing steel strains at ultimate strength
ε_s	Rebar strains
ε_{sm}	Mean rebar strains
ε_{smx}	Mean rebar strains in x-direction
ε_{smy}	Mean rebar strains in y-direction
ε_{sr}	Rebar strains at the crack
$\varepsilon_{sr,y}$	Rebar strains at the crack at yielding
ε_{sx}	Rebar strains in x-direction
ε_{sy}	Rebar strains in y-direction
$\varepsilon_{s,y}$	Rebar strains at yielding
ε_{su}	Rebar strains at ultimate strength
γ_{xy}	Shear strains
γ_{cxy}	Shear strains in concrete
ψ	Factor accounting for plane sections not remaining plane in RC ties
ρ_{sx}	Rebar ratio in x-direction
ρ_{sy}	Rebar ratio in y-direction
σ_c	Stresses in concrete
σ_{c1}	Normal stresses in concrete normal to the crack
σ_{c1b}	Maximum principle stresses in concrete between cracks
σ_{c2}	Normal stresses in concrete parallel to the crack
σ_{cx}	Normal stresses in concrete in x-direction
σ_{cy}	Normal stresses in concrete in y-direction
σ_p	Normal stresses in prestressing steel
σ_{prx}	Normal stresses in prestressing steel at crack in x-direction
σ_{pry}	Normal stresses in prestressing steel at crack in y-direction
σ_s	Normal stresses in rebar in an RC tie
σ_{sr}	Rebar stresses at crack

σ_{srx}	Rebar stresses at crack in x-direction
σ_{sry}	Rebar stresses at crack in y-direction
σ_x	Normal stresses in x-direction
σ_y	Normal stresses in y-direction
τ	Bond stresses at the interface between concrete and steel
τ_{b0}	Bond stresses at the interface between concrete and steel prior to yielding
τ_{b1}	Bond stresses at the interface between concrete and steel after the onset of yielding
τ_{c12}	Shear stresses in concrete at crack
$\tau_{m,y}$	Bond stresses at the interface between concrete and steel at the onset of yielding of rebar at the crack
τ_{xy}	Shear stresses
θ	Modelling uncertainty for crack width predictions
θ_{cr}	Angle between a unit vector normal to the crack and x-direction
ϕ_s	Rebar diameter

References

- Bálasz, G.L. (1993). "Cracking Analysis Based on Slip and Bond Stresses." *ACI Materials Journal*, 90(4), 340-348.
- Barre, F., Bisch, P., Chauvel, D., et al. (2016). "Control of Cracking in Reinforced Concrete Structures: Research Project CEOS.fr (Civil Engineering and Geomechanics)." ISTE Ltd, London, UK.
- Belletti, B., Damoni, C., Hendriks, M.A.N, and de Boer, A. (2014). "Analytical and numerical evaluation of the design resistance of reinforced concrete slabs." *fib Journal Structural Concrete*, 15(3), 1436-1447.
- Bentz, E.C., (2000). "Sectional Analysis of Reinforced Concrete Members." PhD-thesis, Department of Civil Engineering, University of Toronto, Toronto, Canada.
- Bentz, E.C., Vecchio, F.J., and Collins, M.P. (2006). "Simplified Modified Compression Field Theory for Calculating Shear Strength of Reinforced Concrete Elements." *ACI Structural Journal*, 103(4), 614-624.
- Bernardo, L.F.A., Lyrio, A.R.B., Silva, J.R.B., and Horowitz, B. (2018). "Refined Softened Truss Model with Efficient Solution Procedure for Prestressed Concrete Membranes." *Journal of Structural Engineering*, 144(6), DOI: [10.1061/\(ASCE\)ST.1943-541X.0002044](https://doi.org/10.1061/(ASCE)ST.1943-541X.0002044).
- Borosnyói, B., and Balázs, G.L. (2005). "Crack width variation within the concrete cover of reinforced concrete members" *fib Journal Structural Concrete*, 62(3), 53-62.
- CEN. (2004). "EN 1992-1-1 Eurocode 2: Design of Concrete Structures – Part 1-1: General Rules and Rules for buildings." European Committee for Standardization, Brussels, Belgium.
- Cerioni, R., Iori, I., Michelini, P., and Bernardi, P. (2007). "Multi-directional modeling of crack pattern in 2D R/C members." *Engineering Fracture Mechanics*, 75(3-4), 615-628.
- Collins, M.P., and Porasz, A. (1989). "Shear strength for high strength concrete." *Bulletin No. 193, Design Aspects of High Strength Concrete*, Comité Euro-International du Béton, 75-83.
- Collins, M.P., and Mitchell, D. (1997). "Prestressed concrete structures." Prentice Hall, Inc, New Jersey, USA.
- Dabbagh, H., and Foster, S.J. (2006). "A Smearred – Fixed Crack Model for FE Analysis of RC Membranes Incorporating Aggregate Interlock." *Advances in Structural Engineering*, 9(1), 91-101.
- Darwin, D., and Pecknold, D.A. (1977). "Nonlinear biaxial stress-strain law for concrete." *Journal of the Engineering Mechanics Division, ASCE*, 103(2), 229-241.
- Dawood, N., and Marzouk, H. (2011). "Crack width model for thick reinforced concrete plates subjected to in-plane forces." *Canadian Journal of Civil Engineering*, 38(11), 1262-1273.
- Debernardi, P.G., and Taliano, M. (2016). "An improvement to Eurocode 2 and fib Model Code 2010 methods for calculating crack width in RC structures." *fib Journal Structural Concrete*, 17(3), 365-376.
- DIN: EN 1992-1-1/NA. (2011). 2011-01, National Annex – Nationally determined parameters

- Eurocode 2: Design of concrete structures – Part 1-1: General rules and rules for buildings.
- Dörr, K. (1978). “Bond-Behaviour of Ribbed Reinforcement under Transversal Pressure. IASS Symposium on Nonlinear Behaviour of Reinforced Concrete Spatial Structures.” *Werner Verlag*, Düsseldorf, Germany, Vol. 1, pp. 13-24.
- Dyngeland, T. (1989). “Behaviour of Reinforced Concrete Panels.” PhD-thesis, Department of Structural Engineering, Norwegian University of Science and Technology, Trondheim, Norway.
- Edwards, A.D., and Picard, A. (1972). “Theory of Cracking in Concrete Members.” *Proceedings of the ASCE – Journal of the Structural Division*, 98(12), 2687-2700.
- Eligehausen, R., Popov, E.P., and Bertero, V.V. (1983). “Local bond stress-slip relationships of deformed bars under generalized excitations.” Report No. UCB/EERC 83-23, University of California, Berkeley, USA.
- Empelmann, M., Sawicki, P., and Busse, D. (2016). “Comparison of analysis concepts for crack width limitation in accordance with EN 1992-1-1, DIN EN 1992-1-1/NA as well as Model Code 2010. Report Nr. P02-19-1A” *iBMB*, TU Braunschweig, Germany.
- Empelmann, M., and Busse, D. (2018). “Prediction Accuracy of Code Provisions for the Calculation of Crack Widths.” *fib Congress*, October 2018, Melbourne, Australia, ISBN 978-1-877040-14-6.
- Engen, M., Hendriks, M.A.N., Köhler, J., et al. (2017). “A quantification of the modelling uncertainty of non-linear finite element analyses of large concrete structures.” *Structural Safety*, 64(1), 1-8.
- Foster, S.J., and Marti, P. (2003). “Cracked Membrane Model: Finite Element Implementation.” *Journal of Structural Engineering*, 129(9), 1155-1163.
- fib*. (2010). “Structural Concrete. Textbook on behaviour, design and performance. Second edition. Volume 2.” *fib bulletin No. 52*, Lausanne, Switzerland.
- fib*. (2013). “*fib* Model Code for Concrete Structures 2010. International Federation for Structural Concrete.” Ernst & Sohn, Berlin.
- Giordano, L., and Mancini, G. (2009). “Crack Width Evaluation of Reinforced Concrete Membrane Elements.” *Structural Engineering International*, 19(3), 256-261.
- Goto, Y. (1971) “Crack formed in concrete around deformed tension bars.” *ACI Journal*, 68(4), 244-251.
- Hendriks, M.A.N., de Boer, A., and Belletti, B. (2014). “Guidelines for Nonlinear Finite Element Analysis of Concrete Structures (RTD:1016-1: 2017).” *Rijkswaterstaat Centre for Infrastructure*, Utrecht, the Netherlands.
- Hsu, T.T.C. (1988). “Softened Truss Model Theory for Shear and Torsion.” *ACI Structural Journal*, 85(6), 624-635.
- Hsu, T.T.C., and Mo, Y.L. (2010). “Unified theory of concrete structures.” Wiley, Chichester, UK.
- Irgens, F. (2008). *Continuum Mechanics*, Springer, Bergen, Norway.
- JCSS. (2001). “Probabilistic Model Code, 12th draft.” Joint Committee on Structural Safety.
- Jiang, D.H., Shah, S.P., and Andonian, A.T. (1984). “Study of the transfer of tensile forces by bond.” *ACI Journal*, 81(4), 251-259.
- Khalfallah, S. (2006). “Cracking analysis of reinforced concrete tensioned members.” *fib*

- Journal Structural Concrete*, 7(3), 111-116.
- Khalifa, J., (1986). "Limit Analysis and Design of Reinforced Concrete Shell Elements." PhD-thesis, Department of Civil Engineering, University of Toronto, Toronto, Canada.
- Kaufmann, W. (1998). "Strength and Deformations of Structural Concrete Subjected to In-Plane Shear and Normal Forces." PhD-thesis, Institute of Structural Engineering, Swiss Federal Institute of Technology, Zürich, Switzerland.
- Kaufmann, W., and Marti, P. (1998). "Structural Concrete: Cracked Membrane Model." *Journal of Structural Engineering*, 124(12), 1467-1475.
- Kaufmann, W., and Mata-Falcón, J. (2017). "Crack Widths in Structural Concrete Subjected to In-Plane Loading." Workshop proceedings No. 12 on Crack width calculation methods for large concrete structures, Nordic Concrete Federation, Norsk Betongforening, Oslo, Norway.
- Laskar, A., Wang, J., Hsu, T.T.C., and Mo, Y.L. (2007). "Rational Shear Provisions for AASHTO LRFD Specifications: TECHNICAL REPORT. Report No. FHWA/TX-07/0-4759-1." *Department of Civil & Environmental Engineering, Cullen College of Engineering, University of Houston, Houston, Texas, USA.*
- Lutz, L.A. (1970) "Analysis of Stresses in Concrete Near a Reinforcing Bar Due to Bond and Transverse Cracking." *ACI Journal*, 67(10): 778-787.
- Markova, J., and Sykora, M. (2016). "Uncertainties in crack width verification of reinforced concrete structures." *Risk, Reliability and Safety: Innovating Theory and Practice*, DOI: 10.1201/9781315374987-368.
- Marti, P., and Meyboom, J. (1992). "Response of Prestressed Concrete Elements to In-Plane Shear Forces." *ACI Structural Journal*, 89(5), 503-514.
- Marti, P., Alvarez, M., Kaufmann, W., and Sigrist, V. (1998). "Tension Chord Model for Structural Concrete." *Structural Engineering International*, 8(4), 287-298.
- Mlcoch, M., Markova, M., and Sykora, M. (2017). "Uncertainty in crack width estimates according to *fib* Model Code 2010." *Civil Engineering Series*, 17(1), 155-158.
- Mirza, S.M., and Houde, J. (1979). "Study of Bond Stress-Slip Relationships in Reinforced Concrete." *ACI Journal*, 76(1): 19-46.
- Nilson, A.H. (1972). "Internal Measurement of Bond Slip." *ACI Journal*, 69(7), 439-441.
- NPRA. (2015). "N400 Bruprosjektering: Prosjektering av bruer, ferjekaier og andre bærende konstruksjoner." *N400 i Statens vegvesens håndbokserie*, ISBN: 978-82-7207-680-0.
- Pang, X.B. (1991). "Constitutive laws of Reinforced Concrete in Shear." PhD-thesis, Department of Civil and Environmental Engineering, University of Houston, Houston, USA.
- Pang, X.B., and Hsu, T.T.C. (1995). "Behavior of reinforced concrete membrane elements in shear." *ACI Structural Journal*, 92(6), 665-679.
- Pimentel, M., Brüwhiler, E., and Figueiras, J. (2010). "Extended cracked membrane model for the analysis of RC panels." *Engineering Structures*, 32(8), 1964-1975.
- Proestos, G.T. (2014). "Influence of High-Strength Reinforcing Bars on the Behaviour of Reinforced Concrete Nuclear Containment Structures Subjected to Shear." M.Sc-thesis, Department of Civil Engineering, University of Toronto, Toronto, Canada.
- Russo, G., and Romano, F. (1992). "Cracking Response of RC Members Subjected to Uniaxial Tension." *Journal of Structural Engineering*, 118(5), 1172-1190.

- Saliger, R. (1936). "High-grade steel in reinforced concrete." *Proceedings of the 2nd Congress of the International Association for Bridge and Structural Engineering, Berlin-Munich, Germany*. ETH Zürich, Switzerland, 293-315.
- Seelhofer, H. (2009). "Ebener Spannungszustand im Betonbau Grundlagen und Anwendungen." PhD-thesis, Institute of Structural Engineering, Swiss Federal Institute of Technology, Zürich, Switzerland.
- Somayaji, S., and Shah, S.P. (1981). "Bond stress versus slip relationship and cracking response of tension members." *ACI Journal*, 78(3), 217-225.
- Tan, R., Eileraas K., Opkvitne, O., et al. (2018a). "Experimental and theoretical investigation of crack width calculation methods for RC ties." *fib Journal Structural Concrete*, 19(5), 1436-1447.
- Tan, R., Hendriks, M.A.N., Geiker, M., and Kanstad, T. (2018b). "A numerical investigation of the cracking behaviour of reinforced concrete tie elements." *Magazine of Concrete Research*, Ahead of Print, DOI: <https://doi.org/10.1680/jmacr.18.00156>.
- Tan, R., Hendriks, M.A.N., and Kanstad, T. (2018c). "An investigation of the strain profile over the cover in reinforced concrete elements subjected to tension." *Proceedings for the 5th fib Congress*, October 2018, Melbourne, Australia, ISBN 978-1-877040-14-6.
- Tan, R., Hendriks, M.A.N., Geiker, M., and Kanstad, T. (2019). "Analytical calculation model for predicting the cracking behavior of reinforced concrete." Accepted for publication in the ASCE Journal of Structural Engineering.
- Tammo, K., Lundgren, K., and Thelandersson, S. (2009). "Nonlinear analysis of crack widths in reinforced concrete." *Magazine of Concrete Research*, 61(1), 23-34.
- Thorenfeldt, E., Tomaszewicz, A., and Jensen, J.J. (1987). "Mechanical properties of high-strength concrete and applications in design." *Proceedings International Symposium on Utilization of High-Strength Concrete*, Stavanger, Norway, 149-159.
- Vecchio, F.J., and Collins, M.P. (1982). "The response of reinforced concrete to in-plane shear and normal stresses." Department of Civil Engineering, University of Toronto, Toronto, Canada.
- Vecchio, F.J., and Collins, M.P. (1986). "The Modified Compression-Field Theory for Reinforced Concrete Elements Subjected to Shear" *ACI Structural Journal*, 83(2), 219-231.
- Zhang, L.X., and Hsu, T.T.C. (1998). "Behavior and Analysis of 100 MPa Concrete Membrane Elements." *Journal of Structural Engineering*, 124(1), 24-34.

Appendices

Appendix A

Solution procedure for the modified cracked membrane model

It is assumed that external stresses $\sigma_{xy,ext} = [\sigma_x \ \sigma_y \ \tau_{xy}]^T$ are known. The procedure excludes prestressing as well as Regime 2 and 3 in the MTCM.

Step 1 – Use material and geometry properties to determine the crack parameters $\rho_s = A_s/A_c$, $\alpha_E = E_s/E_c$, $\beta = 1 + \alpha$, $\delta = (1 - \alpha)/2$, $\xi = \alpha_E \rho_s / \psi$, $\chi = \zeta \frac{\sum \pi \phi_s}{A_s E_s} (1 + \xi)$ and $\gamma = \chi \tau_{max} / (\beta u_1^\alpha)$ in the reinforcement directions where $\alpha = 0.35$, $\tau_{max} = 5.0$ MPa, $u_1 = 0.1$ mm, $\psi = 0.70$, $\zeta = 1.0$ and $\sum \pi \phi_s$ is the sum of the perimeters of rebars in the section. Determine thereafter the uniaxial crack spacing

$$S_{cr0} = \frac{1}{\delta} \left[\varepsilon_{ct} \frac{1 + \xi}{\psi \xi} \left(\frac{1}{2\gamma} \right)^{\frac{1}{2\delta}} \right]^{\frac{2\delta}{\beta}} \quad (A1)$$

and the steel strain when a crack forms

$$\varepsilon_{sr} = \varepsilon_{ctm} \frac{1 + \xi}{\psi \xi} \quad (A2)$$

Step 2 – Determine the global strain tensor

$$\boldsymbol{\varepsilon}_{xy} = \mathbf{D}_{xy}^{-1} \boldsymbol{\sigma}_{xy,ext} \quad (A3)$$

where \mathbf{D}_{xy} is chosen initially as the elastic material elasticity tensor.

Step 3 – Determine principal strains

$$\boldsymbol{\varepsilon}_{12} = \mathbf{T}(\theta_{cr}) \boldsymbol{\varepsilon}_{xy} \quad (A4)$$

where $\mathbf{T}(\theta_{cr})$ is the transformation tensor and θ_{cr} is the angle between maximum principle strains and the reference x-axis.

Step 4 – Determine concrete principal stresses $\sigma_{c1}(\varepsilon_{c1}, \varepsilon_{c2})$ and $\sigma_{c2}(\varepsilon_{c1}, \varepsilon_{c2})$ from a chosen constitutive law including the effect of transversal strains.

Step 5 – Determine global concrete stresses

$$\boldsymbol{\sigma}_{cxy} = \mathbf{T}(\theta_{cr})^T \boldsymbol{\sigma}_{c12} \quad (A5)$$

Step 6a – Determine concrete stresses between cracks by

$$\sigma_{c1b} = \frac{f_{ct}}{2} (\lambda_x + \lambda_y) - \frac{\tau_{xy}}{2} (\tan \theta_{cr} + \cot \theta_{cr}) \quad (A6)$$

$$+ \sqrt{\left[\frac{\tau_{xy}}{2} (\cot \theta_{cr} - \tan \theta_{cr}) \right]^2 - \frac{f_{ct}}{2} (\lambda_x - \lambda_y) + \tau_{xy}^2} \leq f_{ct}$$

where $\lambda_x = \varepsilon_{cx,max}/\varepsilon_{ct}$ and $\lambda_y = \varepsilon_{cy,max}/\varepsilon_{ct}$. In general,

$$\lambda = \frac{\varepsilon_{c,max}}{\varepsilon_{ct}} \leq 1 \quad (A7)$$

at which

$$\varepsilon_{c,max} = \frac{\psi \xi}{1 + \xi} \varepsilon_{sr} \quad (A8)$$

$$\varepsilon_{sr} = \frac{1 + \xi}{\delta + \xi} \varepsilon_m \quad (A9)$$

where ε_m are mean strains obtained from the global strain tensor in the reinforcement directions, in this case either as ε_x or ε_y .

Step 6b – Determine crack spacing either by CLLM or CHLM.

If $\lambda_x < 1$, $\lambda_y < 1$ and $\sigma_{c1b}/f_{ctm} < 1$ then CLLM governs and the crack spacing is determined as

$$S_r = \begin{cases} 2S_{rx0} \cos|\theta_{cr}| & \text{if } S_{rx0} \cos|\theta_{cr}| \geq S_{ry0} \sin|\theta_{cr}| \\ 2S_{ry0} \sin|\theta_{cr}| & \text{if } S_{rx0} \cos|\theta_{cr}| < S_{ry0} \sin|\theta_{cr}| \end{cases} \quad (A10)$$

where in general

$$S_{r0} = \frac{1}{\delta} \left[\varepsilon_{sr} \left(\frac{1}{2\gamma} \right)^{\frac{1}{2\delta}} \right]^{\frac{2\delta}{\beta}} \quad (A11)$$

If either $\lambda_x = 1$, $\lambda_y = 1$ and $\frac{\sigma_{c1b}}{f_{ctm}} = 1$ occur then CHLM governs and the crack spacing is determined as

$$\left. \begin{aligned} S_{crx} &= S_{crx0} \\ S_{cr} &= S_{crx} \cos|\theta_{cr}| \\ S_{cry} &= \frac{S_{cr}}{\sin|\theta_{cr}|} \end{aligned} \right\} \text{if } S_{crx0} \cos|\theta_{cr}| \geq S_{cry0} \sin|\theta_{cr}| \quad (A12)$$

or as

$$\left. \begin{aligned} S_{\text{cry}} &= S_{\text{cry}0} \\ S_{\text{cr}} &= S_{\text{cry}} \sin|\theta_{\text{cr}}| \\ S_{\text{crx}} &= \frac{S_{\text{cr}}}{\cos|\theta_{\text{cr}}|} \end{aligned} \right\} \text{if } S_{\text{crx}0} \cos|\theta_{\text{cr}}| < S_{\text{cry}0} \sin|\theta_{\text{cr}}| \quad (\text{A13})$$

where the uniaxial crack spacing $S_{\text{crx}0}$ and $S_{\text{cry}0}$ are determined from Eq. (A1).

Step 7 – Determine steel stresses at crack.

If $\lambda_x < 1$, $\lambda_y < 1$ and $\sigma_{\text{c1b}}/f_{\text{ctm}} < 1$ then CLLM governs and steel stresses at crack σ_{sr} are found by multiplying the steel strains obtained by Eq. (A9) with the Young's modulus for steel. The mean strains are obtained as

$$\varepsilon_{\text{sm}} = \varepsilon_{\text{m}} \quad (\text{A14})$$

$$\varepsilon_{\text{cm}} = \frac{\psi\xi}{S_{\text{r}0}} \frac{\varepsilon_{\text{sr}} S_{\text{r}0} - u_{\text{r,CLLM}}}{1 + \xi} \quad (\text{A15})$$

where

$$u_{\text{r,CLLM}} = \left(\frac{1}{2\gamma}\right)^{\frac{1}{\beta}} \varepsilon_{\text{sr}}^{\frac{2}{\beta}} \quad (\text{A16})$$

If either $\lambda_x = 1$, $\lambda_y = 1$ and $\frac{\sigma_{\text{c1b}}}{f_{\text{ctm}}} = 1$ occur then CHLM governs and the steel stresses must be obtained iteratively. The steel strains at a crack is obtained as

$$\varepsilon_{\text{sr}} = \frac{\varepsilon_{\text{m}}}{\beta_s} \quad (\text{A17})$$

where $\beta_s = 1$ is chosen initially. The mean strains are obtained as

$$\varepsilon_{\text{sm}} = \frac{1}{\frac{S_{\text{cr}0}}{2}} \frac{\xi \varepsilon_{\text{sr}} \frac{S_{\text{cr}0}}{2} + u_{\text{r,CHLM}}}{1 + \xi} \quad (\text{A18})$$

$$\varepsilon_{\text{cm}} = \frac{\psi\xi}{\frac{S_{\text{cr}0}}{2}} \frac{\varepsilon_{\text{sr}} \frac{S_{\text{cr}0}}{2} - u_{\text{r,CHLM}}}{1 + \xi} \quad (\text{A19})$$

The maximum slip $u_{r,CHLM}$ is determined iteratively as a function of ε_{sr} using the solution strategy provided for CHLM conditions in Paper III, see also Appendix B. If $\varepsilon_{sm} \neq \varepsilon_m$, new values of $\beta_s = \varepsilon_{sm}/\varepsilon_{sr} \leq 1$, ε_{sr} using Eq. (A17) and ε_{sm} using Eq. (A18) are calculated. Steel stresses at the crack σ_{sr} are found by multiplying Eq. (A17) with E_s .

Step 8 – Determine global steel stress tensor.

$$\boldsymbol{\sigma}_{sxy} = \begin{bmatrix} \rho_{sx}\sigma_{srx} \\ \rho_{sy}\sigma_{sry} \\ 0 \end{bmatrix} \quad (\text{A20})$$

Step 9 – Determine global equilibrium.

$$\boldsymbol{\sigma}_{xy} = \boldsymbol{\sigma}_{cxy} + \boldsymbol{\sigma}_{sxy} \quad (\text{A21})$$

Equilibrium of stresses is obtained if $\boldsymbol{\sigma}_{xy} = \boldsymbol{\sigma}_{xy,ext}$. If not, proceed to Step 10.

Step 10 – Update material elasticity tensor with new secant stiffness.

$$\boldsymbol{D}_{c12} = \frac{1}{1 - \nu_{c12}\nu_{c21}} \begin{bmatrix} E_{c1} & \nu_{c12}E_{c1} & 0 \\ \nu_{c21}E_{c2} & E_{c2} & 0 \\ 0 & 0 & (1 - \nu_{c12}\nu_{c21})G_{c12} \end{bmatrix} \quad (\text{A22})$$

where ν_{c12} and ν_{c21} is the Poisson's ratio's for concrete taken as zero after cracking, and $(1 - \nu_{c12}\nu_{c21})G_{c12} = 1/4[E_{c1}(1 - \nu_{c12}) + E_{c2}(1 - \nu_{c21})]$, while $E_{c1} = \sigma_{c1}/\varepsilon_1$ and $E_{c2} = \sigma_{c2}/\varepsilon_2$. The concrete elasticity tensor is found as

$$\boldsymbol{D}_{cxy} = \boldsymbol{T}(\theta_{cr})^T \boldsymbol{D}_{c12} \boldsymbol{T}(\theta_{cr}) \quad (\text{A23})$$

Steel elasticity tensor is written as

$$\boldsymbol{D}_{sxy} = \begin{bmatrix} \rho_{sx}E_{sx} & 0 & 0 \\ 0 & \rho_{sy}E_{sy} & 0 \\ 0 & 0 & 0 \end{bmatrix} \quad (\text{A24})$$

where $E_{sx} = \sigma_{srx}/\varepsilon_x$, $E_{sy} = \sigma_{sry}/\varepsilon_y$. The global material elasticity tensor is obtained as

$$\boldsymbol{D}_{xy} = \boldsymbol{D}_{cxy} + \boldsymbol{D}_{sxy} \quad (\text{A25})$$

Return to Step 2 and calculate new strains. Repeat procedure until equilibrium is obtained, i.e. $\boldsymbol{\sigma}_{xy} = \boldsymbol{\sigma}_{xy,ext}$.

Appendix B

MATLAB script for CHLM iteration procedure


```

%clc
%clear all
%close all

%%
%%---BEGIN INPUT---%%
format long

% eps_s0 = max(eps_s0,eps_s0_1);           % Steel ✓
strain at crack

% L_itr = L;                               % ✓
Initial length

% The main aim of CHLM algorithm is to obtain the unknown value for u0 as a
% function of eps_s0. The equations in Paper III are used and referred to
% unless denoted otherwise.

while eps_s0

% L = L_itr;                               % Length ✓
of member [mm]

sigma_s0 = eps_s0*Es;                       % Steel ✓
stress at crack [N/mm2]

udCASE = (eps_s0^2/(4*gamma))^(1/beta);     % Eq. (62) ✓
or Eq. (69)

u0max = (eps_s0^2/(2*gamma))^(1/beta);     % Eq. (57)

%%---END INPUT---%%

%%---BEGIN SERIES PARAMETERS---%%

Delta_x = 0.1;                               % Case 2 ✓
parameter dx1 + dx2 (See section 4.4.3 and Fig. 7(b))

Delta_u = 5.8000e-05;                         % Case 2 ✓
parameter du (See section 4.4.3 and Fig. 7(b))

m = 10;                                       % Number ✓
of chosen terms in Eq. (39) and Eq. (40) (MAX 170 TERMS BECAUSE factorial(171) = ✓
infy)

R = -1/2;                                     % Falling ✓
factorial (Pocchhammer) coefficient

%%---END SERIES PARAMETERS---%%

%%---BEGIN CASE CHECK---%%

```

```

% We need to determine whether Case 1 or Case 2 occurs according to the
% discussions in Section 4.4.4. In general, each term in the series is
% calculated before summed in the end.

u0_CHECK = (eps_s0^2/(4*gamma)-Delta_u)^(1/beta); % Eq. (62) ✓
Choose a value of u0 close to the limit value discriminating Case 1 and Case 2

C_CHECK = eps_s0^2/2 - gamma*u0_CHECK^beta; % Eq. (56) ✓
Integration constant for case check

r = zeros(1,m+1); % Vector ✓
for calculating the falling factorial

n = zeros(1,m+1); % Vector ✓
for calculating the factorial k!

bin = zeros(1,m+1); % Vector ✓
for the binomial coefficients

FCASE_CHECK = zeros(1,m+1); % Vector ✓
for function in Case 1 check

fCASE_CHECK = zeros(1,m+1); % Vector ✓
for function in Case 1 check

for k = 1:m

    r(1) = 1;
    r(k+1) = r(k)*(R-k+1); % Falling ✓
factorial

    n(1) = factorial(0);
    n(k+1) = factorial(k); % The ✓
factorial k!

    FCASE_CHECK(1) = (gamma/C_CHECK)^0*(u0_CHECK^(1+0*beta)/(1+0*beta));
    FCASE_CHECK(k+1) = (gamma/C_CHECK)^k*(u0_CHECK^(1+k*beta)/(1+k*beta)); % The ✓
function term in Eq. (61)

end

for i = 1:length(r)

    bin(i) = (r(i)/n(i)); % The ✓
binomial coefficients

    fCASE_CHECK(i) = bin(i)*FCASE_CHECK(i); % Eq. (61) ✓
The binomial coefficients multiplied with the function terms

end

fCASE1_CHECK = L/2 - 1/sqrt(2*C_CHECK)*sum(fCASE_CHECK); % Eq. (61)

if fCASE1_CHECK < 0
    fprintf(' - CASE 1 ')

```

```

else
    fprintf(' - CASE 2 ')
end

%%%---END CASE CHECK---%%%

%%%---BEGIN DETERMINE u0---%%%

% Now that we know which case that occurs, we can determine u0.

FCASE1 = zeros(1,m+1); % Eq. (61) ✓
Vector for function in Case 1

dFCASE1 = zeros(1,m+1); % Eq. (78) ✓
Vector for the derivatives of function in Case 1

F1CASE2 = zeros(1,m+1); % Eq. (66) ✓
Vector for function 1 in Case 2

F2CASE2 = zeros(1,m+1); % Eq. (67) ✓
Vector for function 1 in Case 2

F3CASE2 = zeros(1,m+1); % Eq. (68) ✓
Vector for function 1 in Case 2

dF1CASE2 = zeros(1,m+1); % Eq. (80) ✓
Vector for the derivatives of function 1 in Case 2

dF2CASE2 = zeros(1,m+1); % Eq. (81) ✓
Vector for the derivatives of function 2 in Case 2

dF3CASE2 = zeros(1,m+1); % Eq. (82) ✓
Vector for the derivatives of function 3 in Case 2

FB2 = zeros(1,m+1); % Eq. (60) ✓
Vector for function in integration constant B2

fCASE1 = zeros(1,m+1); % Eq. (61) ✓
Vector for function in Case 1 multiplied with binomial coefficients

dfCASE1 = zeros(1,m+1); % Eq. (78) ✓
Vector for the derivatives of function in Case 1 multiplied with binomial coefficients

f1CASE2 = zeros(1,m+1); % Eq. (66) ✓
Vector for function 1 in Case 2 multiplied with binomial coefficients

f2CASE2 = zeros(1,m+1); % Eq. (67) ✓
Vector for function 2 in Case 2 multiplied with binomial coefficients

f3CASE2 = zeros(1,m+1); % Eq. (68) ✓
Vector for function 3 in Case 2 multiplied with binomial coefficients

df1CASE2 = zeros(1,m+1); % Eq. (80) ✓

```

```

Vector for the derivatives of function 1 in Case 2 multiplied with binomial
coefficients

df2CASE2 = zeros(1,m+1); % Eq. (81)
Vector for the derivatives of function 2 in Case 2 multiplied with binomial
coefficients

df3CASE2 = zeros(1,m+1); % Eq. (82)
Vector for the derivatives of function 3 in Case 2 multiplied with binomial
coefficients

fB2 = zeros(1,m+1); % Eq. (60)
Vector for function in integration constant B2 multiplied with binomial coefficients

if fCASE1_CHECK < 0

    %%--BEGIN CASE 1--%%

    % See section 4.4.4 for solution strategy

    u0itr = udCASE - Delta_u; % Initial
    value for u0 in Case 1

    for j = 1:20

        u0 = min(u0itr,u0max-Delta_u); % Iterated
        value for u0, however not exceeding u0max in Eq. (58) due to Eq. (56)

        C = eps_s0^2/2 - gamma*u0^beta; % Eq. (56)

        for k = 1:m

            FCASE1(1) = gamma^0*(1/C)^(1/2+0)*(u0^(1+0*beta))/(1+0*beta); % Eq. (61)
            FCASE1(k+1) = gamma^k*(1/C)^(1/2+k)*(u0^(1+k*beta))/(1+k*beta); % Eq. (61)

            dFCASE1(1) = gamma^0*((gamma*beta*u0^(beta-1)*(1/2+0)*... % Eq. (78)
                C^(-3/2-0)*u0^(1+0*beta)/(1+0*beta))+C^(-(1/2+0))*...
                *u0^(0*beta));
            dFCASE1(k+1) = gamma^k*((gamma*beta*u0^(beta-1)*(1/2+k)*... % Eq. (78)
                *C^(-3/2-k)*u0^(1+k*beta)/(1+k*beta))+C^(-(1/2+k))*...
                *u0^(k*beta));

        end

        for i = 1:length(r)

            fCASE1(i) = bin(i)*FCASE1(i); % Eq. (61)

            dfCASE1(i) = bin(i)*dFCASE1(i); % Eq. (78)

        end

        fCASE1_u0 = L/2 - 1/sqrt(2)*sum(fCASE1); % Eq. (61)

```

```

dfCASE1_u0 = -1/sqrt(2)*sum(dfCASE1); % Eq. (78)

u0itr = u0 - fCASE1_u0/dfCASE1_u0; % Eq. (70)

if abs(fCASE1_u0) < 1e-4 %
Tolerance for Eq. (61)
    break
end

ITERATIONS(j) = u0itr;

end

%%--END CASE 1--%%

else

%%--BEGIN CASE 2--%%

u0itr = udCASE + Delta_u; % Initial
value for u0 in Case 1

for j = 1:20

u0 = min(u0itr,u0max-Delta_u); % Iterated
value for u0, however not exceeding u0max in Eq. (58) due to Eq. (56)

C = eps_s0^2/2 - gamma*u0^beta; % Eq. (56)

for k = 1:m

F1CASE2(1) = (C/gamma)^0*(u0^(delta-0*beta)/(delta-0*beta)); % Eq. (66)
F1CASE2(k+1) = (C/gamma)^k*(u0^(delta-k*beta)/(delta-k*beta)); % Eq. (66)

F2CASE2(1) = (((C/gamma)^(0/(delta-0*beta)+1/beta)+... % Eq. (67)
    Delta_u*(C/gamma)^(0/(delta-0*beta)))^(delta-0*beta))/...
    (delta-0*beta);
F2CASE2(k+1) = (((C/gamma)^(k/(delta-k*beta)+1/beta)+... % Eq. (67)
    Delta_u*(C/gamma)^(k/(delta-k*beta)))^(delta-k*beta))/...
    (delta-k*beta);

F3CASE2(1) = (gamma^0*((1/gamma)^(1/beta)*C^((2-beta)/... % Eq. (68)
    (2*beta*(1+0*beta))))-(Delta_u*C^(-(1/2+0)/(1+0*beta))))^...
    (1+0*beta)/(1+0*beta);
F3CASE2(k+1) = (gamma^k*((1/gamma)^(1/beta)*C^((2-beta)/... % Eq. (68)
    (2*beta*(1+k*beta))))-(Delta_u*C^(-(1/2+k)/(1+k*beta))))^...
    (1+k*beta)/(1+k*beta);

dF1CASE2(1) = (1/gamma)^0*(C^0*u0^(delta-0*beta-1)-... % Eq. (80)
    ((gamma*beta*0*C^(0-1))/(delta-0*beta))*...
    u0^(beta*(1-0)+delta-1));
dF1CASE2(k+1) = (1/gamma)^k*(C^k*u0^(delta-k*beta-1)-... % Eq. (80)
    ((gamma*beta*k*C^(k-1))/(delta-k*beta))*...

```

```

    u0^(beta*(1-k)+delta-1));

dF2CASE2(1) = ((C/gamma)^(0/(delta-0*beta)+(1/beta))+... % Eq. (81)
    Delta_u*(C/gamma)^(0/(delta-0*beta)))^(delta-0*beta-1))*...
    (-gamma*beta*u0^(beta-1))*((1/gamma)^(0/(delta-0*beta)+...
    1/beta)*(0/(delta-0*beta)+1/beta)*C^(0/(delta-0*beta)+...
    1/beta-1)))+(Delta_u*(1/gamma)^(0/(delta-0*beta))*...
    (0/(delta-0*beta))*C^(0/(delta-0*beta)-1)));
dF2CASE2(k+1) = ((C/gamma)^(k/(delta-k*beta)+(1/beta))... % Eq. (81)
    +Delta_u*(C/gamma)^(k/(delta-k*beta)))^(delta-k*beta-1))*...
    (-gamma*beta*u0^(beta-1))*((1/gamma)^(k/(delta-k*beta)+...
    1/beta)*(k/(delta-k*beta)+1/beta)*C^(k/(delta-k*beta)...
    +1/beta-1)))+(Delta_u*(1/gamma)^(k/(delta-k*beta))*...
    (k/(delta-k*beta))*C^(k/(delta-k*beta)-1)));

dF3CASE2(1) = gamma^0*(((1/gamma)^(1/beta)*C^((2-beta)/... % Eq. (82)
    (2*beta*(1+0*beta))))-(Delta_u*C^(-(1/2+0)/(1+0*beta))))^...
    (0*beta))*(-gamma*beta*u0^(beta-1))*((1/gamma)^(1/beta)*...
    ((2-beta)/(2*beta*(1+0*beta)))*C^((2-beta)/(2*beta*...
    (1+0*beta)-1)))+(Delta_u*((1/2+0)/(1+0*beta))*...
    C^(-(1/2+0)/(1+0*beta)+1))));
dF3CASE2(k+1) = gamma^k*(((1/gamma)^(1/beta)*C^((2-beta)/... % Eq. (82)
    (2*beta*(1+k*beta))))-(Delta_u*C^(-(1/2+k)/(1+k*beta))))^...
    (k*beta))*(-gamma*beta*u0^(beta-1))*((1/gamma)^(1/beta)*...
    ((2-beta)/(2*beta*(1+k*beta)))*C^((2-beta)/(2*beta*...
    (1+k*beta)-1)))+(Delta_u*((1/2+k)/(1+k*beta))*...
    C^(-(1/2+k)/(1+k*beta)+1))));

FB2(1) = (C/gamma)^0*(u0^(delta-0*beta)/(delta-0*beta));
FB2(k+1) = (C/gamma)^k*(u0^(delta-k*beta)/(delta-k*beta)); %Eq. (60)

end

for i = 1:length(r)

    f1CASE2(i) = bin(i)*F1CASE2(i); % Eq. (66)

    f2CASE2(i) = bin(i)*F2CASE2(i); % Eq. (67)

    f3CASE2(i) = bin(i)*F3CASE2(i); % Eq. (68)

    df1CASE2(i) = bin(i)*dF1CASE2(i); % Eq. (80)

    df2CASE2(i) = bin(i)*dF2CASE2(i); % Eq. (81)

    df3CASE2(i) = bin(i)*dF3CASE2(i); % Eq. (82)

    fB2(i) = bin(i)*FB2(i); % Eq. (60)

end

fCASE2 = L/2 - (1/sqrt(2*gamma))*(sum(f1CASE2)-sum(f2CASE2))-... %Eq. (65)
    (1/sqrt(2))*sum(f3CASE2) - Delta_x;

```

```

dfCASE2 = -1/sqrt(2*gamma)*(sum(df1CASE2)-sum(df2CASE2))-... %Eq. (79)
          1/sqrt(2)*sum(df3CASE2);

u0itr = u0 - fCASE2/dfCASE2; %Eq. (70)

if abs(fCASE2) < 1e-4 %↙
Tolerance for Eq. (65)
    break
end

ITERATIONS(j) = u0itr;

end

%%--END CASE 2--%%

end

eps_c_max = xi*(eps_s0-sqrt(2*C))/(1+xi); %Eq. (71)

eps_cm_max = psi*eps_c_max; %Eq. (71)

if eps_cm_max > eps_ctm %See ↙
section 4.4.5
    fprintf('- MEMBER CRACKED i.e. NEW MEMBER LENGTH L = L/2 CHOSEN')
    L = L/2;
else
    break
end

end

u0

u0itr

format short

%%!---END DETERMINE u0---%%
%%

%%

%%!---BEGIN POSTPROCESSING---%%

% We have now determined u0 and can now determine the unknown integration
% constants depending on u0. Finally, we can calculate the crack width.

%%--BEGIN CALCULATE X-VALUES--%%

B1 = L/2; % Eq. (59)

B2 = (1/sqrt(2*gamma))*sum(fB2); % Eq. (60)

```

```

ud = (eps_s0^2/(2*gamma) - u0^beta)^(1/beta); % Eq. (58)

n = 30; % Division ✓
to determine the stepsize in the vector for the slip u

u = 0:u0/n:u0; % Slip ✓
values

x = zeros(1,length(u)); % Vector ✓
for x-values corresponding to the slip values

FX = zeros(length(u),m+1); % Matrix ✓
for functions in Eq. (39) and (40)

fX = zeros(length(u),m+1); % Matrix ✓
for functions in Eq. (39) and (40) multiplied with binomial coefficients

for j = 1:length(u)

    %Filling functions matrix FX with either Eq. (39) or Eq. (40)
    for k = 1:m
        if u(j) < ud
            FX(j,1) = gamma^0*(1/C)^(1/2+0)*(u(j)^(1+0*beta)/(1+0*beta)); % Eq. (39)
            FX(j,k+1) = gamma^k*(1/C)^(1/2+k)*(u(j)^(1+k*beta)/(1+k*beta)); % Eq. (39)
        else
            FX(j,1) = (C/gamma)^0*(u(j)^(delta-0*beta)/(delta-0*beta)); % Eq. (40)
            FX(j,k+1) = (C/gamma)^k*(u(j)^(delta-k*beta)/(delta-k*beta)); % Eq. (40)
        end
    end
end

%MULTIPLYING THE FUNCTIONS IN FX WITH THE BINOMIAL COEFFICIENT
for i = 1:length(r)

    fX(j,i) = bin(i)*FX(j,i);

end

%CALCULATING x-VALUES FOR EACH u-VALUE
if u(j) < ud
    x(j) = B1 - 1/sqrt(2)*sum(fX(j,:)); % Eq. (39)
else
    x(j) = B2 - 1/sqrt(2*gamma)*sum(fX(j,:)); % Eq. (40)
end

end

%%--END CALCULATE X-VALUES--%%

%%--BEGIN BOND STRESS, STRAINS AND FORCES--%%

tau = zeros(1,length(u)); % Vector ✓

```

```

for bond stresses

eps_s = zeros(1,length(u)); % Vector ✓
for steel strains

eps_c = zeros(1,length(u)); % Vector ✓
for concrete strains

Ns = zeros(1,length(u)); % Vector ✓
for steel forces

Nc = zeros(1,length(u)); % Vector ✓
for concrete forces

Ntot = zeros(1,length(u)); % Vector ✓
for total forces

for j = 1:length(u)

    tau(j) = tau_max*(u(j)/u1)^alpha; % Eq. (33)

    eps_s(j) = (xi*eps_s0 + sqrt(2*(gamma*u(j).^beta+C)))/(1+xi); % Eq. (44) ✓
Steel strains

    eps_c(j) = xi*(eps_s0 - sqrt(2*(gamma*u(j).^beta+C)))/(1+xi); % Eq. (45) ✓
Steel strains

    Ns(j) = eps_s(j)*Es*As/1e3; % Steel ✓
forces

    Nc(j) = psi*eps_c(j)*Ac*Ecm/1e3; % Concrete ✓
forces

    Ntot(j) = Ns(j)+Nc(j); % Total ✓
forces

end

%%--END BOND STRESS, STRAINS AND FORCES--%%

%%---END POSTPROCESSING---%%
%%

%%---BEGIN CRACKWIDTH---%

eps_smx = ((xi*eps_s0*(L/2)+u0)/(1+xi))/(L/2);

eps_cmx = (psi*xi*(eps_s0*(L/2)-u0)/(1+xi))/(L/2);

u0m = (1/(1+xi))*(xi*eps_s0*L/2*(1-psi)+u0*(1+psi*xi)); % Eq. (77) ✓
Maximum slip at the loaded end [mm]

w = 2*u0m; % Eq. (76) ✓
Crack width [mm]

```

```
lambda = (1/(1+xi))*(1-(2*u0/(eps_s0*L)));  
in Russo and Romano (1992)
```

```
% Eq. (91) ✓
```

```
%%%---END CRACKWIDTH---%
```

**Doctoral theses at the Department of Structural
Engineering at the Norwegian University of Science and
Technology**

**DEPARTMENT OF STRUCTURAL ENGINEERING
NORWEGIAN UNIVERSITY OF SCIENCE AND TECHNOLOGY**

N-7491 TRONDHEIM, NORWAY
Telephone: +47 73 59 47 00 Telefax: +47 73 59 47 01

"Reliability Analysis of Structural Systems using Nonlinear Finite Element Methods",
C. A. Holm, 1990:23, ISBN 82-7119-178-0.

"Uniform Stratified Flow Interaction with a Submerged Horizontal Cylinder",
Ø. Arntsen, 1990:32, ISBN 82-7119-188-8.

"Large Displacement Analysis of Flexible and Rigid Systems Considering
Displacement-Dependent Loads and Nonlinear Constraints",
K. M. Mathisen, 1990:33, ISBN 82-7119-189-6.

"Solid Mechanics and Material Models including Large Deformations",
E. Levold, 1990:56, ISBN 82-7119-214-0, ISSN 0802-3271.

"Inelastic Deformation Capacity of Flexurally-Loaded Aluminium Alloy Structures",
T. Welo, 1990:62, ISBN 82-7119-220-5, ISSN 0802-3271.

"Visualization of Results from Mechanical Engineering Analysis",
K. Aamnes, 1990:63, ISBN 82-7119-221-3, ISSN 0802-3271.

"Object-Oriented Product Modeling for Structural Design",
S. I. Dale, 1991:6, ISBN 82-7119-258-2, ISSN 0802-3271.

"Parallel Techniques for Solving Finite Element Problems on Transputer Networks",
T. H. Hansen, 1991:19, ISBN 82-7119-273-6, ISSN 0802-3271.

"Statistical Description and Estimation of Ocean Drift Ice Environments",
R. Korsnes, 1991:24, ISBN 82-7119-278-7, ISSN 0802-3271.

"Properties of concrete related to fatigue damage: with emphasis on high strength
concrete",
G. Petkovic, 1991:35, ISBN 82-7119-290-6, ISSN 0802-3271.

"Turbidity Current Modelling",
B. Brørs, 1991:38, ISBN 82-7119-293-0, ISSN 0802-3271.

"Zero-Slump Concrete: Rheology, Degree of Compaction and Strength. Effects of
Fillers as Part Cement-Replacement",
C. Sørensen, 1992:8, ISBN 82-7119-357-0, ISSN 0802-3271.

"Nonlinear Analysis of Reinforced Concrete Structures Exposed to Transient Loading",
K. V. Høiseeth, 1992:15, ISBN 82-7119-364-3, ISSN 0802-3271.

"Finite Element Formulations and Solution Algorithms for Buckling and Collapse
Analysis of Thin Shells",
R. O. Bjærum, 1992:30, ISBN 82-7119-380-5, ISSN 0802-3271.

"Response Statistics of Nonlinear Dynamic Systems",
J. M. Johnsen, 1992:42, ISBN 82-7119-393-7, ISSN 0802-3271.

"Digital Models in Engineering. A Study on why and how engineers build and operate
digital models for decision support",
J. Høyte, 1992:75, ISBN 82-7119-429-1, ISSN 0802-3271.

"Sparse Solution of Finite Element Equations",
A. C. Damhaug, 1992:76, ISBN 82-7119-430-5, ISSN 0802-3271.

"Some Aspects of Floating Ice Related to Sea Surface Operations in the Barents Sea",
S. Løset, 1992:95, ISBN 82-7119-452-6, ISSN 0802-3271.

"Modelling of Cyclic Plasticity with Application to Steel and Aluminium Structures",
O. S. Hopperstad, 1993:7, ISBN 82-7119-461-5, ISSN 0802-3271.

"The Free Formulation: Linear Theory and Extensions with Applications to Tetrahedral
Elements
with Rotational Freedoms",
G. Skeie, 1993:17, ISBN 82-7119-472-0, ISSN 0802-3271.

"Høyfast betongs motstand mot piggedekkslitasje. Analyse av resultater fra prøving i
Veisliter'n",
T. Tveter, 1993:62, ISBN 82-7119-522-0, ISSN 0802-3271.

"A Nonlinear Finite Element Based on Free Formulation Theory for Analysis of
Sandwich Structures",
O. Aamlid, 1993:72, ISBN 82-7119-534-4, ISSN 0802-3271.

"The Effect of Curing Temperature and Silica Fume on Chloride Migration and Pore
Structure of High Strength Concrete",
C. J. Hauck, 1993:90, ISBN 82-7119-553-0, ISSN 0802-3271.

"Failure of Concrete under Compressive Strain Gradients",
G. Markeset, 1993:110, ISBN 82-7119-575-1, ISSN 0802-3271.

"An experimental study of internal tidal amphidromes in Vestfjorden",
J. H. Nilsen, 1994:39, ISBN 82-7119-640-5, ISSN 0802-3271.

"Structural analysis of oil wells with emphasis on conductor design",
H. Larsen, 1994:46, ISBN 82-7119-648-0, ISSN 0802-3271.

"Adaptive methods for non-linear finite element analysis of shell structures",
K. M. Okstad, 1994:66, ISBN 82-7119-670-7, ISSN 0802-3271.

"On constitutive modelling in nonlinear analysis of concrete structures",
O. Fyrileiv, 1994:115, ISBN 82-7119-725-8, ISSN 0802-3271.

"Fluctuating wind load and response of a line-like engineering structure with emphasis
on motion-induced wind forces",
J. Bogunovic Jakobsen, 1995:62, ISBN 82-7119-809-2, ISSN 0802-3271.

"An experimental study of beam-columns subjected to combined torsion, bending and
axial actions",
A. Aalberg, 1995:66, ISBN 82-7119-813-0, ISSN 0802-3271.

"Scaling and cracking in unsealed freeze/thaw testing of Portland cement and silica
fume concretes",
S. Jacobsen, 1995:101, ISBN 82-7119-851-3, ISSN 0802-3271.

"Damping of water waves by submerged vegetation. A case study of laminaria
hyperborea",
A. M. Dubi, 1995:108, ISBN 82-7119-859-9, ISSN 0802-3271.

"The dynamics of a slope current in the Barents Sea",
Sheng Li, 1995:109, ISBN 82-7119-860-2, ISSN 0802-3271.

"Modellering av delmaterialenes betydning for betongens konsistens",
Ernst Mørtzell, 1996:12, ISBN 82-7119-894-7, ISSN 0802-3271.

"Bending of thin-walled aluminium extrusions",
Birgit Søvik Opheim, 1996:60, ISBN 82-7119-947-1, ISSN 0802-3271.

"Material modelling of aluminium for crashworthiness analysis",
Torodd Berstad, 1996:89, ISBN 82-7119-980-3, ISSN 0802-3271.

"Estimation of structural parameters from response measurements on submerged
floating tunnels",
Rolf Magne Larssen, 1996:119, ISBN 82-471-0014-2, ISSN 0802-3271.

"Numerical modelling of plain and reinforced concrete by damage mechanics",
Mario A. Polanco-Loria, 1997:20, ISBN 82-471-0049-5, ISSN 0802-3271.

"Nonlinear random vibrations - numerical analysis by path integration methods",
Vibeke Moe, 1997:26, ISBN 82-471-0056-8, ISSN 0802-3271.

“Numerical prediction of vortex-induced vibration by the finite element method”,
Joar Martin Dalheim, 1997:63, ISBN 82-471-0096-7, ISSN 0802-3271.

“Time domain calculations of buffeting response for wind sensitive structures”,
Ketil Aas-Jakobsen, 1997:148, ISBN 82-471-0189-0, ISSN 0802-3271.

"A numerical study of flow about fixed and flexibly mounted circular cylinders",
Trond Stokka Meling, 1998:48, ISBN 82-471-0244-7, ISSN 0802-3271.

“Estimation of chloride penetration into concrete bridges in coastal areas”,
Per Egil Steen, 1998:89, ISBN 82-471-0290-0, ISSN 0802-3271.

“Stress-resultant material models for reinforced concrete plates and shells”,
Jan Arve Øverli, 1998:95, ISBN 82-471-0297-8, ISSN 0802-3271.

“Chloride binding in concrete. Effect of surrounding environment and concrete composition”,
Claus Kenneth Larsen, 1998:101, ISBN 82-471-0337-0, ISSN 0802-3271.

“Rotational capacity of aluminium alloy beams”,
Lars A. Moen, 1999:1, ISBN 82-471-0365-6, ISSN 0802-3271.

“Stretch Bending of Aluminium Extrusions”,
Arild H. Clausen, 1999:29, ISBN 82-471-0396-6, ISSN 0802-3271.

“Aluminium and Steel Beams under Concentrated Loading”,
Tore Tryland, 1999:30, ISBN 82-471-0397-4, ISSN 0802-3271.

"Engineering Models of Elastoplasticity and Fracture for Aluminium Alloys",
Odd-Geir Lademo, 1999:39, ISBN 82-471-0406-7, ISSN 0802-3271.

"Kapasitet og duktilitet av dybelforbindelser i trekonstruksjoner",
Jan Siem, 1999:46, ISBN 82-471-0414-8, ISSN 0802-3271.

“Etablering av distribuert ingeniørarbeid; Teknologiske og organisatoriske erfaringer fra en norsk ingeniørbedrift”,
Lars Line, 1999:52, ISBN 82-471-0420-2, ISSN 0802-3271.

“Estimation of Earthquake-Induced Response”,
Símon Ólafsson, 1999:73, ISBN 82-471-0443-1, ISSN 0802-3271.

“Coastal Concrete Bridges: Moisture State, Chloride Permeability and Aging Effects”
Ragnhild Holen Relling, 1999:74, ISBN 82-471-0445-8, ISSN 0802-3271.

”Capacity Assessment of Titanium Pipes Subjected to Bending and External Pressure”,
Arve Bjørset, 1999:100, ISBN 82-471-0473-3, ISSN 0802-3271.

“Validation of Numerical Collapse Behaviour of Thin-Walled Corrugated Panels”,
Håvar Ilstad, 1999:101, ISBN 82-471-0474-1, ISSN 0802-3271.

“Strength and Ductility of Welded Structures in Aluminium Alloys”,
Mirosław Matusiak, 1999:113, ISBN 82-471-0487-3, ISSN 0802-3271.

“Thermal Dilation and Autogenous Deformation as Driving Forces to Self-Induced
Stresses in High Performance Concrete”,
Øyvind Bjøntegaard, 1999:121, ISBN 82-7984-002-8, ISSN 0802-3271.

“Some Aspects of Ski Base Sliding Friction and Ski Base Structure”,
Dag Anders Moldestad, 1999:137, ISBN 82-7984-019-2, ISSN 0802-3271.

"Electrode reactions and corrosion resistance for steel in mortar and concrete",
Roy Antonsen, 2000:10, ISBN 82-7984-030-3, ISSN 0802-3271.

"Hydro-Physical Conditions in Kelp Forests and the Effect on Wave Damping and
Dune Erosion. A case study on Laminaria Hyperborea",
Stig Magnar Løvås, 2000:28, ISBN 82-7984-050-8, ISSN 0802-3271.

"Random Vibration and the Path Integral Method",
Christian Skaug, 2000:39, ISBN 82-7984-061-3, ISSN 0802-3271.

"Buckling and geometrical nonlinear beam-type analyses of timber structures",
Trond Even Eggen, 2000:56, ISBN 82-7984-081-8, ISSN 0802-3271.

”Structural Crashworthiness of Aluminium Foam-Based Components”,
Arve Grønsund Hanssen, 2000:76, ISBN 82-7984-102-4, ISSN 0809-103X.

“Measurements and simulations of the consolidation in first-year sea ice ridges, and
some aspects of mechanical behaviour”,
Knut V. Høyland, 2000:94, ISBN 82-7984-121-0, ISSN 0809-103X.

”Kinematics in Regular and Irregular Waves based on a Lagrangian Formulation”,
Svein Helge Gjørund, 2000-86, ISBN 82-7984-112-1, ISSN 0809-103X.

”Self-Induced Cracking Problems in Hardening Concrete Structures”,
Daniela Bosnjak, 2000-121, ISBN 82-7984-151-2, ISSN 0809-103X.

"Ballistic Penetration and Perforation of Steel Plates",
Tore Børvik, 2000:124, ISBN 82-7984-154-7, ISSN 0809-103X.

"Freeze-Thaw resistance of Concrete. Effect of: Curing Conditions, Moisture Exchange
and Materials",
Terje Finnerup Rønning, 2001:14, ISBN 82-7984-165-2, ISSN 0809-103X

"Structural behaviour of post tensioned concrete structures. Flat slab. Slabs on ground",
Steinar Trygstad, 2001:52, ISBN 82-471-5314-9, ISSN 0809-103X.

"Slipforming of Vertical Concrete Structures. Friction between concrete and slipform panel",
Kjell Tore Fosså, 2001:61, ISBN 82-471-5325-4, ISSN 0809-103X.

"Some numerical methods for the simulation of laminar and turbulent incompressible flows",
Jens Holmen, 2002:6, ISBN 82-471-5396-3, ISSN 0809-103X.

"Improved Fatigue Performance of Threaded Drillstring Connections by Cold Rolling",
Steinar Kristoffersen, 2002:11, ISBN: 82-421-5402-1, ISSN 0809-103X.

"Deformations in Concrete Cantilever Bridges: Observations and Theoretical Modelling",
Peter F. Takács, 2002:23, ISBN 82-471-5415-3, ISSN 0809-103X.

"Stiffened aluminium plates subjected to impact loading",
Hilde Giæver Hildrum, 2002:69, ISBN 82-471-5467-6, ISSN 0809-103X.

"Full- and model scale study of wind effects on a medium-rise building in a built up area",
Jónas Thór Snæbjörnsson, 2002:95, ISBN82-471-5495-1, ISSN 0809-103X.

"Evaluation of Concepts for Loading of Hydrocarbons in Ice-infested water",
Arnor Jensen, 2002:114, ISBN 82-417-5506-0, ISSN 0809-103X.

"Numerical and Physical Modelling of Oil Spreading in Broken Ice",
Janne K. Økland Gjøsteen, 2002:130, ISBN 82-471-5523-0, ISSN 0809-103X.

"Diagnosis and protection of corroding steel in concrete",
Franz Pruckner, 20002:140, ISBN 82-471-5555-4, ISSN 0809-103X.

"Tensile and Compressive Creep of Young Concrete: Testing and Modelling",
Dawood Atrushi, 2003:17, ISBN 82-471-5565-6, ISSN 0809-103X.

"Rheology of Particle Suspensions. Fresh Concrete, Mortar and Cement Paste with Various Types of Lignosulfonates",
Jon Elvar Wallevik, 2003:18, ISBN 82-471-5566-4, ISSN 0809-103X.

"Oblique Loading of Aluminium Crash Components",
Aase Reyes, 2003:15, ISBN 82-471-5562-1, ISSN 0809-103X.

"Utilization of Ethiopian Natural Pozzolans",
Surafel Ketema Desta, 2003:26, ISBN 82-471-5574-5, ISSN:0809-103X.

“Behaviour and strength prediction of reinforced concrete structures with discontinuity regions”, Helge Brå, 2004:11, ISBN 82-471-6222-9, ISSN 1503-8181.

“High-strength steel plates subjected to projectile impact. An experimental and numerical study”, Sumita Dey, 2004:38, ISBN 82-471-6282-2 (printed version), ISBN 82-471-6281-4 (electronic version), ISSN 1503-8181.

“Alkali-reactive and inert fillers in concrete. Rheology of fresh mixtures and expansive reactions.”

Bård M. Pedersen, 2004:92, ISBN 82-471-6401-9 (printed version), ISBN 82-471-6400-0 (electronic version), ISSN 1503-8181.

“On the Shear Capacity of Steel Girders with Large Web Openings”.

Nils Christian Hagen, 2005:9 ISBN 82-471-6878-2 (printed version), ISBN 82-471-6877-4 (electronic version), ISSN 1503-8181.

“Behaviour of aluminium extrusions subjected to axial loading”.

Østen Jensen, 2005:7, ISBN 82-471-6873-1 (printed version), ISBN 82-471-6872-3 (electronic version), ISSN 1503-8181.

“Thermal Aspects of corrosion of Steel in Concrete”.

Jan-Magnus Østvik, 2005:5, ISBN 82-471-6869-3 (printed version), ISBN 82-471-6868 (electronic version), ISSN 1503-8181.

“Mechanical and adaptive behaviour of bone in relation to hip replacement.” A study of bone remodelling and bone grafting.

Sébastien Muller, 2005:34, ISBN 82-471-6933-9 (printed version), ISBN 82-471-6932-0 (electronic version), ISSN 1503-8181.

“Analysis of geometrical nonlinearities with applications to timber structures”.

Lars Wollebæk, 2005:74, ISBN 82-471-7050-5 (printed version), ISBN 82-471-7019-1 (electronic version), ISSN 1503-8181.

“Pedestrian induced lateral vibrations of slender footbridges”.

Anders Rönnquist, 2005:102, ISBN 82-471-7082-5 (printed version), ISBN 82-471-7081-7 (electronic version), ISSN 1503-8181.

“Initial Strength Development of Fly Ash and Limestone Blended Cements at Various Temperatures Predicted by Ultrasonic Pulse Velocity”.

Tom Ivar Fredvik, 2005:112, ISBN 82-471-7105-8 (printed version), ISBN 82-471-7103-1 (electronic version), ISSN 1503-8181.

“Behaviour and modelling of thin-walled cast components”.

Cato Dørum, 2005:128, ISBN 82-471-7140-6 (printed version), ISBN 82-471-7139-2 (electronic version), ISSN 1503-8181.

- “Behaviour and modelling of selfpiercing riveted connections”,
Raffaele Porcaro, 2005:165, ISBN 82-471-7219-4 (printed version), ISBN 82-471-7218-6 (electronic version), ISSN 1503-8181.
- ”Behaviour and Modelling of Aluminium Plates subjected to Compressive Load”,
Lars Rønning, 2005:154, ISBN 82-471-7169-1 (printed version), ISBN 82-471-7195-3 (electronic version), ISSN 1503-8181.
- ”Bumper beam-longitudinal system subjected to offset impact loading”,
Satyanarayana Kokkula, 2005:193, ISBN 82-471-7280-1 (printed version), ISBN 82-471-7279-8 (electronic version), ISSN 1503-8181.
- “Control of Chloride Penetration into Concrete Structures at Early Age”,
Guofei Liu, 2006:46, ISBN 82-471-7838-9 (printed version), ISBN 82-471-7837-0 (electronic version), ISSN 1503-8181.
- “Modelling of Welded Thin-Walled Aluminium Structures”,
Ting Wang, 2006:78, ISBN 82-471-7907-5 (printed version), ISBN 82-471-7906-7 (electronic version), ISSN 1503-8181.
- ”Time-variant reliability of dynamic systems by importance sampling and probabilistic analysis of ice loads”,
Anna Ivanova Olsen, 2006:139, ISBN 82-471-8041-3 (printed version), ISBN 82-471-8040-5 (electronic version), ISSN 1503-8181.
- “Fatigue life prediction of an aluminium alloy automotive component using finite element analysis of surface topography”,
Sigmund Kyrre Ås, 2006:25, ISBN 82-471-7791-9 (printed version), ISBN 82-471-7791-9 (electronic version), ISSN 1503-8181.
- ”Constitutive models of elastoplasticity and fracture for aluminium alloys under strain path change”,
Dasharatha Achani, 2006:76, ISBN 82-471-7903-2 (printed version), ISBN 82-471-7902-4 (electronic version), ISSN 1503-8181.
- “Simulations of 2D dynamic brittle fracture by the Element-free Galerkin method and linear fracture mechanics”,
Tommy Karlsson, 2006:125, ISBN 82-471-8011-1 (printed version), ISBN 82-471-8010-3 (electronic version), ISSN 1503-8181.
- “Penetration and Perforation of Granite Targets by Hard Projectiles”,
Chong Chiang Seah, 2006:188, ISBN 82-471-8150-9 (printed version), ISBN 82-471-8149-5 (electronic version), ISSN 1503-8181.

“Deformations, strain capacity and cracking of concrete in plastic and early hardening phases”,

Tor Arne Hammer, 2007:234, ISBN 978-82-471-5191-4 (printed version), ISBN 978-82-471-5207-2 (electronic version), ISSN 1503-8181.

“Crashworthiness of dual-phase high-strength steel: Material and Component behaviour”, Venkatapathi Tarigopula, 2007:230, ISBN 82-471-5076-4 (printed version), ISBN 82-471-5093-1 (electronic version), ISSN 1503-8181.

“Fibre reinforcement in load carrying concrete structures”,

Åse Lyslo Døssland, 2008:50, ISBN 978-82-471-6910-0 (printed version), ISBN 978-82-471-6924-7 (electronic version), ISSN 1503-8181.

“Low-velocity penetration of aluminium plates”,

Frode Grytten, 2008:46, ISBN 978-82-471-6826-4 (printed version), ISBN 978-82-471-6843-1 (electronic version), ISSN 1503-8181.

“Robustness studies of structures subjected to large deformations”,

Ørjan Fyllingen, 2008:24, ISBN 978-82-471-6339-9 (printed version), ISBN 978-82-471-6342-9 (electronic version), ISSN 1503-8181.

“Constitutive modelling of morsellised bone”,

Knut Birger Lunde, 2008:92, ISBN 978-82-471-7829-4 (printed version), ISBN 978-82-471-7832-4 (electronic version), ISSN 1503-8181.

“Experimental Investigations of Wind Loading on a Suspension Bridge Girder”,

Bjørn Isaksen, 2008:131, ISBN 978-82-471-8656-5 (printed version), ISBN 978-82-471-8673-2 (electronic version), ISSN 1503-8181.

“Cracking Risk of Concrete Structures in The Hardening Phase”,

Guomin Ji, 2008:198, ISBN 978-82-471-1079-9 (printed version), ISBN 978-82-471-1080-5 (electronic version), ISSN 1503-8181.

“Modelling and numerical analysis of the porcine and human mitral apparatus”,

Victorien Emile Prot, 2008:249, ISBN 978-82-471-1192-5 (printed version), ISBN 978-82-471-1193-2 (electronic version), ISSN 1503-8181.

“Strength analysis of net structures”,

Heidi Moe, 2009:48, ISBN 978-82-471-1468-1 (printed version), ISBN 978-82-471-1469-8 (electronic version), ISSN 1503-8181.

“Numerical analysis of ductile fracture in surface cracked shells”,

Espen Berg, 2009:80, ISBN 978-82-471-1537-4 (printed version), ISBN 978-82-471-1538-1 (electronic version), ISSN 1503-8181.

“Subject specific finite element analysis of bone – for evaluation of the healing of a leg lengthening and evaluation of femoral stem design”,
Sune Hansborg Pettersen, 2009:99, ISBN 978-82-471-1579-4 (printed version), ISBN 978-82-471-1580-0 (electronic version), ISSN 1503-8181.

“Evaluation of fracture parameters for notched multi-layered structures”,
Lingyun Shang, 2009:137, ISBN 978-82-471-1662-3 (printed version), ISBN 978-82-471-1663-0 (electronic version), ISSN 1503-8181.

“Modelling of Dynamic Material Behaviour and Fracture of Aluminium Alloys for Structural Applications”
Yan Chen, 2009:69, ISBN 978-82-471-1515-2 (printed version), ISBN 978-82-471-1516-9 (electronic version), ISSN 1503-8181.

“Nanomechanics of polymer and composite particles”
Jianying He 2009:213, ISBN 978-82-471-1828-3 (printed version), ISBN 978-82-471-1829-0 (electronic version), ISSN 1503-8181.

“Mechanical properties of clear wood from Norway spruce”
Kristian Berbom Dahl 2009:250, ISBN 978-82-471-1911-2 (printed version) ISBN 978-82-471-1912-9 (electronic version), ISSN 1503-8181.

“Modeling of the degradation of TiB₂ mechanical properties by residual stresses and liquid Al penetration along grain boundaries”
Micol Pezzotta 2009:254, ISBN 978-82-471-1923-5 (printed version) ISBN 978-82-471-1924-2 (electronic version) ISSN 1503-8181.

“Effect of welding residual stress on fracture”
Xiabo Ren 2010:77, ISBN 978-82-471-2115-3 (printed version) ISBN 978-82-471-2116-0 (electronic version), ISSN 1503-8181.

“Pan-based carbon fiber as anode material in cathodic protection system for concrete structures”
Mahdi Chini 2010:122, ISBN 978-82-471-2210-5 (printed version) ISBN 978-82-471-2213-6 (electronic version), ISSN 1503-8181.

“Structural Behaviour of deteriorated and retrofitted concrete structures”
Irina Vasililjeva Sæther 2010:171, ISBN 978-82-471-2315-7 (printed version) ISBN 978-82-471-2316-4 (electronic version) ISSN 1503-8181.

“Prediction of local snow loads on roofs”
Vivian Meløysund 2010:247, ISBN 978-82-471-2490-1 (printed version) ISBN 978-82-471-2491-8 (electronic version) ISSN 1503-8181.

“Behaviour and modelling of polymers for crash applications”
Virgile Delhay 2010:251, ISBN 978-82-471-2501-4 (printed version) ISBN 978-82-471-2502-1 (electronic version) ISSN 1503-8181.

“Blended cement with reduced CO₂ emission – Utilizing the Fly Ash-Limestone Synergy”,
Klaartje De Weerd 2011:32, ISBN 978-82-471-2584-7 (printed version) ISBN 978-82-471-2584-4 (electronic version) ISSN 1503-8181.

“Chloride induced reinforcement corrosion in concrete” Concept of critical chloride content – methods and mechanisms.
Ueli Angst 2011:113, ISBN 978-82-471-2769-9 (printed version) ISBN 978-82-471-2763-6 (electronic version) ISSN 1503-8181.

“A thermo-electric-Mechanical study of the carbon anode and contact interface for Energy savings in the production of aluminium”.
Dag Herman Andersen 2011:157, ISBN 978-82-471-2859-6 (printed version) ISBN 978-82-471-2860-2 (electronic version) ISSN 1503-8181.

“Structural Capacity of Anchorage Ties in Masonry Veneer Walls Subjected to Earthquake”. The implications of Eurocode 8 and Eurocode 6 on a typical Norwegian veneer wall.
Ahmed Mohamed Yousry Hamed 2011:181, ISBN 978-82-471-2911-1 (printed version) ISBN 978-82-471-2912-8 (electronic ver.) ISSN 1503-8181.

“Work-hardening behaviour in age-hardenable Al-Zn-Mg(-Cu) alloys”.
Ida Westermann , 2011:247, ISBN 978-82-471-3056-8 (printed ver.) ISBN 978-82-471-3057-5 (electronic ver.) ISSN 1503-8181.

“Behaviour and modelling of selfpiercing riveted connections using aluminium rivets”.
Nguyen-Hieu Hoang, 2011:266, ISBN 978-82-471-3097-1 (printed ver.) ISBN 978-82-471-3099-5 (electronic ver.) ISSN 1503-8181.

“Fibre reinforced concrete”.
Sindre Sandbakk, 2011:297, ISBN 978-82-471-3167-1 (printed ver.) ISBN 978-82-471-3168-8 (electronic ver.) ISSN 1503-8181.

“Dynamic behaviour of cablesupported bridges subjected to strong natural wind”.
Ole Andre Øiseth, 2011:315, ISBN 978-82-471-3209-8 (printed ver.) ISBN 978-82-471-3210-4 (electronic ver.) ISSN 1503-8181.

“Constitutive modeling of solargrade silicon materials”
Julien Cochard, 2011:307, ISBN 978-82-471-3189-3 (printed ver.) ISBN 978-82-471-3190-9 (electronic ver.) ISSN 1503-8181.

“Constitutive behavior and fracture of shape memory alloys”
Jim Stian Olsen, 2012:57, ISBN 978-82-471-3382-8 (printed ver.) ISBN 978-82-471-3383-5 (electronic ver.) ISSN 1503-8181.

“Field measurements in mechanical testing using close-range photogrammetry and digital image analysis”

Egil Fagerholt, 2012:95, ISBN 978-82-471-3466-5 (printed ver.) ISBN 978-82-471-3467-2 (electronic ver.) ISSN 1503-8181.

“Towards a better understanding of the ultimate behaviour of lightweight aggregate concrete in compression and bending”

Håvard Nedrelid, 2012:123, ISBN 978-82-471-3527-3 (printed ver.) ISBN 978-82-471-3528-0 (electronic ver.) ISSN 1503-8181.

“Numerical simulations of blood flow in the left side of the heart”

Sigrud Kaarstad Dahl, 2012:135, ISBN 978-82-471-3553-2 (printed ver.) ISBN 978-82-471-3555-6 (electronic ver.) ISSN 1503-8181.

“Moisture induced stresses in glulam”

Vanessa Angst-Nicollier, 2012:139, ISBN 978-82-471-3562-4 (printed ver.) ISBN 978-82-471-3563-1 (electronic ver.) ISSN 1503-8181.

“Biomechanical aspects of distraction osteogenesis”

Valentina La Russa, 2012:250, ISBN 978-82-471-3807-6 (printed ver.) ISBN 978-82-471-3808-3 (electronic ver.) ISSN 1503-8181.

“Ductile fracture in dual-phase steel. Theoretical, experimental and numerical study”

Gaute Gruben, 2012:257, ISBN 978-82-471-3822-9 (printed ver.) ISBN 978-82-471-3823-6 (electronic ver.) ISSN 1503-8181.

“Damping in Timber Structures”

Nathalie Labonnote, 2012:263, ISBN 978-82-471-3836-6 (printed ver.) ISBN 978-82-471-3837-3 (electronic ver.) ISSN 1503-8181.

“Biomechanical modeling of fetal veins: The umbilical vein and ductus venosus bifurcation”

Paul Roger Leinan, 2012:299, ISBN 978-82-471-3915-8 (printed ver.) ISBN 978-82-471-3916-5 (electronic ver.) ISSN 1503-8181.

“Large-Deformation behaviour of thermoplastics at various stress states”

Anne Serine Ognedal, 2012:298, ISBN 978-82-471-3913-4 (printed ver.) ISBN 978-82-471-3914-1 (electronic ver.) ISSN 1503-8181.

“Hardening accelerator for fly ash blended cement”

Kien Dinh Hoang, 2012:366, ISBN 978-82-471-4063-5 (printed ver.) ISBN 978-82-471-4064-2 (electronic ver.) ISSN 1503-8181.

“From molecular structure to mechanical properties”

Jiayang Wu, 2013:186, ISBN 978-82-471-4485-5 (printed ver.) ISBN 978-82-471-4486-2 (electronic ver.) ISSN 1503-8181.

“Experimental and numerical study of hybrid concrete structures”

Linn Grepstad Nes, 2013:259, ISBN 978-82-471-4644-6 (printed ver.) ISBN 978-82-471-4645-3 (electronic ver.) ISSN 1503-8181.

“Mechanics of ultra-thin multi crystalline silicon wafers”

Saber Saffar, 2013:199, ISBN 978-82-471-4511-1 (printed ver.) ISBN 978-82-471-4513-5 (electronic ver.) ISSN 1503-8181.

“Through process modelling of welded aluminium structures”

Anizahyati Alisibramulisi, 2013:325, ISBN 978-82-471-4788-7 (printed ver.) ISBN 978-82-471-4789-4 (electronic ver.) ISSN 1503-8181.

“Combined blast and fragment loading on steel plates”

Knut Gaarder Rakvåg, 2013:361, ISBN 978-82-471-4872-3 (printed ver.) ISBN 978-82-4873-0 (electronic ver.) ISSN 1503-8181.

“Characterization and modelling of the anisotropic behaviour of high-strength aluminium alloy”

Marion Fourmeau, 2014:37, ISBN 978-82-326-0008-3 (printed ver.) ISBN 978-82-326-0009-0 (electronic ver.) ISSN 1503-8181.

“Behaviour of threated steel fasteners at elevated deformation rates”

Henning Fransplass, 2014:65, ISBN 978-82-326-0054-0 (printed ver.) ISBN 978-82-326-0055-7 (electronic ver.) ISSN 1503-8181.

“Sedimentation and Bleeding”

Ya Peng, 2014:89, ISBN 978-82-326-0102-8 (printed ver.) ISBN 978-82-326-0103-5 (electric ver.) ISSN 1503-8181.

“Impact against X65 offshore pipelines”

Martin Kristoffersen, 2014:362, ISBN 978-82-326-0636-8 (printed ver.) ISBN 978-82-326-0637-5 (electronic ver.) ISSN 1503-8181.

“Formability of aluminium alloy subjected to prestrain by rolling”

Dmitry Vysochinskiy, 2014:363,, ISBN 978-82-326-0638-2 (printed ver.) ISBN 978-82-326-0639-9 (electronic ver.) ISSN 1503-8181.

“Experimental and numerical study of Yielding, Work-Hardening and anisotropy in textured AA6xxx alloys using crystal plasticity models”

Mikhail Khadyko, 2015:28, ISBN 978-82-326-0724-2 (printed ver.) ISBN 978-82-326-0725-9 (electronic ver.) ISSN 1503-8181.

“Behaviour and Modelling of AA6xxx Aluminium Alloys Under a Wide Range of Temperatures and Strain Rates”

Vincent Vilamosa, 2015:63, ISBN 978-82-326-0786-0 (printed ver.) ISBN 978-82-326-0787-7 (electronic ver.) ISSN 1503-8181.

“A Probabilistic Approach in Failure Modelling of Aluminium High Pressure Die-Castings”

Octavian Knoll, 2015:137, ISBN 978-82-326-0930-7 (printed ver.) ISBN 978-82-326-0931-4 (electronic ver.) ISSN 1503-8181.

“Ice Abrasion on Marine Concrete Structures”

Egil Møen, 2015:189, ISBN 978-82-326-1034-1 (printed ver.) ISBN 978-82-326-1035-8 (electronic ver.) ISSN 1503-8181.

“Fibre Orientation in Steel-Fibre-Reinforced Concrete”

Giedrius Zirgulis, 2015:229, ISBN 978-82-326-1114-0 (printed ver.) ISBN 978-82-326-1115-7 (electronic ver.) ISSN 1503-8181.

“Effect of spatial variation and possible interference of localised corrosion on the residual capacity of a reinforced concrete beam”

Mohammad Mahdi Kioumarsi, 2015:282, ISBN 978-82-326-1220-8 (printed ver.) ISBN 978-82-1221-5 (electronic ver.) ISSN 1503-8181.

“The role of concrete resistivity in chloride-induced macro-cell corrosion”

Karla Horbostel, 2015:324, ISBN 978-82-326-1304-5 (printed ver.) ISBN 978-82-326-1305-2 (electronic ver.) ISSN 1503-8181.

“Flowable fibre-reinforced concrete for structural applications”

Elena Vidal Sarmiento, 2015:335, ISBN 978-82-326-1324-3 (printed ver.) ISBN 978-82-326-1325-0 (electronic ver.) ISSN 1503-8181.

“Development of chushed sand for concrete production with microproportioning”

Rolands Cepuritis, 2016:19, ISBN 978-82-326-1382-3 (printed ver.) ISBN 978-82-326-1383-0 (electronic ver.) ISSN 1503-8181.

“Withdrawal properties of threaded rods embedded in glued-laminated timber elements”

Haris Stamatopoulos, 2016:48, ISBN 978-82-326-1436-3 (printed ver.) ISBN 978-82-326-1437-0 (electronic ver.) ISSN 1503-8181.

“An Experimental and numerical study of thermoplastics at large deformation”

Marius Andersen, 2016:191, ISBN 978-82-326-1720-3 (printed ver.) ISBN 978-82-326-1721-0 (electronic ver.) ISSN 1503-8181.

“Modeling and Simulation of Ballistic Impact”

Jens Kristian Holmen, 2016:240, ISBN 978-82-326-1818-7 (printed ver.) ISBN 978-82-326-1819-4 (electronic ver.) ISSN 1503-8181.

“Early age crack assessment of concrete structures”

Anja B. Estensen Klausen, 2016:256, ISBN 978-82-326-1850-7 (printed ver.) ISBN 978-82-326-1851-4 (electronic ver.) ISSN 1503-8181.

“Uncertainty quantification and sensitivity analysis for cardiovascular models”

Vinzenz Gregor Eck, 2016:234, ISBN 978-82-326-1806-4 (printed ver.) ISBN 978-82-326-1807-1 (electronic ver.) ISSN 1503-8181.

“Dynamic behaviour of existing and new railway catenary systems under Norwegian conditions”

Petter Røe Nåvik, 2016:298, ISBN 978-82-326-1935-1 (printed ver.) ISBN 978-82-326-1934-4 (electronic ver.) ISSN 1503-8181.

“Mechanical behaviour of particle-filled elastomers at various temperatures”

Arne Ilseng, 2016:295, ISBN 978-82-326-1928-3 (printed ver.) ISBN 978-82-326-1929-0 (electronic ver.) ISSN 1503-8181.

“Nanotechnology for Anti-Icing Application”

Zhiwei He, 2016:348, ISBN 978-82-326-2038-8 (printed ver.) ISBN 978-82-326-2019-5 (electronic ver.) ISSN 1503-8181.

“Conduction Mechanisms in Conductive Adhesives with Metal-Coated Polymer Spheres”

Sigurd Rolland Pettersen, 2016:349, ISBN 978-326-2040-1 (printed ver.) ISBN 978-82-326-2041-8 (electronic ver.) ISSN 1503-8181.

“The interaction between calcium lignosulfonate and cement”

Alessia Colombo, 2017:20, ISBN 978-82-326-2122-4 (printed ver.) ISBN 978-82-326-2123-1 (electronic ver.) ISSN 1503-8181.

“Behaviour and Modelling of Flexible Structures Subjected to Blast Loading”

Vegard Aune, 2017:101, ISBN 978-82-326-2274-0 (printed ver.) ISBN 978-82-326-2275-7 (electronic ver.) ISSN 1503-8181.

“Behaviour of steel connections under quasi-static and impact loading”

Erik Løhre Grimsmo, 2017:159, ISBN 978-82-326-2390-7 (printed ver.) ISBN 978-82-326-2391-4 (electronic ver.) ISSN 1503-8181.

“An experimental and numerical study of cortical bone at the macro and Nano-scale”

Masoud Ramenzanzadehkoldeh, 2017:208, ISBN 978-82-326-2488-1 (printed ver.) ISBN 978-82-326-2489-8 (electronic ver.) ISSN 1503-8181.

“Optoelectrical Properties of a Novel Organic Semiconductor: 6,13-Dichloropentacene”

Mao Wang, 2017:130, ISBN 978-82-326-2332-7 (printed ver.) ISBN 978-82-326-2333-4 (electronic ver.) ISSN 1503-8181.

“Core-shell structured microgels and their behavior at oil and water interface”

Yi Gong, 2017:182, ISBN 978-82-326-2436-2 (printed. ver.) ISBN 978-82-326-2437-9 (electronic ver.) ISSN 1503-8181.

“Aspects of design of reinforced concrete structures using nonlinear finite element analyses”

Morten Engen, 2017:149, ISBN 978-82-326-2370-9 (printed ver.) ISBN 978-82-326-2371-6 (electronic ver.) ISSN 1503-8181.

“Numerical studies on ductile failure of aluminium alloys”

Lars Edvard Dæhli, 2017:284, ISBN 978-82-326-2636-6 (printed ver.) ISBN 978-82-326-2637-3 (electronic ver.) ISSN 1503-8181.

“Modelling and Assessment of Hydrogen Embrittlement in Steels and Nickel Alloys”

Haiyang Yu, 2017:278, ISBN 978-82-326-2624-3 (printed. ver.) ISBN 978-82-326-2625-0 (electronic ver.) ISSN 1503-8181.

“Network arch timber bridges with light timber deck on transverse crossbeams”

Anna Weronika Ostrycharczyk, 2017:318, ISBN 978-82-326-2704-2 (printed ver.) ISBN 978-82-326-2705-9 (electronic ver.) ISSN 1503-8181.

“Splicing of Large Glued Laminated Timber Elements by Use of Long Threaded Rods”

Martin Cepelka, 2017:320, ISBN 978-82-326-2708-0 (printed ver.) ISBN 978-82-326-2709-7 (electronic ver.) ISSN 1503-8181.

“Thermomechanical behaviour of semi-crystalline polymers: experiments, modelling and simulation”

Joakim Johnsen, 2017:317, ISBN 978-82-326-2702-8 (printed ver.) ISBN 978-82-326-2703-5 (electronic ver.) ISSN 1503-8181.

“Small-Scale Plasticity under Hydrogen Environment”

Kai Zhao, 2017:356, ISBN 978-82-326-2782-0 (printed ver.) ISBN 978-82-326-2783-7 (electronic er.) ISSN 1503-8181.

“Risk and Reliability Based Calibration of Structural Design Codes”

Michele Baravalle, 2017:342, ISBN 978-82-326-2752-3 (printed ver.) ISBN 978-82-326-2753-0 (electronic ver.) ISSN 1503-8181.

“Dynamic behaviour of floating bridges exposed to wave excitation”

Knut Andreas Kvåle, 2017:365, ISBN 978-82-326-2800-1 (printed ver.) ISBN 978-82-326-2801-8 (electronic ver.) ISSN 1503-8181.

“Dolomite calcined clay composite cement – hydration and durability”

Alisa Lydia Machner, 2018:39, ISBN 978-82-326-2872-8 (printed ver.) ISBN 978-82-326-2873-5 (electronic ver.) ISSN 1503-8181.

“Modelling of the self-excited forces for bridge decks subjected to random motions: an experimental study”

Bartosz Siedziako, 2018:52, ISBN 978-82-326-2896-4 (printed ver.) ISBN 978-82-326-2897-1 (electronic ver.) ISSN 1503-8181.

“A probabilistic-based methodology for evaluation of timber facade constructions”
Klodian Gradeci, 2018:69, ISBN 978-82-326-2928-2 (printed ver.) ISBN 978-82-326-2929-9 (electronic ver.) ISSN 1503-8181.

“Behaviour and modelling of flow-drill screw connections”
Johan Kolstø Sønstabø, 2018:73, ISBN 978-82-326-2936-7 (printed ver.) ISBN 978-82-326-2937-4 (electronic ver.) ISSN 1503-8181.

“Full-scale investigation of the effects of wind turbulence characteristics on dynamic behavior of long-span cable-supported bridges in complex terrain”
Aksel Fenerci, 2018:100, ISBN 978-82-326-2990-9 (printed ver.) ISBN 978-82-326-2991-6 (electronic ver.) ISSN 1503-8181.

“Modeling and simulation of the soft palate for improved understanding of the obstructive sleep apnea syndrome”
Hongliang Liu, 2018:101, ISBN 978-82-326-2992-3 (printed ver.) ISBN 978-82-326-2993-0 (electronic ver.) ISSN 1503-8181.

“Long-term extreme response analysis of cable-supported bridges with floating pylons subjected to wind and wave loads”
Yuwang Xu, 2018:229, ISBN 978-82-326-3248-0 (printed ver.) ISBN 978-82-326-3249-7 (electronic ver.) ISSN 1503-8181.

“Reinforcement corrosion in carbonated fly ash concrete”
Andres Belda Revert, 2018:230, ISBN 978-82-326-3250-3 (printed ver.) ISBN 978-82-326-3251-0 (electronic ver.) ISSN 1503-8181.

“Direct finite element method for nonlinear earthquake analysis of concrete dams including dam-water-foundation rock interaction”
Arnkjell Løkke, 2018:252, ISBN 978-82-326-3294-7 (printed ver.) ISBN 978-82-326-3295-4 (electronic ver.) ISSN 1503-8181.

“Electromechanical characterization of metal-coated polymer spheres for conductive adhesives”
Molly Strimbeck Bazilchuk, 2018:295, ISBN 978-82-326-3380-7 (printed. ver.) ISBN 978-82-326-3381-4 (electrical ver.) ISSN 1503-8181.

“Determining the tensile properties of Arctic materials and modelling their effects on fracture”
Shengwen Tu, 2018:269, ISBN 978-82-326-3328-9 (printed ver.) ISBN 978-82-326-3329-6 (electronic ver.) ISSN 1503-8181.

“Atomistic Insight into Transportation of Nanofluid in Ultra-confined Channel”
Xiao Wang, 2018:334, ISBN 978-82-326-3456-9 (printed ver.) ISBN 978-82-326-3457-6 (electronic ver.) ISSN 1503-8181.

“An experimental and numerical study of the mechanical behaviour of short glass-fibre reinforced thermoplastics”.

Jens Petter Henrik Holmstrøm, 2019:79, ISBN 978-82-326-3760-7 (printed ver.) ISBN 978-82-326-3761-4 (electronic ver.) ISSN 1503-8181.

“Uncertainty quantification and sensitivity analysis informed modeling of physical systems”

Jacob Sturdy, 2019:115, ISBN 978-82-326-3828-4 (printed ver.) ISBN 978-82-326-3829-1 (electric ver.) ISSN 1503-8181.

“Load model of historic traffic for fatigue life estimation of Norwegian railway bridges”

Gunnstein T. Frøseth, 2019:73, ISBN 978-82-326-3748-5 (printed ver.) ISBN 978-82-326-3749-2 (electronic ver.) ISSN 1503-8181.